RIVER BEHAVIOUR AND SENSITIVITY IN ARID ENVIRONMENT: AN ANALYSIS OF LUNI BASIN, INDIA

Dissertation submitted to Jawaharlal Nehru University in partial fulfillment of the requirements for the award of the degree of

MASTER OF PHILOSOPHY

IN

GEOGRAPHY

JAYESH MUKHERJEE

CENTRE FOR THE STUDY OF REGIONAL DEVELOPMENT

SCHOOL OF SOCIAL SCIENCES

JAWAHARLAL NEHRU UNIVERSITY

NEW DELHI – 110067

INDIA

2021

RECOMMENDATION FORM FOR EVALUATION BY THE EXAMINER/S

CERTIFICATE

This is to certify that the *dissertation*/~~thesis~~ titled *River Behaviour and Sensitivity in Arid Environment: An Analysis of Luni Basin, India* submitted by *Mr. Jayesh Mukherjee* for award of degree of *M.Phil.*/~~M.Tech.~~/~~Ph.D.~~ of Jawaharlal Nehru University, New Delhi, has not been previously submitted in part or in full for any other degree of this university or any other university/institution.

We recommend this ~~thesis~~/*dissertation* be placed before the examiners for evaluation for the award of the degree of *M.Phil.*/~~M.Tech.~~/~~Ph.D.~~

Signature of Supervisor

Date: 24/11/2021

Signature of Dean/Chairperson

Date: 24.11.21

Chairperson
Centre for the Study of Reg De
School of Social Sciences
Jawaharlal Nehru University
New Delhi-110067

ACKNOWLEDGEMENT

Date: 24 November, 2021

Place: New Delhi, India

Jayesh Mukherjee

Jayesh Mukherjee

Dedicated to…

Dadu & Didun

CONTENTS

PREFACE

Studies on the science of dryland systems are on the verge on rising ever since we are trying to understand the impact of climate change across the globe. The increasing desertification, community displacement and protruding human impact on the desertscapes are compelling researchers to think a newer way of looking into the paradigm of arid environment which is sensitive to minor adjustments induced by different meteorological phenomenon of the present-day climate change. Such aeolian dryscapes are much eco- and hydro-sensitive in nature where a minor perturbation can lead to some massive changes. Impact of rivers in arid lands are much less explored globally and this research is a first of its kind in the Indian dryland. River science in today's world is untiringly sorting after a vivid investigation of constant alteration activities and its impact on human habitation in both qualitative and quantitative terms. This research seeks to explain river behaviour in arid environment of the Thar desert drained by the only trunk stream Luni, traversing through the central part of Rajasthan and debouching with its ephemeral flow into the Rann of Kutch. A comprehensive flash flood and anthropogenic sensitivity analysis was performed to understand the natural and man-made impact on the landscape of the Luni river basin.

The work done has been divided into the following **six** chapters –

Chapter -1 provides an expatiating introduction of the traditional and modern methods used for understanding river character, behaviour and sensitivity under a detailed review of literature. The research voids were identified with the contextual understanding of the theme of this study which derives out the major objectives. This is followed by the eloquent drafting of the research questions and finally the objectives. The basic framework of methodology along with a vivid listing of research databases were done. A conceptual lens was used based on the literature study to understand the concepts of river 'behaviour' and 'sensitivity' explaining the how the rivers works in a dryland environment.

Chapter -2 provides a detailed description of the various physical and man-made facets of the study area in terms of its physical description, geographical location, administrative boundaries, prevailing meteorological conditions, bioclimatic variables, seasonal vegetation condition, soil cover and its associated characteristics, land resource mapping and outlining the anthropogenic factors like population and transport network densities, and settlement extent.

Chapter - 3 deals with the geoscientific analysis of the Luni river basin with a detailed insight of geological setup, geomorphological conditions, lineaments, tectonic framework, seismic zones, Bouger anomaly, hydrogeological setup and the ephemeral hydrological status.

Chapter - 4 configures the terrain aspects of the Luni river basin including topographic parameters, drainage conditions, watershed shape and size variability, major sub-basin analysis, areal and linear morphometry, basin asymmetry, hypsometric evolution and river long profile analysis along with their derivatives.

Chapter – 5 examines the special arid and fluvial interactions along with the environmental setup of the in-land deltaic system of Luni, followed by the delineation of MCDM based flash flood and anthropogenic sensitivity zones for the entire Luni river catchment.

Chapter – 6 is the conclusion of the dissertation that focuses on the primary findings, presents the challenges and exhibits a future scope of this research with a way forward.

This dissertation report is supplemented with a list of two sixty references in the Bibliography section and has also been substantiated with quite a number of figures, charts and tables.

LIST OF FIGURES

LIST OF TABLES

LIST OF ABBREVIATIONS

Abbreviation	Full Form
ALOS	Advanced Land Observation Satellite
ASF	Alaska Satellite Facility
amsl	Above Mean Sea Level
ASTER	Advanced Spaceborne Thermal Emission and Reflection Radiometer
BE	Basin Eccentricity
BMTPC	Building Materials & Technology Promotion Council
BSI	Bare Soil Index
CAZRI	Central Arid Zone Research Institute
CC	Compactness Coefficient
CGIAR-CSI	Consultative Group on International Agricultural Research - Consortium for Spatial Information
CGWB	Central Ground Water Board
CHIRPS	Climate Hazards Group InfraRed Precipitation with Station
CR	Circularity Ratio
CWC	Central Water Commission
DD	Drainage Density
DEM	Digital Elevation Model
DI	Drainage Intensity
DI	Dissection Index
DSM	Digital Surface Model
DST	Department of Science & Technology
EI	Ellipticity Index
EOC	Earth Observation Centre
EORC	Earth Observation Research Centre
ER	Elongation Ratio
ESA	European Space Agency
FF	Form Factor
FR	Fitness Ratio
GD	Gauge Discharge
GDEM	Global Digital Elevation Model
GDS	Gauge Discharge Station
GEE	Google Earth Engine
GIS	Geographical Information System
GoI	Government of India
GS	Gravelius Shape Index
GSC	German Space Agency
GSI	Geological Survey of India
GWA	Global Wind Atlas
IN	Infiltration Number
IS	Index of Shape
ISRO	Indian Space Research Organization
JAXA	Japan Aerospace Exploration Agency

LoF	Length of Overland Flow
LR	Lemniscate Ratio
LULC	Land Use and Land Cover
LWR	Length Width Ratio
MBI	Mass Balance Index
MCDM	Multi Criteria Decision Model
ME	Mean Elevation
MoES	Ministry of Earth Science
MoJS	Ministry of Jal Shakti
MPI	Morphometric Protection Index
MRN	Milton's Ruggedness Number
MRRTF	Multiresolution Index for the Ridge Top Flatness
MRVBF	Multiresolution Index for Valley Bottom Flatness
NAQUIM	National Project on Aquifer Management
NAI	National Atlas of India
NASA	National Aeronautics and Space Administration
NATMO	National Atlas and Thematic Mapping Organisation
NBSS&LUP	National Bureau of Soil Survey and Land Use Planning
NCS	National Centre for Seismology
NDMI	Normalized Difference Moisture Index
NISCES	National Information System for Climate & Environmental Studies
NRSC	National Remote Sensing Centre
OSM	Open Street Map
RI	Ruggedness Index
RR	Relative Relief
RS	Remote Sensing
RT	Ridge Top
SAVI	Soil Adjusted Vegetation Index
SEDAC	Socio Economic Data & Applications Centre
SF	Stream Frequency
SoI	Survey of India
SPI	Relative Stream Power Index
SRTM	Shuttle Radar Topographic Mission
STI	Sediment Transport Index
TanDEM-X	TerraSAR-X add-on for Digital Elevation Measurement
TPI	Topographic Position Index
TRI	Terrain Ruggedness Index
TSC	Terrain Surface Convexity
TST	Terrain Surface Texture
TWI	Topographic Wetness Index
USGS	United States Geological Survey
VD	Valley Depth
WEI	Wind Exposition Index
WIP	Western India Plate
WSI	Wind Shelter Index

CHAPTER – 1

INTRODUCTION

1.1 Introduction and Literature Review

The fascinating expanse and the environment of deserts worldwide found to be truly interesting to study, especially when exploring the fluvial processes operating over an entire spatial and temporal scale. The arid climate is generally associated with aeolian processes, where wind acts as the key agent to curve out the typical landforms, for instance, the sand dunes, yardangs, loess and others, but a lot of landscaping is contributed by the fluvial actions as well. The impact and imprints of fluvial processes are found in much prominence, even notwithstanding the dryness of the deserts. Like the sparse vegetation cover, specific characteristics of deserts enable water-based erosion to be a potential force (Goudie, 2013). Unlike those rivers of the alluvial plains, arid regions are typically characterized as ephemeral with disappearing nature. In the words of Reid and Frostick (1997, p. 225), rivers play a decisive role in shaping the deserts of the world, although their evanescent channels run through a meagre proportion of the time and proceed towards the nucleus of hyper-arid regions.

The impact-based integration gained from different natural and human factors controlling the river basin needs a defined method by which the relative impact of each controlling factor can be understood, assessed and then combined. The perception of sensitivity has an ability to furnish the foundation for a powerful analytical tool in relating geomorphological diversity. The optimization of sensitivity analysis in the domain of earth sciences are of three types: first, the relative control in the input variables can be appraised by monitoring ensuing changes in the output variable; second, the change effects in constant proportion can be evaluated; and third, the estimate of structural retrieval can be investigated (Huggett, 1988). Past geomorphological studies have explained the concept of sensitivity in various ways, leading to the development of sub-optimal use of the idea and creating a circumstance whereby tests investigating facets of sensitivity and its utilization cannot aptly be compared to the previous studies (Downs and Gregory, 1995). For instance, Thomas and Allison (1993) explain that the implicit understanding of sensitivity relates to the alterations in landscape consequent to adjustments with peripheral perturbations. Till date, no steady approach is used to discern the sensitivity.

To understand one's behaviour, it is commonly said that the way one conducts or acts oneself, especially while interacting with others with some well-defined behavioural traits like

thoughts, words, actions, and habits describing a man's personality, is behaviour. Similarly, river behaviour can be explained as the phenomenon under which it functions in the natural environment. Thus, rivers flowing through various settings like that in a humid tropic to that in a temperate region behaves differently or works uniquely because of the prevailing external and internal agencies like climatic factors, topography, channel processes and hydrological character. So, in relation to the river channel modifications, acting in a different environment, sensitivity leads to how a river would behave and, wherever possible, is defined in terms of the relationship of disrupting forces to a specific threshold condition. Hence the character of a river develops based on its unique behaviour but can be grouped and classified along the lines of some common factors, for instance, climate. The scrutiny of river behaviour upholds how diverse river types can adjust to the amount of modification occurring and the permanence of such modifications. These deliberations determine the behavioural reign of a river reach. Hence, rivers are the great balancers of our landscape, eternally adjusting to the disrupting events and the overall flow and sediment fluxes. Some adjustments are progressive and predictable, while the rest reflect "*dramatic and unpredictable (threshold-breaching) circumstances*". River behaviour shows geomorphic adjustments, those ongoing over a temporal scale in which flux boundary conditions (i.e., flow–sediment regimes and vegetation interactions) remain relatively similar. A reach can retain a characteristic set of the process–form relationships. "*River behaviour is defined as adjustments to river morphology induced by a range of erosional and depositional processes by which water moulds, reworks and reshapes fluvial landforms, producing characteristic assemblages of landforms at the reach scale.*" (Fryirs and Brierley, 2012).

Since our inception days of geographical knowledge, we are accustomed to having a mental picture of dry bed rivers with no such well-defined course, especially for the fingertip streams, which are only found to be in life with water and peak flow during the rainy months of monsoon or western disturbances. The behaviour and character of a river are hence two sides of the same coin, helping to define their variations across a spatial dimension. The combination of factors contributing to the development of a river like – precipitation, topography, slope, soil, land cover, and land use aggravates any fluvial process directly proportional to the development of a sizeable riverine watershed system having different dynamics in an arid environment. Sandy soil helps in a large amount of river water to percolate beneath the ground. At the same time, the rest gets quickly evaporated due to soaring temperatures during the summer months and with meagre rainfall. In today's world, the dimension of fluvial studies has shifted from a

process-based approach to an impact-based approach which needs to have a significant focus to assess the impacts on human beings from both sides, i.e., rivers having a natural impact on the lives of people like during the flash floods which commonly occurs in an arid region along with the human-induced alterations that are majorly changing the landscape, in-channel character and hence only making themselves more vulnerable to hazards. This paradigm shift positively enlightens the need for an impact-based study like the one here intended to be done based on flood recurrence and erosion-based analysis, which can be further taken up seriously as a part of riverscape governance, policymaking and its practical implementation through enforceable laws.

The global scenario of the arid and semi-arid regions is characterized by limited water resources exerting an ever-increasing and tremendous pressure due to fast expansion of population, rising per capita water usage, and irrigation. The different sources of point-based direct or indirect pollution, rising volumes of industrial and domestic effluents and waste, as well as over-drafting of groundwater, cater to a concerning threat to those sporadic resources. Floods are irregular but can be catastrophic, which may threaten lives, and infrastructure is in due rise because of rapid urban expansion leading to high surface runoff. Dryland ecosystems are frail enough to get threatened with groundwater over-extraction and the mismanagement of surface water flows. Added to these, the very existing physical pressure posed due to man-made factors enhance the feelings of changing climate. Hence, compelling strategies and enforceable policies to administer water use is indispensable and requires convenient decision support systems, including modelling tools that can improve the existing resources.

There are many debates about the relative power of fluvial and aeolian processes. Hard and fast empirical data that compare the operation of both types of processes are sparse. Zhang et al. (2011), in their research, provided an exceptional study explaining how water-based actions are dominant in shaping the landscape with rates of water erosion greatly exceeding rates of wind erosion. But they interact in a whole range of ways (Draut, 2012). Aeolian deposits are probably reworked to form the alluvium of desert rivers or source of dune sand or dust, where valley-marginal sand dunes may have a distinctive morphology (Bullard and Nash, 2000). It has been found that the presence of aeolian silt affects the infiltration capacity as well as runoff from desert surfaces where fluvial actions may degrade dunes, rivers may be changing its courses or maybe dammed by dunes and, in tune to recent times, climate change has a profound impact on most deserts with altering humid and arid conditions (Goudie, 2013). The amount of sediment yield is usually related to humid season, but the sediment availability in the aeolian

riverine catchments rises during the torrid phases (Bullard and McTainsh, 2003). Short-lived climatic variability and fluctuations can lead to severe dust devils or flash floods occurring in an area as a matter of course (Bullard and Livingstone, 2002).

Knighton and Nanson (1997) assessed the distinctive, diverse and unique characteristics of dryland rivers. They identified that dryland rivers exist along a continuum from ephemeral to perennial flow, based on the climatic or precipitation-based fluctuations. But concerning their proposition, it was seen that dryland rivers as a group could be distinctive and internally diverse may be seen by some as a possible inconsistency. Prolonged periods of meagre or no channel activity in the arid environment of Luni gets duly interrupted by intense rainfall-runoff events, which lead to the development of short-lived but high-energy flash floods, which leads to the '*Floods in Thar*'. The hillslope vegetation is found to be limited coupled with well-developed slope-channel along the escarpments of Aravalli, and the denuded local remnants across the Luni river basin result in an abundant supply of coarse-grained (gravel, sand) sediment to rivers in confined valleys or too wide, braided channels in piedmont settings (Tooth and Nanson, 2011). The Aravalli escarpment on the southeastern side of the catchment and the presence of in-between ridges present within the river basin of Luni is a significant reason for Luni to behave in a flashy nature. The depth of the river bed is positively related to the hydrological behaviour and the carrying capacity of the sediment load. The insignificant channel depth of the Luni river makes it flashy as the river tends to have a spillover effect due to less depth of river bed and widens out, leaving its course every time with high precipitation events.

Rapid flow velocities and high sediment transport rates are commonly associated with the dominance of horizontal lamination or low angle cross-bedding in fluvial deposits (Tooth and Nanson, 2011). Terrace sequences will have older alluvium deposits preserved within, but active floodplains may be found to be non-existent or limited in extent. Sparse or non-existent vegetation along with a restricted form of sediment cohesion results in unstable river banks. Extensive floods result in extreme (or even catastrophic) alterations within the channel, including pronounced channel widening and deepening (scouring). Hence, the fluvial sensitivity in the arid landscape of Thar provided the shreds of evidence of such discontinuous system behaviour, arousing a tendency to view many dryland rivers across the globe in a state of almost unchanging non-equilibrium (e.g., Thornes, 1980; Rhoads, 1988; Graf, 1988), with channel flows, transportation of sediments and channel morphology rarely in balance. In the context of this previous view and the words of Tooth and Nanson (2011), it can be summed up that dryland rivers were ordinarily seen as the "antithesis of many humid zone perennial rivers"

which possess well-defined feedback mechanisms between channel flow, sediment transport and channel morphology that commonly operates to keep the river channel in a graded condition.

The sensitivity of rivers is inherited within any landscape in the form of historical carvings or as a 'human memory', remembering the former operative processes during the past over a spatial scale. As referred to by Brierley (2010) and Jain et al. (2020), ' landscape memory' brings in the compelling significance for geomorphologists concerning how they discern and decipher the landscapes with a holistic approach. The rivers or any other geomorphic landform tends to get randomly preserved as a source of fragment testimony telling us the tale of the past as of how the rivers flowed, climatic conditions and exhibiting other geo-archaeological evidence. The three significant terms distinguishing the imprints associated with landscape analogy can be geologic, climatic and anthropogenic memory (Brierley, 2010).

The rivers are not detached linear natural bodies but rather an inclusive feature of the landscape with specific hydrogeomorphic characteristics (Jain et al., 2020). Therefore, the present-day observable morphology results from the river feedback mechanism due to particular past external forcing over geological time scale. The river utilizes the available stream power to govern the modern-day valley carvings. The concentration of flood power within the valley and the pertinent incision of the river beds leaves behind paleo-markers which gets selectively preserved over time. So, an in-depth paleo-geomorphological study can help us to go through these 'memories' well preserved by the landscape, same as the remnants of ancient civilizations in the form of their artefacts, manuscripts, etc. reflecting the objectivity to understand the past dynamics of rivers, including the behaviour and sensitivity as well as the driving forces behind them. Brierley (2010) also pointed out that the ingrained ramification of landscapes poses hefty confrontation in the efforts to govern the look and behave in a specific way. So, landscape memory expends an elementary understanding of the natural and man-made relationships, thereby watershed-specific responses to any disturbance events ranging over a magnitude.

The vitality of literature review can be further pacified and substantiated by some latest online search engine tool such as Google Books Ngram viewer developed by Jon Orwant and Will Brockman in mid-December of 2010 exhibits the frequencies of searched keywords or phrases those have occurred in a collection of books (for instance – 'French', 'Spanish', 'US English', etc.) over the searched years. In the tune of the research theme consisting of river 'sensitivity' and 'behaviour', five keywords were selectively chosen, namely, 'dryland rivers', 'landscape

sensitivity', 'river character', 'river behaviour' and 'anthropogenic impact'. The trend of these keywords was searched in Google Ngram viewer for the past century from 1920-2019.
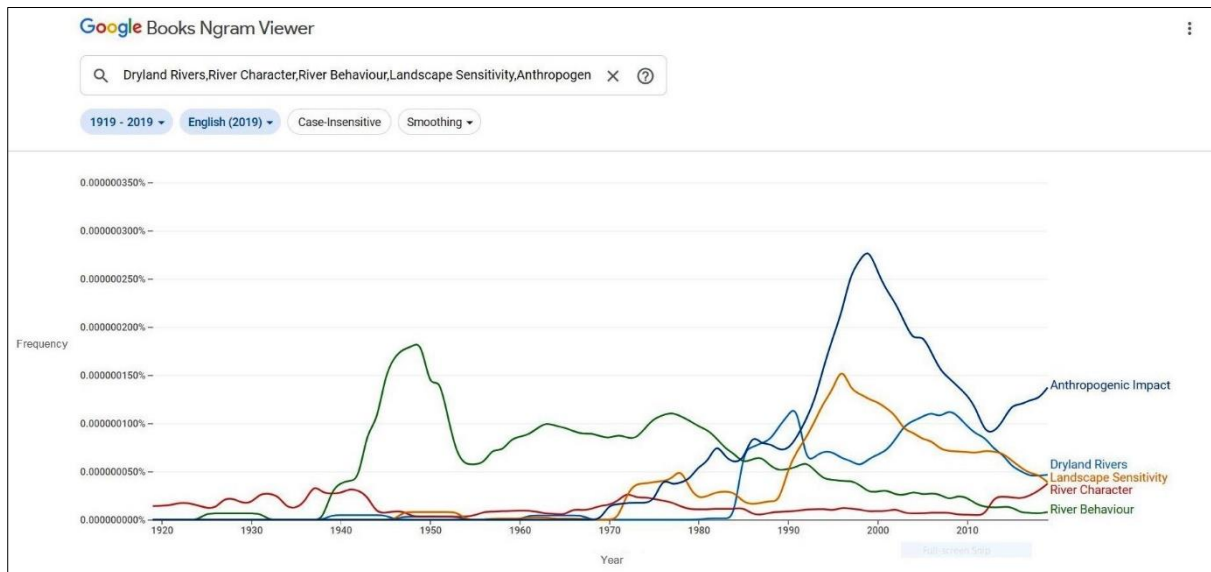
Figure 1.1 Google Books Ngram viewer exhibiting the trend of development and progress of the searched keywords over the past century 1920-2019. Source: Prepared by the researcher.

The general trend of frequency shows a low start in the initial years of the century until from the 1940s the term 'river behaviour' has seen a prominent peak with a gradual decline in the recent years. The technical documents and mention of the river-related behavioural studies in the engineering documents of the US Army corps, USGS, British and French Engineering Services during the World War - II and post War times till the 1990s behavioural studies of rivers in tune to civil constructions within rivers fit the graph for river behaviour. The publications of aeolian or 'dryland rivers' started from the 1970s, reached their peak from 1990-2000 and gradually lowered till recent times. The maximum studies and publications in the form of academic books or research articles came out from the late 1980s till date from famous geomorphologists like Dr. William Graf, Prof. Andrew Goudie, Prof. David S.G. Thomas, Prof. Stephen Tooth, Dr. Parsons and others (Graf and Lecce, 1988; Bull and Krikby, 2002; Parsons and Abhrahams, 2009; Thomas, 2011 and Goudie, 2013). 'River character' is rather found to be less used terminologies unless in the recent times from 2010 the use and analysis of river's unique eco-geomorphic traits are rising and finds a place in recent publications (Fryirs and Brierley, 2012; Fryirs, 2017). The character of rivers and their angle of analysis have a modern thought behind it to describe the working of a river according to its climatic and hydrological setup. The trend line for the term 'landscape sensitivity' comes from Brunsden and Thornes (1979) discussing the concept and examples for the first instance in a

geomorphic sense. The concept went on viral hence after in the discipline, and geomorphic analysis was explained through the lens of landscape 'sensitivity' especially in the 1990s until the early 2000s. This major popularity soon sees a decline in the recent decade, although the concept has not lost its fascinating influence and keeps on surfacing up in some major theoretical as well as practical oriented research articles and books on fluvial geomorphology. The last keyword is the most popularly used terminology, and the concept for analysis is 'anthropogenic impact'. Since the advent of the term after the 1960s, Golomb and Eder (1964) explained how humans could be a source of an active geomorphic agent using the term 'anthropogeomorphology'. The man-made impact analysis on the natural world became day by day increasingly vital and so does the graphical trend show the peak influence of the term during the 1990s till it reaches it peak in 2000s and soon starts to decline till 2010, creating a bell-shaped curve unless again it shows a rising limb of the trend graph.

To further initiate the understanding of the concept of 'sensitivity' in landscape studies and in fluvial science, a timeline chart (Table – 1.1) was listed down showing the list of significant research works with the article title and the keyword(s) used in the study since the very advent of the term 'sensitivity' from 1979. The justification of the research work needs to have an intensive solid base of literature from the past bringing in the various walks of study by researchers all over the globe. The table is pretty self-explanatory where the concept of river 'sensitivity' and 'behaviour has been given a prime focus starting from the recently published Multi-Criteria based Decision Model (MCDM) based Analytical Hierarchical Process (AHP) and Frequency Ratio (FR) techniques to understand river channel sensitivity (Ghosh and Maiti, 2021). Research articles also include a list of major theoretical papers which help in understanding the various facets of river behaviour and sensitivity in the real sense, incorporating dryland river processes and their thresholds to future climate change actions (Larkin et al., 2020), river management and restoration strategies (Khan and Fryirs, 2020; Lisenby, et.al., 2020), need for implementable river policies (García et al., 2021), river ecosystems, river habitat (Fuller et al., 2019) and many such deplorable current issues of river science. Therefore, Table 1.1 is an essential exhibition of the chronology of the evolution of the concept of 'sensitivity' and 'behaviour' in a truly fundamental and applied sense of understanding.

Table 1.1: List of research papers and keyword(s) showing the evolution trend of the concept of river 'sensitivity' and 'behaviour'.

Reference	Research Paper Title	Keywords
Ghosh and Maiti, 2021	Development of new composite index on channel sensitivity using AHP, FR and ensemble model and its application on the Mayurakshi river of Eastern India	Analytical hierarchy process, frequency ratio, Kappa statistics, Mayurakshi river, ROC curve, sensitivity
García et al., 2021	Promoting fluvial geomorphology to "live with rivers" in the Anthropocene Era	Applied fluvial geomorphology, River policy, Process-based management, River restoration
Khan and Fryirs, 2020	An approach for assessing geomorphic river sensitivity across a catchment based on analysis of historical capacity for adjustment	Catastrophic floods, River management, River restoration, Forecasting, Post colonisation, Human disturbance
Lisenby et al., 2020	River sensitivity and sediment connectivity as tools for assessing future geomorphic channel behaviour	Geomorphic forecasting, climate change, catastrophic flood, river restoration, scenario-building, prioritization
Larkin et al., 2020	Identifying threshold responses of Australian dryland rivers to future hydroclimatic change	Dryland rivers, sensitivity, future hydroclimatic changes, threshold
Fuller et al., 2019	Framing resilience for river geomorphology: Reinventing the wheel?	Disturbance, process-response, river ecosystems, river habitat, river science
Gregory, 2019	Human influence on the morphological adjustment of river channels: The evolution of pertinent concepts in river science	Channel changes, concepts, human impact, river channel morphology
Wohl, 2018	Geomorphic context in rivers	Disturbance, management, process domain, resilience, river geometry, river style, context
Fryirs, 2017	River sensitivity: a lost foundation concept in fluvial geomorphology	Threshold; recovery; sediment connectivity; resilience; complex response
Marçal, Brierley and Lima, 2017	Using geomorphic understanding of catchment-scale process relationships to support the management of river futures: Macaé Basin, Brazil	River diversity, Landscape evolution, Channel adjustment, Land use, Landscape connectivity, Future scenarios
Wohl, 2016	Spatial heterogeneity as a component of river geomorphic complexity	River complexity, resistance, resilience, diversity, spatial, heterogeneity
Reid and Brierley, 2015	Assessing geomorphic sensitivity in relation to river capacity for adjustment	River adjustment, River change, Rate of geomorphic adjustment, Threshold, River management
Biron et al., 2014	Freedom Space for Rivers: A Sustainable Management Approach to Enhance River Resilience	Hydrogeomorphology, Meander migration, Floodplain, River management, Wetlands
Fryirs et al., 2009	Post-European settlement response gradients of river sensitivity and recovery across the upper Hunter catchment, Australia	River evolution; river metamorphosis; river sensitivity; river recovery; human disturbance

Werritty and Leys, 2001	The sensitivity of Scottish rivers and upland valley floors to recent environmental change	Landscape sensitivity, Recent environmental change, River stability, Upland Scotland, Floods, Valley floors
Brunsden, 2001	A critical assessment of the sensitivity concept in geomorphology	Landform change, Sensitivity, Resistance, Resilience
Thomas, 2001	Landscape sensitivity in time and space — an introduction	Landscape sensitivity, Earth surface systems, Scale problems, Landscape mosaics, Inherited features
Downs and Gregory, 1995	Approaches to River Channel Sensitivity	Sensitivity, river channel change, thresholds, sensitivity analysis
Downs and Gregory, 1993	The sensitivity of river channels in the landscape system	Human activity, channels landform evolution, fluvial features
Thomas and Allison, 1993	The sensitivity of landscapes	Human action, Climate change, Morphodynamic, Landscape
Brunsden and Thornes, 1979	Landscape sensitivity and change	Constant process, Characteristic form, Transient behaviour, Thresholds, Complex response, Sensitivity to change

Source: Compiled by the researcher.

Figure 1.2: Word cloud highlighting the significant keywords related to river 'behaviour' and 'sensitivity'. Source: Prepared by the researcher based on reviewed literature in Table 1.1.

Table 1.2: Trending terminologies and definitions associated with river 'behaviour' and 'sensitivity' concepts.

Terms	Definition
Fluvial Environment	A type of sedimentary setting where fluvial landforms (geomorphology) and fluvial deposits (facies) are shaped, altered, blighted, and/or conserved through erosion, transport and sediment deposition.
River (dis)continuity	A type of disruption within the interconnected geomorphic network of rivers, though having a continuity, led to breakage of interaction between the channel posed due to natural (e.g., large woody debris) and/or man-made (e.g., causeways) factors.
River Adjustment	The physical adjustments or alterations brought into the riverine system by changing climate or human-based actions can refer to as river adjustment.
River Behaviour	The continuous geomorphic modifications taking over various temporal scales in the flux boundary conditions of a river (e.g., ecological interactions or flow and sediment regimes) remain more or less uniform so that the river reach retains the process-form relationship.
River Capacity	River capacity is defined as the ability to accommodate eco-geomorphic conditions like - river flow, sediments, habitat, etc. by a river winding down the valley till it achieves the immediate base level.
River Change	A wholesome shift in the behavioural reign of a reach yields a distinct river type with a diverse set of process–form relationships.
River Character	The character of a river is describing the river based on the traits that help define its consistency with the lens of climate, underlying geology, operating geomorphic processes and human actions leading to its continuous dynamic evolution and re-development.
River Connectivity	The joining and disjoining of rivers in the form of tributaries and distributaries channelize a natural state of interconnectedness, resulting in a complex geomorphic process-form relationship.
River Diversity	The heterogeneous diversity brought in by climatic, physiographic processes, hydrological regimes, and man-made factors within a river system led to geomorphic variability across various spatial and temporal scales.
River Dynamics	The operative ex-situ or in-situ forcing stimulate the progress, advancement or alterations within the fluvial system.
River Memory	The past archives of riverine processes embedded into the surface or sub-surface layers of the present-day riverscape explain the 'past imprints' left behind by bygone fluvial actions are referred to as river memory.
River Metamorphosis	The continuum evolution of rivers induced by various terrain, climatic, hydrological, and anthropogenic factors drive a river transfiguration and gives rise to an untrodden form over time and space.
River Resilience	The amplitude of a river system and its associated communities to briskly recover from perturbations, comply to transformations without collapsing and improve through innovation and exertion of pliancy strategies.
River Sensitivity	The feasibility and propensity for adjustments along a river course, and the ability of the system to recoup from any given disruptions.
River Space	The interactive geomorphic 'space' of a river continues to have its character without any disturbances posed by anthropogenic actions.
Riverscape	A landscape containing an assemblage of fluvial features, both erosional and depositional landforms, comprises a general riverine panorama.

Source: Compiled by the researcher from various literature as reviewed in Table 1.1

After a detailed understanding of the timeline for the terms 'sensitivity' and behaviour', a trial was initiated to decipher the most important keywords from Table 1.1. For this, a word cloud (Fig. 1.2) was generated online (https://monkeylearn.com/word-cloud/) using the keywords from the research papers. Three essential terms in the respective descending order also seen with graded blue font size in Fig. 1.2 are - 'sensitivity', 'threshold' and 'resilience'. The other vital words among the assemblage of the word cloud is found to be in decreasing order of the font size and diminishing blue colour. The term 'sensitivity' was used nine times, followed by the term 'threshold' five times and 'resilience' four times, respectively. The principal purpose of this word cloud is to bring out the emphasized terminologies used in the tabulated research articles in Table 1.1 so that a better understanding of the focused keywords can be understood and the present research can be used to highlight the current ongoing trend in this specific field of fluvial study.

In tune to the previous keywords, another Table 1.2 was prepared to list out the trending terminologies and their definitions associated with the concepts of river 'behaviour' and 'sensitivity' based on the extensive literature review done for this section and from the research papers in table 1.1. Sixteen words were selectively chosen, and their contemporary definitions were described in their own words to bring out their meaning in a lucid way. All the terms are associated with the 'river' entity, including the 'fluvial environment'. Table 1.2 reflects the present terms of those having a significant scope of discussion and further strengthens the root of the reviewed pieces of literature across this section of the chapter. Some words are very overlapping but have been segregated based on the spirit of the specific terminology, for instance – river 'dynamics' and 'metamorphosis'; riverscape' and 'fluvial environment', which tries to bring out a more or less a similar concept.

A thin line of difference between them has been identified and developed based on the temperament of the ancillary word with the river. Like, the scientific study of the forces involved in the movement is known as 'dynamics', and hence the dynamicity of the rivers means the operative internal or external forcings that stimulate the progress, advancement or alterations within the fluvial system. Similarly, 'metamorphosis' in terms of rivers can be defined as a physical process by which a river grows and develops, alters its channel, and develops certain landforms unique to its stage of evolution. So, the ancillary terms in association with river exemplify the routing of a base concept with a little difference to it but can explain how we probe deep into its definition. "Riverscape" is an overview terminology

that discusses and is encompassed around a landscape engrossed with fluvial landforms. While "fluvial environment" considers everything of a river just within the boundary of riparian buffer or the river channel considering only the erosional, depositional landforms, transportation of sediments and the ecological habitat of the river.

1.2 Research Gaps and Rationale of the Study

The literature review leads us to identify the areas that lack attention and are ardently required to be addressed to bridge the existing gaps within the research domain. The primary findings show that research on the arid environment rivers, especially like that of Luni and other major river basins across the globe, has not tried to address the uniqueness of their river behaviour with response to anthropogenic perturbations and natural calamities like flash floods. The primary objective to date lacks to understand the fluvial behaviour and its sensitivity for an arid environment especially in a unified way. This requires a well-developed infused approach that effectively deals with the relationship between rainfall and surface runoff simulation mutually with a flood inundation model to assess the hazard that can be posed by flash floods (Elfeki et al., 2016) and make the local population residing near to the riverine floodplain vulnerable. Anthropogenic inheritance and the infrastructural load in a river basin need prominent attention to understand the degradational sources within a river basin induced by human-based operations. An analysis of arid river behaviour and its sensitivity also requires a significant drive to spot the impact-based assessment on the local population and their livelihoods thriving on the river. The integrational study still lacks these days where the physical and social impact assessment of rivers are brought together in one place, bridging the gap between both and hence making the analysis more interdisciplinary. This study takes a first of its kind attempt to integrate the river behaviour and the sensitivity factors, both human-based and natural hazards like flash floods in a river basin, firmly contextualizing the concepts in the arid environment of Thar.

These are the widest literature inconsistencies that have been the prime motive of this research, especially in the context of the Great Thar desert of India. Luni is the central river system existing in the Indian part of the Thar, which needs in-depth analysis to understand the fluvial based process-response mechanism in the arid conditions and how it marks its difference or dominance aeolian processes. Conventionally, deserts are known as the driest parts of the globe, but the floods from extreme precipitation can be dangerous to the thriving local population. The very nature of floods is flashy and can inundate a substantial area as it is devoid of a well-defined channel with less channel depth over a concise duration of time. The

floodwaters inundate large areas of land, hampering settlements, agricultural produce by splaying the sands over the channel through its considerable breaching. The Great Indian Thar, which thrives a substantial amount of the human population, needs a sensitive assessment of both anthropogenic disturbances and flash floods within the Luni river basin to understand the zones of higher risks, helping to take appropriate steps and planning to resettle the local villages or agricultural lands away from the sites of higher sensitivity.

1.3 Research Questions

The research questions that arise are those valid, thought-provoking points identified from the research gaps after the exhaustive literature review. These are as follows –

   i.   How is an arid river sensitive to extreme hydrological events like a flash flood?

  ii.   How does the river behave in responding to such extreme flood events?

 iii.   What is the operative process-response mechanism which are responsible for such behaviour?

 iv.   Which anthropogenic factors make an arid river basin sensitive, and how?

  v.   How do the river behaviour and its sensitivity impact human lives and their livelihoods residing within the river basin?

1.4 Research Objectives

The objectives of this study are derived based on the research gaps obtained after the literature review addressing the major unanswered research questions. The objectivity of research needs to address the purpose of this study which can be reasonably achieved with the available resources within a specific timeframe. This research is based on the following enlisted objectives –

1. To formulate a structural framework guide to study aeolian river behaviour and sensitivity based on an in-depth literature survey.
2. To develop a basic understanding of the Luni river basin in the light of physical and anthropogenic factors.
3. To investigate the process-response mechanism operating within the river basin based on the geo-scientific and landscape characterization.
4. To evaluate the behaviour and sensitivity of the study river using the lens of environmental mechanisms associated with aeolian-fluvial synergy and flood out geomorphology.
5. To understand the flash floods and anthropogenic sensitivity within the Luni river basin based on two types of multi-criteria decision making models - AHP and Composite Index.

1.5 Research Datasets

The research datasets include a broad list of secondary datasets collected from various web portals of different data providing organizations which are enumerated in Table 1.3. All the datasets used for the study are freely available and hence comes under the purview of Creative Commons Attribution (CC by 4.0) International License, enabling the researchers to have the datasets freely used, copied or shared globally. Table 1.3 explains the type of data, source of acquisition, spatial resolution and time period for each dataset.

Table 1.3: Enumerated master list containing research datasets used in the present study.

Sl. No.	Parameters	Data Type	Data Source	Spatial Resolution	Period
1	Elevation, Terrain & Drainage	Raster Grid	SRTM DEM (USGS), version 3.0	1 arc-second (30 m)	September, 2014
2	Topography & Luni River Channel	Line and polygon coverage	SoI Topographical Sheets	1: 50,000	2006
3	Geology, Lithology & Lineaments	Spatial Grid	Bhukosh geoportal, GSI/ GSI Quadrangles	1:2,000,000	2018
4	Geomorphology			1:250,000	
5	Tectonic Framework			1:250,000	
6	Seismic Zones	Polygon coverage	Vulnerability Atlas of India v.3, BMTPC	1 cm = 100 km	2019
7	Hydrogeology		NAQUIM, CGWB, MoJS, GoI		2017
8	Soil Distribution		NAI, WIP – 200, NATMO, DST, GoI	1:2,000,000	1981
9	Land Capability		NAI, WIP - 221, NATMO, DST, GoI		
10	Locations of Earthquake Events	Spatial Grid	NCS, MoES, GoI	1:250,000	2020
11	Temperature, CV of rainfall, Diurnal range of temperature, Solar radiation & Water vapour pressure	Raster Grid	WorldClim v.2.1	2.5 min. x 2.5 min. (~5 km^2)	1970-2000
12	PET & AI		CGIAR-CSI	30-arc second	
13	Rainfall		CHIRPS v. 2.0	0.05 x 0.05 degree	1981-2019

14	Wind Speed (10 m & 50 m)		Global Wind Atlas (GWA) 3.0	10-arc second (300 m)	2019
15	Wind Power Density				
16	Soil Texture, Depth & Carbon Density		NISCES, Group: Terrestrial Sciences, SLARD, NRSC, ISRO	5 km x 5 km	Feb 2016
17	Land Degradation		WMS Layer, NRSC, ISRO	1:50,000	2015-16
18	Wasteland				
19	Cropland		SEDAC, NASA	~10 km	2000
20	Pastureland				
21	LULC	Raster Grid	Global Landcover, ESA	100 m	2009 & 2019
22	VCI		Copernicus Global Land Service, ESA	1 km x 1 km	May & Oct 2019
23	Satellite Image based Indices (floodout)		Landsat 8 OLI/TIRS C1 L1; Path/Row: 150-43	30 m	May & Oct/Nov 2019
24	Global surface water		Joint Research Centre, European Union	30 m	1984-2020
25	Fluvial Signatures	Polygon coverage	Google Earth Imagery	2 cm = 1 km	2020
26	Population Density	Raster Grid	SEDAC, NASA	30 arc second	2015
27	Population per Pixel and Settlement Extent		WorldPop, Univ. of Southampton, U.K.	100 m	2020
28	Transport Networks (Road & Railways)	Spatial Grid	Open Street Map	Extracted using Luni's watershed polygon	2020
29	Settlements				
30	Village/Block / District/State Boundaries		Census of India, 2011		2011
31	River Point Hydrology	Daily Water Level & Flow Timeseries	Executive Engineer, Mahi Division, Gandhinagar, CWC, MoJS, GoI	Two Gauge-Discharge monitoring stations on Luni River - Balotra & Gandhav, Rajasthan	1990-2016 & 1979-2016

Source: Compiled by the researcher.

1.6 Research Methodology

This research is encompassed in various methodologies used to bring out multiple results from the different datasets (Table 1.3). The primary usage of the dataset is based on fulfilling the research objectives (section – 1.4). The first objective tries to achieve new structural framework guidance to study and better understand river behaviour and sensitivity. This framework is developed by going through an exhaustive and more than eighty literature including research articles, short communications, commentaries, oral and poster presentation abstracts of various conferences over the past forty years. The second objective needs a GIS-based methodology to prepare the basic maps of the Luni river basin directly from the acquired raster or spatial layers exhibiting the climatic, bioclimatic, vegetation condition and other physical and anthropogenic factors. Similarly, the third objective is fulfilled based on using an extensive geoprocessing of the raster and spatial datasets in the GIS environment to develop the geo-scientific and landscape characterization of the Luni river basin. Analytical tables, charts and graphs are prepared based on such processed datasets. The fourth objective is based on developing conceptual diagrams after going through the landscape of the Luni river, especially in the floodout region, using the help of GIS/RS techniques, Landsat and Google Earth imageries. The last objective to decipher the flash flood and anthropogenic sensitive zones is fulfilled using various thematic layers in the GIS environment based on the MCDM-AHP and CSI modelling. The specific methodologies are later discussed in details specifically under each individual chapter.

1. 7 Framework for River Behaviour and Sensitivity Study

Any study or research needs to have a well-defined structure or framework in mind or document which can be utilized to take up a step-wise approach in understanding a concept. The development and prosperity of the idea depending on how well the researcher designs the framework. The collective research efforts can be supported only with a good research framework that provides an underlying structure to clinch onto the core concept of the study. Hence, the scope of the study can have better attention with the guidance of a better framework. The research framework does not *"presuppose a normative stand of the analyst"* (Biermann and Kalfagianni, 2020).

This research aims to develop new structural framework guidance to study the aeolian river behaviour and sensitivity based on an in-depth literature survey. After going through various pieces of literature over the past forty years, a two-fold framework has been conceptualized and put into work to understand the main two keywords of the title of this research – 'river

behaviour' and 'river sensitivity'. Figure 1.3 tries to encapsulate river behaviour in a cyclical impact framework. The behaviour of a river can be understood as the *expected adjustments* that occur for a *specific environment*-based river. The inspiration to draw up a comprehensive framework for river behaviour can justify the reason and the way of personifying rivers their behaviour and its impact on the local landscape.
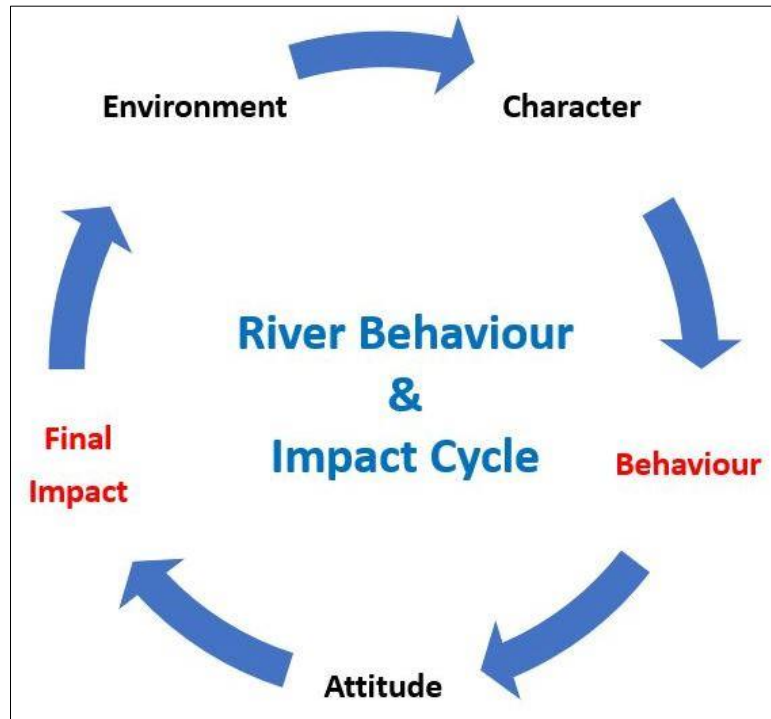
Figure 1.3: River Behaviour and Impact Cycle. Source: Devised by the researcher.

Based on the above, the primary five components of the river behaviour and impact cycle are described step-wise below –

1. Environment: The cycle starts with an environmental setup in which the study area is located. As the study involves the Luni river basin, consider arid/dryland as the dominant environment in which the river behaviour would be studied.

2. Character: Character is the traits of qualities that make a river different from others. Here, the character of a river is directly derived from the first step, i.e., an environment that determines the river's character. So, Luni being a dryland river is based on certain unique qualities like zero river flows, splayed channels, ephemeral flow lines, and other traits defining its character and helping better to understand the present-day river metamorphosis and channel dynamics.

3. Behaviour: River behaviour is known as the actions made by the riparian systems in conjunction with their physical environment, including the other systems. So, the interactive phases of rivers based on external or internal forcing define how a river will behave based on the specific environment defined characteristics. Thus, Luni being a dryland river and based on the previous traits, the behaviour of the river channel will be flashy during extreme precipitation over a short duration of time, creating flash floods. As the channel depth is less than the channel width, the floodwaters easily spill out of the channel and inundate the local settlements and farmlands. Hence, environment derived characteristics of a river shape its actions, and the immediate impact is studied in this research to fulfil the overlooked research area through the set objective.

4. Attitude: In human psychology, 'attitude' is defined as a mental and emotional entity that characterizes a person. It is often said to 'personify an individual' or describes 'a way of behaviour'. This concept can be used to understand the complex and intermediate multi-step micro-processes that operate on and within the fluvial landscape, resulting in a broader manifestation of the river behaviour and sensitivity. The attitude of a river involves all the unseen background hydro-geomorphological operations, both in-situ and ex-situ, that withheld the river's character-induced behaviour in a particular environment. For instance, the behavioural expression of the river in Luni, in the form of flash floods, includes the small determinant factors like slope curvature and slope angle, helping to instigate a flash flood event during a very high rainfall event.

5. Final Impact: After going through the exhaustive understanding of the previous four steps in the river behaviour and impact cycle framework, the final impact assessment can be outlined linking all the major traits, actions and minor processes which defines the reason and objective of the studying flash flood event (natural) & geohazard assessment for the riparian settlements (human). After enlisting the factors and going through all possible methods the best approach can be chosen to identify the highly sensitive zones of flash floods and significant concentration of anthropogenic footprints. In this study, the MCDM-AHP and CSI methods are used to understand the final impact of various processes and thematic parameters affecting the sensitivity.

The first framework clarifies the step wise approach in studying river behaviour and its impact through sensitivity analysis both in natural and man-made terms. The second framework is called the river 'psyche' pyramid (Fig. 1.4). This is instead a simplified version of the first

framework. Behavioural studies of a river can be best described once the characteristic traits are clubbed or segregated based on a broader class; for example, the natural factors like climate, topography, slope etc. are all clubbed under physical aspects while the population density, settlement density, transport network density etc. are segregated under anthropogenic factors.
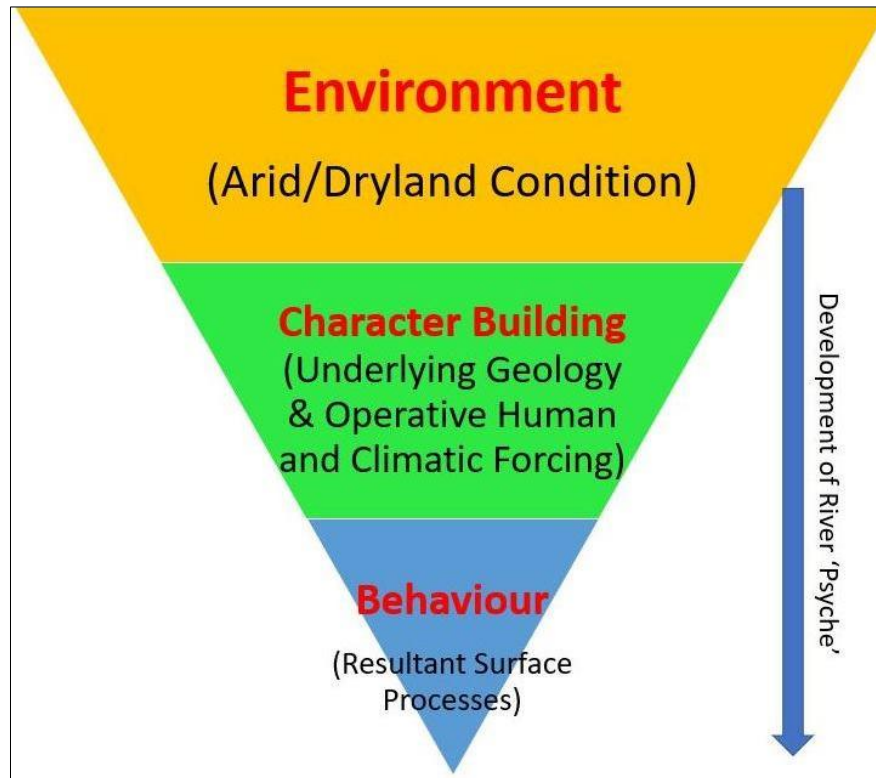
Figure 1.4:River 'Psyche' Pyramid. Source: Devised by the researcher.

This framework is based on a human psychology framework used to understanding a person's behaviour based on a series of psychometric tests or questionnaires as used by a psychologist or psychiatrist to treat a behavioural disorder. As used metaphorically in journalism, the' inverted pyramid' is kept intentionally in this framework to set up the most vital information (or what might even be considered the summary) at first. The framework is called a river 'psyche' pyramid because it deals with the soul or spirit of a river as 'psyche' in standard terms means the "deepest feelings and attitudes". To study river behaviour, 'psyche' is the best fit name given to the framework. The best experience to understand the actions based on the traits of a river is best described through the three steps in the inverted pyramidical diagram.

a. **Base (Environment)**: The pyramidical base defines how a river would develop and reflect its known or unknown traits determined by the *environment* in which it thrives. Behavioural psychology is a proven theory that a child personifies the traits that they learn from their specific household environment. Childhood learning, both physical and household, impacts

that child's behaviour as a man/woman they grew up to. Similarly, the arid environment of the Thar desert is entirely different from that of a tropical/glacial setup. The uniqueness of each environment makes the rivers develop unique traits (like a tropical river is characterized by profound channel depths compared to their channel widths in its mid-stage of evolution, while a dry river has a shallow channel depth and a broader channel width) and respond uniquely based on their character traits (for instance, in a tropical river, extreme rainfall will gradually increase the river water level and then will lead to gradual flooding, while in a dry river, extreme precipitation events will add on a sudden high amount of water in the shallow channel which is incapable of withholding a large amount of water incoming within a short period of time leading to flash floods).

b. **Mid (Character Building)**: Along with the environment, the middle part of the river 'psyche' diagram incorporates *character* building. This includes developing the river character based on the operative environmental forcing both in-situ and ex-situ. For instance, the factors that lead to the development of ephemeral streamflow in the dryland Luni river. The only source of river water is the rain flowing down the Aravalli range, and its tributary streams also have the same source. The river flow is zero to almost nil along the entire year, with the highest annual zero flow days compared to any other tropical or sub-arid rivers in the plateau region of India. Due to less water, river-based erosional forces like lateral downcutting are almost negligible. The river bed and banks' sandy nature tend to splay and out-migrate from the original channel, resulting in channel depth < channel width. The climatic setup includes temperature, rainfall intensity, wind speed, underlying geology, lineaments, geomorphological attributes, and their continuous interactions with anthropogenic features like population density, transport networks, etc. help a river basin develop its environment-oriented character like humans.

c. **Apex (Behaviour)**: The resultant behaviour or the manifestation that we see on the earth's surface is finally determined based on the previous two steps of the river 'psyche'. The 'psyche' of the river develops from the environment, a critical discussing element to understand its behaviour. The sensitivity is also much discerned once the character-building factors are known and enlisted. This conceptual framework is a concise way to decipher the reasons for a river's behavioural actions in a specific environmental or climatic setup. The differences found in the various climatic setup brings in changes in the river sediments, ecological composition and hydrological regimes. Studying a river and figuring out a complete layout of the complex internal and external processes entrust the researcher to

take forward the sensitivity analysis and a significant display of characteristic traits of each river in their climatic setup.

1.8 Summary

The chapter presents engaging details of various kinds of literature reviewed to understand the development of the concepts of river 'behaviour' and 'sensitivity'. Genuine and profound impacts of literature have been systematically surveyed and tabulated in various tables to understand the developing trend of literature in the past fourty years since the advent of the concept of 'sensitivity' by Brunsden and Thornes (1979). The keywords used in the different research articles were studied and analysed to develop significant research gaps either in the global or Indian context of studying river behaviour and sensitivity in dryland regions. Luni river, in this case, has been a unique selection and perfectly matches the conditions to study such exciting themes under the pretext of river behaviour and its sensitivity. The identification of research gaps was followed by explaining the rationale of the study. This was next converted into meaningful research questions trying to address the unanswered. The five primary objectives of the research were framed and consolidated together in the context of the research questions. The requisite secondary research datasets were tabulated to understand the study's various requirements, keeping in mind the research objectives. The research methodology is given in a nutshell depending on the fulfilment of each objective. The chapter ends with two research frameworks – the 'river behaviour and impact cycle' and the river 'psyche' pyramid. This fulfils the first objective of the research, i.e., to formulate a structured framework to study the river behaviour and the sensitivity using a methodological toolkit. The analysis factors can be classified and well fitted to discern the conceptual understanding of the objective study. Such a formulation is a new finding in fluvial science, which is entirely based on the author's realisation of the topic and after going through several pieces of literature. The author's enrichment and methodological understanding through the quantification of qualitative works of literature have resulted in developing two such impactful research frames that can have a universal application. It can also be used to decipher the river behaviour in any part of the globe within any climatic setup.

CHAPTER – 2
THE STUDY AREA

2.1 Introduction

The nature of physical and human-based factors operating within the Luni river basin, ranging from its basic location, elevation, climate, soil, croplands, pasturelands, land use, population, and transport network are studied in this chapter. The raster and vector layer-based maps define each of the parameters as discussed vividly under each sub-heading of this chapter and look to substantiate the need for sensitivity analysis of the Luni river basin in the preceding chapters. This chapter presents a prelude for discerning the facts of Luni's fluvial behaviour.

2.2 Objective

This chapter deals with the second objective of the research, which focuses on exploring all the generic natural and anthropogenic facts and figures of the Luni river basin.

2.3 Methodology

The secondary raster and spatial datasets were procured from different sources and used to shape the maps for this chapter and analyze them further to fulfil the objectivity of this research (Table 2.1). The procedure includes geoprocessing and analyzing the various secondary datasets in the GIS environment (ArcGIS v.10.3, QGIS v.3.14 and SAGA GIS v.2.3.2). The location map includes the delineated Luni river basin and the main Luni river channel from the SoI topographical maps and the latest base map imagery available in the ArcGIS environment. The contour map for the entire Luni river basin was generated from the SRTM DEM 1-arc second with a contour interval (CI) of 75 m. The administrative state, district, CD blocks, and village boundaries were obtained per the Census of India, 2011 records and clipped for the entire study river basin. The various types of raster and spatial layers of different scales obtained from the sources as enlisted in Table 2.1, shows the individual thematic parameters for the Luni river basin like climate (rainfall, temperature, cv of rainfall, wind speed, wind power density); bioclimatic variables (PET and AI), soil conditions (soil type, depth, texture and carbon density); cropland and pastureland distribution; vegetation condition; anthropogenic factors (population density, settlement extent, transport networks). Each layer was either obtained as a global or national level raster or spatial dataset and was clipped only for the study area boundary for further analysis. This chapter includes all the possible natural and human-based generic facts about the Luni drainage basin.

Table 2.1: List of Datasets used for analysis in chapter 2.

Parameters	Data Type	Data Source	Spatial Resolution	Period
Elevation & Drainage	Raster Grid	SRTM DEM (USGS), version 3.0	1 arc-second (30 m)	September, 2014
Luni River Channel	Digitized	SoI Topographical Sheets	1: 50,000	2006
Soil Distribution	Polygon Coverage	NAI, WIP – 200, NATMO, DST, GoI	1:2,000,000	1981
Land Capability		NAI, WIP - 221, NATMO, DST, GoI		
Temperature, CV of rainfall, Diurnal range of temperature, Solar radiation & Water vapour pressure	Raster Grid	WorldClim v.2.1	2.5 min. x 2.5 min.	1970-2000
PET & AI		CGIAR-CSI	30-arc seconds	
Rainfall		CHIRPS v. 2.0	0.05 x 0.05 degree	1981-2019
Wind Speed (10 m & 50 m)		Global Wind Atlas (GWA) 3.0	10-arc seconds (300 m)	2019
Wind Power Density				
Soil Texture, Depth & Carbon Density	Raster Grid	NISCES, Group: Terrestrial Sciences, SLARD, NRSC, ISRO	5 km x 5 km	February 2016
Land Degradation		WMS Layer, NRSC, ISRO	1:50,000	2015-16
Wasteland				
Cropland		SEDAC, NASA	~10 km	2000
Pastureland				
LULC		Global Landcover, ESA	100 m	2009 & 2019
VCI		Copernicus Global Land Service, ESA	1 km x 1 km	May & October, 2019
Population Density		SEDAC, NASA	30-arc seconds	2015
Population per Pixel and Settlement Extent		WorldPop, Univ. of Southampton, U.K.	100 m	2020
Transport Networks (Road & Railways)	Spatial Grid	Open Street Map	Extracted using Luni's watershed polygon	2020
Settlements				
Village/Block/District/State Boundaries		Census of India, 2011		2011

Source: Compiled by the researcher.

2.4 The Luni River Basin

The Luni river and its major tributaries constitute the prime drainage system in the Indian part of the Thar desert, originating in the pre-Cambrian Naga hills along the western slopes of the Aravalli range near Puskar valley of Ajmer district, Rajasthan. The two initial order headwater streams, one originating from the lower Aravalli foothills in Ajmer known as Sagarmati river confluences just north of the Govindgarh village with the Saraswati river descending from the dissected hills in Nagaur district to become the Luni river evidently observed in the topographical map 45 J/7. It flows through northwards and north-westwards over a short distance before turning south-westward to Balotra from where it takes a southerly turn and eventually discharges into the inland drainage system of the Great Rann of Kutch, forming a floodout, which finally meets the Arabian Sea (Bajpai, 2004 and Jain et al., 2005). The seasonal river traverses a distance of about 500 km, leaving Rajasthan at Chitalwana village in Jalore before it disappears in the Rann of Kutch in Gujarat. The river Luni has a monsoonal discharge regime season and remains dry during the rest of the year. The study river basin is bounded by the ranges of Aravalli and extended Gujarat plains on the east, followed by the Great Thar on the north and west and the marshy land of Kutch in the south. The general layout of the Luni Basin is shown in Fig. 2.1. The river water of Luni is fresh and potable up to Balotra but soon the water becomes overwhelmingly saline further downstream as it meets up in the Rann. The main tributaries of Luni on the left are Sukri, Mithri, Bandi, Khari, Jawai, Guhiya, Sagi while Jojari river is the only one joining it on the right side. The total area of the Luni river basin is 39,278.80 km^2 including ten districts of Rajasthan namely – Ajmer, Barmer, Bhilwara, Jalor, Jodhpur, Nagaur, Pali, Rajsamand, Sirohi and Udaipur along with the fringing areas of Banas Kantha and Kachchh districts of Gujarat (Table – 2.2).

There are 12 major sub-basins in Luni Basin namely Bandi (770.11 km^2), Bandi (Hemawas) 1,649.30 km^2, Guhiya 3,854.20 km^2, Jawai 2,640.50 km^2, Jojri 7,046.00 km^2, Khari 2,638.30 km^2, Khari (Hemawas) 1,098.60 km^2, Mithari 1,702.70 km^2, Sagi 1,218.70 km^2, Sukri (Nadi) 3,166.60 km^2, Sukri Sayala (river) 995.70 km^2. Out of these 12 sub-basins, seven major sub-basins are used for analysis in the present study, each with > 1,000 km^2 basin area (Fig. 4.8).

During the dry summer and winter season, discharge is minimal to absent (Kar, 1994; Bajpai, 2004). Aeolian sand accumulates within the main channel, only to be eroded by floods during the subsequent southwest monsoon. Accordingly, the Luni displays characteristics typical of many ephemeral streams, especially the downstream concentration of sediment load resulting

from transmission losses (Sharma et al., 1984), and the drainage network can appear locally disconnected owing to aeolian obstructions.
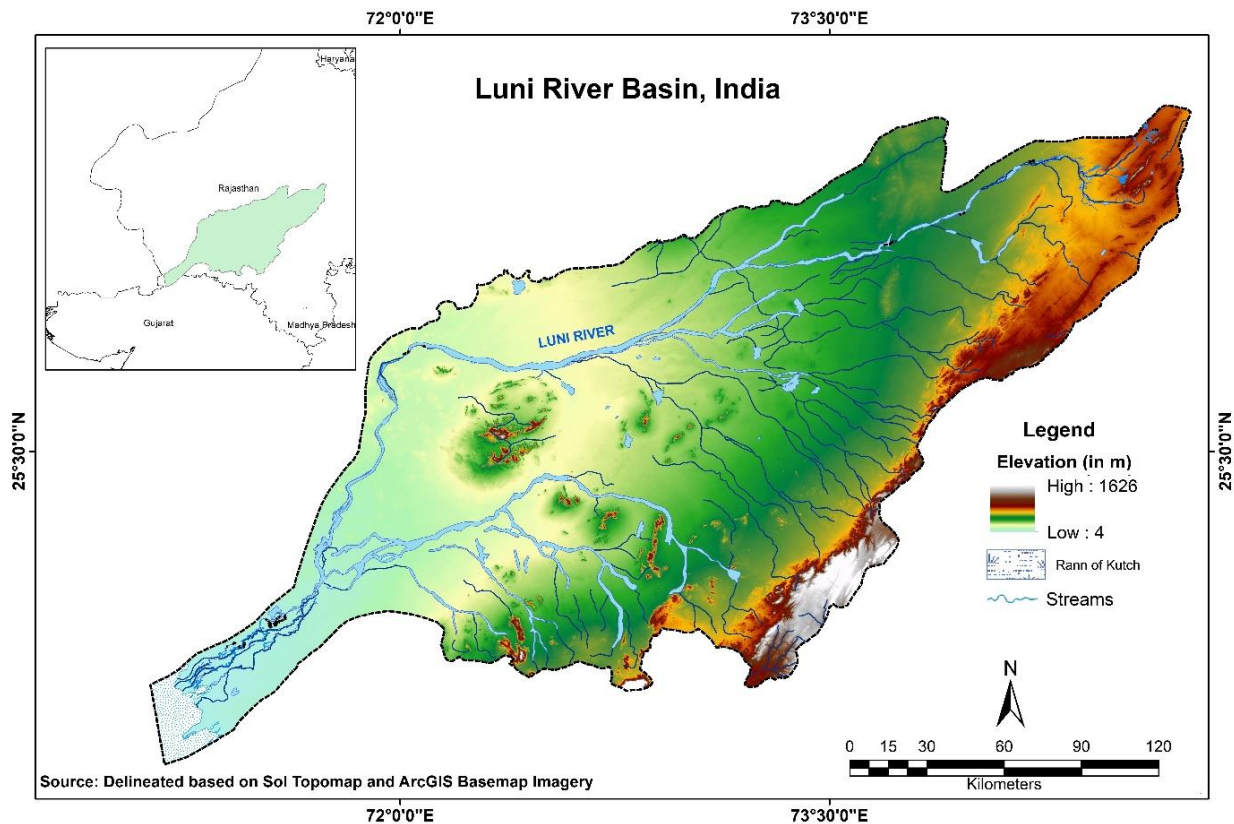
Fig. 2.1: Study Area and Location of Luni River Basin, India. Source: Prepared by the researcher based on SoI Topomaps and ArcGIS base map imagery.

2.5 Topography and Elevation Distribution

The basin's topography varies from plain areas occupying the western part characterized by flat, sandy terrain to mountainous regions of the east, made up of various igneous rocks, including some Limestone outcrops. The contour map of the Luni basin (Fig. 2.2) explains the presence of high elevated Aravalli in the east of the river basin and a circular outcrop adjacent to the western end of the basin or on the eastern bank of the Luni river. The drainage lines cross the contours helping to carve a plain land with remnants of residual hills and monadnocks throughout the basin. The contour interval for the basin is placed at 75 m so that the higher elevation cluster could be quickly identified from those sparsely placed contours representing the plane lands. Table 2.1 shows the elevation summary of the basin with minimum elevation contour at Chotan block in Barmer district with an elevation of 4 m amsl. The highest peak is 1626 m amsl located at the Abu roadblock in the Sirohi district of Rajasthan. The mean height and the relative relief for the entire Luni basin are 230 m and 1622 m amsl, respectively.
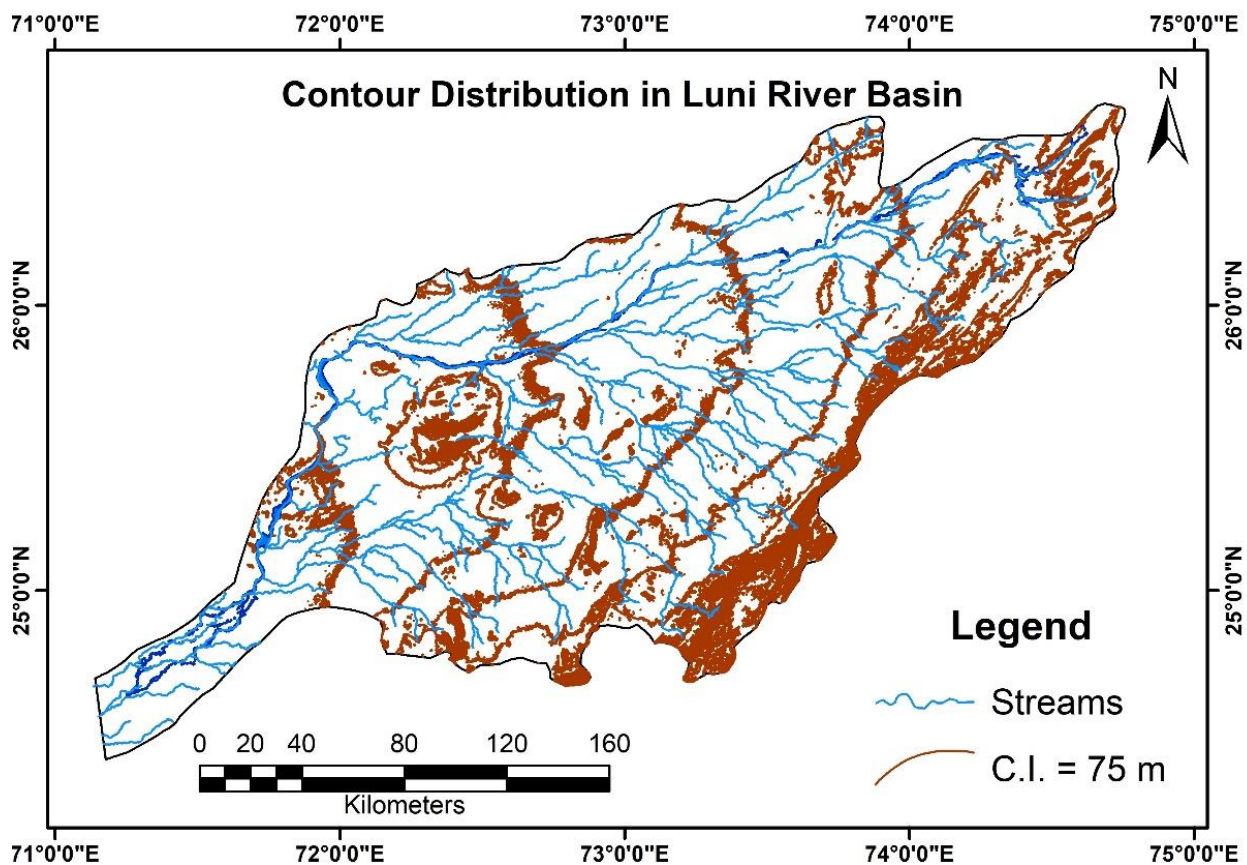
Fig. 2.2: Distribution of contours across the Luni river basin. Source: Prepared by the researcher based on the USGS SRTM DEM 1-arc second.

Table 2.2: Elevation Summary of Luni river basin

Elevation Type	Elevation (m amsl)	CD Block	District	Location
Minimum	4	Chotan	Barmer	71°8'23.011"E 24°41'3.176"N
Maximum	1626	Abu Road	Sirohi	72°48'26.363 "E 24°40'50.946"N
Mean	230	-	-	-
Relative Relief	1622	-	-	-

Source: Computed by the researcher.

2.6 Administrative Boundaries

The distribution of the administrative boundaries within the Luni basin starts from the states, districts, CD Blocks and ends up with the villages. The basin spreads across a massive expanse with ~40,000 km^2 area covering two western states of India– Rajasthan from where Luni originates and Gujarat, where the river ends at the Rann of Kachchh (Fig. 2.3a). Ten districts from Rajasthan and two districts of Gujarat cover up the entire expanse of the Luni basin as

enlisted in Table – 2.2 and shown in Fig. 2.3b. Under the districts of Rajasthan, there are 38 Community Development (CD) blocks or tehsils or sub-districts and three CD blocks under the districts of Gujarat. These CD blocks are majorly known for drought proneness, for which government programmes for watershed development and management is carried out in these districts or blocks for community development and effective dealing of droughts through projects like Drought Prone Area Programme (DPAP), *Neeranchal* and *Haryali* sponsored by the State and/or Central Government. The enormous scale political boundary is the villages which are over 3112 from Rajasthan and 27 villages from Gujarat that covers the entire Luni basin and hence have a direct or indirect link with the watershed. Each hamlet or more than two villages often form micro-watersheds which are essential to study and explore better soil conservation, watershed management, irrigation development, groundwater recharge and agricultural enhancement practices. Learning a river basin from the perspective of political or administrative boundaries enhances the understanding of underdeveloped areas. Hence, it helps to motivate the development projects to get channelized to such areas where there is utter need of overall infrastructural and socio-economic upliftment and sustainable conservation of available natural resources.

Table 2.3: Summary of Administrative boundaries within the Luni river basin

States	Rajasthan	Gujarat
Districts	Ajmer, Barmer, Bhilwara, Jalor, Jodhpur, Nagaur, Pali, Rajsamand, Sirohi & Udaipur (10)	Banas Kantha & Kachchh (2)
CD Blocks	38	3
Villages	3112	27

Source: Census of India, 2011

Fig. 2.3: Administrative Boundaries within Luni river basin; a – States, b - Districts, c – CD Blocks and d – Village. Source: Prepared by the researcher based on the administrative boundaries of Census of India, 2011.

Fig. 2.4: Climatic Parameters in Luni river basin; a –Annual Average Precipitation, b – CV of Rainfall, c –Average Annual Temperature and d – Mean Diurnal Range of Temperature. Source: Prepared by the researcher based on CHIRPS v.2.0, 1981-2019 (Rainfall) and WorldClim v.2.1, 1970-2000.

2.7 Climatic Parameters

The climate of an aeolian environment typically characterized by scanty precipitation and extreme daytime and nighttime temperatures. Summer months are dry with hot winds called *loo* blowing over the entire Luni basin. The mean temperature across the basin found to be 33.51˚C with the average precipitation as 388.20 mm, while in monsoon months, the mean rainfall stands out to be 358.10 mm only (Table – 2.3). The maximum rainy days last for about only one month and eight days, i.e., 38 days/year, indicating the region's arid nature. The only precipitation comes from the south-west monsoon winds of the Arabian Sea branch as the rain-bearing clouds pass the Aravalli ranges and some from local atmospheric phenomenon during the summer or winter months. The other climate parameters like wind speed, sunshine hours, relative humidity, and annual evaporation are also included under the climate statistics to have a wholesome view of the various climate forcing operating over the study river basin.

Table 2.4: Climate Statistics for Luni river basin

Climate Parameter	Minimum	Maximum	Mean	Standard Deviation	Coefficient of Variation
Mean Maximum Temperature (˚C)	26.83	35.00	33.51	0.81	0.02
Highest Maximum Temperature (˚C)	37.20	46.70	44.84	1.03	0.02
Mean Minimum Temperature (˚C)	12.81	20.90	19.22	0.90	0.05
Lowest Minimum Temperature (˚C)	-2.05	6.00	3.48	0.99	0.28
Annual Precipitation (mm)	221.50	1048.10	388.20	104.20	0.27
Monsoon Months Precipitation (mm)	191.60	1007.70	358.10	99.80	0.28
Rainy Days (days/yr.)	12	38	19	3.90	0.20
Wind Speed (km./hr.)	1.90	7.16	4.38	0.96	0.22
Sunshine hours (hr./day)	7.98	8.61	8.39	0.09	0.01
Relative Humidity (%)	43.50	60.54	49.19	3.23	0.07
Annual Evaporation (cm)	141.10	263.58	216.23	24.46	0.11

Source: IMD monthly dataset (1990-2009); Rainfall statistics based on IMD, RD and WRD dataset (1957-2010)

The annual average precipitation (Fig. 2.4a) depicts the maximum amount of precipitation in form rainfall is visualized in the south-eastern fringe of the river basin with a range of 934.05 – 1491.35 mm as extracted from the CHIRPS grided dataset over a time period of 1981-2019. The most important part is the western part of the river basin where the rainfall is least as the average annual range is found to be 354.43-452.52 mm only. The eastern part of the river basin receives the highest amount of rainfall from the south-west monsoon winds of the Arabian Sea

branch and hence from the map it is evidently clear that the average annual precipitation diminishes towards the west, confirming the impact of arid Thar desert.

The percentage of annual coefficient of variation (CV) of rainfall (Fig. 2.4b) is the most important characteristics of desert rainfall with high annual variability. The average annual rainfall levels are very low with sudden high intensity individual storms generating peak runoff flows generating flash flood like events but the impression of desert rainfall and such local storms should not give any wrong impression from its singular event of ferocity (Goudie, 1987). The highest precipitation area is found in the south-eastern part of the basin corroborates with the highest CV% of rainfall amounting in between 159-172%, followed by the lower part of the basin demarcated with yellow shade exhibits a lower CV% of rainfall from the previous higher range amounting in between 154-159%. Interestingly, the lowest CV% of rainfall is seen along the eastern leeward sides of Aravalli and the western part of the river basin, both receiving the least amount of rainfall for their geographical orientation or location.

The annual average temperature (Fig. 2.4c) of the study river basin lies in between 21.48 – 27.78˚C as obtained from the climate gridded dataset from WorldClim v.2.1. This range is typical for the arid regions of Rajasthan and Gujarat as the river basin is situated over the Tropic of Cancer (23.5 ˚N). The variability of the annual average temperature is almost evenly distributed with a minor variation of about 1-2 ˚C. The maximum range of annual average temperature is observed over the western and central part of the river basin indicating the increasing aridity while the leeward slopes of Aravalli experience the minimal range lying in between 21.48-24.16 ˚C.

The mean diurnal range of temperature (Fig. 2.4d) records the difference in between mean maximum and mean minimum temperature for range of years. The eastern fringe records the least diurnal range while the western part of the river basin where the river flows experience the highest diurnal range indicating the extremities brought forth by the arid conditions prevailing in this adjoining region of the Thar desert. The major diurnal range is observed along the south-western tract of the river basin where Luni takes a sharp western turn immediately after Balotra till it continues to bifurcate and anabranch in the floodout region of Rann of Kutch.

The average annual wind speed (Fig. 2.5a) as obtained from extracting the raster dataset for the study basin from the Global Wind Atlas 3.0, 2019 for the wind speed observed at two levels 10 and 50 meters above the ground level with a spatial resolution of 10-arc second is an

exemplary example among the climatic parameters which needs a special understanding for dryland rivers as wind speed plays a crucial role in shaping and altering the riverscape in the arid regions of Thar. The combination of surface level wind speed at 10 and 50 meters can give a wholesome overview of how sands are entrained and hence the interaction between the dynamic agencies of wind and water could be better explained in a dryland river basin like that of the Luni. The average annual wind speed is highest over the maximum elevation zones, i.e., over the Aravalli and the residual hillocks adjoining the Luni near Balotra ranging in between 6.57-9.9 ms^{-1}. The entire stretch of Luni's main channel falls under the range of a very nominal wind speed 4.93-5.27 ms^{-1}, while the adjacent leeward slopes of the Aravalli experience the least wind speed of 3.1-4.92 ms^{-1}. The wind speed in the Rann of Kutch where the Luni forms inland delta experiences moderate to high wind speed with the influence of its massive expanse and adjacency to the Thar dessert from the side of Nagar Parkar in Pakistan.

The mean annual wind power density (Fig. 2.5b) corroborates with the former map of average wind speed. Wind power density is a parameter to understand the potentiality of the wind speed either to generate wind-based electricity (Saxena and Rao, 2016), shift the sand dunes (Yizhaq, Ashkenazy and Tsoar, 2009; Goudie, 2013), wind erosion (Goudie, 2013), generate dust storms (Goudie and Middleton, 2006; Goudie, 2013) or entrain the sand grains to block the aeolian river channels with an indication of complex interaction (Bullard and Livingstone, 2002; Bullard *et al.*, 2003; Belnap, Munson and Field, 2011). Wind Power Density is calculated as – (1/2 x air density of the site x wind speed cubed). The spatial variability of the wind power exists across the dryland river basin of Luni because of topographic control (Goudie, 2013). Here the maximum mean annual wind power density is recorded in the peak region of Aravalli and the residual hills near the Luni river with a range of 409.73-1018.42 Wm^{-2}. The downslopes of leeward side of the Aravalli records high wind power density when compared with the pediment-pediplain zone build up by the tributaries of the Luni. The least wind power density is observed in the plains which is dominated by the rivers, showing a range in between 42.2-145.56 Wm^{-2}. Therefore, the wind power density is overpowering in the zones of highest elevation and progressively decreases in the plains, but has a short-range high variability over the zone of Rann of Kutch due to its massive expanse.

The average annual solar radiation (Fig. 2.5c) records the highest exposure along the south-western and southern part of the Luni river basin with a range of over 20,351.42-20,776.92kJm^{-2}day^{-1}, while it continuously decreases towards the northern part of the basin with the lowest value of 19,515.25 kJm^{-2}day^{-1}. A variable range of low, moderate and high solar radiation is

recorded along the eastern part of the river basin, including the Aravalli. Hence, the Luni river is observed under the zone of highest average annual solar radiation, which also contributes to the drying up of the river bed as the river approaches the southern part of its watershed.

The average annual vapour pressure (Fig. 2.5d) explains the amount of water present in the air directly proportional to the water vapour's partial pressure in the air. So, a direct measure of the water content present in the air. The map shows that the highest amount of water vapour pressure is found in the river basin's southern part, ranging between 1.79-1.89 kPa. As the southern part is both geomorphologically and anthropogenically crucial with the highest amount of agriculture and tributary confluence and distributaries of the Luni river. The amount of water vapour pressure progressively decreases towards the north with the lowest over the Pushkar area from where the Luni originates and along the Aravalli with a range of 1.28-1.53 kPa. The consequent zones of low, moderate and high progress towards the south with a small exception for the residual hills on the left bank of the Luni near Balotra.

Fig. 2.5: Climatic Parameters – II in Luni river basin; a –Average Annual Wind Speed, b –mean annual Wind Power Density, c –Average Annual Solar Radiation and d – Average Annual Water Vapour Pressure. Source: Prepared by the researcher from the raster layers of GWA v.3, 2019 and WorldClim v.2.1, 2000.
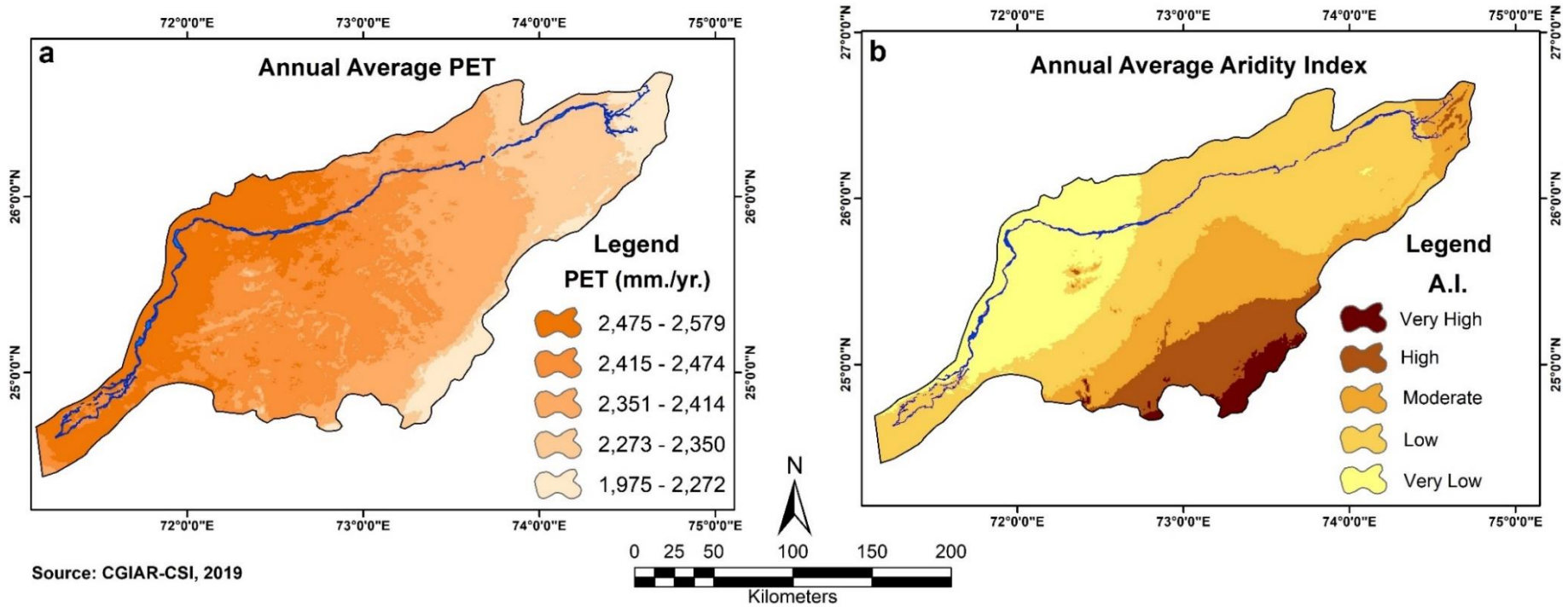
Fig. 2.6: Bioclimatic variables – a. Annual Average Potential Evapotranspiration (PET) & b. Annual Average Aridity Index in the Luni river basin. Source: Prepared by the researcher from the raster layers of PET and AI, CGIAR-CSI, 2018.

2.8 Bioclimatic Parameters

The bioclimatic parameters in the Luni basin are explained through the annual average potential evapotranspiration (PET) (Fig. 2.6a) and annual average aridity index (AI) (Fig. 2.6b). Potential evapotranspiration includes the summation of the potential of evaporation from soils and transpiration by plants. It only occurs at the likely rate when the water available for this process is non-limiting. The evaporation rate depends on various prevailing climatic conditions, specifically the sun's radiative energy, the vapour deficit of the air, temperature and wind. PET is essential to analyze the sensitivity on climate, which would, in turn, redirect us to understand any climate change occurrence with various simulation studies (McKenney and Rosenberg, 1993). The profound implications on hydrologic processes and the performance of crop induced by PET (Chattopadhyay and Hulme, 1997) indicate the importance of including such a bioclimatic parameter. River basins in drylands can be sensitive enough to the changing PET, which explains the maximum range is observed in between 2,475-2,579 mmyr^{-1} along the western, south-western and southern edges of the basin through which the main channel of Luni drains the region. The PET tends to lower progressively towards the north and eastern borders of the river basin adjoining Aravalli with a range of 1,975-2,272 mmyr^{-1}.

The annual average aridity index (AI) is an important predictor for understanding precipitation availability over atmospheric water demand (UNEP, 1997). The generalized function of precipitation, temperature, and/or PET is known as AI, which is calculated as:

$$AI = MAP / MAE \qquad \text{(Eq. 1)}$$

where, MAP = Mean Annual Precipitation and MAE = Mean Annual PET. Projected aridity studies, especially for dryland rivers, are vital to understand the climatic forcing on such arid rivers and how alterations occur geomorphologically (Larkin *et al.*, 2020). The higher AI values show a humid region, while the lower AI values indicate an arid region (UNEP, 1997). So, the annual average AI values indicate a humid region with maximum AI scores in the south-eastern fringes along with the Aravalli where it records the maximum AI values indicating a humid zone as it receives comparatively highest moisture from the south-west monsoon winds of Arabian Sea branch. The AI value decreases distinctively towards west from very high to very low. The Luni river flows through from moderate to very low AI zone. Humidity is hence understood to have been diminishing towards the west as it nears to the Thar desert.

2.9 Vegetation Condition

Vegetation condition in a dryland river basin is a major factor of the river channel environment though the continuous interactions in between the fluvial processes and vegetation in arid river channels have not been studied with such priority (Sandercock et al., 2007). A dryland river is characteristically different compared to the alluvial or humid environment rivers with a degree of abruptness in morphology and riparian vegetation, sensitive to climate change with a considerable variation in ecology and local climate complexities followed by alterations in sedimentation rates and resistance to erosion. Ecosystem and human society in arid regions has a symbiotic relationship in context of natural vegetation condition prevailing in the dryland riverscape (Mo *et al.*, 2019). So, inorder to study and identify the temporal changes of vegetation over a spatial scale, the use of remote sensing and such other information technology facilitates the large-scale ecological research (Xing et al. 2009; Parker et al. 2018).

In the following figure 2.7 (a) and (b), the general vegetation condition present across the Luni river basin is being portrayed for the two seasons, i.e., Pre-Monsoon (May, 2019) and Post-Monsoon (October, 2019). The pre and post monsoon scenarios, clearly indicate the typical monsoon type of climate with alterations of wet and dry seasons. During the pre-monsoon period it is observed that, a moderate to very low amount of vegetation is spatially distributed during the summer months with an exception in the central patches of the river basin portrayed with yellow. After the monsoon retreats, the amount of vegetation distinctively increases across the entire Luni river basin as seen in yellow, while the chronic drylands adjoining the arid Thar region in the west and some of the degraded or uncultivable wastelands are seen in patches of blue having least vegetation. But, here the main form of vegetation condition is being contributed by the extensive agricultural lands as this region is dominated by cultivation which is later discussed in details with the land use and landcover map of the Luni river basin (Fig. 2.11). Natural vegetation in form of forests is found only in fewer part of the river basin especially adjoining the leeward slopes of Aravalli and down in the Rann where the Luni finally drains out. Thus, the eastern part of the Luni river represents a better vegetation condition compared to its western bank which is covered with extensive drylands, sand dunes and the Thar landscape.

Vegetation Condition Index of Luni River Basin
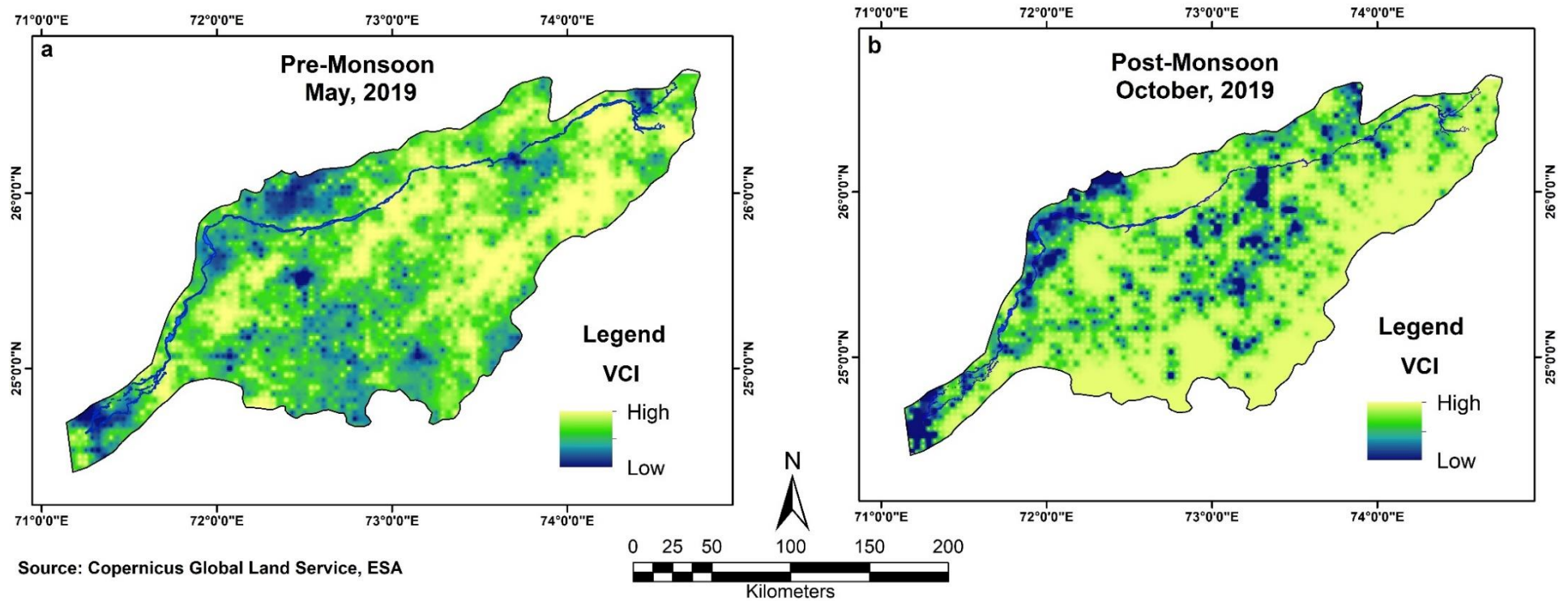
Fig. 2.7: Variations observed in vegetation condition through VCI during (a) pre (May, 2019) and (b) post (October, 2019) monsoon seasons within the Luni river basin. Source: Prepared by the researcher from the raster layer of VCI, Copernicus Global Land Service, ESA.

2.10 Soil Condition

Soil or pedogenic studies are very relevant to understand the dominant soil groups, their formation processes, characteristics and erodibility rates found in a river basin. The soil formation processes depend on the external climatic and natural forcing responsible for curving out the specific landscape depending on the parent rock material. Information related to the textures of soil, soil depths and carbon densities enrich the understanding of soil condition and its erodibility for a river basin study. Geomorphic assessment could be well accomplished with undergoing an entire soil profile study, while modelling soil loss equations can give better results to assess its prevailing soil conditions, hence helping to zone out the erosion prone regions which will help to take up better conservation practices in order to minimize the soil loss.

Table 2.5: Areal distribution of Soil cover found within the Luni river basin

Sl. No.	Soil Type	Area	
		km²	%
1	Red & Yellow Soil	2841.36	7.23
2	Calcareous Sierozemic Soil	3095.23	7.88
3	Red Gravelly Soil	4959.69	12.62
4	Red Sandy Soil	1947.99	4.96
5	Grey Brown Soil	14879.64	37.87
6	Lithosolic Desert Soil	1685.87	4.29
7	Regosolic Desert Soil	6742.24	17.16
8	Shallow Black Soil	31.55	0.08
9	Saline and Saline Alkaline Soil	3095.23	7.88

Source: Computed by the researcher from vector layers of soil cover.

The pedogenesis of the study basin (Fig. 2.8) is explained by the presence of nine major soil groups also represented in Table 2.4 showing their individual areal coverage and percentage composition within the Luni river basin. The map clearly depicts the major dominance of grey brown soil (Calciorthrids) over the western and central part of the river basin with a coverage of 37.87%. Regosolic desert soil (Ustipsamments) constitutes the second major soil group constituting about 17.16%, found in the adjoining areas of grey brown soils. The third major soil group constitutes of red gravelly soil as derived from the regoliths of Aravalli hills contributing 12.62% of the entire major soil groups. The other three soil groups found mostly in few patches are calcareous sierozemic soil, saline and saline alkaline soil as well as red and yellow soil respectively with a contributing composition of greater than 7% (Table 2.4). Unlike the other river basins of northern India, alluvial content is least in the Luni river basin, hence

making it a unique one to have a secondary origin and derived grey brown soil and desert regosolic soil.
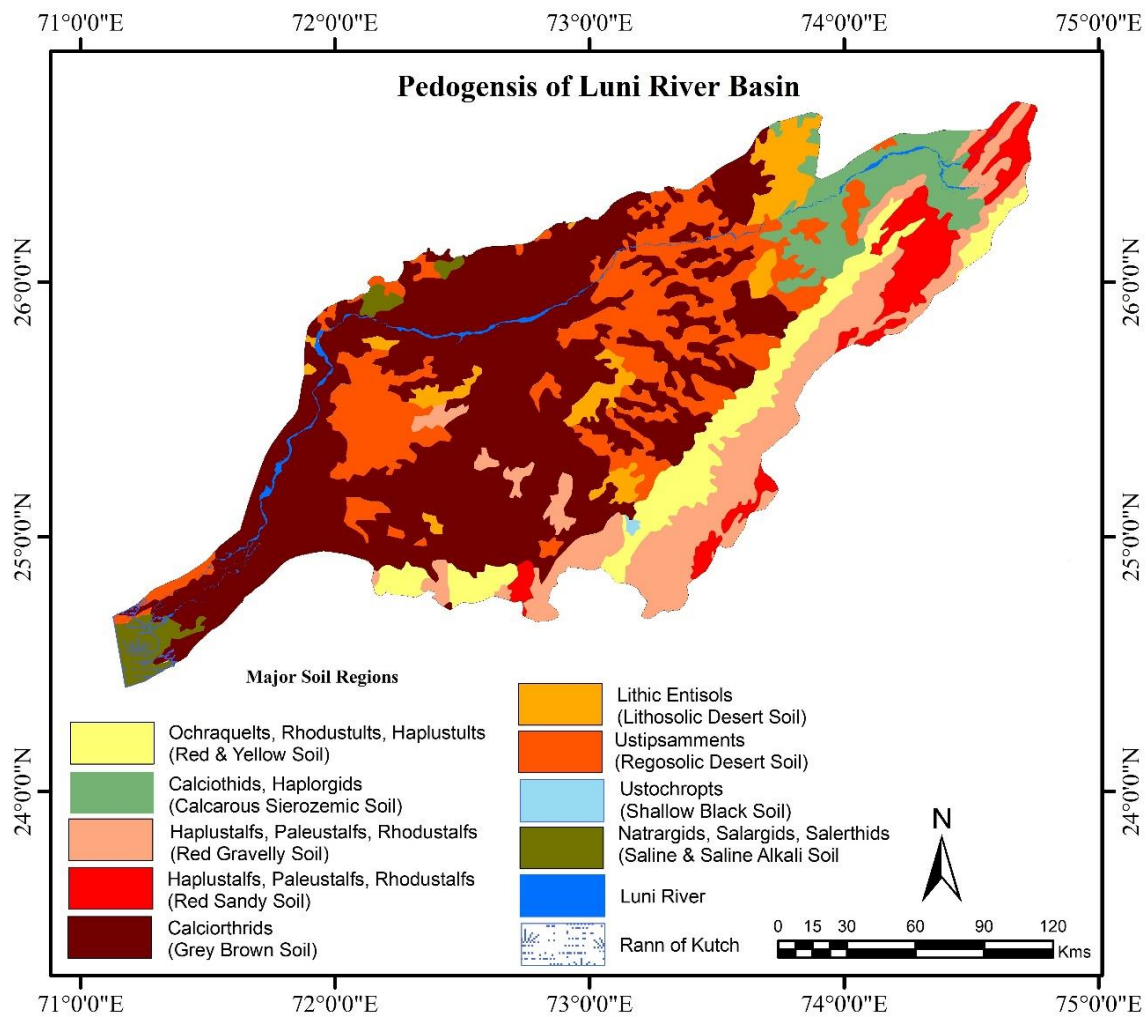
Figure 2.8: Major types of soil found across the Luni river basin. Source: Prepared by the researcher based on the NAI, WIP – 200, NATMO, GoI, 1981.

The major soil textures (Fig. 2.9 a and b) represent the two dominant soil textures across the river basin in form of loamy and sandy soil respectively. The soil texture is represented in binary form, that is, one for the areas having the specific soil texture and zero for those areas having no presence of that soil texture. Loamy soil texture (Fig. 2.9 a) is the most dominant form found across the entire central and the northern part of the river basin., with few patches towards the south as well. The sandy soil texture (Fig. 2.9 b) is found southern parts of the river basin especially after the Luni crosses Balotra, specifically on its left or eastern banks indicative of the sand dune trails in this region, while few patches are located in the central part of the river basin. The binary form of representation makes it easy to identify the distribution in the following maps.

53
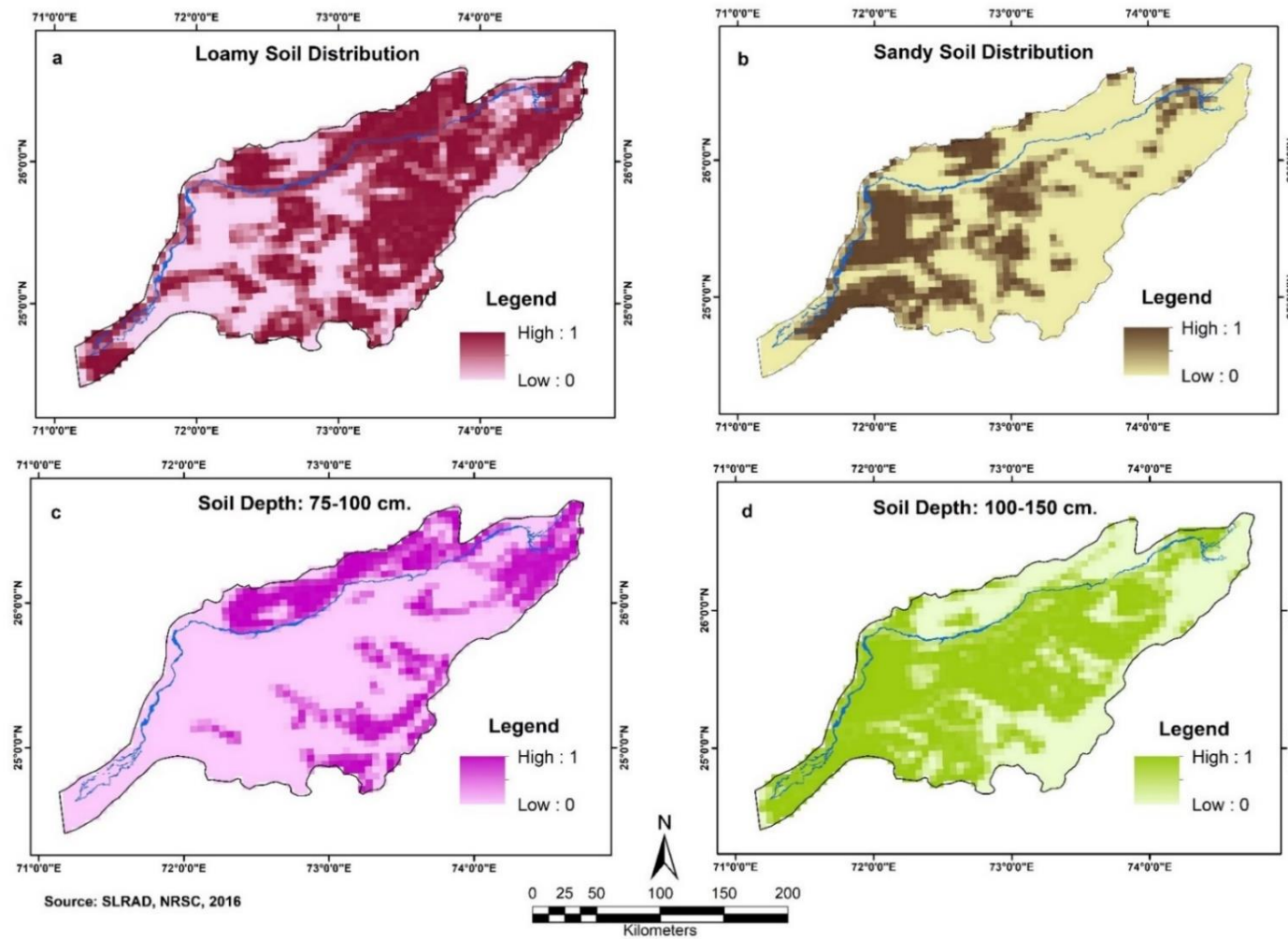
Fig. 2.9: Major Soil Textures (a. Loamy & b. Sandy) and Soil Depths (c. 75-100 cm & d. 100-150 cm) in the Luni river basin. Source: Prepared by the researcher based on the raster layers of SLRAD, NRSC, 2016.
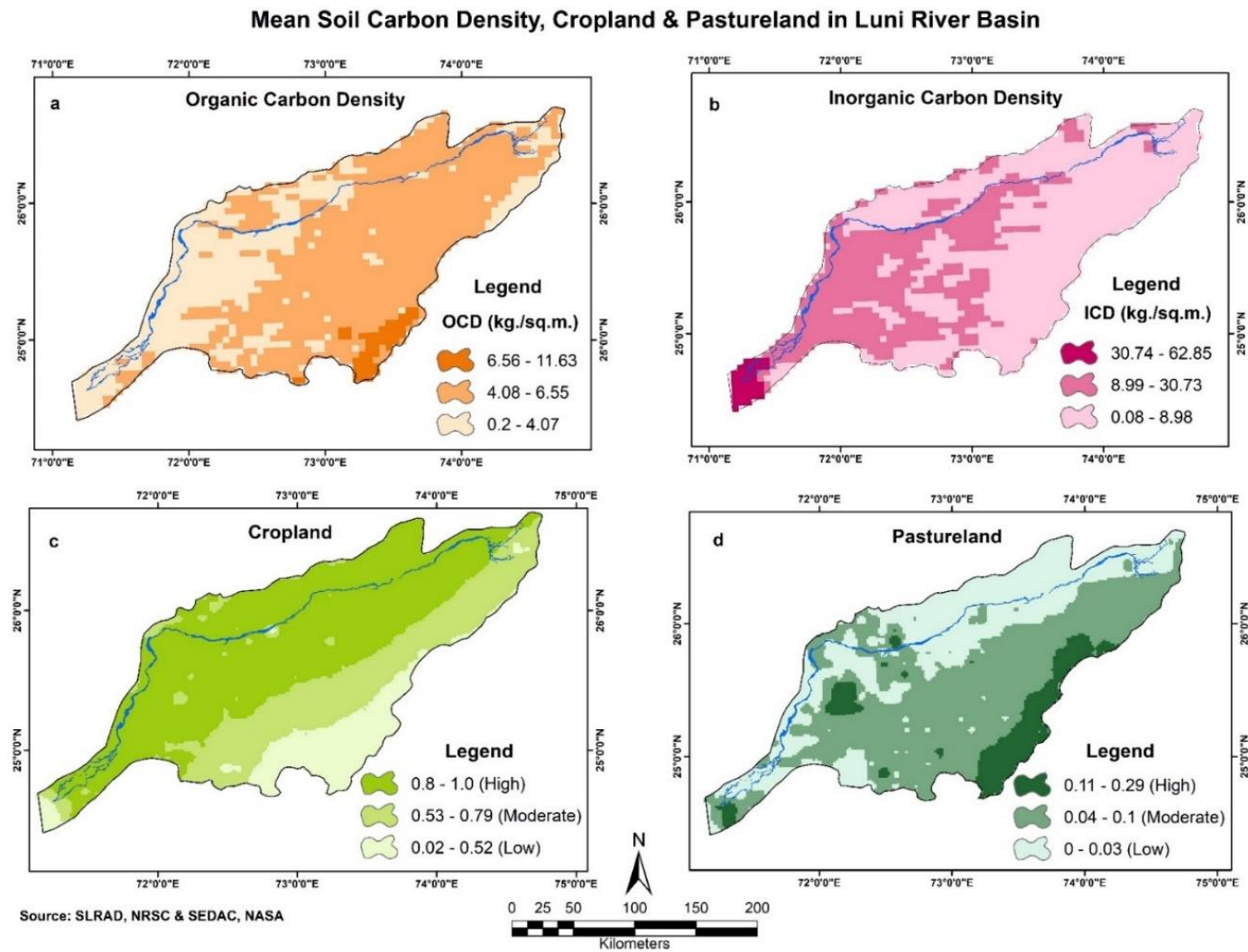
Fig. 2.10: Mean Soil Organic (a) and Inorganic (b) Carbon Density, Cropland (c) and Pastureland (d) in the Luni river basin. Source: Prepared by the researcher based on the raster layers of SLRAD, NRSC, 2016 and SEDAC, NASA, 2000.

The major soil depths range from 75 -100 cm (Fig. 2.9c) in the north western part of the Luni river basin, place of Luni's origin near Pushkar hills and also in the leeward slopes of Aravalli in the south-eastern part of the river basin. The dominant soil depth ranging from 100-150 cm as represented in Fig. 2.9 d explains the maximum coverage of soil depth in between 100-150 cm ranges in the central and southern part of the entire Luni watershed. The binary form of zero and one clearly helps to understand the spatial distribution of the soil depth across the entire watershed and hence is essential to comprehend the status of soil depth and its prevailing condition in the river basin.

Soil organic carbon is a quantifiable component of soil organic matter. Organic matter of soil is composed of 2–10% of most soil's mass and has a vital part in the physical, chemical and biological use of pastoral soils. Nutrient retention and turnover, soil structure, ability of moisture retention and availability, degradation of pollutants and carbon sequestration are some of the important components of soil organic matter. The organic carbon density represented in the map (Fig. 2.9a) shows that it is the major form of carbon density found within soils of the Luni river basin covering almost the entire central portion of the watershed. The organic carbon density of maximum in the south eastern part near to the Aravalli ranges represented in a darker shade of peach with a quantity of 6.56-11.63 $kg^{-1}m^{-2}$. The organic carbon density in the soil decreases towards the west as the maximum watershed's coverage of organic carbon density comes under 4.08-6.55 $kg^{-1}m^{-2}$, followed by the least presence of organic carbon density in the western and southern part of the watershed with 0.2-4.7 $kg^{-1}m^{-2}$.

The inorganic carbon density distribution of Luni river basin is shown in Fig. 2.9b, where the maximum inorganic carbon density ranging in between 30.74-62.85 $kg^{-1}m^{-2}$ is concentrated in the floodout region adjoining the Rann, followed by a quantity of 8.99-30.73 $kg^{-1}m^{-2}$ in the adjoining areas of the Luni floodout and in the entire eastern banks of Luni after the river crosses Balotra[1]. Sandy soil texture is found to have a correlational existence with higher inorganic carbon density and loamy soil corroborates well with organic carbon density in soil.

The cropland and pastureland distribution within the Luni river basin (Fig. 2.9 c and d) is meant for a better overview of the land use pattern as obtained from the georeferenced binary raster datasets of NASA. The entire Luni river falls under heavily cropped land and the distribution

---

[1] The eastern banks of the Luni river after Balotra and the floodout region located in the Jalore district of Rajasthan is marked with high intensive cropping associated with heavy use of fertilizers and better irrigation facilities has led to rise of inorganic carbon density compared to the eastern side of the river basin as can also be validated in Fig. 2.9 c with the cropland map of the Luni catchment.

of cropland shows a progressive decline of farmlands towards the east of the watershed especially the leeward slopes of Aravalli. A moderate amount of farming is found in the central axis of the watershed. The pastureland distribution perfectly corroborates the cropland map and depicts the maximum pastureland adjoining the eastern part of the watershed where the number of farmlands is the least. Pastureland is also found to exist in the areas near the floodout and also adjoining the residual hill situated on the eastern bank of Luni after Balotra, demarcated with dark green shades.

2.11 Land Resource Mapping

The land resource mapping for a river basin brings out the definite land capability which is vital to understand the type of available land within a river basin. Land capability is an indicative factor derived from the generic regional land status map of India giving us an idea regarding the land utility which can further be enhanced with explanation and mapping of land degradation, wasteland and landuse/landcover mapping. The land resource is a prime indicator of economic condition found within the river basin reflecting enough to superficially understand the social condition of people residing in the specific study area.

2.11.1 Land Capability Mapping

FAO (1983) elucidate land capability as the "quality" of land meant for producing commonly cultivated crops and pasture plants without falling over a long-time spell. Wells (2001) explained land capability as the "ability" of land to assist a certain type of use without bringing about any sort of permanent damage. The land capability classification is a blueprint for the assessment of soil inhibitions and land governance recommendations meant for a range of scales including state, catchment and the property planning level (Murphy et al., 2004 and Gad, 2015).

The land capability map of the Luni river basin (Fig. 2.10) is a basic indicator to understand the land utility status and its potentiality in terms of cultivation, wasteland, pastureland and other forms of using the available landscape except for the settlement areas which are nowadays prime essential information to understand the overview of the land competence of a designated area. Table 2.5 explains the land capability map with the figures of areal coverage in square kilometers and percentage coverage. The distribution of poor land stands out to be the highest among the land capability found along the north-western edges and central part of the river basin, constituting 28.93%, shown in sea green shade. The second group of land capability is marked as very good land, those can be primarily used for agriculture are found

along the western bank of Luni river and in few fragments within the basin, portrayed in meadow green shade, constitutes 22.63%, followed by moderately good land contributing 21.56%, shown in pink shade. Such land can be used for cultivation, grazing cattle as well as for some secondary industries. The areas adjoining the western slopes of Aravalli can only be suitably used for forestry and grazing of cattle mainly as here being classified based on its limitation severity.

Table 2.6: Areal distribution of categories in the Land capability of Luni river basin.

Sl. No.	Land Capability Categories	Area	
		Km.^{2}	%
1	Poor Land	11358.40	28.93
2	Very Good Land	8883.51	22.63
3	Moderately Good Land	8462.94	21.56
4	Land suitable for wildlife, Watershed Management etc	774.43	1.97
5	Land with severe Limitation suitable for forestry and grazing	4681.75	11.92
6	Land with very severe limitations suitable for forestry and grazing	5099.26	12.99

Source: Computed by the researcher from vector layers of land capability.
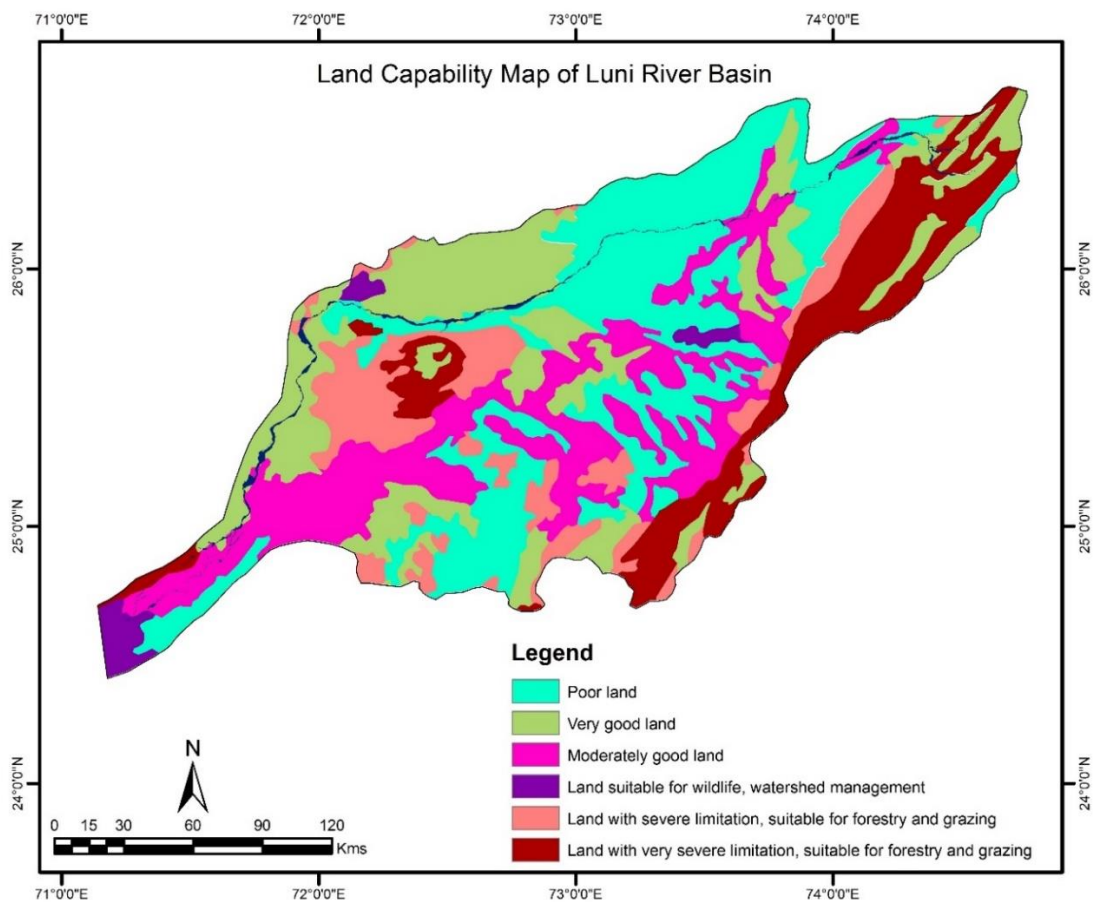
Fig. 2.11: Land capability map of Luni river basin. Source: Prepared by the researcher based on NAI, WIP – 200, NATMO, GoI, 1981.

2.11.2 Land Degradation and Wasteland Mapping

The land degradation status as seen from the map (Fig. 2.11a) is majorly representative which shows that the western flank of the Luni river basin portrayed in green shade demarcates the zone of wind erosion. The other source of land degradation in the Luni river basin is salinization and alkalinization due to the high rate of evaporation and residual soil group found in few excerpts across the river basin represented in the pink shade in the map. The rest part of the river basin in white shade represents normal land cover without any degradation or demarcated as cultivation lands. Canal water misuse with excessive irrigation has initiated waterlogging leading to excessive rise of salinization (Kar and Kumar, 2020).

The wasteland map (Fig. 2.11b) shows various wasteland categories under which the dominant type is found to be shrublands, salt-affected areas across the river basins majorly located in the areas adjoining the Aravalli, the river channels of Luni and its major tributaries respectively. Some patches with green shades show degraded forest lands due to extensive forest clearing and cattle grazing. The slopes of residual hills of Aravalli and pediment foot slopes are also marked by ravines and gullies which are a sort of degraded wasteland although have a low presence. The arid landscape of the Thar brings in an entire sand complex which is itself a wasteland followed by the Rann where the Luni drains out forming an extensive splaying and series of avulsion channels indicating a progressive wasteland generate from fluvial signatures.

2.11.3 Landuse and Landcover Mapping

The Landuse and Landcover (LULC) mapping is a quintessential tool that reflects the major spatial coverage of any study unit with a synergic exhibition of the major land uses in form of anthropogenic activities on the land surface as well as natural land unit coverage like water bodies and forests. LULC mapping has become a reasonable practice with a wide range of applications in various fields making it lucid derived from various types of remotely sensed imageries (Khan et. al. 2020; Johnson and Iizuka, 2016). Mapping LULC and identification of geomorphic features are an integral part of developing a conceptual framework and management of land and water resources (Khan et. al., 2020; Steinhausen et. al., 2018; Haas and Ban, 2017). The process of change detection is observing the alterations occurring for various LULC classes, both anthropogenic and natural over a temporal scale using multi-date images to assess the differences in the designated classes for a study area due to various human actions and environmental conditions (Singh, 1989).

The LULC change detection for the Luni river Basin is being extracted, quantified and mapped in Fig. 2.12 for a temporal period of ten years, i.e., 2009 (ESA and UCLouvain, 2009) and 2019 (Buchhorn, 2020) from ESA global landcover dataset in order to bring out the major shifts and alterations within land use and landcover classes. The decadal shift in the LULC pattern is being put up in Table – 2.6 to explain the change matrix comprehensively. The classes of LULC are divided into natural and anthropogenic units each having three classes designated under it according to the NRSC scheme. Here, the traditional way of extracting LULC through supervised or unsupervised classification from the spectral signatures of Landsat/LISS-III could not be performed. This is because the areal coverage of the Luni basin is extensive for which multiple uniform and cloud-free images could not be procured from the web platforms of USGS or NRSC.

Land Degradation & Wasteland Mapping of Luni River Basin
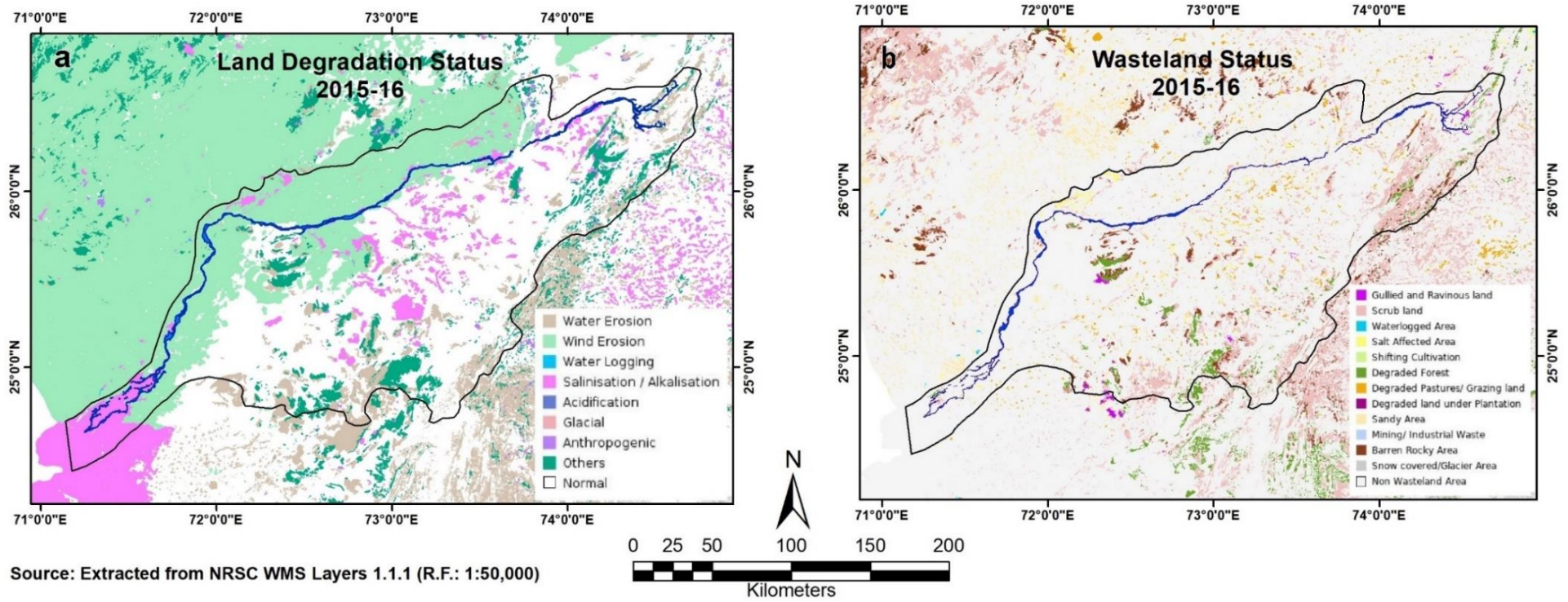
Fig. 2.12: Major types of Land Degradation factors and Wasteland status of Luni river basin. Source: Prepared by the researcher based on the NRSC WMS layers, 2015-16.
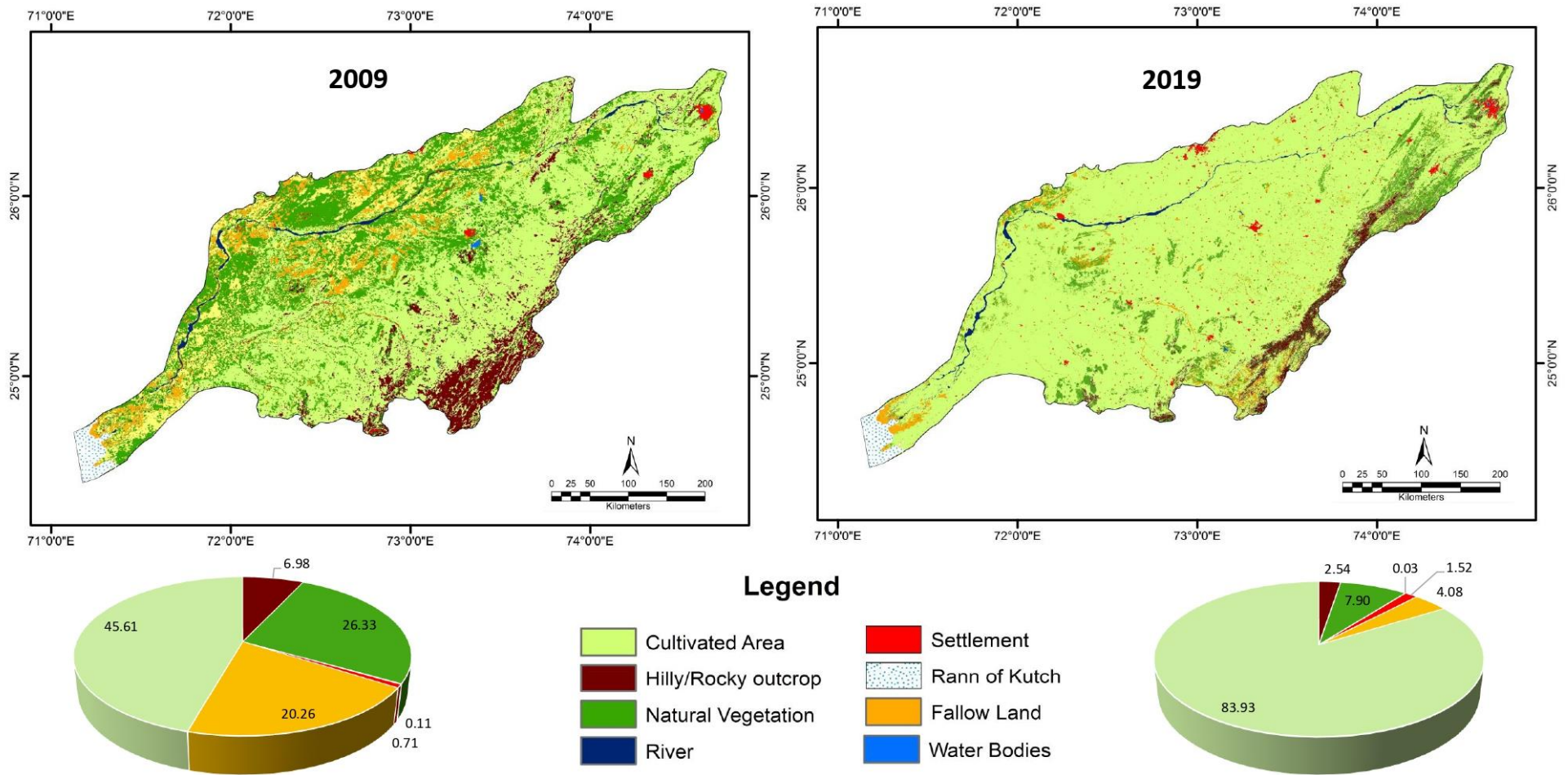
Fig. 2.13: Landuse and Landcover (LULC) changes in the Luni river basin for 2009 & 2019. Source: Prepared by the researcher based on the classified raster layers of Global Landcover, ESA.

Table 2.7: Decadal shift in Landuse and Landcover (LULC) pattern within the Luni river basin.

Sl. No.	LULC Units	LULC Class	2009		2019		Change Matrix				Interpretation
			Area				2019-2009 (km.^{2})	% Change	Avg. % Change		
			km.^{2}	%	km.^{2}	%			LULC Unit	Overall	
1	Natural	Hilly/Rocky Outcrop	2741.15	6.98	998.22	2.54	-1742.93	-63.58	-67.57	-14.16	Increase in mining, quarry activities.
2		Natural Vegetation	10342.28	26.33	3101.61	7.90	-7240.67	-70.01			Major rise of land area under cultivation and or drought-like situations during previous years.
3		Water Bodies (except rivers)	43.6	0.11	13.47	0.03	-30.13	-69.11			Dry season or Drought spells.
4	Anthropogenic	Settlement	278.86	0.71	595.62	1.52	+316.76	113.59	39.25		Major growth of urban centres
5		Fallow Land	7958.35	20.26	1602.04	4.08	-6356.31	-79.87			The considerable area under agricultural land use.
6		Cultivated Area	17914.56	45.61	32967.86	83.93	+15053.3	84.03			Converting uncultivable fallow lands & area under natural vegetation into potential farmlands.

Source: Compiled by the researcher.

The small lakes, water reservoirs, open water tanks, water checked behind the semi-permanent dam structures and the remnants of ephemeral river channels with water content were classified as waterbodies. But the river channel of Luni and its major tributaries were found to be dry for which they have got classified as fallow land/farmlands or even as natural vegetation. The ESA landcover dataset has a major disadvantage of overlooking the minor physical or man-made features at a local or sub-national scale, which is a rather obvious one for being a global level data. In the floodout region of Luni, the area has been mainly classified as fallow or agricultural land with the major river distributaries coming in either purview of such types of LULC units. The river width plays a significant role in highlighting its presence in the LULC class maybe for a local level analysis for example – river reach or a specific river stretch. But here it can be ignored assuming the importance of LULC of the entire Luni catchment. Pixel-based object classification for such an extensive catchment is not always feasible within a GIS platform and requires greater computational power to enhance such features segregating the spectral signatures. The main reason for Luni's absence except for few perennial reaches from the waterbody class is because of the presence of exposed sand beds having high reflectance value getting classified as fallow or barren land and for those reaches having an agricultural presence or vegetation growth along the banks of the river gets classified into their respective LULC units.

The hilly/rocky outcrop has seen a decline of its areal coverage due to a probable rise in mining and quarrying activities near the Aravalli, distinctively observed in the maps. Many isolated monadnocks and residual hills are cleared off for mining stone chips which has led to vanishing of smaller hills at unprecedented rates (Kar and Kumar, 2020). The amount of natural vegetation and water bodies have also seen a steep decrease of its areal coverage in 2019 compared to 2009 maybe because of increased conversion of forest lands into farmlands as well as the rise of dryland signatures due to lingering short spells of droughts that occur in this watershed in alternative years.

The anthropogenic units of LULC consist of three distinct classes as settlements, fallow land and cultivated area. The areal coverage of settlements and cultivation lands have shown a sharp rise in 2019 compared to the base year 2009 as there has been a major growth of urban centres namely the district towns and headquarters. The farmlands have increased their share in 2019 may be due to certain progressive agrarian policies of the local government where the extensive fallow or uncultivable lands have been converted into agricultural lands with irrigation facilities. Thus, the share of fallow lands has also decreased over the decade may be due to the

rise of better farming facilities like availability of irrigation, fertilizers and other socio-economic welfare schemes for agricultural upliftment in the districts of Rajasthan.

The figures of the change matrix for the LULC classes are expressed well in Table 2.6. The overall percentage of the change matrix shows an alteration rate of -14.16% over the past decade. While individual LULC units show a massive fall and rise of change matrix by -67.57% and 39.25% for natural and anthropogenic units respectively. Natural LULC units have recorded the maximum extent of alterations showing a decrease of their share among the entire Luni watershed, while the anthropogenic units show an average increase of the share of LULC classes[2]. The eye-catching alterations in LULC are seen along the course of the Luni river especially on the western banks as well as in the southern edges in the flood out region. The major conversion of fallow lands and area under natural vegetation has undergone alterations in these areas with a dominant rise of cultivation lands. The other possible reason for the major decline in the LULC classes over the decade is the technicality of classification of satellite images provided by ESA for maybe two different seasons using separate geo-computational approaches. But both the temporal maps of 2009 and 2019, has been verified using accuracy assessment against the google earth imagery in a geospatial platform.

2.12 Transportation Condition

The transportation network is an indispensable part of human life and its unprecedented growth over the past years are joining up the remotest corners of the nation. It is a progressive signature of a nation's economic growth, infrastructural facelift and is an essential element in the process of regional development (Roy, 2021). The significant rise of global demand, especially in the last few decades for transportation mediums like roadways, railways and underground tunnels, have been trying to meet up the needs of exponential population growth and lengthening of continuous supply of goods, freights and passengers (Mouratidis and Kehagia 2014). The incessant expansion of linear transport network infrastructures like roadways, railways, bridges, culverts, dams, etc. has proved to be a major threat to the fragmentation of the landscape, causing (dis)connectivity in the riverine system (Roy, 2021). Major constructions of lateral roads or railways are leaving anthropogenic footprints and disrupting the fluvial system with longitudinal (dis)connection (Roy and Sahu, 2018) within the fluvial corridor, which in turn, are affecting the riverine ecology and natural biomass (Hu et al. 2017; Cong et

---

[2] Rising anthropogenic activities especially farming and mining has increased over the last decade with better facilities for both the sectors and conversion of unutilsed barren and fallow lands into farmlands with improved agricultural facilities has claimed more lands under human activities from their natural lineage.

al. 2014). The transport networks are the cause behind having enough barriers, obstructing the free movement of river water, sediments, organisms and nutrients in between the active channel and its buffer area or floodplain, leading to (dis)connectivity of the fluvial landscape (Roy and Sahu 2017; Blanton and Marcus 2014, 2009). Therefore, the issues arising out in geomorphic connectivity due to encroaching human activities in a fluvial system, especially because of the rise in infrastructural constructions and linear transport networks, has been a food of thought in the contemporary world. The transfer of river water, sediments and their complete role in maintaining biodiversity has made the study of transport networks and their impact on a riverine watershed a rising matter of interest among river researchers. (Roy, 2021; Singh et al. 2020; Wohl 2017; Roy and Sahu 2017, 2018; Parson et al. 2015; Blanton and Marcus 2014, 2009). Hence, in this study in order to fulfill the final objective for understanding the human induced sensitive hotspots within the study basin, the transportation parameters are considered to analyse the maximum and minimal hotspots of anthropic perturbations.

Open Street Maps are the crowdsourced free available data sets providing up to date information regarding transport networks like roadways and railway routes embedded with accurate information. In figure 2.13a, a transport network consisting of both rail and road networks has been extracted for the entire Luni river basin from the global dataset. District towns and headquarters exhibit maximum assemblage of road networks, while the entire watershed almost has an even distribution of transport networks. The Luni river and its corridor has a considerable proportion of transport networks on its corridor and hence is creating a fluvial (dis)continuity by fragmentation of the present geomorphic landscape. Anthropogenic dynamism induced by human-based linear infrastructure on the fluvial corridor of Luni has been put out to be a major source of interest to be studied under the title of river behaviour and its sensitivity. The transport networks and population density are the two major forms of human-based parameters which leads to alterations in the natural landscape creating possibilities to carve out a new landform made out from the anthropogenesis. Such parameters will help in deciphering their impact on the riverscape and will portray the sensitivity posed by such man-made activities on the Luni catchment area.

The transport network density map (Fig. 2.13b) is being derived from the vector layer of transport routes with a unit of $km^{-1}km^2$. The entire Luni watershed has a very meagre amount of transport network density amounting in between a range of 0.01–0.47 $km^{-1}km^2$ This is followed by the range of 0.48-1.05 $km^{-1}km^2$ demarcated with yellow patches across the entire river basin. The further higher concentration of transport networks leading to a higher density

ranging from 1.08 till 5.26 $km^{-1}km^2$ is found in proximity to the cities of Jodhpur in the north-west on the right bank of river Luni and Ajmer on the northern part of the watershed distinguishable with colour shades of green to blue in respect of the hierarchical density order.

Proximity or near distance from the transport network within the Luni river basin (Fig. 2.13c) is the best way of representing near distance analysis between the transport lines and the entire watershed. The most prominent form of the proximity of transport network is found to be zero for almost the entire Luni river basin which is represented by the yellow shade. This is because the entire river basin has an even distribution of transport networks with a combination of both the road and rail networks as evidently seen in Fig. 2.13a. Some rural settlements which are placed a bit far apart from one another show a greater distance from the transport networks starting from 2479.64 m (or 2.48 km) to the maximum extent of 11,291.2 m (or 11.29 km). The largest interstice is found near the Rann where the Luni drains out forming an inland delta. Inorder to assess, a watershed's sensitivity anthropogenic footprints, especially in form of infrastructure development, has led to (dis)integration of the landscape morphology within the active riverine floodplain as well as in the river corridor. The expression of riverine alterations posed due to such intertwined transportation networks elevates the need for a human impact assessment on riverine morphology and its biodiversity.

Fig. 2.14: Transportation condition in Luni river basin. Source: Prepared by the researcher based on the vector layers obtained from Open Street Map, August 2020.

Fig. 2.15: Population Dynamics in Luni river basin. Source: Prepared by the researcher based on the raster layers obtained from SEDAC, NASA, 2015 and WorldPop., University of Southampton, 2020.

2.13 Population Dynamics

The population residing within a river basin is a key indicator to understand the continuous active human dynamism within the river basin. The ever-increasing exponential rise of the human population over the past few decades has threatened the natural flow of rivers and their related landscape where the river is taken for granted. The "living space" of rivers are being continuously compromised with the continuous encroachments of ever-increasing population and man-made infrastructure without considering the natural entity and ecology of the fluvial system.

The population count (Fig. 2.14 a) and the population density (Fig. 2.14b) are mapped within the Luni river basin using the SEDAC, NASA gridded global dataset for the year 2015 (CIESIN, 2018) to understand the zones of sparse to highest population density thriving in the watershed. The cities of Ajmer in the north and Jodhpur in the north-west represents both the highest population count of 12,964-19,676 along with the highest density of 847.46-1022.67 person/sq. km. Both the population count and density map corresponds to each other helping us to understand the distribution of population within the Luni river basin. In the eastern part, a comparatively low population count and density are observed as this region is inhabited by a rural and semi-urban population. The entire western part where the Luni flows through represents the lowest figure of population count below 2932 and a density of population in between 29.75-166.03 person/sq. km.

The average population per pixel (Fig. 2.14c) and settlement extent (Fig. 2.14d) for the year 2020 are the most recent global gridded datasets showing pixel-wise classified population and the extent of settlements (including towns, cities and settlements along the linear roads or railways) provided by the University of Southampton as WorldPop data. This dataset is classified based on remote sensing satellite imagery using random forest-based dasymetric redistribution of available census data projections (Stevens et al., 2015). Both the maps help us to understand the recent population projection over the entire river basin of Luni. The highest population per pixel is found over the major two cities of Jodhpur and Ajmer followed up by the district headquarters, small towns and sparsely spaced rural settlements. Since these are satellite imagery-based information, it helps in providing a real-time scenario of the study area. Assessment of the population and settlement impact can be well judged with the binary colour of settlement extent showing the settled area in red patches and the sparse settlements in yellow. The significance and impact of anthropogenic sensitivity in the watershed are hence derived.

2.14 Summary

The chapter provides a detailed insight into the generic facts of the Luni river basin. The natural and human-based factors are discussed in detail providing an insight into the character traits of visualizing the tendency of the Luni river to behave in a specific way as determined by the environmental settings. Luni river basin drains the central portion of Rajasthan with an area of 39,278.80 km^2 covering ten districts of Rajasthan and two minor portions of the districts of Gujarat. The Luni river is typically having a distribution of semi-arid to arid climatic conditions based on the annual mean temperature and rainfall. The amount of rainfall decreases from Aravalli in the east to the extensive sand dune plains of Thar in the west. Other meteorological and bioclimatic factors like wind speed, solar radiation, water vapour pressure, AI and PET were seen to correspond to the nature of a dryland area. Pre-monsoon VCI exhibits a drier condition compared to the post-monsoon scenario when the VCI shows a better state due to the rise of agriculture. The dominant type of soil is found to be grey-brown soil or calciothirds and a variable carbon density in form of organic and inorganic is distributed based on the dominant Kharif agricultural practices. Poor land quality dominates the land capability but in recent years found to have decreased considerably due to the rise of better farming facilities. Land degradation due to wind erosion, alkalinization/salinization and dune encroachment from the Thar is a major cause of localized LULC disruptions. Wastelands are mainly formed due to gullies and ravines in the hill related pediment pedeplain complex and salinization which is through a very local process. The LULC mapping for the years 2009 and 2019 exhibits major changes with more areas being proclaimed under mining and farming with better facilities and rising population. An increase of drought spells, less rainfall and major radial expansion of the urban towns and cities are seen in the temporal analysis of LULC over the last decade. The transportation conditions are mapped to bring out the present infrastructure present in the catchment area and how the population dynamics are distributed over the entire drainage basin area based on which the sensitivity analysis is performed in the successive chapter.

CHAPTER – 3

GEOSCIENTIFIC CONFIGURATION OF LUNI RIVER BASIN

3.1 Introduction

The nature of a river basin can be better understood by observing and analyzing the underlying geological factors as well as the surface processes and their interrelated dynamics. The climatic agents of erosion are constantly acting on the surface and shaping new landforms, in turn, curving out the riverscape. These elementary in and ex-situ processes operate continuously and try to venture out new landform units that are carved out from the synergy. The studies of geology, geomorphology and tectonic influence on river basins (Castelltort et al., 2012; Taloor et al., 2017; Vijith et al., 2017; Menier et al., 2017; Das and Pardeshi, 2018; Anand and Pradhan, 2019; Taloor et al., 2021) has been the best way to decipher the type, character and in turn the behaviour of a watershed which also helps to explain the response to natural or human-induced sensitivity.

3.2 Objective

The first part of the third objective of this study is addressed in this chapter which focuses on investigating the process-response mechanism operating within the Luni river basin based on the geoscientific characterization.

3.3 Methodology

This chapter entails the Luni river basin's geological and morphological records, extracted from various sources as mentioned in Table 1.3. This is mainly based on the GSI's geological quadrangles. The geology, geomorphology, lineament, tectonic framework, hydrogeology, neo-tectonics and seismic zones maps have been extracted from the base maps listed in Table 3.1 using vector tools like polygons, polylines and point features in the ArcGIS environment, and the area was calculated for of the thematic classes. The vector-based format helped in developing the geoscience datasets for further analysis of the sensitivity parameters discussed in chapter 5. The hydrological datasets for the Luni river are obtained from the Central Water Commission (CWC) for two Guage-Discharge Stations (GDS) located uniformly along the Luni river channel, one upstream of the river at Balotra and the other in the downstream at Gandhav. The different hydrological analysis for the Luni river is performed in Microsoft Excel and IBM SPSS so that the hydrological character can be assessed. The daily GD datasets go through an exhaustive sorting and arranging process and are converted into either monthly and/or annual basis. The datasets for hydrological investigation include water level, discharge, stream power, rating curve and zero flow index for both the GD stations. All the hydrological

calculations are described in the preceding part of the chapter with detailed explanations for each.

Table 3.1: List of datasets used in chapter 3.

Sl. No.	Parameters	Data Type	Data Source	Spatial Resolution	Period
1	Geology, Lithology & Lineaments	Spatial Grid	Bhukosh geoportal, GSI/ GSI Quadrangles	1:2,000,000	2018
2	Geomorphology			1:250,000	
3	Tectonic Framework			1:250,000	
4	Seismic Zones	Polygon coverage	Vulnerability Atlas of India v.3, BMTPC	1 cm = 100 km	2019
5	Hydrogeology		NAQUIM, CGWB, MoJS, GoI		2017
6	Locations of Earthquake Events	Spatial Grid	NCS, MoES, GoI	1:250,000	2020
7	River Point Hydrology	Daily Water Level & Flow Timeseries	Executive Engineer, Mahi Division, Gandhinagar, CWC, MoJS, GoI	Two Gauge-Discharge monitoring stations on Luni River - Balotra & Gandhav, Rajasthan	1990-2016 & 1979-2016

Source: Compiled by the researcher.

3.4 Geology

The underlying records of the earth surface and studying their significance is a prime part of geo-scientific investigation for a river basin to understand and develop a framework for its process-response (sensitivity) mechanism. Geological study amplifies the major comprehension of sensitivity for the physical earth processes operating in a watershed. The geological framework could better apprehend using the sequence study Table as provided in Table 3.1. The initiation of the geological sequence starts with Alwar and Ajabgarh group which are classified under the Delhi supergroup belonging to the mid-Precambrian age. This is followed by the intrusives of the post-Delhi supergroup belonging to the upper and lower Precambrian age. The granites, rhyolites, porphyries and tuffs are found as a rock formation. Next in sequence is the Vidhyan or Marwar supergroup of upper to lower Precambrian age. Sedimentary rock formations such as sandstones and limestones are a part of this supergroup comprised of local place-based groups like Nagaur, Bhilwara and Jodhpur. The Palna group of rock formations belonging to the lower Eocene consists of sandstones, bentonitic clays etc. In the recent geological formations, the quaternary deposits derived due to natural wind or water-based erosive actions have led to the formation of aeolian and fluvial deposits leading to

expressive geomorphological features like sand dunes, alluvial sands, clays and gravels, scientifically explored to bring out their formation, geological timing, nature and characteristics (Mishra *et al.*, 1998; Jain *et al.*, 1999, 2005; Kale, Singhvi and Mishra, 2000; Kar *et al.*, 2001; Jain and Tandon, 2003; Bajpai, 2004; Singhvi and Kar, 2004). A series of unconformities are also found to exist in between the Quaternary, Cenozoic, upper Proterozoic to lower Proterozoic eras. The Quaternary and Cenozoic formations are only found to be exposed on the ground surface of the river basin, while the rest of the formations are recorded only at the sub-surface level.

The Luni river basin is comprised of igneous, metamorphic, carbonate and sedimentary rocks. The alluvium occupies an extensive part and extends in a north-southwest direction through the central part of the drainage basin. Granites and gneissic rocks also cover large basin areas as large outcrops in the north-central part and as small outcrops rising out of alluvium. Sandstone and Bilwara Limestone is found to be exposed along the northern extremity of the basin bordering its outer part. Metamorphic rocks, including gneisses, phyllite and schists, extend in the northeast-southwest belt along the eastern and southern part of the catchment.

The geological formations (Fig. 3.1) as mapped from the base map of geological quadrangle maps of GSI express various types of rock formations from different geological eras each belonging to various super groups. The quaternary deposits in undifferentiated fluvial or aeolian sediments cover up the most extensive area with a coverage of 60.09%. This is followed by the coarse-grained intrusive igneous Erinpura granite formations, which is the main source of mining activity found in a stretch of the north-west to south-east represented in pink shade comprises 16.13% of the Luni river basin. The third group of geological rock formations includes the Kumbhalgarh group, which contains carbonate, mafic volcanic and argillaceous rocks. It is a part of the Aravalli formation with 7.23% of the entire Luni basin. The Punagarh group comprising of sandstones of Trans Aravalli (Khan and Khan, 2016) region portrayed in the yellow shade on the north-central part of the Luni watershed has a coverage of 4.11%. Table 3.2 shows various other geological formation units in negligible percentage cover starting from Malani volcanic, undifferentiated Delhi supergroup, Gogunda Sirohi group till traces of sill and dykes in the Aravalli ranges. Localized geological formations contribute 12.44% in a consolidated group.

Table 3.2: Geological Sequence in the Luni river basin

Era	Age	Supergroup	Group	Rock Formation
Quaternary	Recent to sub-recent	-	Aeolian & Fluvial Deposits	Wind-blown sands, sand dunes, Alluvial sands, clays & gravels, etc.
----- x -------- x -------- x -------- x ---- Unconformity---- x -------- x -------- x -------- x----				
Cenozoic	Lower Eocene	-	Palana	Sandstones, bentonitic clays, Fuller's earth and lignite seams
(Not exposed on the surface in the basin but sub-surface presence recorded)				
------- x -------- x -------- x -------- x ---- Unconformity---- x -------- x -------- x -------- x----				
Upper Proterozoic to Lower Palaeozoic	Upper Precambrian to Lower Cambrian	Vindhyan (Marwar Super-group)	Nagaur, Bilwara, Jodhpur	Sandstone Limestones mainly with cherty dolomite Sandstone
------- x -------- x -------- x -------- x ---- Unconformity---- x -------- x -------- x -------- x----				
Upper Proterozoic	Upper Precambrian to Lower Precambrian	(Post-Delhi) Intrusives	Jalore-Granite, Malani Rhyolites Idar Granites, Erinpura Granites*	Granites, rhyolites, porphyries and tuffs, etc.
Middle Proterozoic	Middle Precambrian	Delhi	Ajabgarh	Dolomitic marbles, quartzites, meta-basites, Schistand gneiss
			Alwar	Quartzites, mica-Schistand Phyllite

Source: Compiled by the researcher based on the technical reports of GSI, GoI & Water Resource Department, Government of Rajasthan (2013).
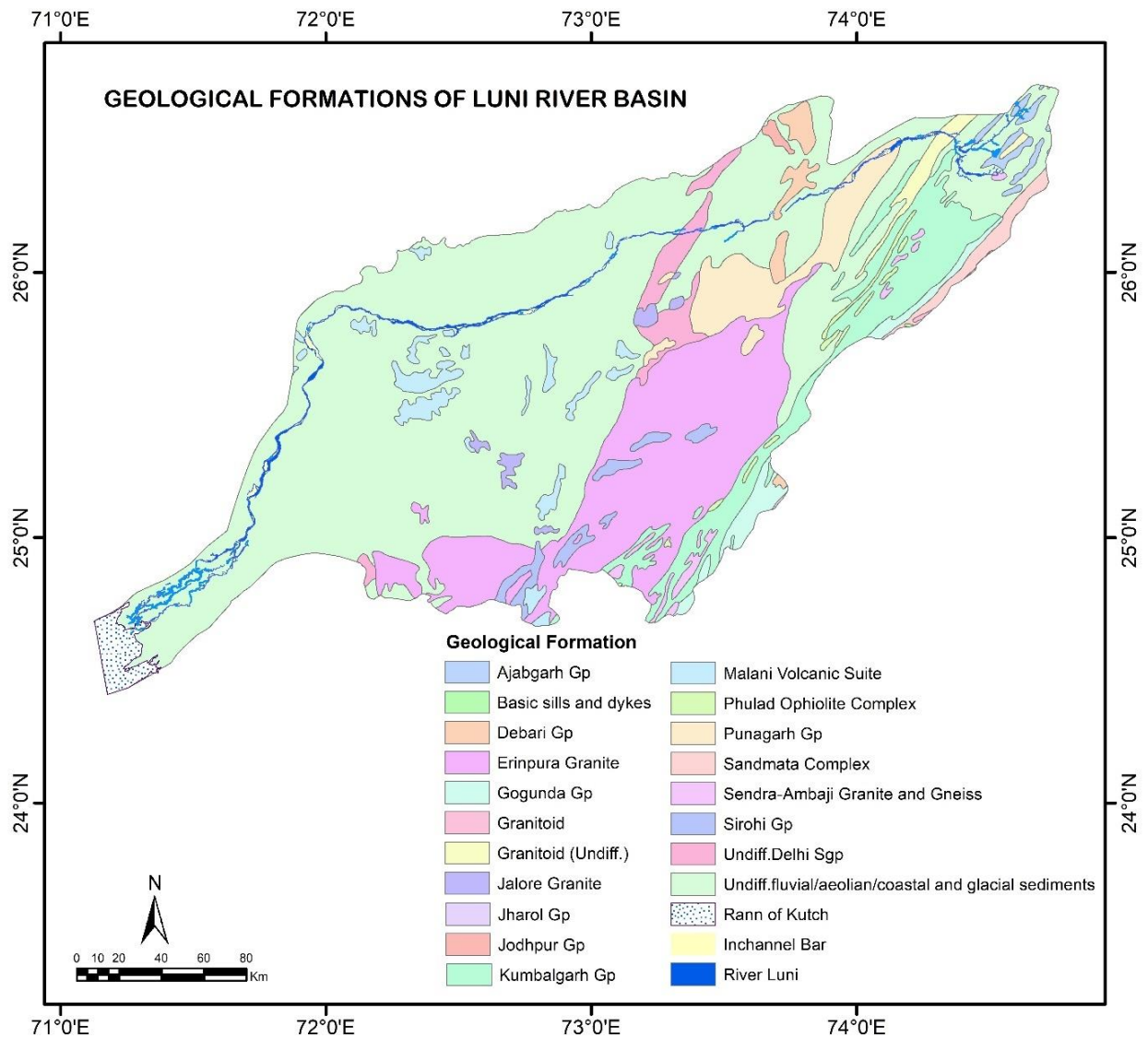
Fig. 3.1: Geological formations of Luni river basin. Source: Prepared by the researcher based on the GSI quadrangle maps of Rajasthan and Gujarat, 2018.

Table 3.3: Geological Units found in Luni river basin

Geological Units	Area (km^2)	Coverage (%)
Undiff Fluvial/Aeolian sediments	23601.15	60.09
Erinpura Granite	6336.22	16.13
Kumbhalgarh Gp	2839.44	7.23
Punagarh Gp	1613.23	4.11
Malani Volcanic Suite	917.29	2.34
Undiff.Delhi Sgp	817.83	2.08
Gogunda Gp	560.07	1.43
Sirohi Gp	457.74	1.17
Debari Gp	424.73	1.08

Sandmata Complex	362.20	0.92
Granitoid (Undiff.)	340.46	0.87
Ajabgarh Gp	259.89	0.66
Sendra-Ambaji Granite and Gneiss	248.45	0.63
Jalore Granite	223.67	0.57
Phulad Ophiolite Complex	191.29	0.49
Jodhpur Gp	61.82	0.16
Granitoid	14.40	0.04
Jharol Gp	5.52	0.01
Basic Sill and dykes	3.42	0.01

Gp – Group, Sgp – Supergroup, Undiff – Undifferentiated. Source: Computed by the researcher.

3.5 Geomorphology

Geomorphology is a proportional product of the geological formations with the curving out of erosive natural agents like wind and running water for a dryland river basin like Luni. The progression of semi-arid to arid climatic conditions from the eastern to the western part of the river basin (Kale et al., 2000), immensely influences geomorphic formations by the principle of origin. The Aravalli range, running southwest to northeast with its expressive escarpments, ridges and relict hills in the east, is the vital portion of the river basin. In terms of geomorphology, the basin is structurally controlled. The presence of elongated synclinal and anticlinal valleys is found to exist amidst the parallel ridges of the Aravalli hills. These valleys range in width from 1 to 10 km and are surrounded by hills with discontinuous upland elevations of 300 m amsl. The valley plains are generally in the form of pediments (integrated Alluvial fans), which are partly aggradational (near the foothills) and partly denudational (away from the hills), are covered in the latter case with a thin mantle of soil and regolith. In Ajmer district, the Pushkar and Sagarmati valleys are synclinal, whereas the Anasagar valley is anticlinal. Alluvial and sandy plains are extensively associated with relict hills and scattered sandy hummocks in the Luni basin, essentially west of the Aravalli hill range. The stable and shifting sand dunes are deposited both on the alluvial plains and the windward side of the ridges, facing the Thar. The elongation length of such dunes is generally parallel to the wind direction, governing the morphological features such as hill ranges, wind gaps, etc.

The geomorphological formations mapped (Fig. 3.2) across the Luni river basin is tabulated with areal coverage and its percentage share as well in Table 3.3. The quaternary studies have shown that medium to fine-grained aeolian sand sheets (Kar et al., 2001; Kar, 2020) are represented in the map with dotted shade along the western part of the Luni basin most dominant geomorphic composition of 27.62%. The dominant impact of sand grain and dune

migration from the Thar desert in the western part of the watershed wraps the western central portion. The older alluvial plain of Luni and its tributary prominently adjoining the rivers with yellow shade comprises 25.63% of the river basin. The pediment pediplain complex adjoining the northern hills in Ajmer, southeastern parts of Aravalli and the north-western fringes of the watershed comprises 12.73% of the Luni basin representing the Luni basin continuous dissection and erosion of such landscape units by the initial stream orders. The younger alluvial plain with 8.82% coverage is found across the Luni and its tributaries within the buffer area of its respective channels. The highly dissected structural hills and valleys in Aravalli comprise of 5.50% share. The other geomorphic units are enlisted in Table 3.3 with their percentage share. Aeolian dune complex, parabolic dunes, moderately dissected structural and denudational relict hills. characterize the local geomorphic units. It comprehends the active yet localized geomorphic processes that continue to operate with the dryland riverscape.

Table 3.4: Geomorphic units in Luni river basin

Geomorphic Units	Area (km^2)	Coverage (%)
Aeolian Sand Sheet	10848.91	27.62
Older Alluvial Plain	10068.07	25.63
Pediment Pediplain Complex	4999.60	12.73
Younger Alluvial Plain	3465.43	8.82
Highly Dissected Structural Hills and Valleys	2158.95	5.50
Moderately Dissected Structural Hills and Valleys	1643.76	4.18
Active Flood Plain & Older Flood Plain	1468.08	3.74
Aeolian dune complex	978.87	2.49
Parabolic dune	802.76	2.04
Moderately Dissected Denudational Hills and Valleys	758.88	1.93
Older Coastal Plain	630.77	1.61
River	285.87	0.73
Aeolian dissected dune complex	253.71	0.65

Source: Computed by the researcher.
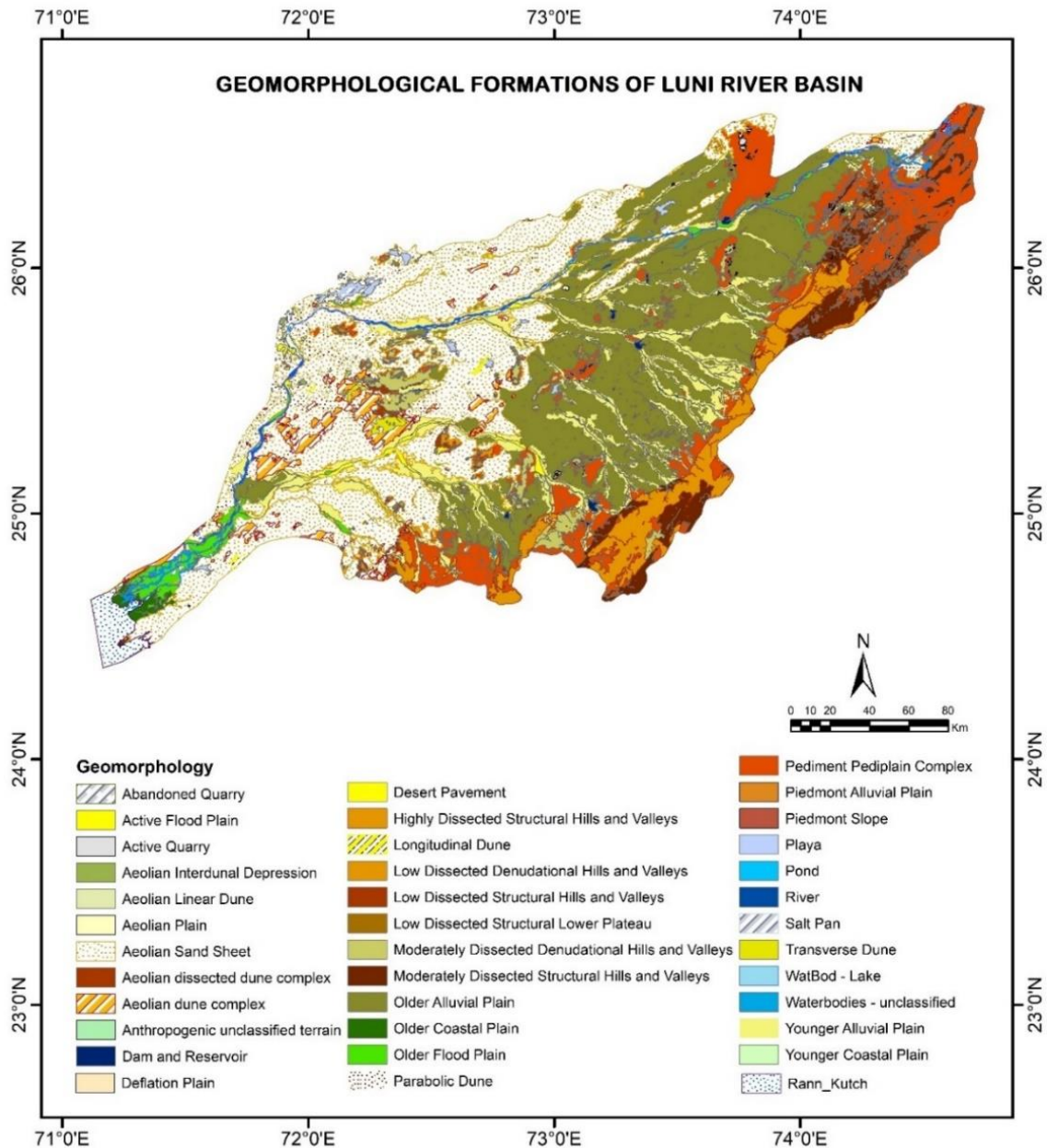
Fig. 3.2: Geomorphological formations of the Luni river basin. Source: Prepared by the
researcher based on the GSI geomorphology maps of Rajasthan & Gujarat, 2018.

3.6 Lineaments

The structural or geomorphic foundation of lineaments expresses its type and nature found to be
responsible for altering the riverine flows across a river basin. Lineaments are found to rule the present-
day channel processes (Kar, 1994), deflecting the direction of river flow hence affecting the steadiness
of long profile gradient from its regular concave shape (Keller and Pinter, 2002; Ambili and Narayana,
2014; Antón et al., 2014; Sonam and Jain, 2018; Boulton, 2020). The study of lineaments is vital to
understand the dynamism and vitality of tectonics influencing drainage pattern, watershed shape and its
asymmetry factor, deflection of streams, flow turn angle and river incision rates (Cox, 1994).

Lineaments are vital in studying potential groundwater zones as Kumar and Krishna (2018) explained how the occurrence and progress of groundwater are monitored by secondary porosity, which is related to the presence of fractures and lineaments initiating maximum percolation of water into the ground. The intersection points and those areas around the lineaments are favourable sites for high infiltration rates and groundwater storage (Gupta and Srivastava, 2010; Mukherjee et al., 2012).

The map in figure 3.3 shows the types of lineament distribution across the Luni river basin. The total length of lineaments and their percentage cover is enlisted for each form of lineament in Table 3.4. The geomorphic lineaments represent drainage parallel form covering 21.08% of the watershed. The tributaries and certain initial stream orders make parallel drainage form orienting the streams straight and parallel to each other, leading to the development of straight lineaments. The structural form of lineaments is enlisted in the Luni watershed as faults, joints/fractures, axial traces of folds, dykes and shear zones. Among these, faults constitute 36.43%, followed by joints/fractures for 27.35% (Table 3.4) among the types of lineaments. Hence, lineament types are key to understanding the direction of river flow, the orientation of the rivers and flow turn angles, and deciphering the need for inclusion in a river behaviour study. These lineaments found along the long profile can decipher the key areas where the river has a tectonic influence in form of upliftment rejuvenation or down warping.
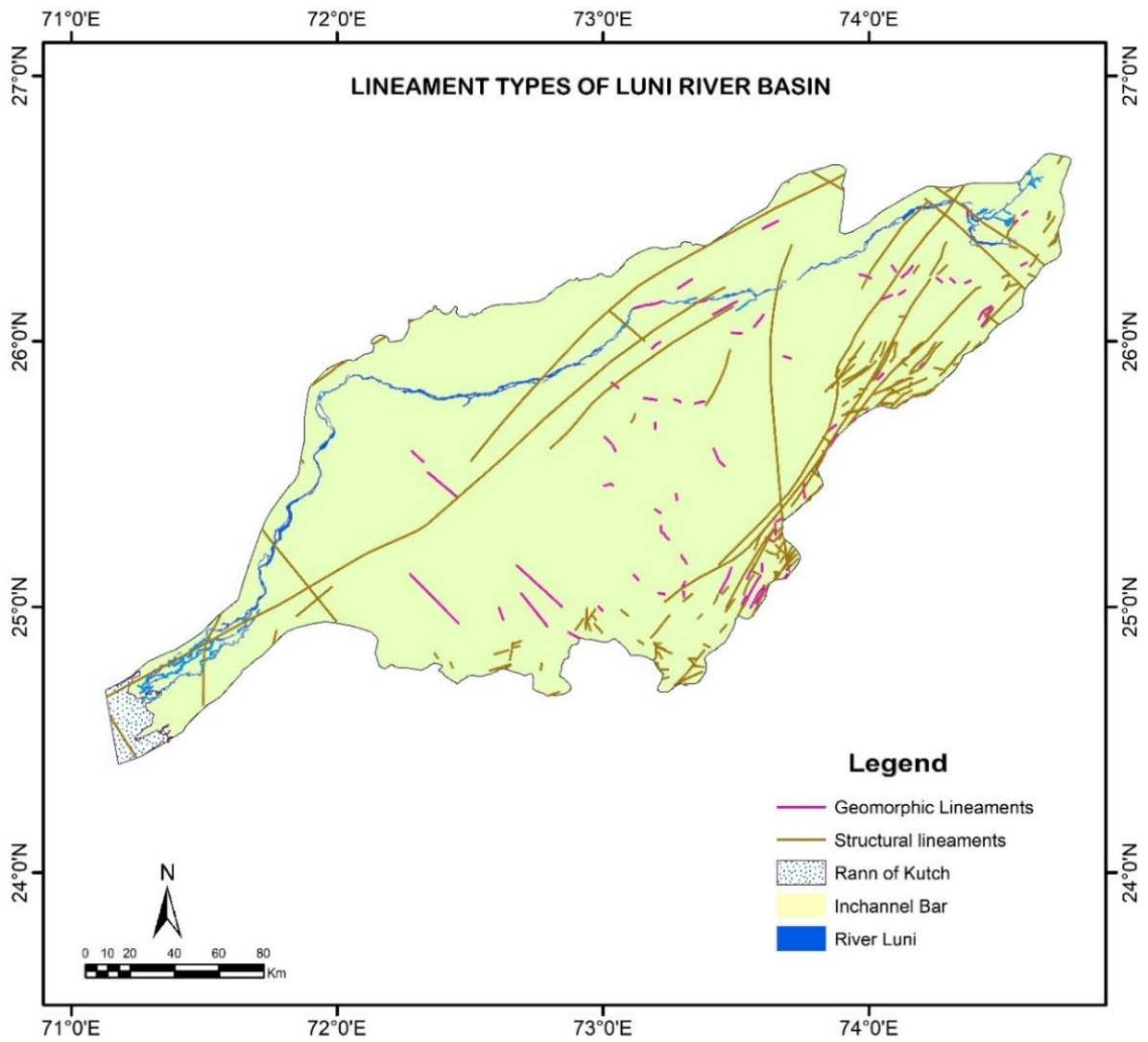
Fig. 3.3: Types of Lineament distribution across Luni river basin. Source: Prepared by the researcher based on the GSI quadrangle maps of Rajasthan and Gujarat, 2018.

Table 3.5: Lineament form and types of Luni river basin

Lineament Form	Lineament Type	Length (km)	Coverage (%)
Drainage parallel	Geomorphic	995.94	21.08
Fault		1721.27	36.43
Joint/Fracture		1292.03	27.35
Axial trace of fold		333.73	7.06
Shear zone		182.73	3.87
Ridge parallel		166.36	3.52
Break-in slope		22.36	0.47
Dyke	Structural	9.82	0.21

Source: Computed by the researcher.
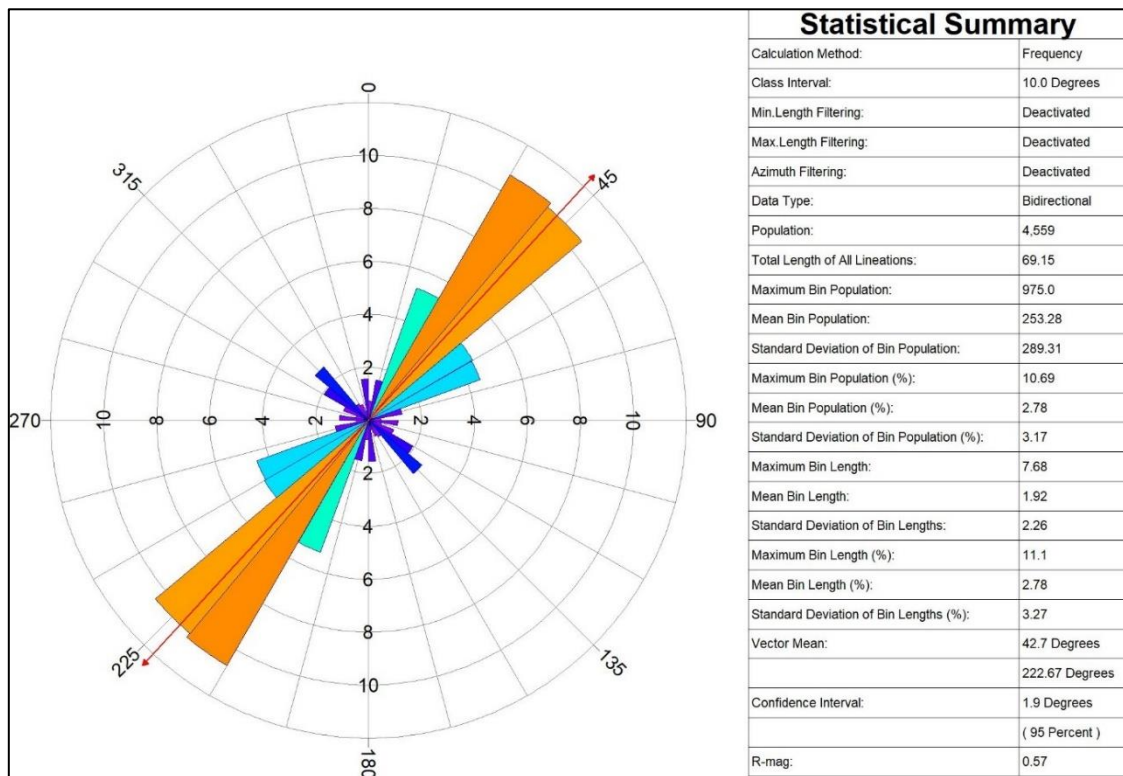
Fig. 3.4: Sequential orientation of Lineaments in Luni river basin. Source: Prepared by the researcher based on the lineament vector files.

The sequential orientation of lineaments in the entire Luni river basin as shown in Fig. 3.4 exhibits the direction of lineaments. The major lineaments show a North-East-South-West (NE-SW) trend. Frequency-based analysis was performed in RockWorks v. 17 software to extract the orientation of the major lineaments of the river basin. This trend was also validated from the previous literature which explained the similar form of trend in the lineaments within the Luni watershed (Bajpai, 2004). The major faults observable from the map (Fig. 3.4) are found to traverse the Luni river basin are – the North-West-South-East (NW-SE) Jaisalmer Barwani lineament, NE-SW trending Luni-Sukri lineament (Ramasamy et al., 1991; Dhir et al., 1992) which is intersected in the SW part of the basin at Jhab (Pal, 1991) and to some extent by the Tonk - Raisinghnagar lineament oriented in NW-SE direction (Roy and Jakhar, 2001) and also by numerous parallel large to small sized lineaments (Bajpai, 2004).

3.7 Tectonism and Seismic Zonation

The Luni river catchment is a sedimentary basin with active tectonics (Agnihotri et al., 2021), explaining the major component of the tectonic framework of the river basin. A tectonic framework helps understand the overall impact of tectonics and the pulse of its impact on the surface processes. The fabric of tectonostratigraphic, sequence of basin sediment composition, and the crust's basic evolution are crucial to understanding the tectonic framework (Li et al., 2015; Roy and Chatterjee, 2015; Biswas, 2016; Zhang et al., 2018). Bajpai, Roy and Tandon (2001) explain Luni's high tectonic activeness with ≥300 m of sediment accumulation coverage.

In the Fig. 3.5, the composition of the tectonic framework for the Luni river basin is based on eight types of classes. The above figure is being substantiated by Table 3.5 defining the areal coverage and percentage cover of the tectonic framework. As observed in the map, the dominant class is found to be represented in a shade of mustard yellow, representing the alluvial fill in intra-cratonic depression constituting 46.36%. The Luni river basin has been being a part of the famous paleo-Swaraswati river with its major orientation of drainage along the Indus cutting across the region of Ghaggar - Hakra river traced from the geochemistry of sediments (Chatterjee and Ray, 2018) of Punjab plains and the other along the region of Thar desert. Advanced sediment dating and quaternary isotopic analysis conducted by different researchers (Khonde et al., 2017; Chatterjee et al., 2019; Saini, Alok and Pant, 2020; Roy, Tandon and Singh; 2021) in this region has shown how the inter-cratonic linear depression has been

systematically filled up with alluvial sediments from the time of evolution. The central portion of the Luni watershed as observed in the shade of grey represents Late to Post Tectonic Granitoid with a composition of 30.2%. A granitoid complex is a unit of the tectonic framework which has a stable cratonic base demarcated as a low-risk earthquake zone (Zone -II) as also can be validated by observing the seismic zones in Fig. 3.6. The Aravalli on the east contributes 15.97% to the next important tectonic contribution in the form of the Proterozoic fold belt being part of the relict mountains dating back to the days before the Himalayas were formed. The rest types of the tectonic framework are all scattered in between the previous three dominant framework classes in form of Shelf facies cover in intra-cratonic sag (including low - moderate strained folded cover), Acid Volcanics, Ophiolite / Melange, Unclassified Gneissic Complex and Eperic Sea/Marginal Overlap Cover (in Pericratonic Sag). These complexes are either intrusive types or resultant formation of high-grade metamorphosis. Hence, the tectonic characteristics of the Luni watershed are much understood through the alluvial fill in intra-cratonic linear depression, which is vital to explain the river channel character, types of river sediments, and paleo form in the past. Behavioural study of Luni can be undertaken to incorporate the tectonic fabric, which can help conceptualize the reasons for specific behavioural patterns of the Luni river.
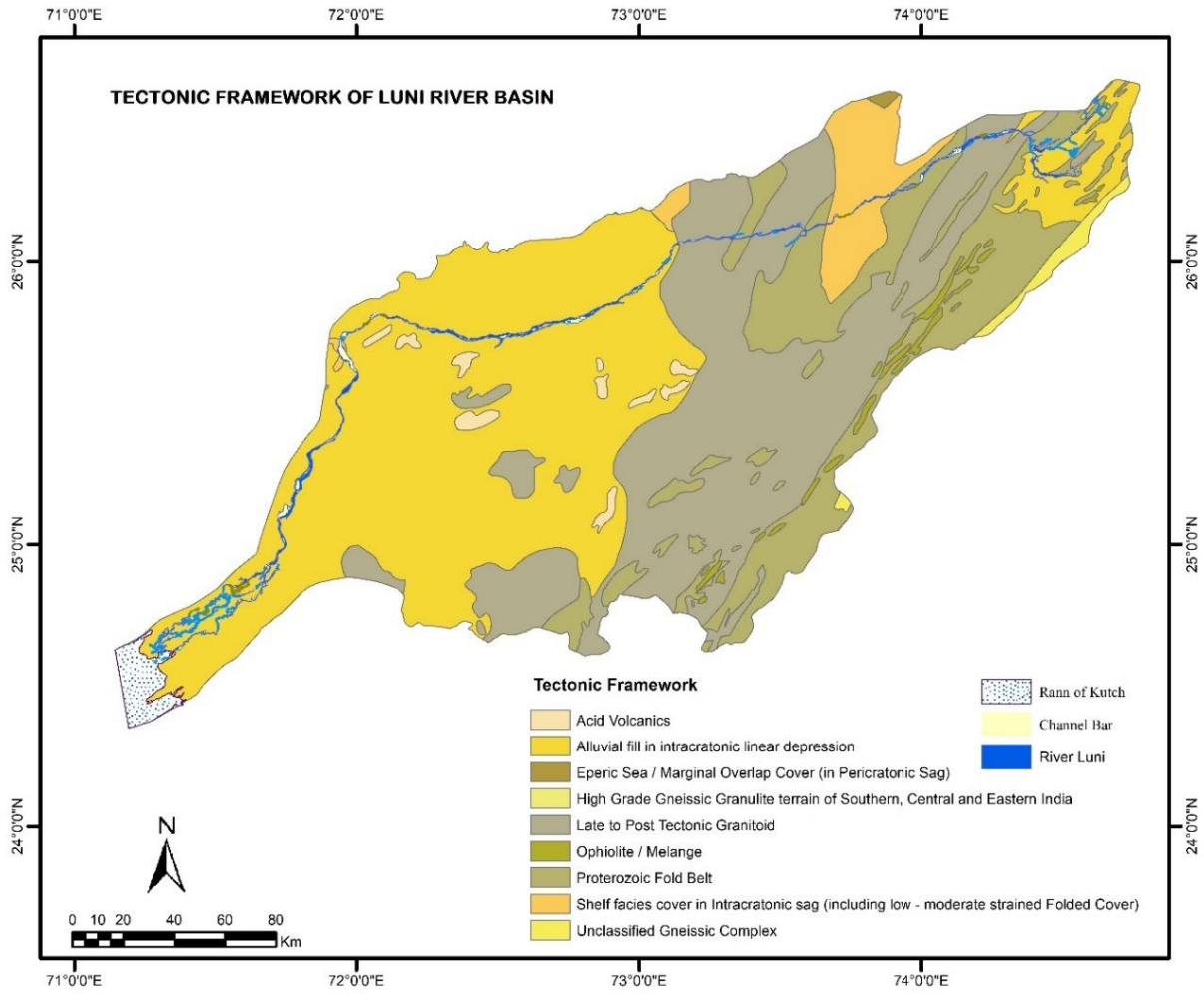
Fig. 3.5: Tectonic Framework of Luni river basin. Prepared by the researcher based on the GSI tectonic framework maps of Rajasthan and Gujarat, 2018.

Table 3.6: Distribution of Tectonic framework of Luni river basin

Tectonic Framework	Area (km²)	Coverage (%)
Alluvial fill in intra-cratonic linear depression	18209.33	46.36
Late to Post Tectonic Granitoid	11860.48	30.20
Proterozoic Fold Belt	6272.05	15.97
Shelf facies cover in intra-cratonic sag (including low - moderate strained folded cover)	1785.85	4.55
Acid Volcanics	396.28	1.01
Ophiolite / Melange	380.13	0.97
Unclassified Gneissic Complex	334.60	0.85
Eperic Sea / Marginal Overlap Cover (in Pericratonic Sag)	39.46	0.10

Source: Computed by the researcher.

The neotectonics and seismic zonation map in Fig. 3.6 explains the range of the Bouguer anomaly and the earthquake or seismic hazard zones present within the Luni river basin. In simpler terms, Bouguer anomaly can be defined as the datum level showcasing reduction of gravity for an arbitrary elevation. It is referred to as geoid by the difference between the gravity observed reduced to the particular geoid and the gravitational reference upon the geoid (Nozaki, 2006). The variations of Bouguer anomaly are used by geologists and geophysicists to investigate geological discontinuities and variations on land. In the above figure, the values of Bouguer anomaly vary from +40 to -60 milli-gal (mgal). The negative gravity anomalies across the Luni river basin ranging from -1 to -60 mgal represent the deposition of sediments over an uneven basement (Bajpai, Roy and Tandon, 2001) consisting of Marwar Supergroup formations (Bajpai, 2004). Such values are observed in the eastern and northern sections of the basin over the Aravalli and the extensive pediment-pediplain complex. Positive anomalies are observed over the western part of the basin as well as near the source of Luni, ranging in between +10 to +40 mgal primarily due to more even basement formed from the quaternary alluvial fills of Luni river and the aeolian sediments from Thar. The anomaly profiles also indicate the activation of the basement along with horst and graben structures for which most of the rivers within the catchment align and lie within the gravity low structure or grabens (Bajpai, Roy and Tandon, 2001). Such a study reveals the gravitational variation in various watershed parts and is essential to substantiate the neo-tectonic impact for finding out the geological aberrations.
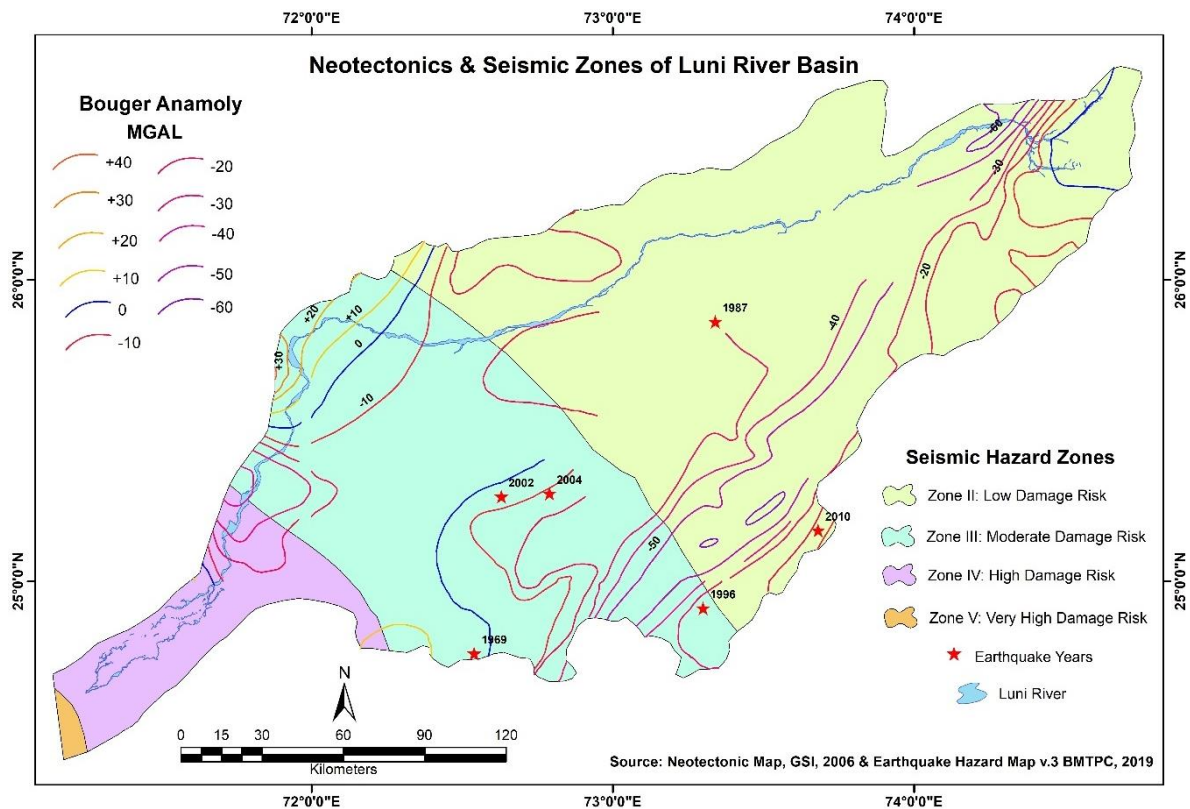
Fig. 3.6: Neotectonics and Seismic Zones in Luni river basin. Source: Prepared by the researcher based on the neo-tectonic and seismic zone maps of Rajasthan and Gujarat, 2019.

The second part of the map exhibits the most interesting part of the Luni catchment. Luni river basin is one of those rare natural units that consists of all significant four types of earthquake hazard zones. These hazard zones are classified according to the BMTPC Vulnerability Atlas of India v. 3.0, 2019. The maximum coverage of the basin comes under Zone II: Low Damage Risk zone (56.08%), followed by the Zone II: Moderate Damage Risk zone (35.32%), Zone III: High Damage Risk zone (8.20%) and Zone IV: Very High Damage Risk zone (0.39%). The progression of earthquake risk declines from mouth to source, the maximum risk is found at the inland deltaic region of Luni adjoining the Rann of Kutch, noted for very high intra-plate seismicity associated with major lineaments in the form of faults and joints/fractures (e.g. Bhuj earthquake, 2001). Inorder to substantiate the hazard intensity of earthquake zones, past fifty years earthquake event data was collected from National Centre for Seismology. Very low to moderate magnitude earthquakes were recorded in 1969, 1987, 1996, 2010, 2002 and 2004, majorly falling under Zone III. Hence, the earthquake hazard zones, their perpetual risk-based intensity, and Bouger anomalies observed over the riverscape make a novel approach in understanding the sensitivity of the landscape, its seismic activeness, and characterizing the river behaviour.

3.8 Hydrogeology

Hydrogeological studies reveal the internal processes, movements, distribution of groundwater water. The context of hydrogeology also indicates how a river is a significant constituent of surface water helps in groundwater formation, movement and storage. Luni is a central river basin of the entire state of Rajasthan and is vital to understand its hydrogeology for taking up groundwater condition and survey, helpful for devising vital agro-economic and public welfare policies. In the perspective of river behaviour, groundwater movement plays an essential role in understanding river water flow and the related dynamics. The concept of 'gaining' or 'losing' streams help to understand the groundwater and riverine interactions better.

The aeolian deposits in the Luni river basin extensively vary from fine to very fine sand and slit, which are majorly alluvial. The aeolian deposits of Thar occurring in west Rajasthan have moderate to high yield potentials of groundwater. These are well-sorted and permeable with a poor natural recharge and deep-water Table. According to the reports of GWD, Govt. of Rajasthan (2013), the aquifer type predominantly found over the entire Luni river basin is composed of alluvium both younger near the active floodplain of Luni and the major tributaries and the older ones near the pediment-pediplain complex. Alluvial aquifers are present in most of the central and western parts of the basin, with few intrusions in the north. Granite is the next dominant type of aquifer present in the south and southeastern parts of the basin.

The map in Fig. 3.7 contains the most engrossing information about the Luni river basin's hydrogeological status and groundwater potentiality. The aquifer deposition is fairly thick and discontinuous in the southern and along the northern section of the river basin with a regional extensive unconfined to confined aquifer down to 330 meters below ground level (mbgl). The north-western section comprises of discontinuous unconfined to semi-confined aquifer down to 375 mbgl. The central area of the basin has discontinuous confined aquifers down to 80 mbgl, restricted on weathered mantles and fractures. The eastern part of the watershed is covered with discontinuous unconfined to semi-confined aquifers down to 150 mbgl determined within fractures and weathered mantle roots of the Aravalli. The entire basin is dominated by aquifers having secondary intergranular porosity and fractures ranging in between 5-25 litres per second (lps) with the only exception in the northwestern section having a lower value of 1-5 lps. Compact formation with meagre yields of ≤1 lps is found near the Aravalli and scattered in the entire basin represented in red. The water level contours show that the southern section of the river basin has a water level ≤100 m while it increased to ≥300 m in the northern part and then a sharp decline in the northeastern tip of the basin. The

groundwater potential yield in lps is based on the primary intergranular porosity. Majorly <10 lps is the groundwater yield of the Luni river basin but in the southern section near the Luni and Sukri river confluence, the yield of groundwater is found to be 10-25 lps and with a major highest yield patch (represented in the deep blue shade) >40 lps.
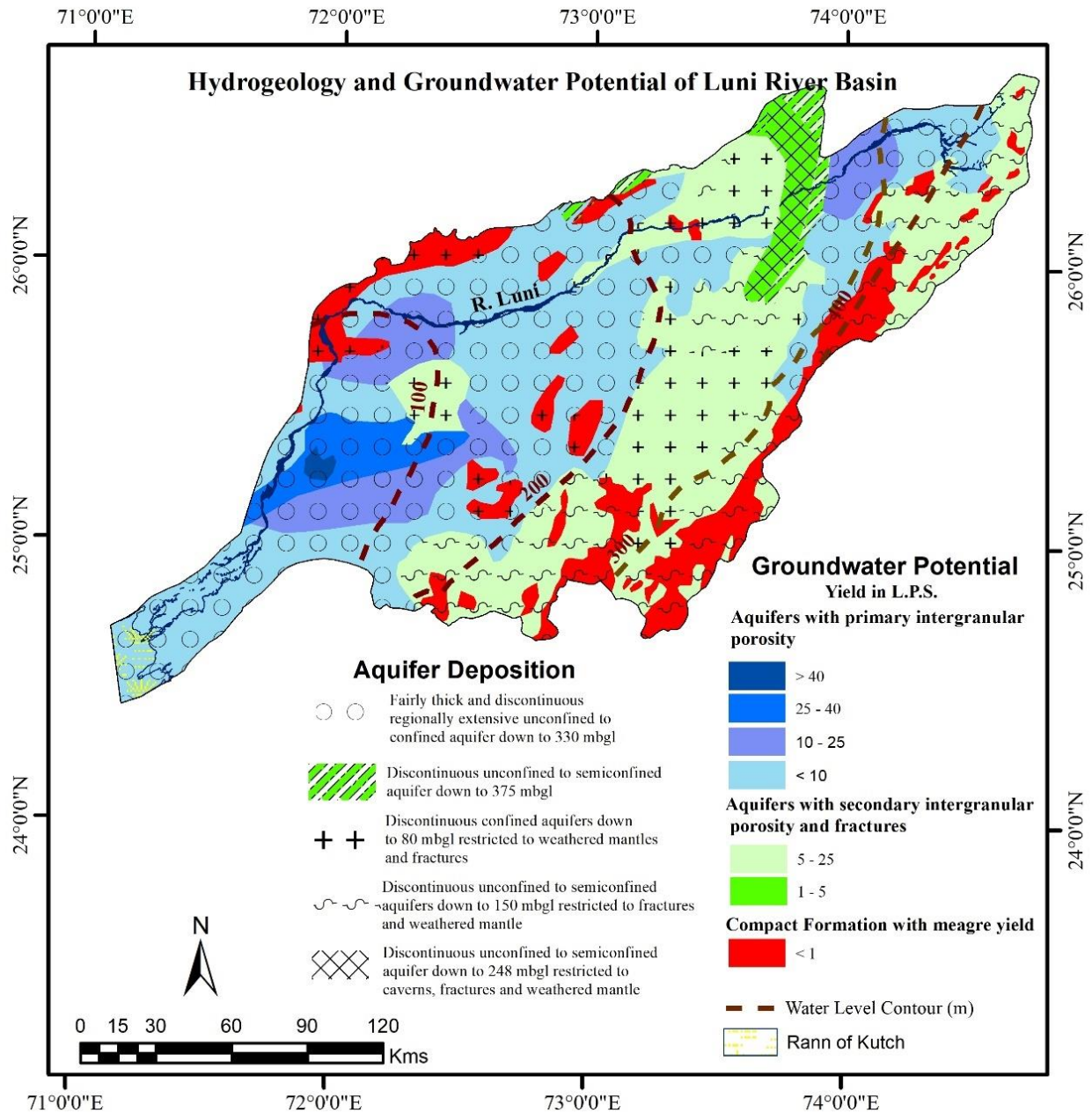
Fig. 3.7: Hydrogeological status and Groundwater Potentiality of Luni river basin. Source: Prepared by the researcher based on the NAQUIM maps of CGWB of Rajasthan and Gujarat, 2017.

The groundwater conditions are further explored from the reports of GWD, Govt. of Rajasthan (2013) showing the basic depth to the water level in the basin ranges in between 10-40 mbgl

which is also seen in the groundwater potential yield layers. These depths to water level are seen in western, central, northeastern and southwestern parts of the watershed. Two pockets, one in the west (Balotra-Siwana-Sayla-Bhinmal region) and the other in the north (around Merta), have water quite deep-water levels varying from 70-100 mbgl and sometimes reaching up to 130 mbgl. The water level fluctuation is another important parameter to showcase the stability of groundwater, its usage, availability and storage. Wide fluctuations are observed in between -8 m to +18 m. The instability is a rise from nominal to a compelling high level in Sirohi and the hilly areas of the other districts in the east. The alluvial fill areas of Jalor, Barmer, and Nagaur has the most minor fluctuation level within a range of ±2 m. Certain localized phenomena like high groundwater exploitation due to industrial or farming activities showcase a fall in water levels or high unfavourable fluctuation.

3.9 Hydrological Behaviour

The studies related to hydrological sciences, especially for a river basin is time and space only factor. The increasing interruptions posed by anthropogenic activities like agriculture, irrigation, alterations in land use, reservoir management, rapid urbanization are consequently modifying the flow regimes of rivers and the landscapes at unprecedented rates (Grant, 1997). These factors have highly transformed the riverine systems with specific damaging impacts, which are irreversible and have hampered the ecological flow and the natural habitat of the riverine corridor. The climatic implications and topography, soil and slope conditions are considered the key determinants of hydrological alterations that affect the river's flow.

Aeolian or dryland rivers are typically characterized by zero flow throughout the year except for any high precipitation events, which bring a sudden gushing flow into the stream with a considerable peak discharge which alters the channel morphology depending upon the flow velocity. Being a dryland river of the Thar, Luni imbibes these characteristics and behaves differently from any other river belonging to a commonly found climatic setup like those in the semi-arid or tropical parts of India having a perennial or a non-perennial source of water.

The hydrological study is conducted for Luni using the Gauge-Discharge (GD) data collected from the office of Executive Engineer, Mahi Division, Gandhinagar, Gujarat for the years 1990 till 2016 for Balotra station (25°49'17.22"N, 72°14'30.91"E) situated in the upstream part of Luni and from 1978 till 2016 for Gandhav station (24°59'22.73"N, 71°40'57.18"E) in the downstream part just before the Luni channel splays into the floodout. Data is recorded manually during 08:00 am IST especially in the monsoon season when the river receives the

most regular flows. The GD data is a mixture of mostly computed form with few observed data. Maintenance of hydrological data in this river is mostly neglected due to the absence of riverine flow throughout the year which is a major loss for scientists to analyze the character and nature of the river providing a detailed insight into the river behaviour. Prolonged maintained water level and discharge data can help in understanding the pattern and flow regimes of the river and sort out the uncertainty and stochastic events with special emphasis on studying anomaly events like flash flood occurrences. The GD dataset for Balotra is available from 1990-2016 and for Gandhav, the dataset is available from 1978-2016. Gandhav is the oldest GD monitoring station maintained by CWC, while the one at Balotra is established years after the infamous 1979 floods in Luni. The channel width of Luni at Balotra is 424.60 m and at Gandhav is 756.12 m which are determined from the Google earth platform using a ruler tool to measure the approximate distance of the channel just along the local bridges in which the scale for measuring water level is drawn on the bridge pier. The locations of the two GD stations of Balotra and Gandhav are shown in figure 3.8. Thus, for a better geomorphological investigation, the hydrological purview needs to be well documented especially for an arid river like Luni which has unique streamflow movements unlike those of the major glacier-fed perennial channels or the bedrock non-perennial river channels of Deccan India.

Fig. 3.8.: Location map of CWC GDS along the Luni river – Balotra (Upstream) and Gandhav (Downstream). Source: Prepared by the researcher based on the Google Earth imagery.

3.9.1 River Regime and Annual Hydrograph

The regime of a river refers to the seasonal pattern of flow over the year. River regimes have been identified by Haines et al. (1988) as having an important influence on the different river attributes such as its ecology. Regime identification is essential for understanding the river's nature; the seasons of a high regime (potential water availability) and low regime (shortage periods) correspond to ecological impacts along the channel. The riparian vegetation, the river organisms as well as the human population which inhabits the corridor behave following the river's regime. The changes in the seasonal regime of the Luni could be analyzed by plotting the mean monthly discharge of the station (Fig. 3.9). This is the simplest means of understanding the flow patterns of the river. It is seen that the mean monthly discharge for August is the highest, whereas it is the lowest in May. Thus, it can be generally concluded that the Luni river has a monsoonal regime, which means that its flow condition is highest after receiving the highest rainfall during the monsoon months of July and August. There is no increase in the mean discharge after the winter months because the basin does not receive water from snowmelt or very high rainfall from the western disturbances. By using the Haines et al. (1988) method of classification of river regime into 15 classes, the Luni river falls in the Group 7 class, which is the 'Extreme late summer' regime. The average flows are expressed as percentages of the mean annual flows.

The annual average discharge of the Luni river (Fig. 3.10) is found to be generally nil or dry throughout the years typifying its arid ephemeral nature. The modal peaks of hydrographs are observed in 1990 and 1995 with a considerable annual average discharge for Balotra. Low peaks are observed in 1997, 2007 and 2016. A similar type of annual hydrograph is observed for the downstream GD station Gandhav. High peak flows indicated by the multi-modal peaks of the hydrograph in 1979, 1983, 1990 and 1995 exhibit the annual average high flows. Shorter peaks are observed for the years 1992, 1997, 2002, 2007 and 2016. The yearly average values provide a contained idea about the minimal and high event-based flow of the Luni river, hence catering for the behaviour of Luni as a dryland riverine system.

A considerable data gap with no such predictable trend is found for flood frequency in the Luni river. Dryland rivers are purely dependent on precipitation to have streamflow and the nature of peak flow events are restricted to the non-conventional flash floods marked by high intensity rainfall over a short timeframe which are a bit unpredictable. The return period of the highest magnitude discharge recorded for Balotra is 27 years with a discharge of 2907 m^3s^{-1}, while the

infamous 1979 floods in Luni recorded at Gandhav with ever highest discharge recorded in a single day is 4300 m^3s^{-1} has a return period of 39 years.
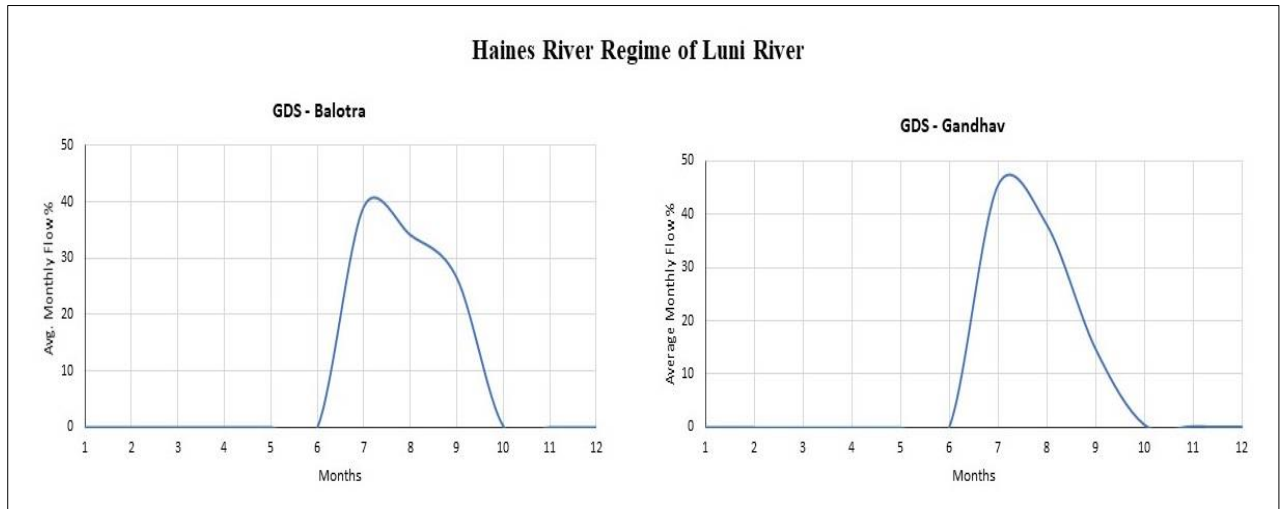
Fig. 3.9.: Haines River Regime of Luni river derived for two GDS – Balotra (Upstream) and Gandhav (Downstream). Source: Computed by the researcher based on the CWC GD data.
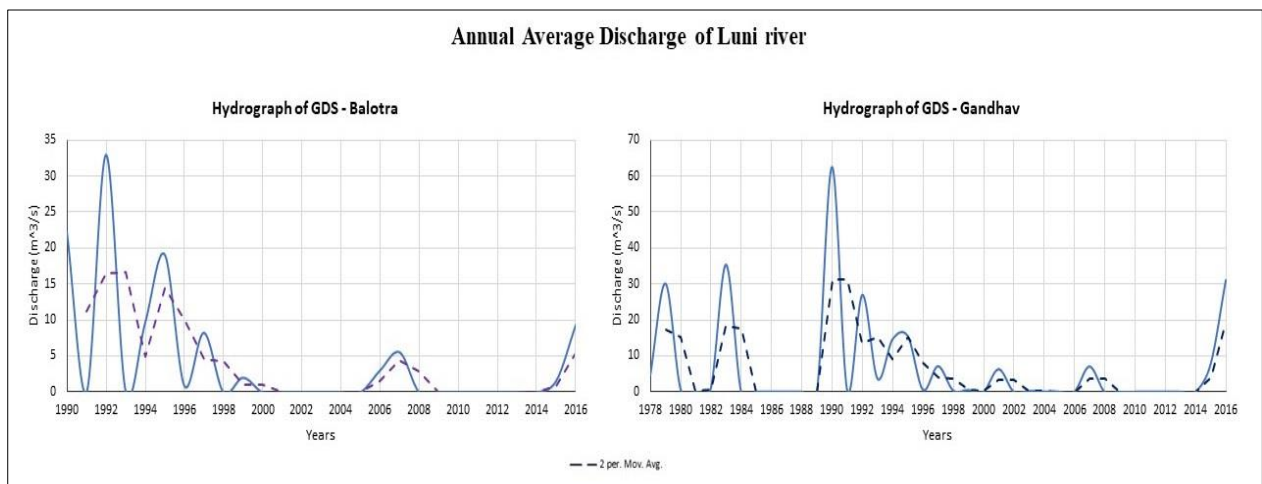
Fig. 3.10.: Annual Average Discharge of Luni river derived for two GDS – Balotra (Upstream) and Gandhav (Downstream). Source: Computed by the researcher based on the CWC GD data.

3.9.2 Hydrological Data Analysis for two GDS on Luni river

- **Annual Monthly Water Level –** The AMWL is based on the water level observed along with the GDS of Balotra recorded daily (Fig. 3.11). Each day's water level (WL) is measured to have the idea of how much amount of water is flowing through the river. The

daily dataset is converted into a monthly scale and superimposed over each other from 1990-2016. The reduced level (RL) of zero gauge for the Balotra GDS is 102 m above mean sea level. Thus, each observation of WL needs to be subtracted from the RL value to get the actual level of water flowing in the river. For instance, on the 22nd July of 1990, Balotra records a WL of 128.65 m, which means the actual flow in the river is (113.65-102) m = 11.65 m from the river bed. The WL is found to concentrate over the monsoon months from June till the first week of October with few years having AMWL above the RL of zero gauge, indicating its ephemeral character.

Gandhav experiences a similar water level showing a peak exclusively in monsoon months. The RL of zero gauge is 31 m above mean sea level. The distribution of observable high flow events of 1979 and 1990 can be discerned from the water level (Fig. 3.14). The Sukri confluence with the Luni river just above the GDS of Gandhav and hence has its flow contributed into the Luni channel, for which even beyond the monsoon months meagre water flow is observed during the pre-winter months.

- **Annual Monthly Discharge** – The AMQ is computed from the raw daily dataset which is converted into a monthly scale and superimposed over each other from 1990-2016 (Fig. 3.11). The AMQ records maximum discharge during the monsoon months from June to September and perfectly complements the AMWL. Balotra being situated on the upstream part of Luni gets the maximum amount of flowing water from the adjacent runoff channels and the upstream tributaries during the monsoon season. The year 1990 shows the maximum AMQ at Balotra.

The GDS at Gandhav experiences a similar monsoonal unimodal peak of discharge (Fig. 3.14) having perfect synchrony with the AMWL. Throughout the years the AMQ is limited from June to September with a further extension till the first week of November in few exceptional years. This condition suggests the dry non-perennial river regime of the Luni river. The highest discharge leading to flash floods in 1979 is also evident from the graph.

- **Annual Monthly Stream Power –** Stream power is hence defined as the amount of energy lost against the river banks and its bed per unit of the downstream distance. It is the potential energy lost when the river water flows due to friction or the specific work done by the river against its bed and banks. Stream power can also be equated as the decline of the potential energy to the force exerted against the bed and banks of the river. The actions associated with the stream power are the discharge, river bed slope, supply of sediment and action of gravity which is balanced by the strength of bedrocks materials, sediment particle size and

the force needed to shift the materials. The AMSP is calculated based on the annual monthly discharge dataset fitted into the equation,

$$\omega = \rho g Q S \quad \text{(Eq. 2)}$$

where ω is stream power expressed in $W^{-1}m^{-2}$, ρ is the river water density assumed to be as 1000 $kg^{-1}m^{-3}$, similar to the freshwater density, g as the gravitational acceleration of 9.8 $m^{-1}s^{-2}$, Q is the amount of discharge in $m^{-3}s^{-1}$ and S as the local slope of the channel which is measured as 0.0003 $m^{-1}m$ at Balotra and 0.0007 $m^{-1}m$ at Gandhav.

Balotra (Fig. 3.12) and Gandhav (Fig. 3.15) exhibits the highest AMSP during the monsoon months from June to September for most of the years having a positive correlation with the discharge. Peak flow events like flash flood conditions extrapolate the amount of erosion by the gushing streamflow. The lesser channel depth and greater channel width in both the gauging stations put forth the possibility of an average stream power eroding the bank of the Luni because of its less resistant and fragile composition with sand. Hence, stream power is vital for Luni's behaviour in channel development to procure the ongoing consistency with channel avulsions and splay outlays. The channel tends to break away during a high flow event associated with isolated greater impact of stream power events.

- **Annual Rating Curve –** The ARC is showing the relation of the water level (gauge height) to the discharge. This is a positive correlation since as the discharge increases, the water level rises as well, with the cross-sectional area of the river remaining largely static here. Points are plotted versus the accompanying stage, and a smooth curve is drawn through the points. A high positive correlation is represented by the polynomial trendline of ARC for GDS Balotra (Fig. 3.12) with an R^2 value of 0.93. The GDS at Gandhav represents a very low positive polynomial trend with an R^2 value of 0.05 for the ARC due to a longer dataset from 1979-2016 compared to that of Balotra from 1990, having more years of zero flow.

Table 3.7: Comparative status of hydrological parameters computed for the Luni river along its two GDS.

Sl. No.	Hydrological Parameter	Abbreviation	Unit	GD Monitoring Stations		Reference
				Balotra (Upstream)	Gandhav (Downstream)	
1	Annual Monthly Water Level	AMWL	m	Increase of water level during peak flows in the monsoon months.	The rising water level in the monsoon and contribution of river water from adjoining Sukri river, adjoining with Luni just upstream of Gandhav,	Fig. 3.11 & 3.14
2	Annual Monthly Discharge	AMQ	m^3s^{-1}	Only monsoon-based discharge in the river from June to September up to November as water remains flowing in Luni.		
3	Annual Monthly Stream Power	AMSP	$W^{-1}m^2$	Stream power is directly proportional to the river discharge found to be present in monsoon months only.		Fig. 3.12 & 3.15
4	Annual Rating Curve	ARC	Unitless	A rising water level with increasing discharge in the river with a positive trend and a stable cross-sectional area.		
5	Zero Flow Months	ZFM	%	Dry months except the monsoon has zero streamflow in the river.	Zero flow in the river is found to dominate in the maximum except the monsoon season with fewer exceptional flows due to local precipitation events and local flows from the Sukri river.	Fig. 3.13 & 3.16
6	Zero Flow Months Index	ZFMI	Unitless	Higher values indicating no flowing river water in the GDS and lower values indicate years having low to considerable discharge as observed.		
7	Decadal Trend of Average ZFM	DTAZFM	%	The rising trend of zero flows with a decline in the recent decade.	The falling trend of zero flows during the second decade with a recent rising trend.	
8	Flashiness Index	R-B Index	Unitless	GDS based analysis observing the flashy flows during a daily flow event indicated by R-B Index = 1 meant for a sudden rise in discharge from a minimal or zero flow.		Table 3.8 & Fig. 3.17

Source: Compiled by the researcher.
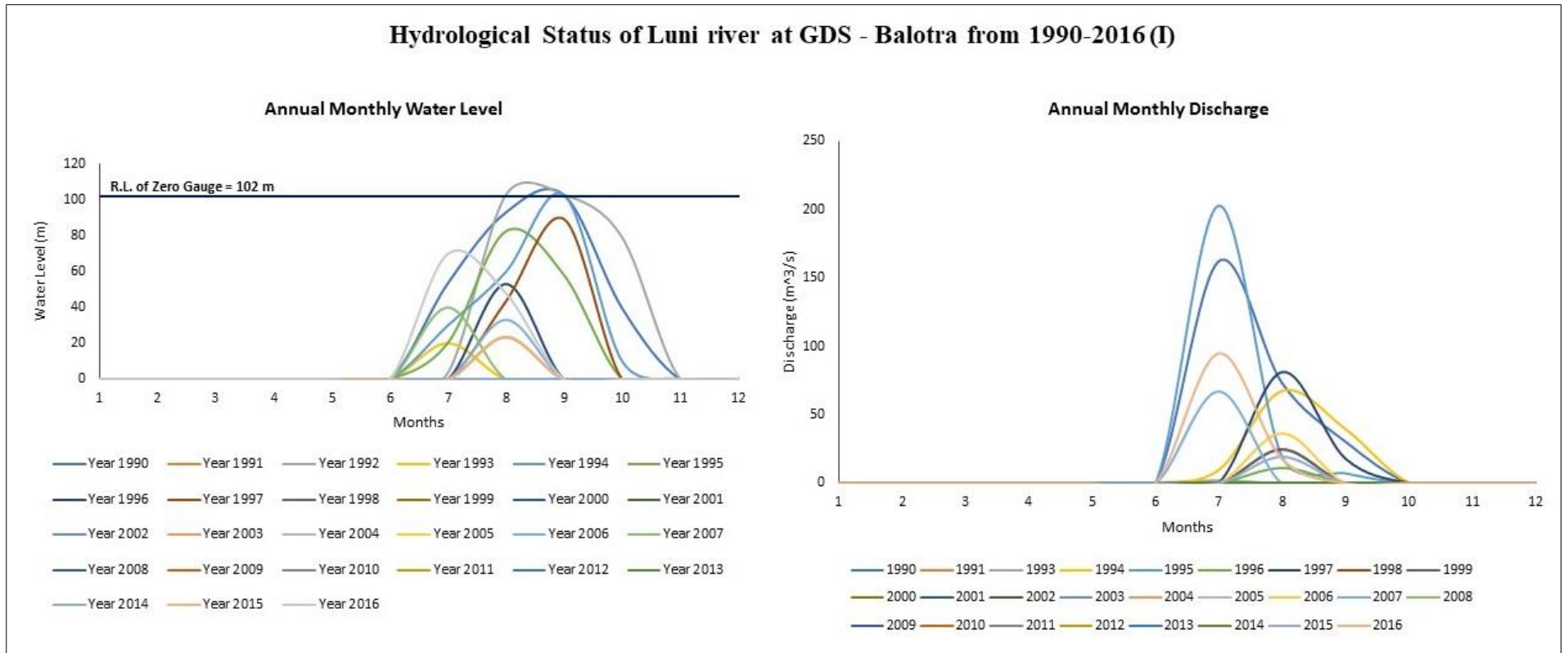
Fig. 3.11.: Annual Monthly Water Level and Discharge observed at GDS- Balotra from 1990-2016. Source: Computed by the researcher based on the CWC GD data.
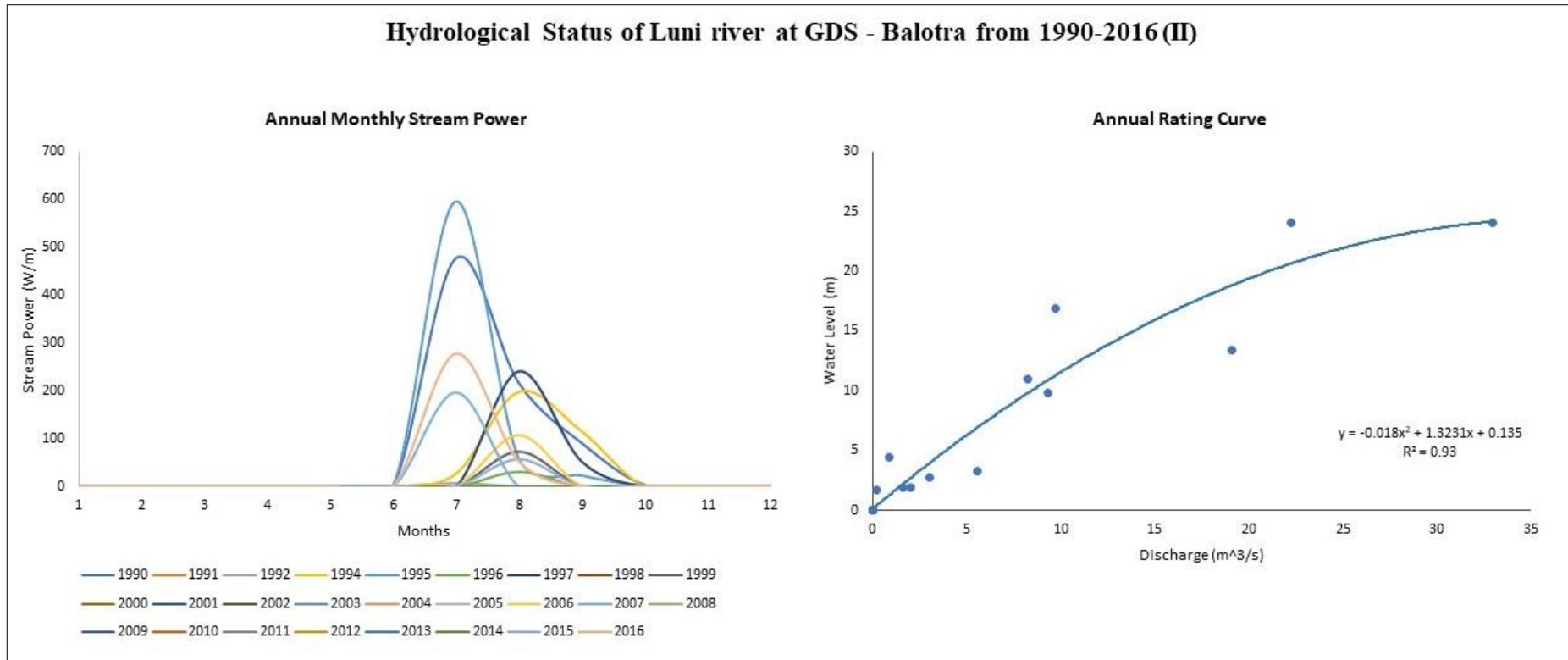
Fig. 3.12: Annual Monthly Stream Power and Annual Rating Curve observed at GDS- Balotra from 1990-2016. Source: Computed by the researcher based on the CWC GD data.

Fig. 3.13: Hydrological evaluation of Zero Flow Months at GDS – Balotra (1990-2016). Source: Computed by the researcher based on the CWC GD data.

- **Zero Flow Months –** Zimmer et al. (2020) explain the seasonal zero-flow readings can be caused due to various factors like arid conditions as dominates in the Luni river for most of the days in the year, both in pre and post-monsoon seasons. But, the other range of natural factors leading to zero flow gauge readings are frozen surface water, reversal of flow in tidal mouths, equipment or data error, evapotranspiration and transmission losses at the gauging site, bypassing the gauge due to sub-surface flow. The human-based factors like excessive pumping of groundwater or water withdrawals from the river channel due to farming activities can also lead to zero flow conditions in the Luni river. Kar (2018) highlights that due to the construction of local water check dams and anicuts in the upstream areas of the tributaries of the Luni river along the Aravalli ranges has led to dry river conditions downstream with no flowing water and restricting the natural function of streams in the sandy plains.

The maximum days throughout the year is found to have a zero-water flow and discharge at both the gauging sites of the Luni river. Thus, the zero flow days are converted to ZFM for a better and lucid analysis of the zero flow conditions, making the data concise. At GDS Balotra (Fig. 3.13) and Gandhav (Fig. 3.16), the lower percentage represents those years having some amount of streamflow while the years having a higher percentage represents no flowing water observed at the respective gauging stations. A two-year moving average trendline was fitted in order to discern the tendency of the dataset.

- **Zero Flow Months Index –** ZFMI is computed based on the ZFM where the values have been normalized and plotted with a scatter plot to have an enhanced understanding of the ZFM. The ZFMI for Balotra (Fig. 3.13) and Gandhav (Fig. 3.16) shows that values tending towards 1 are marked by nil streamflow, while the lower values tending towards zero shows the river having considerable discharge. Hence, ZFM and ZFMI share a negative correlation with streamflow, i.e., higher ZFM or ZFMI is associated with zero flow in the gauging site and vice-versa.

- **Decadal Trend of Average ZFM –** DTAZFM gives the trend-setting of the zero flow months in the past decades for both the GDS. A rising trend with a power trend line and a positive R^2 value of 0.75 represents an increasing trend of zero flow in the Luni river at Balotra over the past three decades at Balotra (Fig. 3.13). While a different scenario is observed at Gandhav (Fig. 3.16) where a polynomial trend line fits the dataset of DTAZFM with a moderately positive R^2 value of 0.49. The trend of decadal zero flow at Gandhav goes through a declining stage for the initial decade from 1979-1989, followed by an increasing condition of zero flow from 1990 onwards matching with the decadal ZFM

conditions at Balotra. This decadal trend over a longer time frame helps to comprehend the angle of increasing incidences of dry climatic conditions (suggestive of climate change) over the Luni catchment with fewer instances of flashy peak flow events occurring due to local, short duration and high-intensity rainfall events.
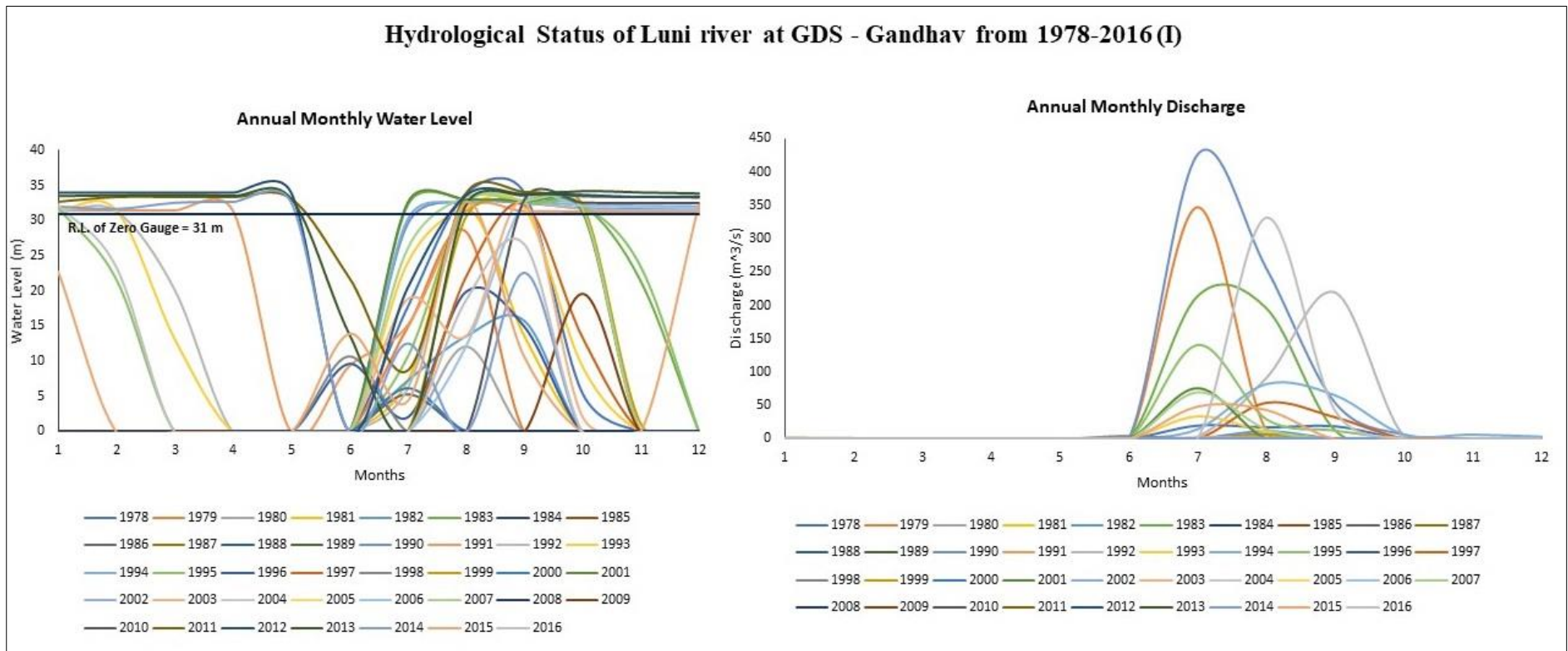
Fig. 3.14: Annual Monthly Water Level and Discharge observed at GDS- Gandhav from 1978-2016. Source: Computed by the researcher based on the CWC GD data.
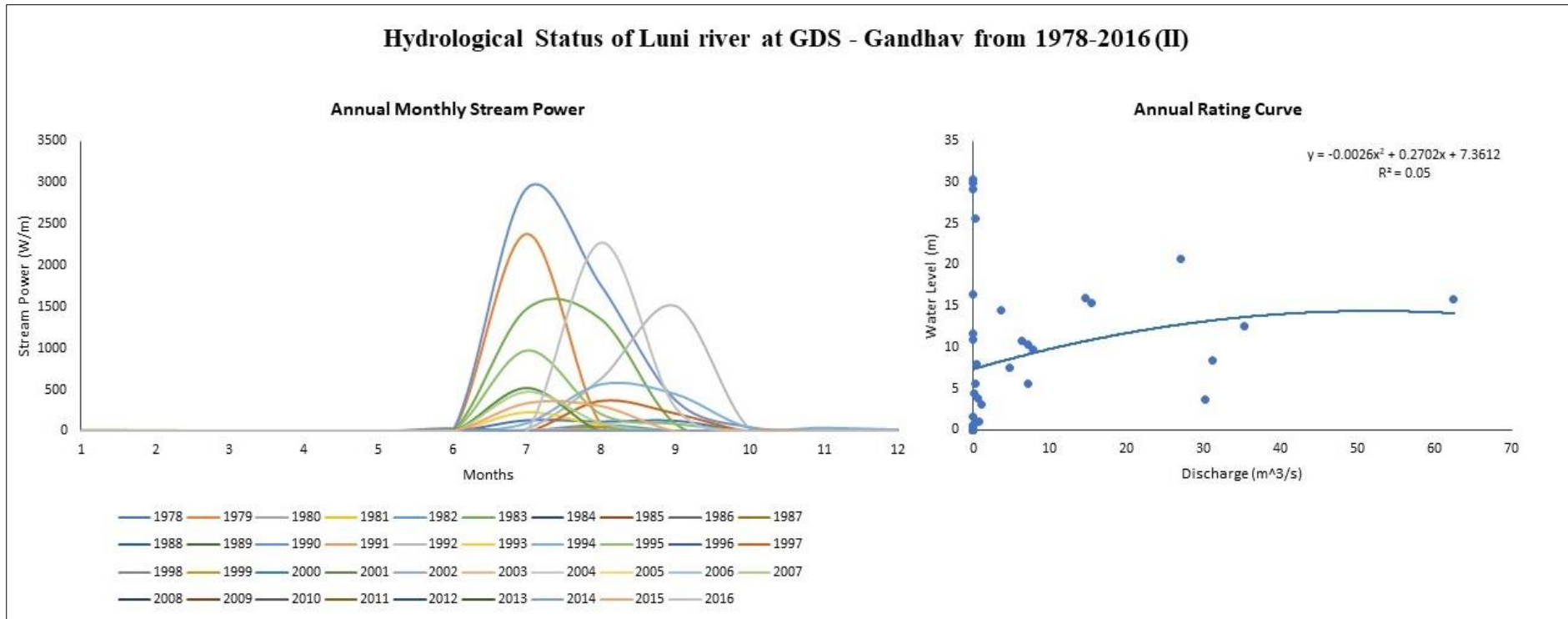
Fig. 3.15.: Annual Monthly Stream Power and Annual Rating Curve observed at GDS- Gandhav from 1978-2016. Source: Computed by the researcher based on the CWC GD data.

Fig. 3.16: Hydrological evaluation of Zero Flow Months at GDS – Gandhav (1978-2016). Source: Computed by the researcher based on the CWC GD data.

3.9.3 Flashiness Index

The flashiness index or known as the Richards-Baker Flashiness Index popularly abbreviated as R-B Index is used to determine the recurrence and swiftness in the river flow as a response to short-term storm events like flash floods (Baker et al., 2004; Fongers et al., 2007). The ephemeral character of the river introduces large flows during a high-intensity event where the stream water rises and declines quickly making them flashy by behaviour. R-B index brings forth the oscillations in the daily streamflow when compared to that of the average or summative scenario. It is computed as the proportion of the summation of variation of flows on two consecutive days to the total daily average flow in the river. The R-B index is positioned on the flow variability where it is found to be more susceptible to the altering trends compared to the discharge data (Baker et al., 2004; Fongers et. al., 2007; Pratama and Kusratmoko, 2018). The equation for computing R-B index is –

$$R - B \ Index = \sum_{i=1}^{n} |Qi - Qi - 1| / \sum_{i=1}^{n} Qi - 1 \qquad \text{(Eq. 3)}$$

where, Qi and $Qi\text{-}1$ are the average daily discharge (m^{3}s^{-1}) on day i and day i-1 (day after the ith day), respectively. The R-B index is unitless and a similar result can be procured when the discharge is replaced by the total daily discharge volume. The original values are found to be negative and in order to eliminate the negative sign the resultant value is kept within the parallel bracket. The inconsistencies over a while are usual in a river's R-B index values. The prolonged trend of fluctuations is an outcome of hydrological variations which are due to alterations in land use or modification in dam operations. The flashiness index is based on the gauging site observations only. The streams that are predominantly flashy at a particular location can become steady in downstream due to the devitalization of flashy flows by the tributaries of the trunk stream. Alike, flashy flows in the stream above the gauging station can be in a latent form by the merged flows of contributing tributaries at the gauge.

The Luni river has an ephemeral flow throughout the year except in the monsoon months as nourished by the rainfall from the southwest monsoon winds of the Arabian Sea branch. Since, minor fluctuations are generally observed in such a riverine condition, indicating the development of certain flashy events within the river. The conditional flashiness response of the Luni river is therefore obtained from the two famous flash floods events which were documented from the GDS of Balotra (upstream) in 1990 and at Gandhav (downstream) in 1979. In Table 3.8, the two peak flow events are evident from the daily flow data obtained from CWC. The GDS of Balotra is observed with a sudden discharge of 304.3 m^{3}s^{-1} on 5th July 1990

immediately after a day which was having zero flow. Thus, the value of the R-B Index = 1 shows the flashy or sudden peak discharge event at the gauging site. The days preceding 5th July 1990, discharge went up to 1875 and 1449 m³s⁻¹ respectively and an R-B Index value of 084 and 0.29 respectively.

Table 3.8: R-B Index for two prime peak flow events in the GDS on the Luni river.

GDS	Balotra (Upstream)		Gandhav (Downstream)		
Date	Discharge (m³s⁻¹)	|R-B Index|	Date	Discharge (m³s⁻¹)	|R-B Index|
04/07/1990	0	-	18/07/1979	0	-
05/07/1990	**304.3**	**1**	19/07/1979	**4300**	**1**
06/07/1990	1875	0.84	20/07/1979	2655	0.62
07/07/1990	1449	0.29	21/07/1979	1790	0.48
08/07/1990	0	-	22/07/1979	1050	0.70
09/07/1990	**356**	**1**	23/07/1979	550	0.91
10/07/1990	160.3	1.22	24/07/1979	188	1.93
11/07/1990	61.09	1.62	25/07/1979	100	0.88
12/07/1990	34.83	0.75	26/07/1979	56	0.79
13/07/1990	26.12	0.33	27/07/1979	36	0.56
14/07/1990	15.69	0.66	28/07/1979	24	0.50
15/07/1990	8.51	0.84	29/07/1979	20	0.20
16/07/1990	5.67	0.50	30/07/1979	11	0.82
17/07/1990	3.03	0.87	31/07/1979	3	2.67
18/07/1990	1.91	0.59	01/08/1979	1	2
19/07/1990	1.31	0.46	02/08/1979	1	0
20/07/1990	0.96	0.36	03/08/1979	1	0
21/07/1990	0	-	04/08/1979	1	0
22/07/1990	0	-	05/08/1979	1	0
23/07/1990	0	-	06/08/1979	1	0
24/07/1990	0	-	07/08/1979	11	0.91
25/07/1990	0	-	08/08/1979	46	0.76
26/07/1990	0	-	09/08/1979	110	0.58
27/07/1990	0	-	10/08/1979	96	0.15
28/07/1990	0	-	11/08/1979	64	0.50
29/07/1990	0	-	12/08/1979	45	0.42
30/07/1990	0	-	13/08/1979	24	0.88
31/07/1990	0	-	14/08/1979	8	2
01/08/1990	0	-	15/08/1979	1.5	4.33
02/08/1990	0	-	16/08/1979	1	0.50

Source: Computed by the researcher.

Similarly, the most dangerous flash floods observed in the Luni river was measured at Gandhav on 19th July 1979 with a sudden discharge of 4,300 m³s⁻¹ just after a day having no flow in the river. So, the R-B Index values of 1 exhibit flash flow in the river through the gauging site.

Higher R-B index values are obtained from large fluctuations in streamflow followed by index values close to zero indicating stable streamflow. Fig. 3.17 has been used to depict the relationship between discharge (X-axis) and R-B Index (Y-axis). Peak discharge events are found to be spread out as outliers in the graph for both the GDS. Gandhav has a more stable daily flow compared to Balotra as lower R-B Index scores of Gandhav represent the same. Balotra has more fluctuation in its flow with R-B Index values possibly due to series of rainfall events, evident from the daily flow data as well where a high discharge event was followed by a zero flow with a repetitive increase of discharge.
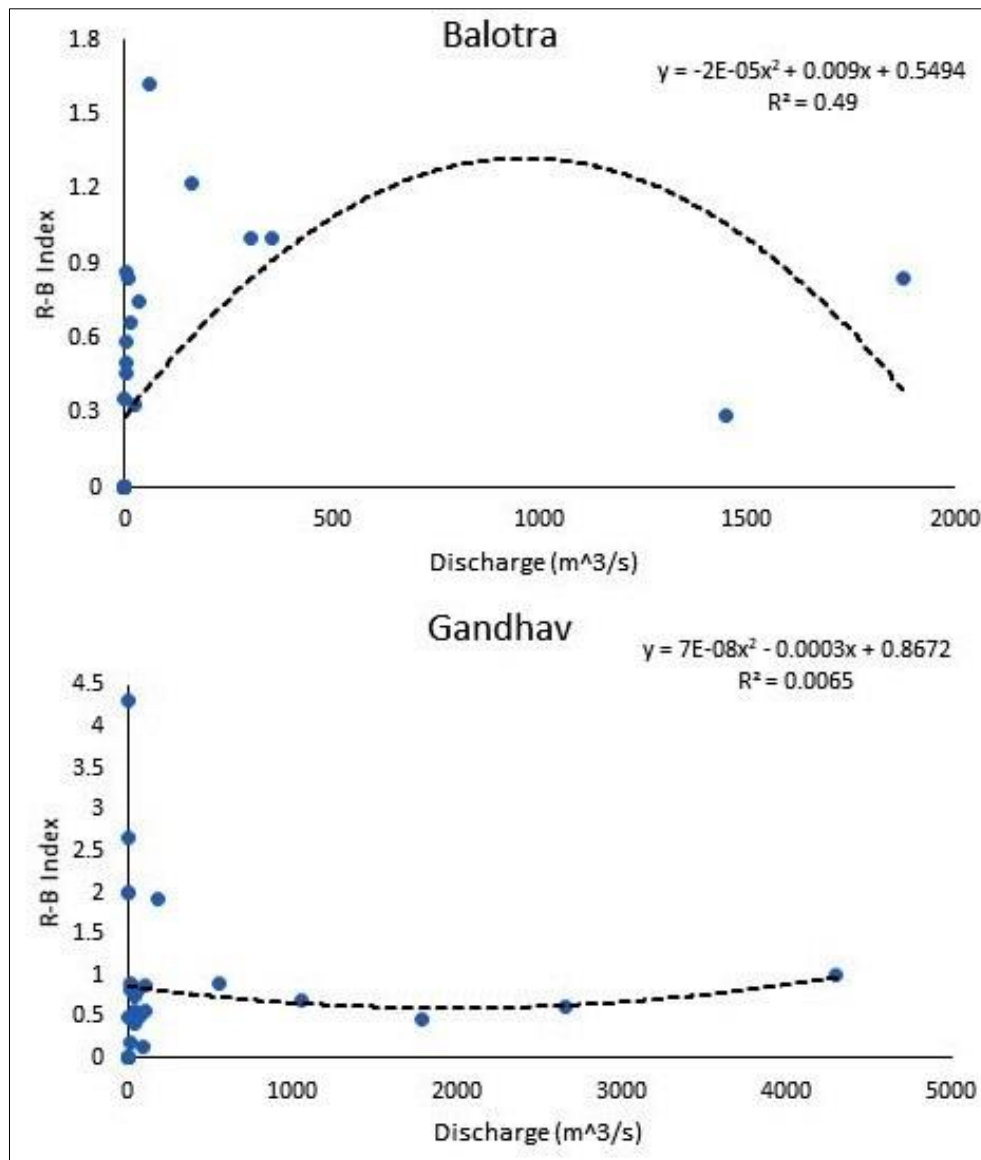
Fig. 3.17: Relation and trend of R-B Index with discharge observed for two peak flow events in the GDS on the Luni river. Source: Computed by the researcher.

3.9.4 Statistical Analysis of Annual Average Discharge

The descriptive statistical analysis for the Luni river comprehends the provided set of compiled average discharge data for each year, showcasing the scenario for upstream GDS Balotra from 1990-2016 and that of GDS Gandhav downstream of Luni from 1978-2016. Descriptive statistics are divided into two popular quantum – a measure of central tendency and measures of variability (or extent of the dataset). Mean, median and mode are the measures of central tendency, while minimum and maximum observations, range, variance, standard deviation, skewness and kurtosis are the measures of dispersion.

Table 3.9: Statistical parameters for annual average discharge for two GDS on the Luni river.

Sl. No.	Statistical Parameters	Annual Avg. Discharge Values		Interpretation
		Balotra	Gandhav	
1	Mean	4.26	6.58	Very low mean discharge, characterizing the arid/ephemeral riverine condition.
2	Median & Mode	0	0	Maximum months are having zero flows.
3	Standard Deviation	11.41	16.76	Higher SD indicating the spread of discharge values over a broader range, a few days experience peak discharge in a year while rest remains meagre to zero flow days.
4	Variance	551.90	1346.11	Variability of discharge with the extent of their spread out from the mean.
5	Minimum	0	0	Ephemeral flows or dry river beds with no discharge.
6	Maximum & Range	38.45	53.99	Monsoonal maximum flow with a lower range supporting the dry riverine conditions.
7	Skewness	1.42	1.68	High positive skewness.
8	Kurtosis	4.58	4.85	Leptokurtic

Source: Computed by the researcher.

The Table 3.9 explains the values of measures of central tendency and dispersion in the context of the average discharge of the Luni river. The mean values are very low enough for annual average discharge to be described for the individual designated periods. This is suggestive of dryland river conditions. The median and mode are zero as maximum months except the monsoon season have no discharge values. The standard deviation with considerable high values indicates the spread of discharge values over a broader range, a few days experience peak discharge in a year while rest remains meagre to zero flow days. The variability of discharge with the extent of their spread out from the mean explain the variance of the annual average discharge dataset. Minimum flows are found to be zero suggesting the non-perennial status. Maximum and range of annual average discharge suggest the dry river conditions and flows generated from precipitation events.

The lucid way to determine the variations in the monthly discharge is by plotting the mean and coefficient of variations which shows the influence of climatic parameters as well as other basin parameters. The skewness and the kurtosis of the GDS hydrological data gives an idea about the flow conditions concerning the distribution of discharge. The skewness and the kurtosis of the data gives an idea about the flow conditions. The discharge data is found to have a high positive skewness with a greater asymmetry for both the GDS. The kurtosis is defined by wider shape and bulky tails indicating a higher chance of positive event which is meant to be leptokurtic as observed from the respective values. The years having peak discharge are found to have a symbiotic relationship with the kurtosis curve. Lower peaks of kurtosis indicate minimal to zero flow in the river.
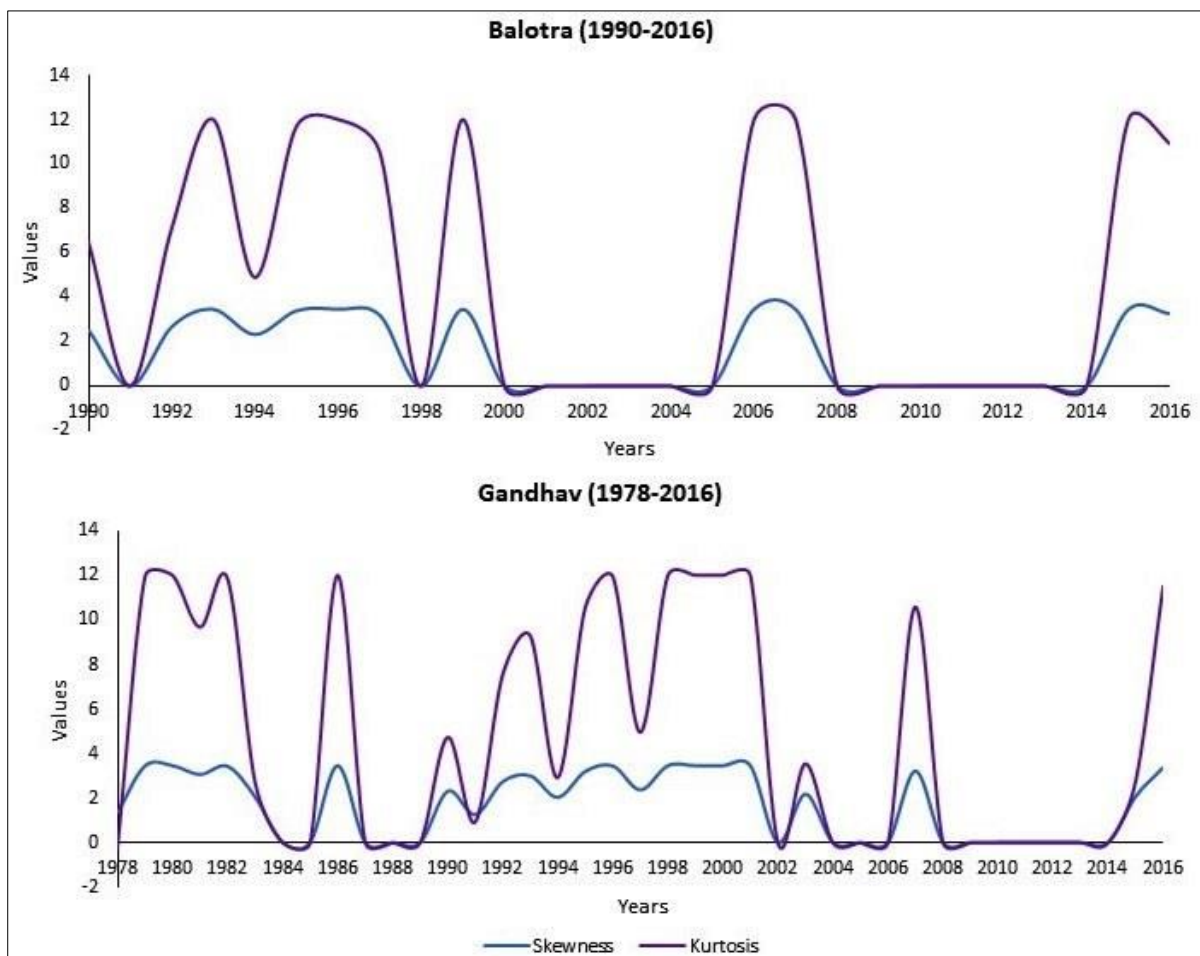
Fig. 3.18: Statistical Moments (Skewness and Kurtosis) for annual average discharge for two GDS on the Luni river. Source: Computed by the researcher.

3.9.5 Comparison of Discharge in upstream and downstream of Luni river GDS

The annual average discharge of Luni for both the GDS – Balotra and Gandhav needs to be compared in order to observe the variations of discharge in upstream and downstream gauging

stations. Since, the discharge data for Balotra is available from 1990, the inter-comparison of both Balotra at upstream and Gandhav downstream is done from the same year. The usual idea is that discharge in a river increases downstream when compared to upstream as a greater number of tributaries join the main trunk stream at downstream reaches having a flatter or circular shape compared to the upstream area of a river basin. Thus, the difference of annual average discharge increases downstream of Luni with more number to tributaries contributing to the streamflow in the main Luni channel as observed at Gandhav.

The difference of discharge (Table 3.10) is found to be positive which indicates it to be a 'gaining stream', in which discharge amount is gained by the Luni channel at Gandhav from the tributary streamflow. Fewer negative values as highlighted in the table, indicate an exceptional situation when higher discharge value is noted compared to the downstream gauging station may be due to less amount of streamflow from the adjoining Sukri river joining the Luni river before Gandhav, making it a 'losing stream'. Higher rates of groundwater percolation, excess over-drafting of Luni's surface water for domestic and farming uses as well as high rates of evapotranspiration accompanied with hot dry winds can lead to lower discharge downstream gauging sites. The stretch of Luni in between Balotra and Gandhav traverses a long arid path adjoining the sand dunes of Thar especially along the west bank, which leads to arid conditions, initiating drying up of the river flow leaving a meagre amount of discharge downstream at Gandhav. The principle of maximum downstream discharge compared to the upstream gauging site of Balotra opens up the prospect of characterizing Luni based on the hydrological condition and flow movement in the river channel. Such epitome of river character infuses the ephemeral behaviour of the river as exhibited with minimal to zero flows in most of the times for such a central dryland river system in Rajasthan.

Table 3.10: Annual average discharge differences for two GDS on the Luni river.

| Year | Annual Avg. Discharge (m^3s^{-1}) | | |
	Balotra (Upstream)	Gandhav (Downstream)	Difference*
1990	22.26	62.45	40.19
1991	0.00	0.37	0.37
1992	32.96	26.93	**-6.03**
1993	0.17	3.66	3.49
1994	9.69	14.68	4.99
1995	19.11	15.47	**-3.64**
1996	0.90	0.58	**-0.32**
1997	8.27	7.12	**-1.15**
1998	0.00	0.35	0.35
1999	2.04	0.54	**-1.50**
2000	0.00	0.05	0.05
2001	0.00	6.31	6.31
2002	0.00	0.00	0.00
2003	0.00	0.25	0.25
2004	0.00	0.00	0.00
2005	0.00	0.00	0.00
2006	3.05	0.00	**-3.05**
2007	5.57	7.06	1.49
2008	0.00	0.00	0.00
2009	0.00	0.00	0.00
2010	0.00	0.00	0.00
2011	0.00	0.00	0.00
2012	0.00	0.00	0.00
2013	0.00	0.00	0.00
2014	0.00	0.00	0.00
2015	1.59	7.76	6.17
2016	9.34	31.05	21.70

*Difference = Gandhav (Downstream) – Balotra (Upstream). Source: Computed by the researcher.

3.10 Summary

This chapter discerns the various exhaustive geo-scientific findings of the Luni river basin. The documentation of geology, geomorphology, lineament, tectonic framework, Bouguer anomaly and seismic zones helps understand the crucial form of river behaviour acting as traits in determining its behaviour. Geology and geomorphology layers explain the unique presence of undifferentiated aeolian and fluvial quaternary sediments throughout the river basin. The tectonic framework of the Luni river basin is based on intra-cratonic alluvial fills eroded from the Aravalli and the Thar from the inception of the landscape. The presence of four types of seismic zones with the dominance of low and moderate earthquake risk lays the tectonic foundation of the basin accompanied with the past 50 years of earthquake events. Such a study

helps to show the status of tectonism and its possible impact on the riverine system. Bouger anomaly was used to see the distribution of gravity anomalies in the entire basin. The hydrogeological systems help in determining the rich or prospective groundwater zones with the characterization of aquifers. This also helps in identifying the prospective areas of groundwater recharge overlaid by the major and minor lineaments. Hydrological behaviour of Luni is reflected through the 'Group 7' of Haines' River regime classifying it under 'extreme late summer regime'. Different hydrological parameters (Table 3.7) like AMWL, AMQ, AMSP, ARC, ZFM, ZFMI, DTAZFM and R-B Index are used to quantify the hydrological gauge and discharge datasets available for the two GDS – Balotra (upstream) and Gandhav (downstream). The river behaviour is hence established as ephemeral, dry and non-perennial with monsoonal flow only and incurring flashy flows due to certain extreme precipitation events.

CHAPTER – 4

LANDSCAPE CHARACTERIZATION OF LUNI RIVER BASIN

4.1 Introduction

The landscape of a river basin is a dynamic product that keeps on altering its shape, morphology and surface landforms due to climatic and tectonic disposition over various temporal and spatial scales. Diversified indices are used to comprehend the characteristics of a landscape unit and hence discern the development of behavioural traits of a river, sensitive to changing climate and human-induced disturbances. The generic meaning of 'terrain' is the 'surface of the landscape', which is the basic unit of any geomorphic analysis and can be attributed to a well-defined topographical model to extract the surface dynamics of the earth. The various rates of geomorphic processes operating over different spatial and temporal scales play a significant role in developing present-day landforms (Thornbury, 1954). The current open-source digital elevation models with various spatial resolutions like the SRTM, ASTER, CARTOSAT, ALOS PALSAR, TanDEM-X and others are a vital part of terrain modelling, topographic characterization and geomorphometric analysis (Patel and Sarkar, 2009). The nature of topographic variations and their curvature profiles, aspects of relief, lineament patterns, surface slopes types, the interrelationship between geology and terrain, attributes of landscape hypsometry and the hierarchy of altimetric sub units decipher the terrain characteristics of a region or river basin (Patel and Sarkar, 2010; Patel, 2013). Inorder to discern the behaviour of a river basin, terrain-based aspects need to be included in the study to bring out the best geomorphological explanation for the Luni river basin. The geomorphometric analysis is the best framework for terrain and drainage disposition of a river basin based on the fabric of mathematics, earth system analysis and computer science. Morphometric exercises are now primarily undertaken by geo-computational advances and new plugins or modules in the GIS environment (Maune, 2001). Harinath and Raghu (2013) explained how in-situ landscape and terrain evaluation methods are laborious, time-consuming, and capital intensive, while geomorphometric analysis provides far easier evaluative measures of drainage basins.

4.2 Objective

This chapter seeks to examine the landscape character of the Luni river basin with the operative process-response mechanism to fulfil the second part of the third objective of this research. The characterization of terrain reflects the operative surface processes on the basin topography and evolution of the Luni's drainage system.

4.3 Methodology

As represented in figures 4.1 to 4.7, the landscape terrain features were done using the SRTM DEM 1 arc-second. The DEM was geo-processed in ArcGIS and SAGA GIS to extract the thematic layers of various terrain aspects and then was used for an inter-comparative overview and analysis in describing the watershed. The same DEM was used to delineate the significant sub-basins of the Luni river. The river basin shape and size inter-comparison was done using different DEMs of various spatial resolutions and those from the top-cited literature. This is followed by the shape based morphometric analysis, erodibility analysis using compound ranking for all the basins derived from various sources in Microsoft Excel and SPSS. The same analysis was also performed to understand the sub-basin morphometry and its areal perspective. The riverscape's stage of evolution for the study river basin and its sub-basins was calculated and graphically represented using the hypsometric curves. The data was extracted from the SRTM DEM and then analyzed in Microsoft Excel. The tectonic analysis of the Luni river and its tributaries was done using long profile analysis by superimposing the main streams over the SRTM DEM in QGIS and plotting the final data in Microsoft Excel. The stream length (SL) index was calculated based on three moving window average techniques to capture the range of tectonic influence on the main Luni river and its major sub-tributaries.

Table 4.1: List of datasets used in analysis of the present chapter.

Sl. No.	Parameters	Data Type	Data Source	Spatial Resolution	Period
1	Elevation, Terrain & Drainage	Raster Grid	SRTM DEM (USGS), version 3.0	1 arc-second (30 m)	September, 2014
2	Topography & Luni River Channel	Line and polygon coverage	SoI Topographical Sheets	1: 50,000	2006

Source: Compiled by the researcher.

4.4 Slope Factors

The slope-based factors enlisted in Table 4.2 are obtained from the SRTM DEM 30 m tiles used for the first-order analysis of various types of slopes and profiles curvatures. These factors are enlisted below -

- **Slope**: A curve fitted according to the topographic surface and modelled out from a DEM for a given spatial location best defines a slope (Burrough, 1986). It is the first-order derivative of the DEM surface (Table 4.1). The slope manifests the gradient and is the rate of optimal alteration in z-values or elevation. Slope can also be defined as the ratio between

altitudinal variations between two points on the earth's surface, corresponding to the ground distance between the two points (Das et al., 2020). In Fig. 4.1a, almost the entire Luni basin is having a classic lower slope ranging in between 0˚-6.81˚ represented in the shades of yellow. The only exception is found in the residual remains in the western part of the catchment and along the entire eastern part consisting of the Aravalli ranges with a slope of 25.76˚-75.47˚, as observed with the shades of brown. These high slopes are associated with a greater amount of erosion and sediment transportation.

- **LS-Factor**: The Universal Soil Loss Equation (USLE) has six input parameters. The combination of slope length and slope angle (LS-factor) is defined to have a major impact on the soil loss at a regional scale. The L-factor stands for the impact of slope length, while the S-factor measures the effectivity of slope steepness. Both the factors of LS define the potential zones of soil erosion, indicating the nature and type of regional topography. In the Fig. 4.1b, the variation of LS-factor values is maximum over the higher altitudinal areas like the Aravalli and the residual remains of hillocks in the west, while the entire Luni basin has no such erosion potentiality as represented with lowest values or observable with the shades of brown and yellow.

- **Curvature**: Goudie (2004) defined curvature as the rate of slope change in degrees per hundred meters. The slope surfaces are classified as concave, convex and rectilinear based on positive, zero or negative values. In Fig. 4.1c, the negative values of curvature (-27.8 to -0.8) are associated with concave slope surfaces, which denotes a gradual decrease of slope found along the eastern part of the Luni basin, rightly showcasing the residual character of the Aravalli ranges undergoing slow erosion. The rectilinear surfaces are represented by zero curvature. The most dominant form of curvature for the entire study river basin ranges in between -0.31 to 0.17 represented with green. Slope values increasing downstream are signs of topographic abnormality due to tectonic or human influences that are rarely found within the watershed represented with positive curvature values.
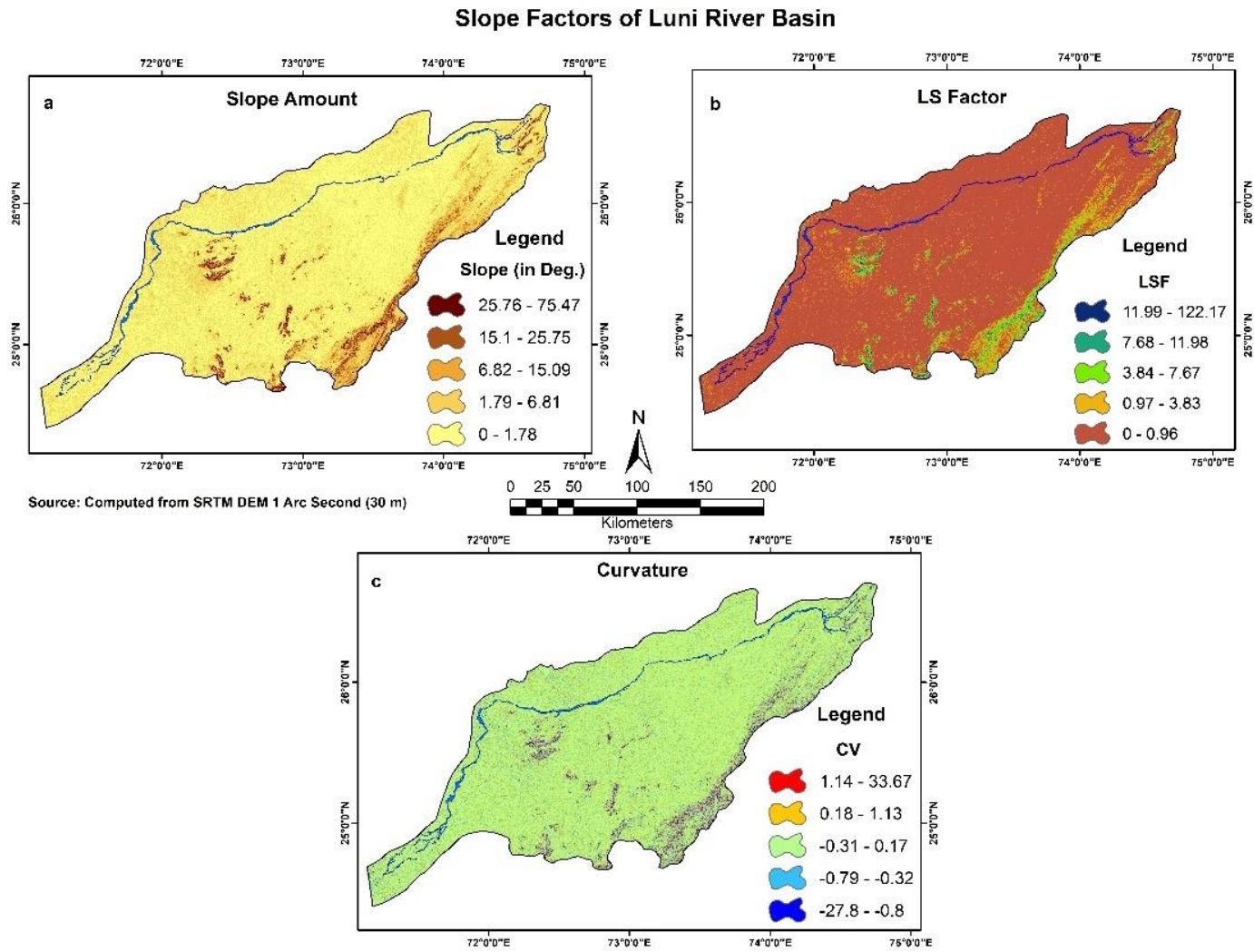
Fig. 4.1: Slope factors of Luni river basin; a. Slope Amount, b. LS factor and c. Slope Curvature. Source: Prepared by the researcher based on the SRTM DEM 30 m tiles.

Table 4.2: List of morphometric parameters used for slope, terrain, drainage and basin characterization of Luni river.

Sl. No.	Chapter Reference	Morphometric Parameter	Abbreviation	Unit	Formula	Variables	Citation
1	Slope Factor (Fig. 4.1)	Slope	θ	degrees (°)	First order derivate of DEM surface	-	Evans, 1980
2		Curvature	C_V	Dimensionless	Second-order derivative of DEM surface/ Curvature in the direction of contour line	-	
3		LS Factor	LS		LS = (n + 1) (α/22.13) n x (sinβ/0.0896) m	Constant values of n = 0.4, and m = 1.	Moore et al., 1991
4	Terrain Characterization (TC) – I (Fig. 4.2)	Mean Elevation	ME	meters (m)	Average elevation of DEM surface	-	-
5		Relative Relief	RR		$RR = h_{max} - h_{min}$	h_{max} = Maximum elevation and h_{min} = Minimum elevation	Smith, 1935
6		Dissection Index	DI		$DI = RR / h_{max}$	RR = Relative relief and h_{max} = Maximum elevation	Nir, 1957
7		Hypsometric Integral	HI		$HI = (h_{mean} - h_{min}) / (h_{max} - h_{min})$	h_{mean} = Mean elevation of the basin, h_{min} = Minimum elevation of the basin and h_{max} = Maximum elevation of the basin	Pike and Wilson, 1971
8	TC – II (Fig. 4.3)	Terrain Ruggedness Index	TRI	Dimensionless	Index of topographical homogeneity	-	Reiley et al., 1999

9	Terrain Characterization – II (contd.) (Fig. 4.3)	Terrain Surface Texture	TST		Spatial intricacy per unit area (i.e., drainage density and changes in sign of slope aspect or curvature)	-	Iwahashi and Pike, 2007
10		Terrain Surface Convexity	TSC		Segregation of high and low relief features		
11		Topographic Wetness Index	TWI		$TWI = \ln [A_S / \tan(\theta)]$	A_S = Specific catchment area derived from the accumulation matrix, θ = Slope in degrees	Beven and Kirkby, 1979
12	Terrain Characterization – III (Fig. 4.4)	Morphometric Protection Index	MPI		Evaluation of positive topographic openness describes how an area's relief is protected considering the DEM elevation profile.	-	Yokoyama et al., 2002
13		Mass Balance Index	MBI		Index showing the presence of unconsolidated terrain mass of the study area		Friedrich, 1996
14		Topographical Position Index	TPI	Dimensionless	Measuring topographic slope positions and automating landform classifications.		Guisan et al., 1999

No.	Category	Parameter	Symbol	Unit	Formula	Variables	Source
15	TC – III (contd.) (Fig. 4.4)	Sediment Transport Index	STI		$STI = (m + 1) \times (A_s / 22.13)^m \times \sin(B / 0.0896)^n$	A_s = upslope contributing area per unit contour length, B is the local slope gradient in degrees; the contributing area exponent, m, = 0.4 and the slope exponent, n, = 1.4.	Moore and Burch, 1986
16	Terrain Characterization – IV (Fig. 4.5)	Multiresolution Valley Bottom Flatness	MRVBF	Dimensionless	Identification of valley bottoms from DEM surface	-	Gallant and Dowling, 2003
17		Multiresolution Ridge Top Factor	MRRTF		Identification of ridge tops from DEM surface	-	
18	Drainage Characterization (DC) – I (Fig. 4.6)	Drainage Density	D_D	km./km.^{2}	$DD = L_u / B_A$	L_u = Total length of all the streams in the basin, B_A = basin area	Horton, 1945
19		Stream Frequency	S_F	No. of streams/km^2	$SF = N_u / B_A$	N_u = Total number of all streams, B_A = basin area	
20		Drainage Intensity	D_I	Dimensionless	$D_I = D_D/S_F$	D_D = Drainage density, S_F = Stream frequency	Faniran, 1968
21		Drainage Texture	D_T		$D_T = S_F \times D_D$		Smith, 1950
22	DC – II (Fig. 4.7)	Constant of Channel Maintenance	CCM	km.^{2}/km.	$CCM = 1/D_D$	D_D = Drainage Density	Schumm, 1956
23		Length of Overland Flow	LOF		$LOF = 1/2 \times D_D$		Horton, 1945

No.	Category	Parameter	Symbol	Unit	Formula / Description	Variables	Reference
24		Infiltration Number	IN		$IN = D_D \times S_F$	D_D = Drainage density, S_F = Stream frequency	Faniran, 1968
25	DC – II (contd.) (Fig. 4.7)	Stream Power Index	SPI	Dimensionless	$SPI = \ln [A_S \times \tan (\theta)]$	A_S = Specific catchment area derived from the accumulation matrix, θ = Slope in degrees	Moore et al., 1991
26	Linear Characterization (Table 4.3 & 4.7)	Basin Length	B_L	km.	The maximum length of the river basin from source to mouth	-	-
27		Basin Perimeter	B_P	km.	A path that outlines the river basin shape		
28		Basin Area	B_A	km.^{2}	Areal coverage of river basin		
29		Basin Width	B_W	km.	The breadth of the river basin		
30		Straight length from the watershed mouth to the centre of mass of the watershed	Lcm		Perpendicular length from the basin mouth to the centre of mass of the basin		Black, 1972
31		Width of the watershed at the centre of mass and perpendicular to Lcm	Wcm		The breadth of the watershed from the centre of mass and perpendicular to Lcm		
32	Areal Characterization (Table 4.3 & 4.7)	Index of Shape	I_S		$I_S = B_L^2/B_A$	B_A = Basin Area, B_L = Basin Length	Horton, 1932
33		Circularity Ratio	C_R	Dimensionless	$C_R = 12.57 \times (B_A/B_P^2)$	B_A = Basin Area, B_P = Basin Perimeter	Miller, 1953
34		Elongation Ratio	E_R		$E_R = (1.128\sqrt{B_A})/B_L$	B_A = Basin Area, B_L = Basin Length	Schuum, 1956
35		Form Factor	F_F		$F_F = B_A/B_L^2$		Horton, 1932

#		Parameter	Symbol		Formula	Variables	Source
36		Lemniscate Ratio	L_R		$L_R = B_L^2/ (4 \times B_A)$		Chorely et al., 1957
37		Compactness Coefficient	C_C		$C_C = 0.2841 \times B_P/B_A^{0.5}$	B_P = Basin Perimeter, B_A = Basin Area	Gravelius, 1914
38		Ellipticity Index	E_I		$E_I = \prod (B_L^2/4 \times B_A)$	B_A = Basin Area, B_L = Basin Length	Stoddart, 1965
39		Length-Width Ratio	LW_R		$LW_R = B_L/B_W$	B_L = Basin Length, B_W = Basin Width	-
40	Areal Characterization (contd.) (Table 4.3 & 4.7)	Gravelius Shape Index	G_S	Dimensionless	$0.28 \times (B_P/\sqrt{B_A})$	B_P = Basin Perimeter, B_A = Basin Area	Bendjoudi & Hubert, 2002
41		Fitness Ratio	F_R		$F_R = B_L/B_P$	B_L = Basin Length, B_P = Basin Perimeter	Melton, 1957
42		Basin Eccentricity	B_E		$B_E = (Lcm^2 - Wcm^2)^{0.5}/Wcm$		Black, 1972

Source: Compiled by the researcher.

4.5 Terrain Characterization – I

The first set of geomorphometric units is computed based on the SRTM DEM 30 m tiles for the entire Luni basin and enlisted in Table 4.2. The parameters are discussed below –

▪ **Mean Elevation**: The average elevation obtained based on geoprocessing the DEM used for terrain analysis. The mean elevation is highest over the Aravalli in the eastern part of the basin 649.68-1473.25 m (Fig. 4.2a). The mean elevation gradually decreases towards the west and the southern section records the lowest mean elevation values ranging between 4.62-131.33 m.

▪ **Relative Relief:** The difference in elevation between the highest and lowest points in an areal unit is relative relief (Smith, 1935). Kuhni and Pfiffner (2001) explain how relative relief is a crucial yet simple form of geomorphometric expression to give an overview of the studied terrain with varying intensity of erosional processes operating within a river basin. Almost the entire Luni river basin records a low RR value ranging between 2.18-34.88 m (Fig. 4.2b) suggesting the high amount of erosion that has been prudential for landscaping the alluvial plains of the entire basin. The values of RR gradually rise upslope towards the east in Aravalli which are still in a process of gradual erosion. The highest RR values are found along the crest of the hills with a value ranging between 298.83-597.79 m.

▪ **Dissection Index:** The proportion of the relative relief and the highest elevation expressing the dissection or magnitude of a terrain. Miller (1953) and Nir (1957) defined the dissection index of terrain as the ratio between the relief energy (relative relief) and the perpendicular distance from the erosional base, taking into account the dynamicity of the topography of an area. In Fig. 4.2c, the higher elevations of Aravalli and the southern section of the basin is highly dissected by the different stream orders. The inland delta or the floodout region has the greatest number of tributaries cutting the planform and dissecting the region. The entire central section of the basin has the lowest dissection.

▪ **Hypsometric Integral:** Hypsometric integral is the area underneath the hypsometric curve (or the area height relationship) and ranges from 0 to 1. The intensity of erosional processes operating within a basin shares a direct correlation with the HI. In Fig. 4.2d, maximum erosion is observed in the floodout region, while most of the area is moderately eroded and the high slopes of Aravalli are found to have the least erosion. The progression of gradual erosion can be well understood from the map. A geomorphic unit like the pediment-pedeplain complex exhibits low to high-grade erosion.
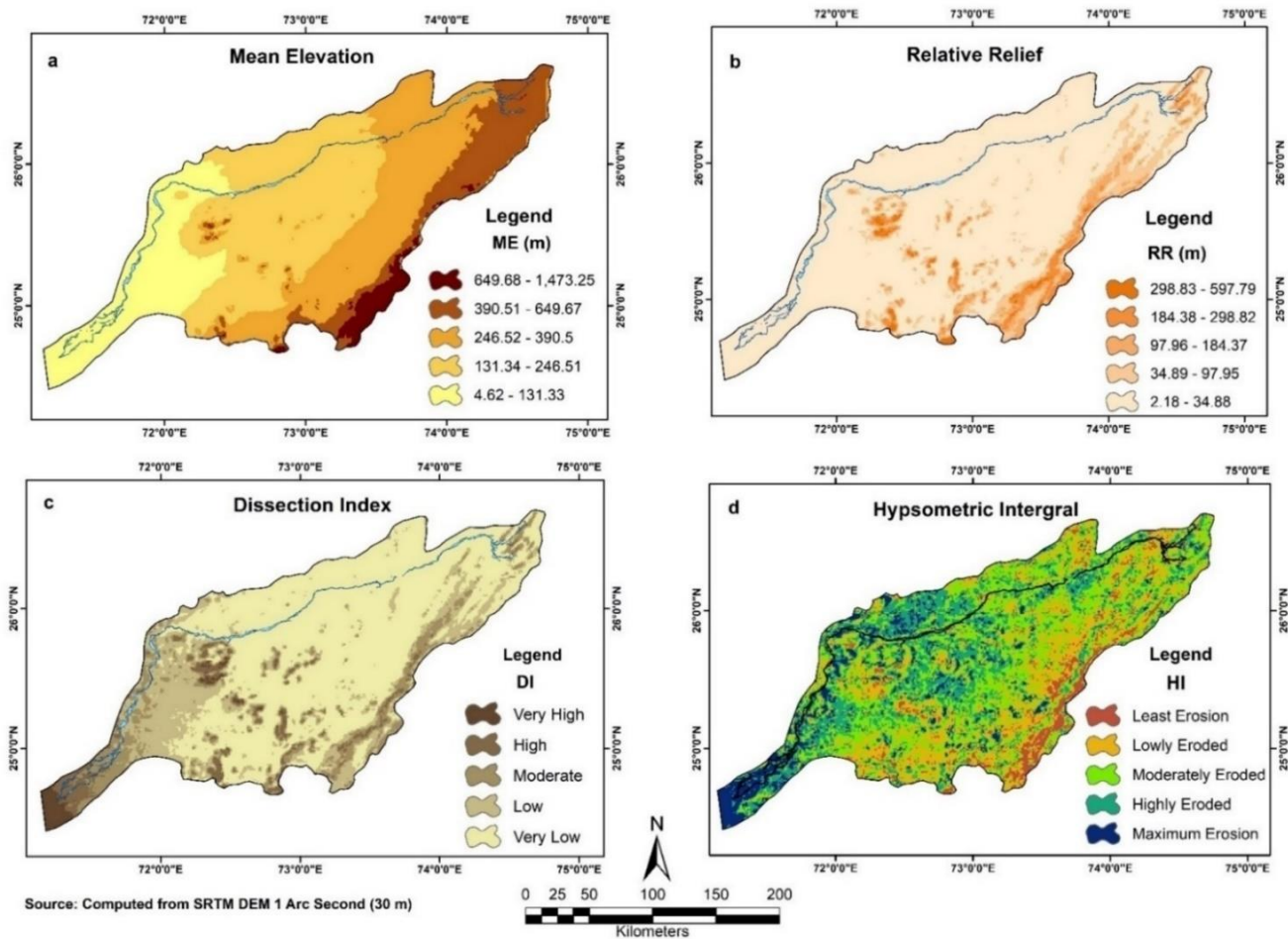
Fig. 4.2: Terrain Characterization – I parameters of Luni river basin; a. Mean Elevation, b. Relative Relief, c. Dissection Index and d. Hypsometric Integral. Source: Prepared by the researcher based on the SRTM DEM 30 m tiles.
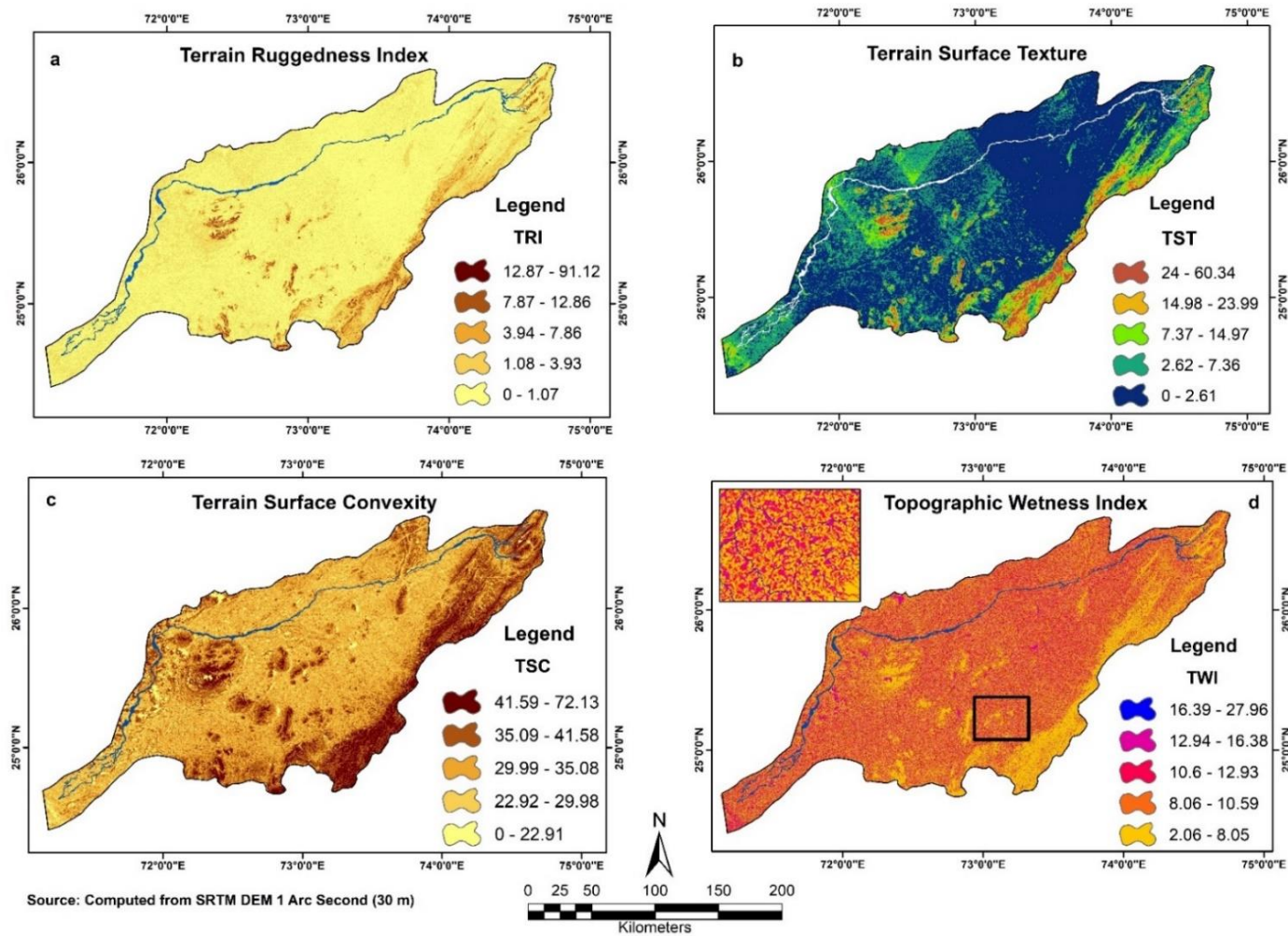
Fig. 4.3: Terrain Characterization - II parameters of Luni river basin; a. Terrain Ruggedness Index, b. Terrain Surface Texture, c. Terrain Surface Convexity and d. Topographic Wetness Index. Source: Prepared by the researcher based on the SRTM DEM 30 m tiles.

4.6 Terrain Characterization – II

The second set of geomorphometric units is computed based on the SRTM DEM 30 m tiles for the entire Luni basin and enlisted in Table 4.2. The parameters are discussed below-

- **Terrain Ruggedness Index:** TRI is explained as homogeneity of terrain distribution of elevation (Riley et al., 1999). The flatness or ruggedness of a riverscape can be defined using this high valuable geomorphometric parameter. Regions having a lower TRI value denote a high probability of flooding since such areas are flat, e.g., floodplains (Das, 2021a). A higher amount of ruggedness is observed in higher slopes of Aravalli in the eastern section (Fig. 4.3a), while the entire basin is found to be flat with the least undulations with few exceptions.

- **Terrain Surface Texture:** Terrain textures considers relief (z factor) and spacing (x, y factors), which represent measures of spatial intricacy per unit area, incorporating the drainage density and slope curvature (Iwahashi and Pike, 2007). In Fig. 4.3b, explains the texture of almost the entire river basin is flat with a lower amount of terrain surface roughness. While the higher elevation region in the eastern part shows higher texture values suggesting topographic ruggedness.

- **Terrain Surface Convexity**: For automatic classification of a high gradient topography, slope gradient and surface texture of the topography plays a combinational and fundamental role, but are inadequate to classify low relief features, for instance, segregating older river terraces from the younger ones. So, to better demarcate these, the local convexity or positive surface curvature was utilized by Iwahashi and Pike (2007). It is commonly seen in Fig. 4.3 c, low surface convexity conforms to broad valleys and mountain foot slopes, while higher values are typically associated with features like alluvial fans or terraces.

- **Topographic Wetness Index**: The TWI parameter measures the relief effect on runoff generation (O'Loughlin 1986) and thereby approximates surface saturation zones (Beven and Kirkby 1979; Barling et al. 1994). The terrain's influence on the generation of runoff and the volume of flow accumulation is best represented by TWI (Hong et al., 2018, Das, 2021). The most low-lying points with a higher TWI value (Fig. 4.3d) has a higher risk of flood and vice versa. The inset marked layer shows a zoomed-in section of the foot slope region of Aravalli having the best combination values of TWI and the drainage accumulation points could be well understood.

4.7 Terrain Characterization – III

The third set of geomorphometric units is computed based on the SRTM DEM 30 m tiles for the entire Luni basin and enlisted in Table 4.2. The parameters are discussed below-

- **Morphometric Protection Index**: MPI is defined as evaluating positive topographic openness describing how the relief of an area is protected considering the DEM elevation profile (Yokoyama et al., 2002). The Fig. 4.4a explains that most of the Luni river basin is having a poor to moderate morphometric protection based on the elevation with the only exception for the high slopes of Aravalli.

- **Mass Balance Index**: MBI is an index showing unconsolidated terrain mass of the study area (Friedrich, 1996). The Fig. 4.4b, shows how the terrain mass is compensated by the erodible lower floodplains and slow erodible hills of Aravalli. Higher mass balance index values are seen over the residual blocks of Aravalli and gradually decreases towards the western part of the basin, which is highly erodible.

- **Topographical Position Index**: The TPI parameter (Guisan et al., 1999) is an automated algorithm that measures topographic slope positions and enables landform classification. Positive TPI values (Fig. 4.4c) are discerned for the central point that is located above their surroundings, and negative values indicate lower topographic positions. The TPI range thus depends on the predetermined radius and elevation difference (Grohmann and Riccomini, 2009). Higher predetermined radius values usually denote major landforms while lower values correspond to minor valleys and ridges (De Reu et al., 2013).

- **Sediment Transport Index**: STI is a vital part of morphometry used in a data-sparse environment to compute the potential amount of sediment that can be transported by a geomorphic agent based on the upslope contributing area and an assumption that how it is directly related to slope and discharge (Moore and Burch, 1986). This index is deduced from the unit stream power theory and used for slope lengths <100 m and slope <14˚. The highest sediment transporting areas are seen along higher slopes of Aravalli, which gradually lowers down in the plains of the watershed (Fig. 4.4d).
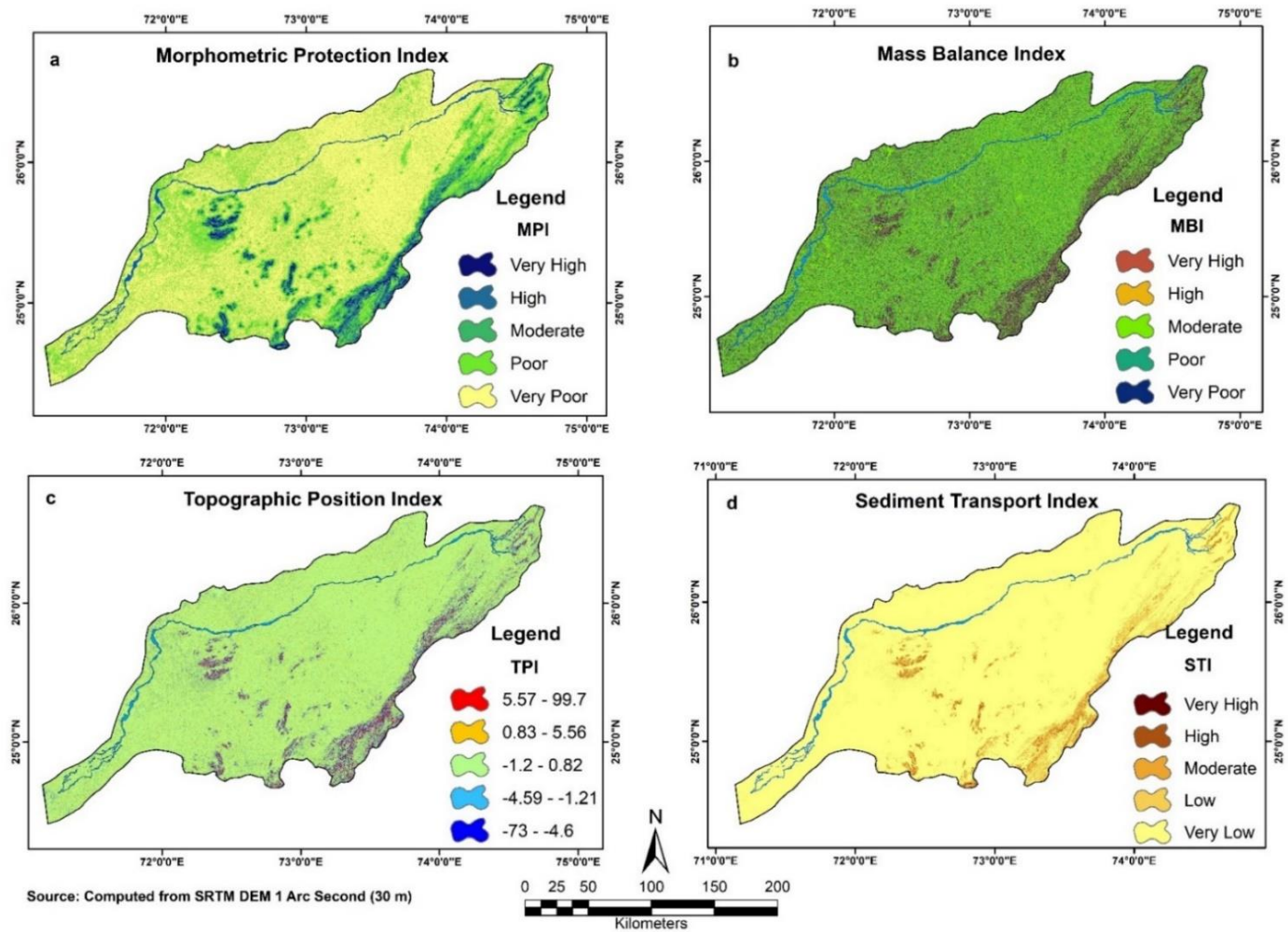
Fig. 4.4: Terrain Characterization - III parameters of Luni river basin; a. Morphometric Protection Index, b. Mass Balance Index, c. Topographic position Index and d. Sediment Transport Index. Source: Prepared by the researcher based on the SRTM DEM 30 m tiles.
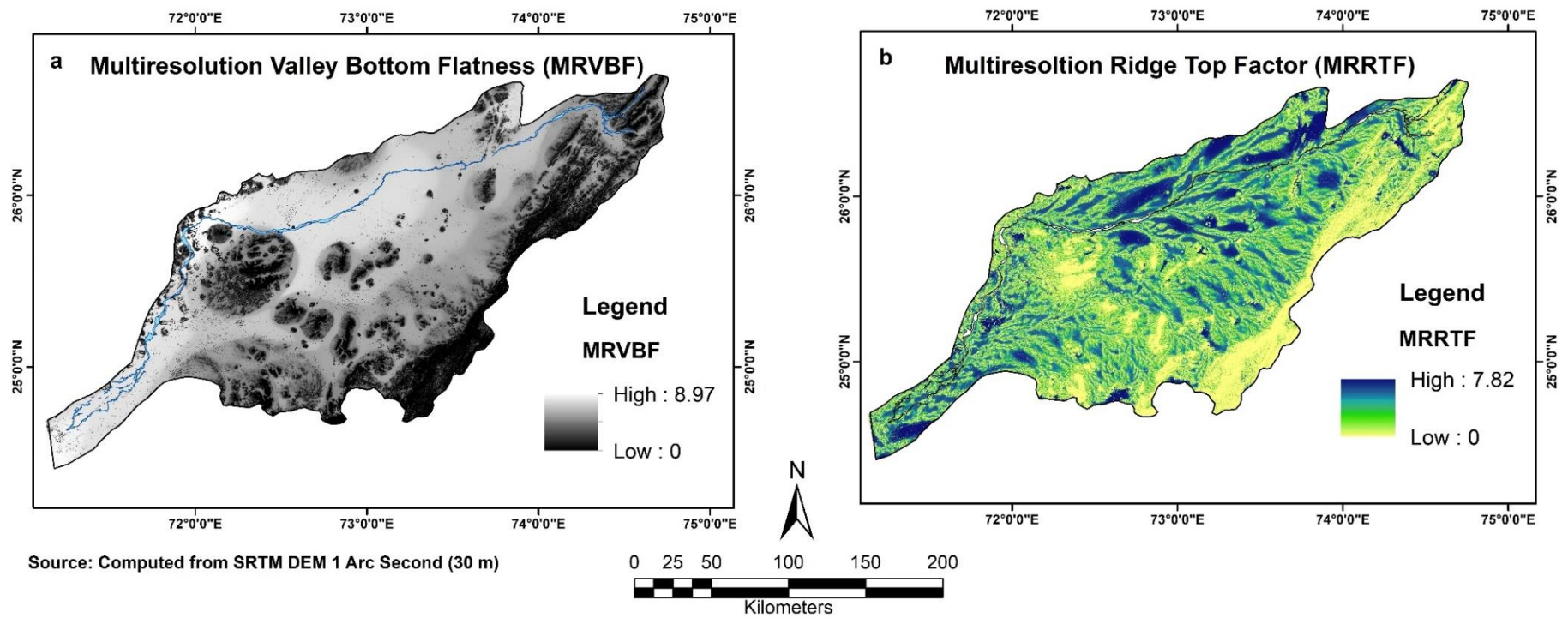
Fig. 4.5: Terrain Characterization - IV parameters of Luni river basin; a. MRVBF and b. MRRTF. Source: Prepared by the researcher based on the SRTM DEM 30 m tiles.

4.8 Terrain Characterization – IV

The fourth set of geomorphometric units is computed based on the SRTM DEM 30 m tiles for the entire Luni basin and enlisted in Table 4.2. The parameters are discussed below-

- **Multi-Resolution Valley Bottom Flatness and Multi-Resolution Ridge Top Factor**: MRVBF and MRRTF is a DEM classification automated algorithm which is used to identify the low-lying flat areas as valley bottoms and higher altitudinal areas as ridge top respectively (Gallant and Dowling, 2003). Slope and elevation are extracted from DEM to classify the MRVBF and MRRTF as both are corresponding one another. These are computed through a network of neighbourhood classification systems with a progressively coarser-resolution to identify small and large valleys. In Fig. 4.5 a and b, the flat valley bottom or the ridge tops are represented with zero or the lowest values. The higher values in MRVBF shows the higher elevation areas, while those of MRRTF represents the lowest points obtained from a DEM surface.

4.9 Drainage Characterization - I

Drainage characteristics are associated with the hydrological condition of a river basin. The DEM surface helps to generate the drainage lines based on the geoprocessing and hydrologically condition flow accumulation raster from which we can compute various sets of drainage characteristics related to the studied basin's terrain. This form of characterization is of sheer importance to comprehend the development of a riverscape and how it behaves. The first set of drainage parameters as given in Table 4.2 are as follows –

- **Drainage Density**: DD is defined as the proportion of the sum of all stream lengths within the basin to its total area (Horton, 1945). Gregory and Walling (1968) document how DD combines stream power potency and erosional processes operating within a river basin. Higher DD values indicate more significant fluvial process potency and characterize a higher erosional regime and vice versa. In Fig. 4.6a, the lowest drainage densities (<0.13 km./km.^{2}) were observed over the Aravalli in the eastern part of the Luni watershed. The amount of DD gradually increases towards the western part of the watershed with maximum concentration (indicated with dark blue shade) over the areas through which Luni and its main tributaries flow having an amount of 0.54-0.83 km./km.^{2}

- **Stream Frequency**: It denotes the total number of streams flowing per unit area (Horton 1945) and is closely related to the drainage density and the various parameters that influence drainage density. It is indicative of the nature of runoff in an area, giving insights

into the overland flow length and channel spacing. The Fig. 4.6b, the lowest SF values are found in the higher altitudes of the eastern region, while the moderate to maximum SF values are seen in those areas where the tributaries are joining, avulsing and anabranching along with the main channel of Luni. The floodout region is also having a significant-high SF value because of the channel debranching leading to an inland delta.

- **Drainage Intensity**: DI is the ratio of stream frequency to drainage density (Faniran, 1968). The higher values of DI (Fig. 4.6c) implies that DD and SF have a huge impact on the extent to which the agents of denudation have eroded the surface. The pediment-pediplain complex or the footslope of the Aravalli region has the highest amount of DI as observed with the shades of blue. While the central drainage lines of Luni and its tributary streams form a low DI and the top slopes of the Aravalli show the lowest DI values.

- **Drainage Texture**: The total number of stream segments from all the river basin orders per perimeter is described as DT (Horton, 1945). The closeness of channel spacing is measured by DT which mainly depends on rainfall, lithology, vegetation, infiltration capacity, relief aspect of the topography (Smith, 1950). The entire eastern part of the river basin (Fig. 4.6d) exhibits very coarse DT and it progressively becomes very fine near the main Luni channel and its associated tributaries marked with purple shade.

4. 10 Drainage Characterization – II

The second set of drainage characteristics as given in Table 4.2 are discussed below –

- **Constant of Channel Maintenance**: CCM is a popular index that is used as the inverse of DD or the constant of maintaining a river channel as landform property. This constant indicates the number of sq. km. of a basin surface that is needed to form and sustain a channel of length 1 km (Schumm, 1956). Almost 85% of the river basin is most erodible (Fig. 4.7a), while the footslope zones and higher reaches of Aravalli are found to be low to moderately erodible except few patches which are least erodible.

- **Length of Overland Flow**: LOF is defined as the length of the flow of rainwater before its concentration leading to the formation of a definite first-order stream (Horton, 1945). It is calculated as the reciprocal of twice of DD. The smaller value of LOF represents higher runoff associated with high erosion, and vice-versa. The highest channel erosion dominates the entire Luni river basin (Fig. 4.7b), while only the footslope zones of Aravalli and the residual tracks of the west show low to intermediate channel erosion and the few patches of least erodible zones are having sheet erosion.

- **Stream Power Index**: Data sparse regions especially the desert landscapes known for extreme weather conditions and irregular stream flow pose a challenge to initiate any research work but advanced satellite procured elevation datasets have made it possible through high-level geo-computation. SPI is such an index that works as a proxy to quantify the potentiality of stream power. Moore et al. (1991) and Chen and Yu (2011) show how SPI values tend to shoot up in the areas of an active erosional regime (Fig. 4.7c). The marked inset area offers the zoomed-in feature of SPI classes ranging from very poor to high. Slope and SPI values are positively correlated, as the gradient of slope influence the SPI classes and thus, the entire Luni river basin has a comparatively low SPI value.

- **Infiltration Number**: It is expressed as the product of the density of drainage (DD) and frequency of streams (SF) in a river basin (Faniran, 1968). DD and SF both shares a positive relation (directly proportional) with IN. The Luni river basin is classified with five major classes from very low to very high IN (Fig. 4.7d). The Luni basin is of no exception, as the high values of DD coincide with the very high class of IN. The highest infiltration is found along the major tributary streams and the main Luni channel. IN also exhibits the best sites of surface water infiltration and potential recharge of groundwater.
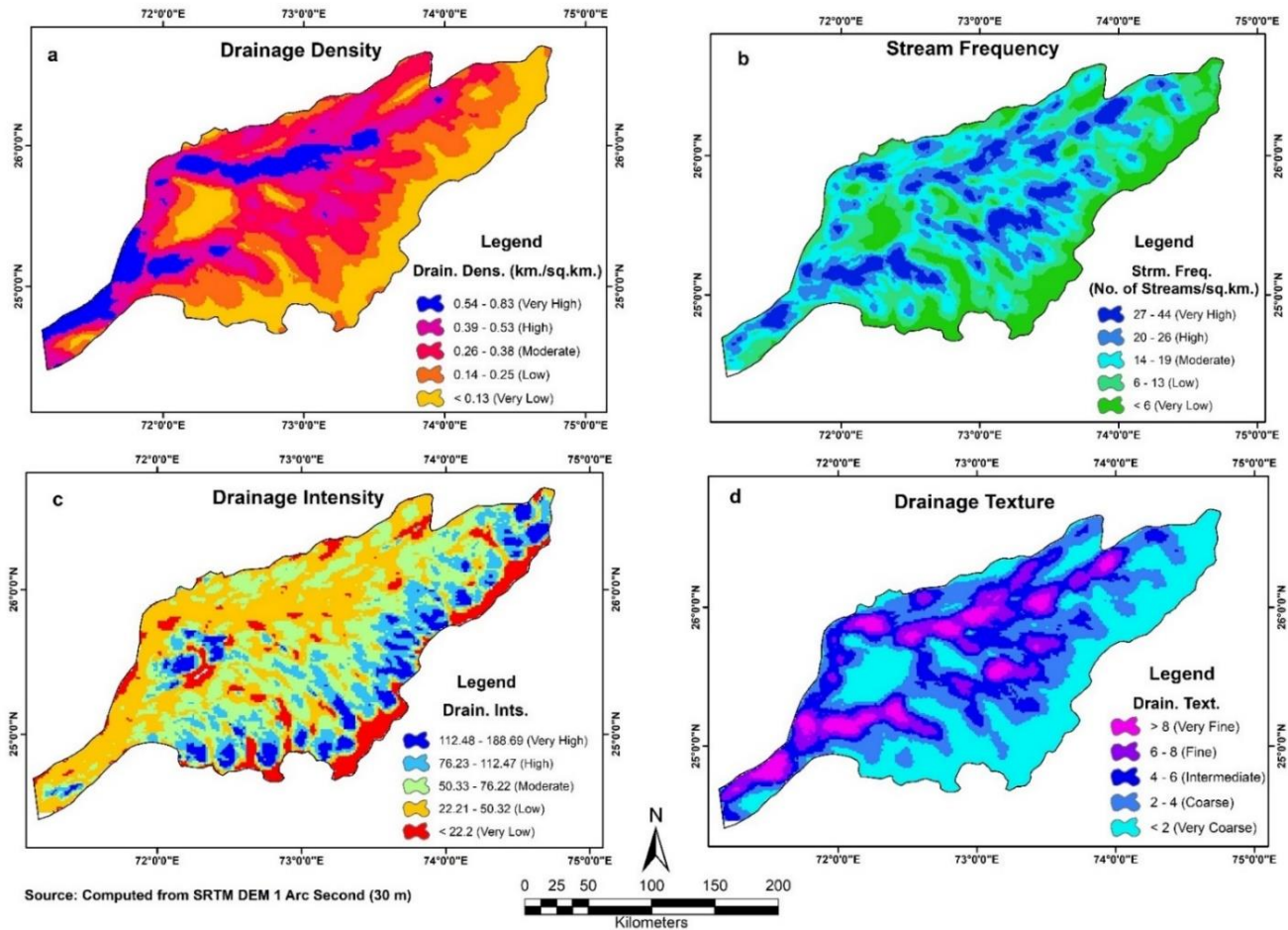
Fig. 4.6: Drainage Characterization – I parameters of Luni river basin; a. Drainage Density, b. Stream Frequency, c. Drainage Intensity and d. Drainage Texture. Source: Prepared by the researcher based on the SRTM DEM 30 m tiles.
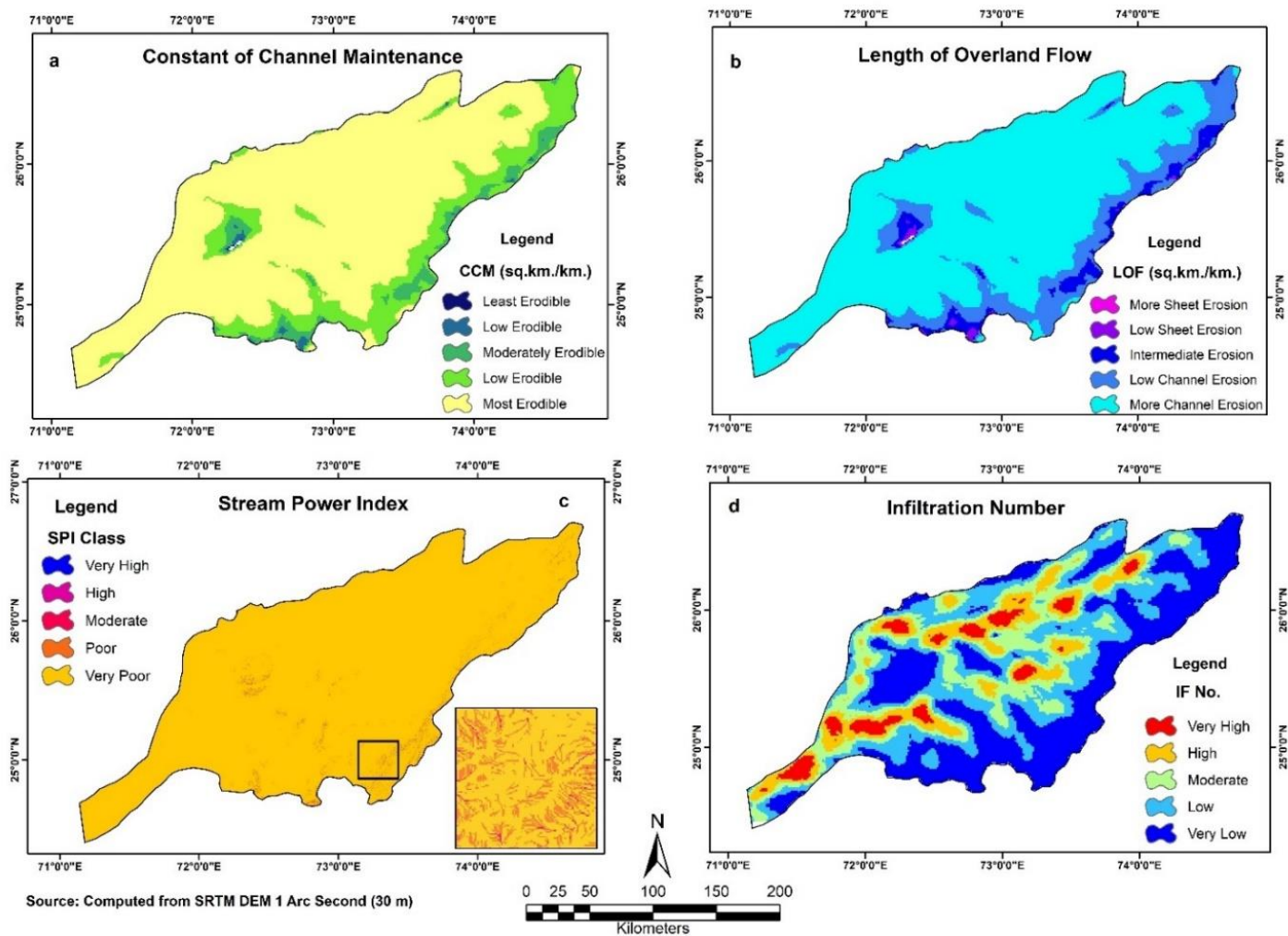
Fig. 4.7: Drainage Characterization – II parameters of Luni river basin; a. Constant of Channel Maintenance, b. Length of Overland Flow, c. Stream Power Index and d. Infiltration Number. Source: Prepared by the researcher based on the SRTM DEM 30 m tiles.

4.11 Areal Characterization of major sub-basins of Luni river basin

The Luni river basin consists of several small to large sub-basins which are having typical sub-arid to dryland characteristics. The major issue that was discovered while delineating the sub-basins from a DEM was that, while automated delineation of sub-basins using the ArcHydro tool in the ArcGIS environment, the sub-basin boundaries were substantially different and found to cross over the presently used Luni basin boundary for the study. This is due to the indigenous delineation of the present study basin which has been extracted from the SRTM DEM 30 m and then rectified using the SoI topographical maps and the present-day Google Earth imagery. So, inorder to avoid any sort of erroneous interpretation, each of the sub-basins of Luni was delineated individually from the geo-processed flow accumulation raster with the pour points digitized from the SoI topographical maps. According to the various reports of CGWB (2012) and CWC (2014), Luni consists of ~30 sub-basins. These sub-basins are majorly minor with initial stream orders and have an area <1,000 km^2 which are mainly based on the local runoff channels generating during the monsoon or high rainfall events and remain mostly dry throughout the year. After analyzing these minor sub-basins, the present study mainly focuses on the seven major sub-basins of Luni with an area of >1,000 km^2 which primarily feeds water and sediment to the Luni river.

In Fig. 4.8, the major sub-basins of Luni are mapped with their major streams. Since Luni's orientation of flow is towards the western side of the drainage basin, it has a greater number of left bank or eastern tributaries than that to its bank. Two right bank basins are Mithri/Jojri and Jojari, while the five left bank river basins are Lilri, Guhiya, Sukri N., Kher Nawala and Sukri R. from north to south. The linear and areal morphometric analysis was performed to bring out the shape based morphometric indices for each of the Luni's sub-basins. Table 4.2, defines the list of linear and areal parameters that have been used to analyze the shape of these sub-basins. The different shape based morphometric parameters (Table 4.3) were used to bring out a comparative analysis of erodibility. Shape parameters such as E_R, C_R, F_F, C_C, basin shape have a negative relationship with erodibility, i.e., lower the value, more is the erodibility and vice-versa.

The three prime areal parameters – E_R, C_R and F_F are represented in Fig. 4.9 as dot and line graph for each of the seven sub-basins of Luni. These three-shape based morphometric features explain the combination and compliment the potentiality of erosion and flood risks. Lower E_R values are meant for structurally controlled and youth stage of river basin evolution with lower potency of flood risks. Higher E_R values explain a more circular shaped river basin with a high

modal hydrograph and higher risk of erosion. E_R can be classified into five classes as more elongated (<0.5), elongated (0.5-0.69), less elongated (0.70-0.79), oval (0.80-0.89) and circular (>0.9) (Chandrashekar et al., 2015). The E_R values vary between 0.40 to 0.68 inferring more to the elongated shape of the Luni sub-basins. The C_R credits the circularity of a river basin which in turn helps to decipher the range of sediment contribution through erosion, structural control and the stage of evolution. A minimal amount of C_R indicates no such structural control, while the maximum values of C_R indicate the presence of higher lithological control on the drainage basin (Vittala et al., 2004; Sukristiyanti et al., 2018). The C_R values vary from 0.13 to 0.27 for the seven sub-basins of Luni, indicating a minimal structural control. Flood hydrograph affects the F_F of a drainage basin (Abboud and Nobal, 2017; Sukristiyanti et al., 2018). High values of F_F indicate the circular shape of the river basin having high peak flows over a peak flow of shorter duration. Lower F_F values indicate an elongated form of the river basin with low peak flows over a long duration. The values of F_F for the Luni sub-basins vary between 0.12 to 0.36, indicating elongated shapes and validates the major ephemeral behaviour of these sub-basins.

The other geomorphometric parameters used in the analysis for sub-basin shapes of Luni are meant for a more comprehensive understanding and development of a unique compound score for priority analysis of the sub-basins. The L_R helps in determining the slope of the drainage basins and the value varies from 0.91-2.04 indicating a higher concentration of area towards the upper and central parts of the sub-basins. The C_C values vary between 1.93-2.49 indicating a compact and elongated sub-basin type. E_I shares an inverse relation with F_F and the value ranges from 1 to infinity. Low values of E_I represents a higher rate of runoff each value of Luni sub-basins show a comparative high runoff characteristic LW_R is the ratio of length to width of the sub-basins which shows that the measure of the fit into the landscape. The G_S index is a parameter meant for understanding the shape type of a watershed and the values indicate that the sub-basins are elongated in generic nature with a tendency of an oval to the circular stage in the later stage of evolution. F_R is a measure of topographic fitness and the value ranges between 0.24-0.34, meaning a good fit of the basins aligned with the terrain. The mathematic shape of a sub-basin is derived based on the B_E factor. Since all the basins are having a value >1, the eccentric shape of the sub-basins is that of a hyperbola.
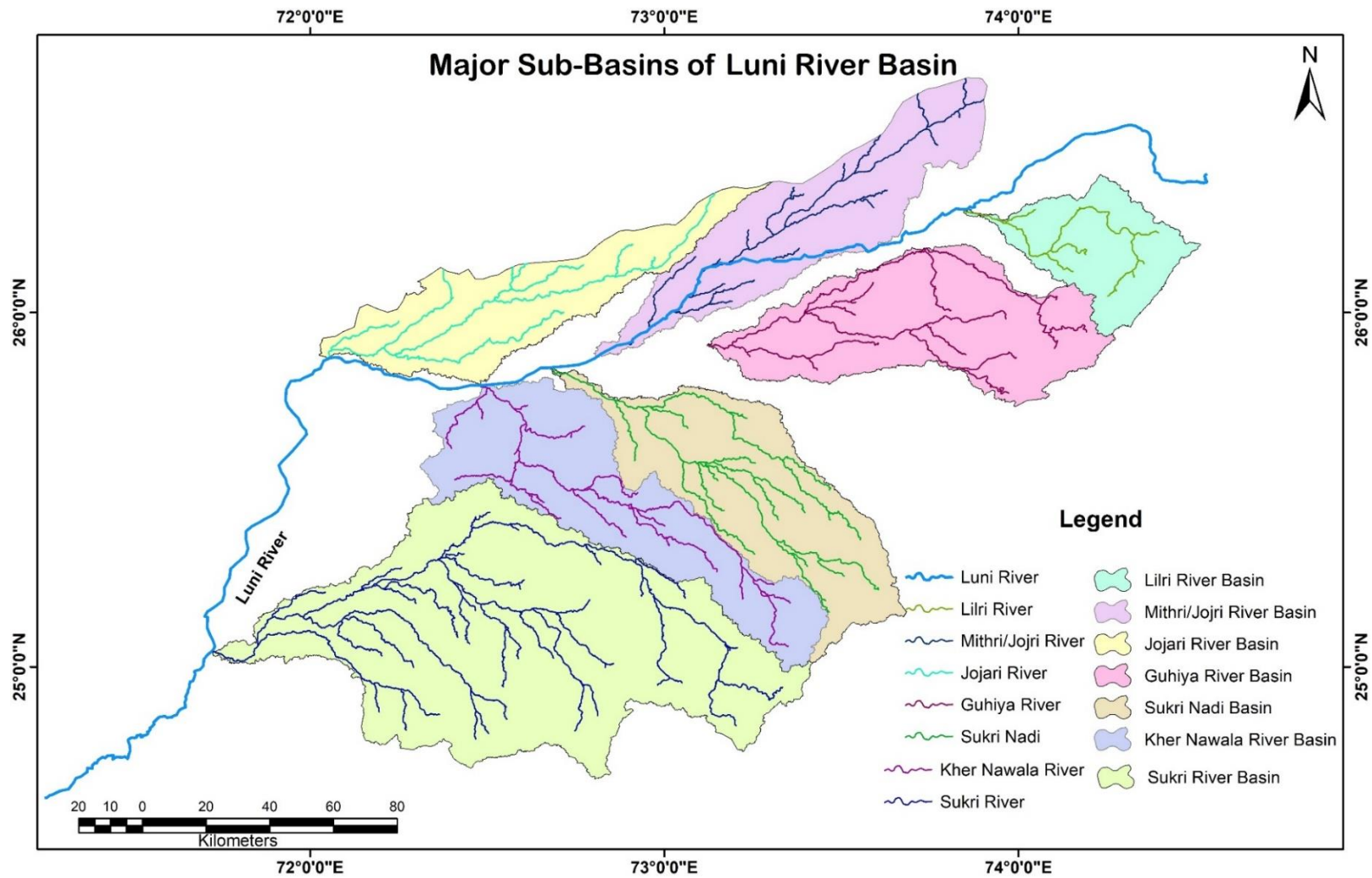
Fig. 4.8: Major sub-basins of Luni river. Source: Prepared by the researcher based on the SRTM DEM 30 m tiles.

Table 4.3: Values of linear and areal morphometric parameters for Luni river sub-basins.

Sub Basin ID	Sub Basin Name	B_L	B_A	B_P	B_W	Lcm	Wcm	I_S	C_R	E_R	F_F	L_R	C_C	E_I	LW_R	G_S	F_R	B_E	C_p
1	Lilri River	62.38	1411.51	257.54	50.56	39.95	19.79	2.76	0.27	0.68	0.36	0.69	1.93	2.17	1.23	1.92	0.24	1.75	1.27
2	Mithri or Jojri River	139.06	2943.49	530.94	29.04	81.94	16.86	6.57	0.13	0.44	0.15	1.64	2.76	5.16	4.79	2.74	0.26	4.76	2.67
3	Jojari Nadi	138.33	2348.34	404.02	38.22	58.52	14.54	8.15	0.18	0.40	0.12	2.04	2.35	6.40	3.62	2.33	0.34	3.90	2.71
4	Guhiya Nadi	115.68	3218.43	404.63	50.42	62.12	24.24	4.16	0.25	0.55	0.24	1.04	2.01	3.27	2.29	2.00	0.29	2.36	1.68
5	Sukri Nadi	126.88	3139.32	463.60	40.51	71.02	20.23	5.13	0.18	0.50	0.20	1.28	2.33	4.03	3.13	2.32	0.27	3.37	2.07
6	Kher Nawala Nadi	126.71	3286.34	506.55	58.54	52.09	13.28	4.89	0.16	0.51	0.20	1.22	2.49	3.84	2.16	2.47	0.25	3.79	2.00
7	Sukri River	169.41	7869.79	682.40	100.55	88.70	40.76	3.65	0.21	0.59	0.27	0.91	2.17	2.87	1.68	2.15	0.25	1.93	1.52

B_L: Basin Length, B_A: Basin Area, B_P: Basin Perimeter, B_W: Basin Width, Lcm: Straight length from the watershed mouth to the centre of mass of the watershed, Wcm: Width of the watershed at the centre of mass and perpendicular to Lcm, I_S: Index of Shape, C_R: Circularity Ratio, E_R: Elongation Ratio, F_F: Form Factor, L_R: Lemniscate Ratio, C_C: Compactness Coefficient, E_I: Ellipticity Index, LW_R: Length-Width Ratio, G_S: Gravelius Shape Index, F_R: Fitness Ratio, B_E: Basin Eccentricity, C_p: Compound Score. Source: Computed by the researcher.

Table 4.4: Compound scoring, priority ranking and erodibility of Luni river sub-basins.

Sub-Basin ID	Sub-Basin Name	Cp Score	P_R	Interpretation	Erodibility
1	Lilri R.	1.27	1	High	**Most Erodible**
7	Sukri R.	1.52	2	High	
4	Guhiya N.	1.68	3	Moderate	
6	Kher Nawala N.	2.00	4	Moderate	
5	Sukri N.	2.07	5	Moderate	
2	Mithri or Jojri R.	2.67	6	Low	
3	Jojari N.	2.71	7	Low	**Least Erodible**

P_RPriority Rank. Source: Computed by the researcher.

Table 4.5: Frequency analysis of Luni river sub-basin erodibility

Priority Ranking Ranges	Erodibility Risk	Frequency
<3	High	2
3 to 6	Moderate	3
>6	Low	2

Source: Computed by the researcher.
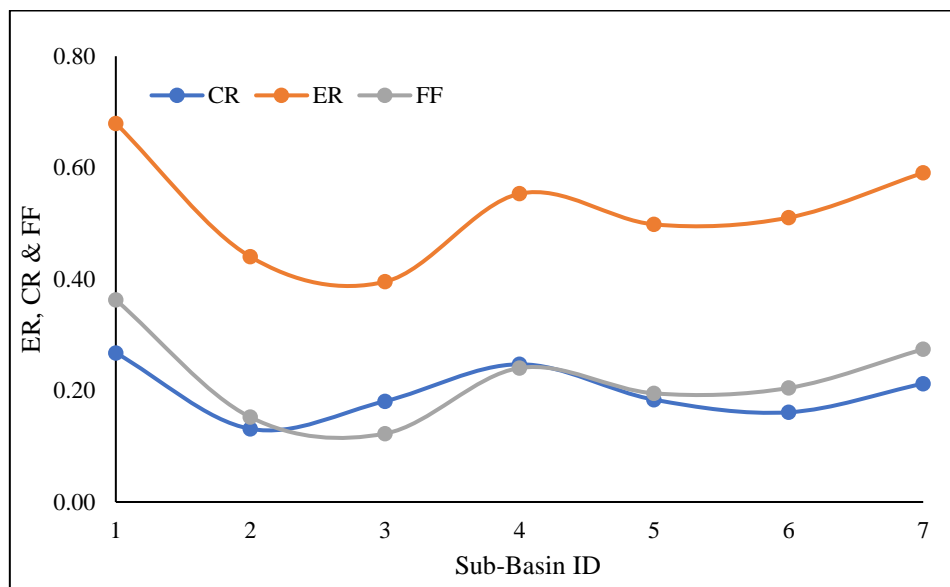
Fig. 4.9: Dot and line graph showing the variation of ER, CR and FF for the major Luni sub-basins Source: Computed by the researcher.

An average value of each of the areal parameters was compiled as a compound score and then a priority ranking was done in a hierarchic order based on the method of Vittala et al. (2008) (Table 4.4). Low compound scores were given higher priority ranks while those with higher scores were given lower ranks. The higher priority sub-basins are the most erodible ones with a lower compound score, while those sub-basins lower ranking and high compound score represent the least erodible. The risk of erodibility is judged based on the compound scoring

and sub-basin priority ranking (Table 4.4), while the frequency of erodibility of such sub-basins is compiled in Table 4.5. Priority rank of <3 fall under the class of highest risk of erodibility which are evaluated as Lilri and Sukri R. sub-basins. The risk of erosion is moderate for the Guhiya, Kher Nawala and Sukri N. sub-basins which are having a priority rank between 3 to 6. Lower chances of erosion are recorded for the right bank tributaries of the Luni - Mithri/Jojri and Jojari river >6 P_R.

4.12 Analysis of Luni River Basin Boundary Delineation

Luni is a classical dryland river system of India and is a most interesting one to study the variation of basin boundary. Unlike any other river basin/sub-basin boundaries, that drains out with a single main river channel (e.g., Yamuna or Son), without forming any sort of anabranching or distributaries (like those formed by - Mahanadi, Godavari, Kaveri etc.), the Luni river basin cannot be delineated from a single pour point. Luni river forms an inland delta after meeting the last tributary Sukri and after crossing Gandhav, the channel debranches out into the extended sandy floodplains of the Rann of Kutch. The exact pour point is hence not possible to be defined as an input to delineate the exact river basin out of a DEM. Mishra et al. (2019) show how the Varuna river (near Varanasi, U.P.) basin boundary varies as the different types of DEMs with the varying resolution was used to delineate the basin boundary.

In this present study, the Luni river basin is delineated using the SRTM DEM 30 m which was then corroborated with the available SoI topographical maps and the present-day Google Earth imagery (September 2020). The present basin boundary extracted from the SRTM DEM 30 m was altered following the contours of the SoI topographical maps and the Google Earth basemap in ArcGIS. The southern part of the basin boundary was altered and a broad mouth was digitized to consider all the anabranching channels of the Luni. The western section of the SRTM DEM 30 m-based basin boundary was eliminated as the ephemeral flows are found not to contribute to the Luni river channel directly (Fig. 4.10). After hydrological conditioning of the DEM as a pre-processing requirement to extract the watershed in the GIS environment, the automated D-8 algorithm derives the pixel-based elevation values (Nardi et al., 2013) to draw out the Luni river basin. Since the process is pre-determined within the GIS system and cannot be altered if a specific condition base algorithm code is written for such an exceptional case. It is obvious that the western part of the Luni river basin lies in the arid environment of Thar and due to higher rates of evaporation and least amount of precipitation makes no streams to sustain, leaving behind the remanent of few ephemeral channels. All such western streams of Luni are initiated and fed by rain water. These streams carry themselves few kilometers downstream

with an exception during high intensity and daylong rainfall that turns such runoff channels violent and prone to flash floods. In Fig. 3.17, the inset red rectangles exhibit the local initial stream orders which flow eastwards towards the Luni river channel is unable to sustain the extreme climatic conditions of the Thar and hence perishes before reaching the main Luni river. Thus, the right bank tributaries of Luni are found to be most fragile and lean with the least channel width and streamflow. Even the most cited previous researchers have mainly considered the eastern part of the Luni river as its major basin area (Kale et al., 2000; Bajpai, 2004; Sharma, 2008) and therefore this fact has been considered while the inter-comparison of the basin boundary was done.
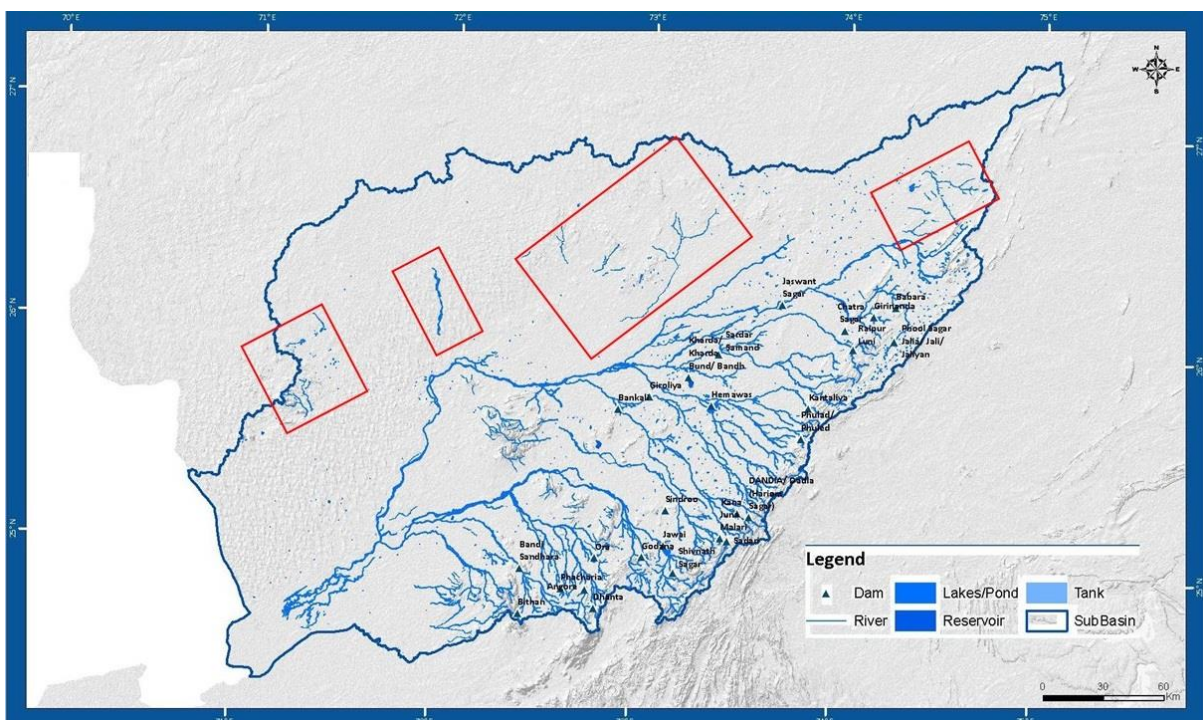
Fig. 4.10: The red marked areas showing the ephemeral nature of streams which eventually fail to join up the main Luni channel and hence raise a point on whether to consider such arid part into the regular basin system of Luni. Source: Adopted by the researcher from the CWC Basin report on west-flowing rivers of Saurashtra and Kutch including Luni (2014).

Apart from the three major cited research articles and the presently used basin boundary, various types of DEMs of the different resolution was used to see how the DEM based basin boundary varies from one another. Seven types of DEMs (Table 4.6) were used to show the major basin area using an approximate pour point in the Luni floodout area digitized from the SoI topographical map - 40 P/6 (Fig. 5.3). After pre-processing the DEM, and making them hydrologically connected in the GIS environment, the pour point extracted from the

topographical map was adjusted according to the flow accumulation layer obtained from the respective DEM. Thus, various shapes of the Luni river basin were obtained mainly based on the pixel-wise hydrological delineation of the watershed using the predetermined automated D-8 algorithm in the GIS platform. The other sources considered for the inter-comparison of the Luni river basin boundary was incorporated from the river basin reports published by the CWC (2014) and CGWB (2012) and the open-source major river basins of the world dataset made available by the data catalogue of the World Bank (2017). These river basins are also based on some hydrological corrected DEM and found to be much correlated with the one delineated from the DEMs by the researcher.

Table 4.6: Enlisted DEMs used in the analysis of Luni river basin boundary differentiation.

Sl. No.	DEMs	Spatial Resolution	Data Type	Data Source	Time Period
1	ASTER GDEM v.003	1 arc second (30 m)		Earthdata, NASA	Nov., 2013
2	CartoDEM v.3 R1			NRSC, ISRO	Apr., 2015
3	SRTM v.3.0			Earth Explorer, USGS	Sept., 2014
4	ALOS GDSM World 3D (AW3D30) v. 3.1		Elevation Raster Grid	EORC, JAXA	May, 2020
5	SRTM v.4.0	3 arc second (90 m)		CGIAR-CSI	2008
6	TanDEM-X			Earth Observation Centre (EOC), German Aerospace Centre	2015
7	SRTM v.4.0	250, 500 m and 1 km		CGIAR-CSI	2008

Source: Compiled by the researcher.

4.12.1 Areal morphometric analysis of Luni river basins obtained from various sources

The various source-based Luni river basins were overlayed on each other along with the present study river basin to bring out the areal difference observed in each river basin boundary (Fig. 4.11). Linear and areal morphometry of these river basins were performed to bring out the structure-based analysis of these river basins, pertinent in understanding the variation of morphometric attributes in comparison to the present study basin boundary. In Table 4.7, the linear and areal morphometric parameters are enlisted to give an overview of how the river basin boundaries vary from one another and with that of the present boundary. The highest and lowest basin area is observed for SRTM DEM 90 m with 75,042.87 km^2 and Sharma (2008) with 30,146.80 km^2 respectively. The areal morphometry considers the same listed factors that were analyzed for the Luni river sub-basins as provided in Table 4.2. The E_R, C_R and F_F are represented in Fig. 4.12 as dot and line graph exhibits the relationship between these three key

morphometric factors. The Luni basin boundaries delineated from different DEMs and obtained from various articles and reports show a moderate elongation with a lower form factor corresponding them each other. The minimal amount of structural influence is registered with a lower circularity ratio. The other indices of shape exhibit the vast expanse of the central and southern portion of the river basins with a peaky upper section. The main mass concentration of the river basin lies in the centre with a variation of over ~50 km. as derived from the CG point analysis. The topographic fitness of the river basins is unique to be fitted within the landscape of Thar and the relics of Aravalli hills.

The Fig. 4.13 and Table 4.8 are complementary and represents the basin area and their difference from the area of the present study basin of Luni. The highest difference is observed for the SRTM 90 m derived Luni basin of 35,764.07 km^2. Negative values of basin area difference were observed for the river basins obtained from Kale et al. (2000) and Sharma (2008) with -3877.79 and -9132 km^2 respectively. This means that the basin area used by Kale and Sharma are less than the area of the present study basin. The DEM and the report based Luni river basins have a higher area than that those taken from the research articles. The DEMs tend to draw the watershed polygon based on the entire hydrologically conditioned flow accumulation raster and do not have control over the decision of which part is not to be considered.

The compound scoring and the priority ranking of the various Luni basins are done based on the different enlisted areal morphometric parameters (Table 4.9). The lowest compound scores with the highest priority rank were obtained for the SRTM DEM 1 km derived Luni basin, while the highest compound score with the lowest priority rank was observed for the Luni basin obtained from the open-source dataset of World Bank (2017). The risk of erosion is compiled in Table 4.10 with the frequency analysis of the Luni basins divided into five major classes. A higher risk of erosion is observed for the various DEM derived six basins with a priority ranking range of <2 and 2-4. The rate of erosion is found to be the least with a priority ranking range of 6-8 and >8. These are all article and report based Luni basins having lower erosion potentiality. Only three basins have a moderate erosion potential and are in a transition stage of elevating them towards a low erosion risk zone as the priority rank ranges between 4-6.
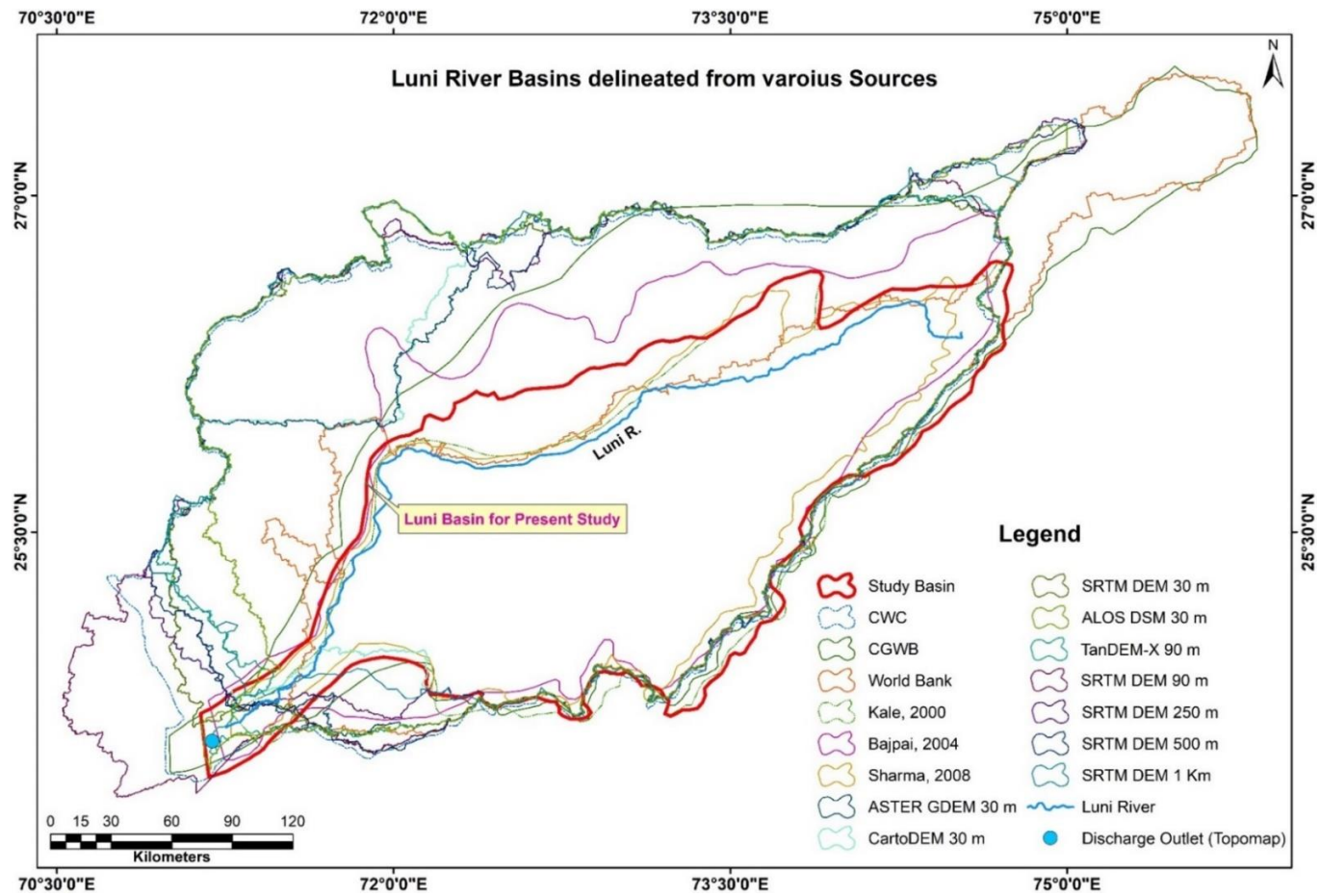
Fig. 4.11: Luni river basin boundary derived from DEMs of different resolutions and cited literatures. Source: Prepared by the researcher based on the listed DEM tiles in Table 4.6 and cited research articles.

Table 4.7: Values of linear and areal morphometric parameters for Luni river basins derived from different sources.

Basin ID	Basin	B_L	B_A	B_P	B_W	Lcm	Wcm	I_S	C_R	E_R	F_F	L_R	C_C	E_I	LW_R	G_S	F_R	B_E	C_S
1	Present Study Basin	433.16	39278.80	1188.58	183.74	221.27	91.26	4.78	0.35	0.52	0.21	1.19	1.69	3.75	2.36	1.68	0.36	2.21	1.74
2	CWC (2014)	518.10	72948.30	1573.52	286.32	229.49	126.96	3.68	0.37	0.59	0.27	0.92	1.64	2.89	1.81	1.63	0.33	1.51	1.42
3	CGWB (2012)	585.93	59965.90	1427.06	224.68	283.83	93.27	5.73	0.37	0.47	0.17	1.43	1.64	4.50	2.61	1.63	0.41	2.87	1.99
4	Kale et al. (2000)	412.42	35401.01	1093.07	194.19	208.78	75.35	4.80	0.37	0.51	0.21	1.20	1.64	3.78	2.12	1.63	0.38	2.58	1.75
5	Sharma (2008)	393.21	30146.80	1069.87	171.51	204.93	68.52	5.13	0.33	0.50	0.19	1.28	1.74	4.03	2.29	1.73	0.37	2.82	1.86
6	World Bank (2017)	524.88	40303.30	1974.09	215.83	207.59	67.71	6.84	0.13	0.43	0.15	1.71	2.77	5.37	2.43	2.75	0.27	2.90	2.34
7	Bajpai (2004)	431.02	44190.96	1170.05	219.82	215.83	92.21	4.20	0.41	0.55	0.24	1.05	1.57	3.30	1.96	1.56	0.37	2.12	1.58
8	ASTER GDEM 30 m	421.76	60805.20	2019.93	271.77	198.16	112.51	2.93	0.19	0.66	0.34	0.73	2.31	2.30	1.55	2.29	0.21	1.45	1.36
9	CartoDEM 30 m	422.58	59032.36	1879.06	249.04	200.11	105.82	3.03	0.21	0.65	0.33	0.76	2.18	2.38	1.70	2.17	0.22	1.61	1.38
10	SRTM DEM 30 m	437.84	69430.55	1915.06	275.89	256.30	147.67	2.76	0.24	0.68	0.36	0.69	2.05	2.17	1.59	2.04	0.23	1.42	1.29
11	SRTM DEM 90 m	486.04	75042.87	1890.89	275.22	242.39	140.67	3.15	0.26	0.64	0.32	0.79	1.95	2.47	1.77	1.93	0.26	1.40	1.36
12	SRTM DEM 250 m	471.65	68918.1	1691.94	264.17	193.00	122.76	3.23	0.30	0.63	0.31	0.81	1.82	2.54	1.79	1.80	0.28	1.21	1.34
13	SRTM DEM 500 m	475.17	70098.39	1621.121	275.40	195.02	145.53	3.22	0.34	0.63	0.31	0.81	1.73	2.53	1.73	1.71	0.29	0.89	1.29
14	SRTM DEM 1 km	428.33	67620.69	1415.76	272.43	190.67	142.29	2.71	0.42	0.68	0.37	0.68	1.54	2.13	1.57	1.52	0.30	0.89	1.17
15	TanDEM-X 90 m	442.17	68715.2	1780.12	276.07	214.57	117.75	2.85	0.27	0.67	0.35	0.71	1.92	2.24	1.60	1.90	0.25	1.52	1.30
16	ALOS World 3D-30m	497.40	68211.5	2085.47	276.15	228.24	144.24	3.63	0.20	0.59	0.28	0.91	2.25	2.85	1.80	2.24	0.24	1.23	1.47

B_L: Basin Length, B_A: Basin Area, B_P: Basin Perimeter, B_W: Basin Width, Lcm: Straight length from the watershed mouth to the centre of mass of the watershed, Wcm: Width of the watershed at the centre of mass and perpendicular to Lcm, I_S: Index of Shape, C_R: Circularity Ratio, E_R: Elongation Ratio, F_F: Form Factor, L_R: Lemniscate Ratio, C_C: Compactness Coefficient, E_I: Ellipticity Index, LW_R: Length-Width Ratio, G_S: Gravelius Shape Index, F_R: Fitness Ratio, B_E: Basin Eccentricity, C_S: Compound Score. Source: Computed by the researcher.
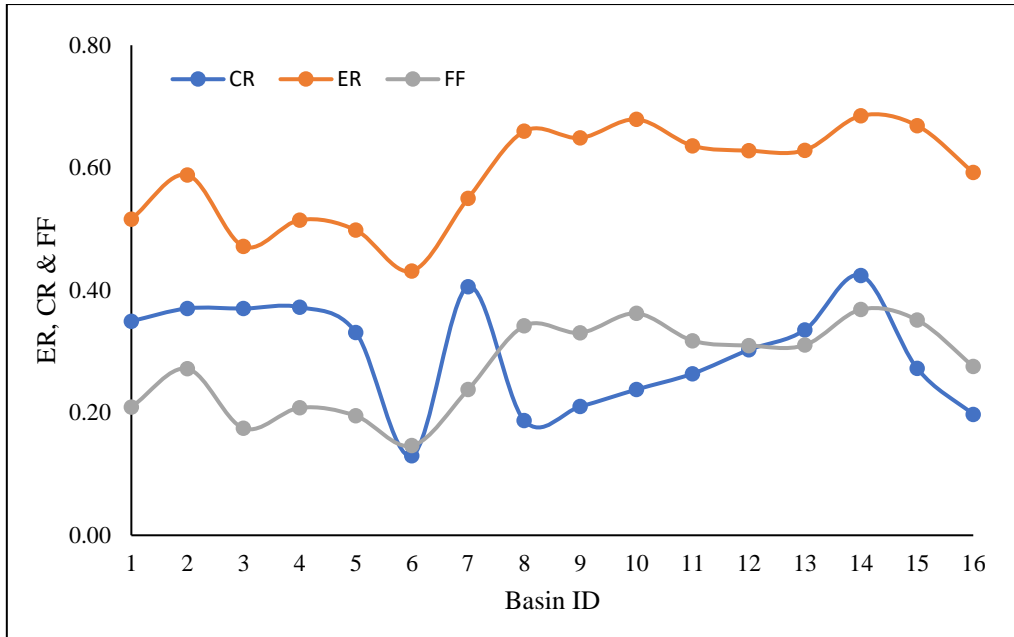
Fig. 4.12: Dot and line graph showing the variation of ER, CR and FF for the Luni river basins derived from various sources. Source: Computed by the researcher.

Table 4.8: Area of the Luni river basins obtained from various sources and their areal differences.

Basin Source	Basin Area (km²)	Basin Area for Present Study (km²)	Areal Difference (km²)
CWC (2014)	72948.3	39278.80	33669.50
CGWB (2012)	59965.90		20687.10
Kale et al. (2000)	35401.01		-3877.79
Sharma (2008)	30146.80		-9132.00
World Bank (2017)	40303.30		1024.50
Bajpai (2004)	44190.96		4912.16
ASTER GDEM 30 m	60805.20		21526.40
CartoDEM 30 m	59032.36		19753.56
SRTM DEM 30 m	69430.55		30151.75
SRTM DEM 90 m	75042.87		35764.07
SRTM DEM 250 m	68918.1		29639.30
SRTM DEM 500 m	70098.39		30819.59
SRTM DEM 1 km	67620.69		28341.89
TanDEM-X 90 m	68715.20		29436.40
ALOS World 3D-30m	68211.50		28932.70

Source: Computed by the researcher.

Fig. 4.13: Basin area and the areal differences for Luni river basin as obtained from various sources. Source: Computed by the researcher.

Table 4.9: Compound scoring, priority ranking and erodibility of Luni river basins derived from various sources.

Basin	Compound Score	Priority Ranks	Interpretation	Erodibility
SRTM DEM 1 km	1.17	1	Very High	**Most Erodible**
SRTM DEM 500 m	1.29	2	High	
SRTM DEM 30 m	1.29	2	High	
TanDEM-X 90 m	1.30	3	High	
SRTM DEM 250 m	1.34	4	High	
SRTM DEM 90 m	1.36	5	Moderate	
ASTER GDEM 30 m	1.36	5	Moderate	
CartoDEM 30 m	1.38	6	Moderate	
CWC (2014)	1.42	7	Low	
ALOS World 3D-30m	1.47	8	Low	
Bajpai (2004)	1.58	9	Low	
Present Study Basin	1.74	10	Low	
Kale et al. (2000)	1.75	11	Very Low	
Sharma (2008)	1.86	12	Very Low	
CGWB (2012)	1.99	13	Very Low	
World Bank (2017)	2.34	14	Very Low	**Least Erodible**

Source: Computed by the researcher.

Table 4.10: Frequency analysis of erodibility for Luni river basins derived from various sources.

Priority Ranking Ranges	Erodibility Risk	Frequency
<2	Very High	1
2 to 4	High	4
4 to 6	Moderate	3
6 to 8	Low	4
>8	Very Low	4

Source: Computed by the researcher.

4.12.2 Centre of Gravity analysis

The Centre of Gravity (CG) is the imaginary point where the total body weight of an object either regular or irregular, is anticipated to be concentrated. CG analysis is an unexplored part of watershed studies which gives a newer dimension of understanding how a drainage basin area has its mass distributed with a major concentration over a point generally at the centre of the river basin. River behaviour could be analysed by observing the distribution of the river basin mass and hence the weightage of the main trunk stream could be deciphered and the basic reason for its present channel flow could be interpreted. The CG is calculated based on the channel length measured from the outlet of the river basin to a point on the river nearest to the centre of the basin. The CG points for all the river basins were obtained using the feature to point tool in the ArcGIS environment. The centroid points of each basin were obtained and a proximity analysis was performed to bring out the distance of each CG point from that of the present study basin. In Table 4.11 and Fig.4.14, the distance of the CG points of each derived Luni basins from that of the present study basin of Luni is provided with a Table and a radar plot respectively, complementing one another. The maximum distance was observed for the SRTM DEM 90 m derived Luni basin (49.49 km) and that of the reported basin of CGWB (49.05 km). The least distance of 3.74 km was observed for the Luni basin obtained from the research article of Sharma (2008). Therefore, the range of concentration of the mass represented by the CG points for the different source derived Luni basins are found determines the propensity of variation of the mass concentrated over its respective centre in accordance.

Based on the CG points spread over an approximate distance of 50 km, a buffer range analysis was performed to see which derived river basins come closer to the present study basin, while others move back further to the highest proximal distances. In Table 4.12, five buffer zones are shown as derived in the ArcGIS environment based on the buffer tool with the frequency of CG points meant for each of the river basins. Out of the fifteen river basins, only two basins come close to the CG point of the present study basin i.e., within 10 km buffer zone, as obtained

from the research articles of Kale et. al. (2000) and Sharma (2008). While nine of the river basins mainly derived from the various DEMs as well as that of CWC (2014) and CGWB (2012) comes under the buffer range of 40-50 km.

Table 4.11: Distance of Centre of Gravity (CG) from the present study river basin of Luni

Basin Source	Distance of CG Points from the Present Study Basin (km)
CWC (2014)	42.20
CGWB (2012)	49.05
Kale et al. (2000)	9.73
Sharma (2008)	3.74
World Bank (2017)	27.59
Bajpai (2004)	14.21
ASTER GDEM 30 m	30.29
CartoDEM 30 m	32.41
SRTM DEM 30 m	43.47
SRTM DEM 90 m	49.49
SRTM DEM 250 m	42.55
SRTM DEM 500 m	41.87
SRTM DEM 1 km	44.31
TanDEM-X 90 m	43.15
ALOS World 3D-30m	41.16

Source: Computed by the researcher.

Table 4.12: Buffer ranges of CG points for the Luni river basins obtained from various sources from the present study basin.

Buffer Ranges (km)	No. of CG Points	Name of CG Basin Points
<10	2	Kale et al. (2000) and Sharma (2008)
10 to 20	1	Bajpai (2004)
20 to 30	1	World Bank (2017)
30 to 40	2	CartoDEM 30 m and ASTER GDEM 30 m
40 to 50	9	ALOS World 3D DSM - 30m, TanDEM-X 90 m, CWC (2014), CGWB (2012), SRTM 30, 90, 250, 500 m and 1 km

Source: Computed by the researcher.
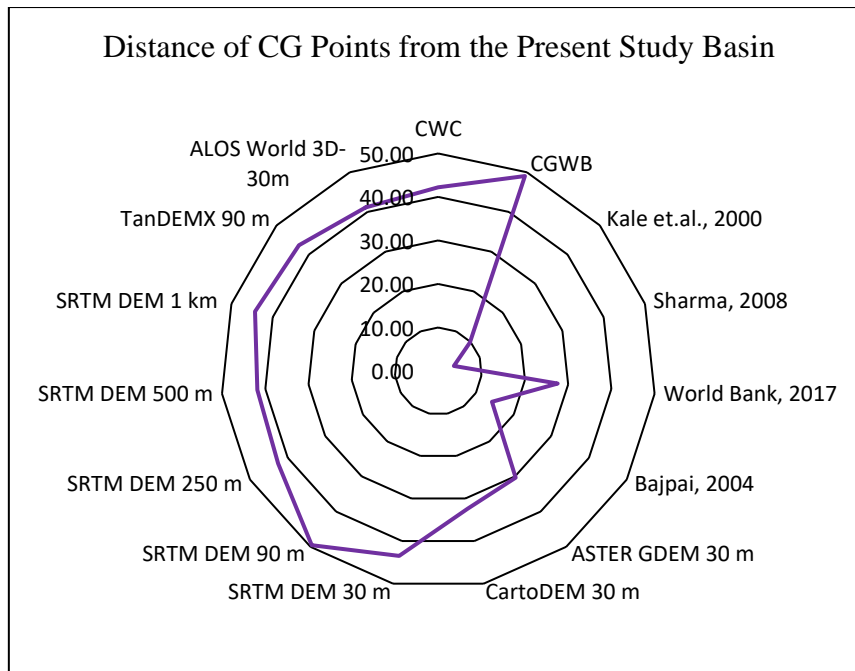
Fig. 4.14: Distance of the CG points from the present study basin. Source: Computed by the researcher.

4.12.3 Luni river basin Asymmetry Factor (AF Index)

The assessment of tectonic tilting within the river basin along with its tilt direction is defined as the AF index (Cox, 1994; Kale et al., 2014; Roy and Sahu, 2015). It is vital for understanding the river basin tilting perpendicular to the direction of the Luni channel. The AF index is calculated using the formula –

$$AF = 100 \, (^{Ar}/_{At}) \quad \text{(Eq. 4)}$$

where Ar is the hypsographic right area of the Luni river basin and At is the total basin area of the Luni river. The AF index is computed based on the present study basin only. The AF index value ~50 suggests a uniform lithology in a stable setting which is said to be an ideal condition for conceptual understanding. An unstable setting that is normally found for more or less very natural drainage basins would have a deviation from the normal value as greater or less than 50 (Keller and Pinter, 1996). The AF index value for the Luni river basin is 21.42 suggesting an entire rightward tilting of the entire drainage basin. The Luni river flows through the western section of the river basin (Fig. 2.1) with an area of only 8,414.94 km^2 to its right and an area of 30,863.9 km^2 to its left side. The regional slope and structural setting have led to a wider left side area compared to that of right in the Luni catchment and hence all the major tributaries flow into the Luni river from its left.

4.13 Landscape characterization through Hypsometry Curve

The graphical representation of an empiric aggregate distribution function of terrain in a river basin is known as hypsometric curve. Hypsometry can be unpacified with the definition of distribution of terrain for a functional area covered under each contour interval, as computed manually from a topographical map. These curves are drawn on a normalized scale with cumulative area on the X-axis and cumulative height on the Y-axis inorder to bring out the variations in the drainage basin and its sub-basins. The significance of hypsometric integral (HI) values are associated with the different kinds of morphometric parameters. A strong positive relation is found in between basin geometry and stream networks. The foundation of hypsometry was laid down by Langbein (1947) and was further utilized and explained by Strahler (1953) to cover the area-elevation curve and HI. The underneath area of the hypsometric curve is computed to determine the HI representing the residual volume, while the erosion integral (EI) represents the area of the basin that has already been eroded by the forces of denudation.

The various geometric forms for the hypsometric curve state the present stage of life cycle for a river basin landscape. The HI primarily figures out the dissection intensity of upland areas in a drainage basin. A young topography with soaring elevation is illustrated with an upward-convex arc within the graphical axes. A mature topography is represented with near about straight-line curves having marginal sinuosity. The senile erosional stage is observed with the down warping gradient upslope-concave curves.

The hypsometric curves of the Luni river basin and its major sub-basins (Fig. 4.15) represents a senile topography where the geomorphic agents of fluvial and aeolian actions have already denuded the riverscapes leaving behind a meagre amount of the unconsumed topography left to be eroded. The monadnocks of Aravalli in the eastern section of the river basin and some of the few remnants on the western part of the basin just adjoining the river Luni near Balotra are undergoing slow and progressive erosion because of their ancient hard crustal pre-Cambrian granitic origin. The HI% and EI% in Table 3.17 distinguish every sub-basin of Luni including itself based on their present stage of erosion. The mean HI% of the entire Luni river basin is 20.21 suggesting that the basin is in the middle old stage. The senile/old stage of the basin's topography can be further classified into three micro-stages –

- Late old stage (EI ≤15%) - where the curve drops sharply down vertically and then is quite flat or very gently sloping

- Middle old stage (EI = 15-25%) - where the curve slopes down sharply initially but diagonally and then assume an even gentler gradient for the rest of its course

- Early old stage (EI = 25-35%) - where the initial steeply dropping segment is minimal and then the curve assumes a constant slope for the rest of its course.

Table 4.13: Percentage of HI & EI of Luni river basin and its major sub-basins.

River Basin	Sub-Basin ID	HI%	EI%	Generic Hypsometric Stage	Micro Hypsometric Stage
Luni River	-	**15.20**	**84.80**		**Late Old Stage**
Lilri River	1	27.27	72.73		Early Old Stage
Mithri or Jojri River	2	32.15	67.85		
Jojari Nadi	3	30.38	69.62	Monadnock/Senile	
Guhiya Nadi	4	19.96	80.04		Middle Old Stage
Sukri Nadi	5	13.73	86.27		Late Old Stage
Kher Nawala Nadi	6	10.71	89.29		
Sukri River	7	12.27	87.73		
Mean	-	**20.21**	**79.79**		**Middle Old Stage**

Source: Computed by the researcher.

The superimposition of the hypsometric curves of the Luni river basins along with the major seven sub-basins (Fig. 4.16) reveals that all of the basins have been dissected to below the equilibrium line, with an exception of Mithri or Jojri river basin which has not yet initiated toe erosion in the topography as the curve of hypsometry rise above the equilibrium line. These basins are progressively in the early old to the late senile stage in their evolutionary process. Some of the sub-basins have very similar hypsometric curves. The above superimposition also allows three distinctive groupings to be made on the basis of the attitude of the hypsometric curve (Table 4.13). The treemap distribution (Fig. 4.16) explains the hierarchical arrangement of the HI% values in accordance with the denudation of the sub-basin. The two right-side tributary river basins Mithri and Jojari are found to be in their early old stage of the evolutionary process while the rest are progressing towards the late old stage, where the Luni river basin itself is in the brim of the senile topographic stage. Similar representation to further distinguish the EI% and HI% values a bar diagram is represented in Fig. 4.16 to give an easy overview of its distribution.
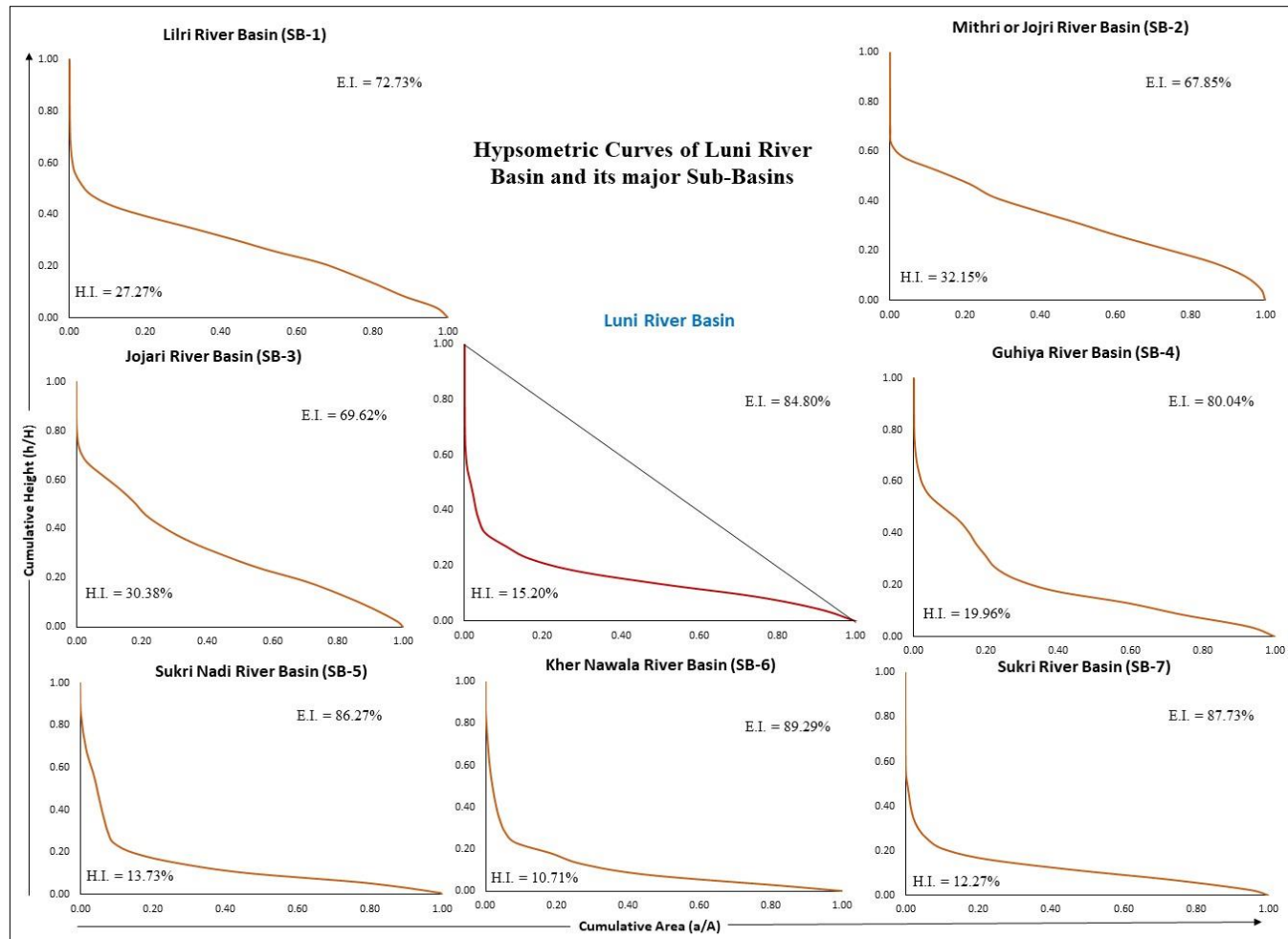
Fig. 4.15: Hypsometric curves of Luni river basin and its major sub-basins. Source: Computed by the researcher based on the SRTM DEM 30 m tiles.
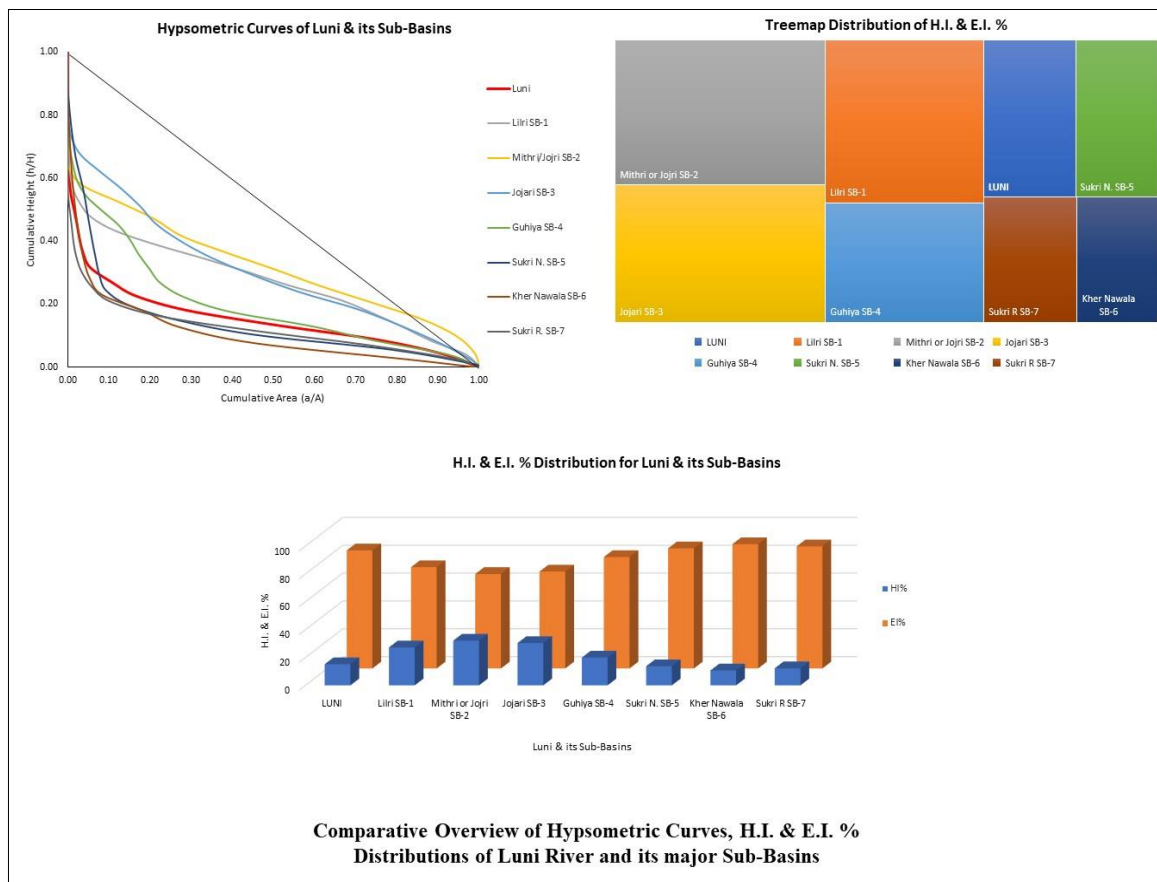
Fig. 4.16: Superimposed hypsometric curves, treemap distribution and distribution of HI% and EI% for Luni river basin and its major sub-basins. Source: Computed by the researcher based on the SRTM DEM 30 m tiles.

4.14 River Behaviour Analysis of Luni using Long Profile

A river's long profile is its general distribution of gradient along the entire channel from source to sink. It is the proportional graphical representation of decline in the channel's slope to its segment over a particular reach. It is therefore the configuration of the channel bottom in longitudinal view (Knighton, 1998). In most cases and particularly in humid regions and for established (mature) stream channels, it is concave – upwards. It is an important element of riverine behavioural study together with the channel network discerning the frontier conditions for hillslope processes. The longitudinal profiles of natural rivers, though concave upward, rarely tend to be smooth. Convexities are generally found in a long profile which shows how steep local channel gradient can result from one of several causes like defiant strata of bedrocks, the addition of a coarser sediment load and/or tectonic actions. This 'concave up' shape of the long profiles has also often been described in terms of the graded profile.

Thus, a river's long profile exhibits its prolonged adjustment to morphology of the drainage basin landscape, induced by the varying conditions of lithology, climatic setup and tectonic actions. River channel slope, determining the erosional rates, are accommodated such that diversified rates of uplift are matched by variable amount of erosion. Hence, hasty changes in slope due to certain ex-situ perturbations along the river profiles (Montegomery and Brandon, 2002; Kirby and Whipple, 2012) may express active faults that cross these rivers (Seeber and Gornitz, 1983). Due to the profiles being extracted from the DEM surface through polyline overlay, the comparatively poorer resolution DEM than those ideally required for longitudinal profile analysis can also at times cause an artificial break to appear, but these have been largely smoothened out using eleven-point moving average window (Kale et al., 2014).

The long profile of the Luni river shows a general 'concave-upward' slope with certain alteration points or 'breaks' in the slope. A segment distance of 10 km was chosen after going through a series of six sets of permutation segment lengths inorder to judge the best distance suitable for covering the entire Luni river for long profile analysis. Thus, the approximate river length of >500 km was divided into 10 km segments having 50 sets of observations with cumulative distance downstream of Luni (X-axis) and elevation (Y-axis). The Fig. 3.24 helps to interpret the Luni's long profile with the major 'breaks' observed from the intersection of major faults cutting across the river channels in various points through the entire Luni river (highlighted in red rectangles), corresponds exactly with the red circles in the inset long profiles curves drawn on linear and logarithmic scales. Hence, the tectonic influence from the major structural faults and the degree of its exposure, alignment and deflection controls the behaviour of the river and its sensitivity to the riverscape. The flow turn angle and deviation of the straight channel leads to the breaks in the long profile curve of the Luni river.

The various associated parameters used to characterize the lithological control and geomorphic evolution based on tectonic activities of the Luni river basin are explained using the following ancillary parameters of the long profile which are discussed as given below –

- **Normalized Long Profile**: Normalization of the long profile is a process of structuring the DEM derived raw long profile database on a scale of 0 to 1. Both the elevation and distance datasets are standardized and a plot of the long profile is obtained in a normalised framework. The normalised long profile of the Luni river (Fig. 4.18) explains the influence of knickpoints or tectonic perturbations of the major fault lines cutting across the river at various sites (Fig. 3.24). A polynomial trend line was found to suitably fitting the long

profile curve with the highest goodness of fit or R^2 value as 0.99. Normalizing a long profile helps to pinpoint the exact breaks or knickpoints inorder to locate the exact point(s) of influence of tectonics on the river metamorphosis.

Due to differences in the length and amount of fall of the channel, a simple comparison of the long profiles does not bring light to all the facets. Hence, the length of long profile and channel fall were standardized (Fig. 3.25) to reduce the effects of variable basin size and relief by the elevations and lengths being divided by the highest catchment relief and the total stream length respectively to standardize the profiles (Lee and Tsai, 2009).

- **Stream gradient index (SL)**: The geophysical variables like climate, local lithology, sediment flux, tectonics, alterations in base level brings in a change in a typical concave-shaped long profile (Kirby and Whipple, 2012). Hack (1973) postulated a simple and classical approach to denote any sort of deviation in a river long profile through the stream-gradient index (SL). It can also be shown as a function of distance towards a river's downstream, expressing the changes in channel slope (Nexer et al., 2015). The computation of SL index is based on segment slope along the river channel ($\frac{\Delta H}{\Delta L}$) and the distance between the source of the river to a selected segment (L) –

$$SL = \frac{\Delta H}{\Delta L} \times L \qquad \text{(Eq. 5)}$$

Seeber and Gornitz (1983) have used the SL index in an active orogeny to identify the tectonic influence on the river channel. Interpretation of SL values should be done with caution as it directly banks on the shape of the equilibrium profile and its dynamic relationship between the contributing catchment area and sediment flux (Nexer et al., 2015 and Das et al., 2021b). Higher SL index values represent a stronger influence of tectonics, while the lower SL index values represent a minimal influence of tectonics on the river channel. Hence, the SL index and tectonic influence share a direct and positive correlation.

The SL index for the entire Luni river channel (Fig. 4.18) is determined with a segment distance of 10 km. The river Luni flows through a gradual slope indicating a progressive range of SL index showcasing the differential erosion rate and lithological control imposed by the faults. The long profile is dominated by certain reminisces of active tectonics because of the underlying faults (Ayaz and Dhali, 2020). The rate of change is documented separately to find out the major location of the change in the SL index. The average SL value for the Luni river channel is 153.78, and the minimum and maximum values range between 3.80 to 448.47 (Appendix, Table B). A second-order polynomial trend line was found to fit the best. It

represented the SL index dataset with a low positive curvilinear trend with the R^2 value of 0.38, meaning anomalous changes with sudden low and contrasting high values of SL index bringing in the fact of major sharp knickpoints or steep knickzones (Das et. al., 2021b) induced by the faults underneath the Luni river channel.

- **Comparison of Long Profiles drawn on Arithmetic and Logarithmic scale**: The interface to compare long profiles on two mathematical scales helps in understanding and locating the exact points of changes in the long profile induced by an external perturbation including active tectonics or variable grade of erosion. The long profiles plotted along the base of cumulative distance downstream (km) is based on the two types of Y-axes one with the arithmetic and the other with a logarithmic scale. The logarithmic scale inverses the long arithmetic profile curve and helps in highlighting the major knickpoints along the curve to have a better view and exact locations of them as shown in Fig. 4.18 with the inset red circles.

- **Change of Segment Slope**: The shift in segment slope along the Luni river channel (Fig. 4.18) is recorded in m km^{-1} on the base of the cumulative distance downstream (km). The graph's initial part shows a sloping decline with rising segments indicating the positive rise in slope anomaly due to underlying faults and erosion-based differences. The logarithmic trend line was most suitably representing the dataset. A high positive R^2 value of 0.8 was noted, indicating the changes of slope to be progressive with minor perturbations.

- **Changing Rate of SL Index**: The amount of change of the SL index (Fig. 4.18) suggests the rate of alterations observed within the Luni river channel due to tectonic influence as found from the lineament intersections. The major faults crossing the Luni channel endorse a gradual to high rate of change in the SL index. The mean amount of change of the SL index is 2.02, while the changing rates vary from -169.99 to 311.49 (Appendix, Table B). Such anomaly showcases the ex-situ disturbances in the long profile's gradient. Slight to significant variations on the graph indicate the frequency and propensity of the changing rates in the SL index.
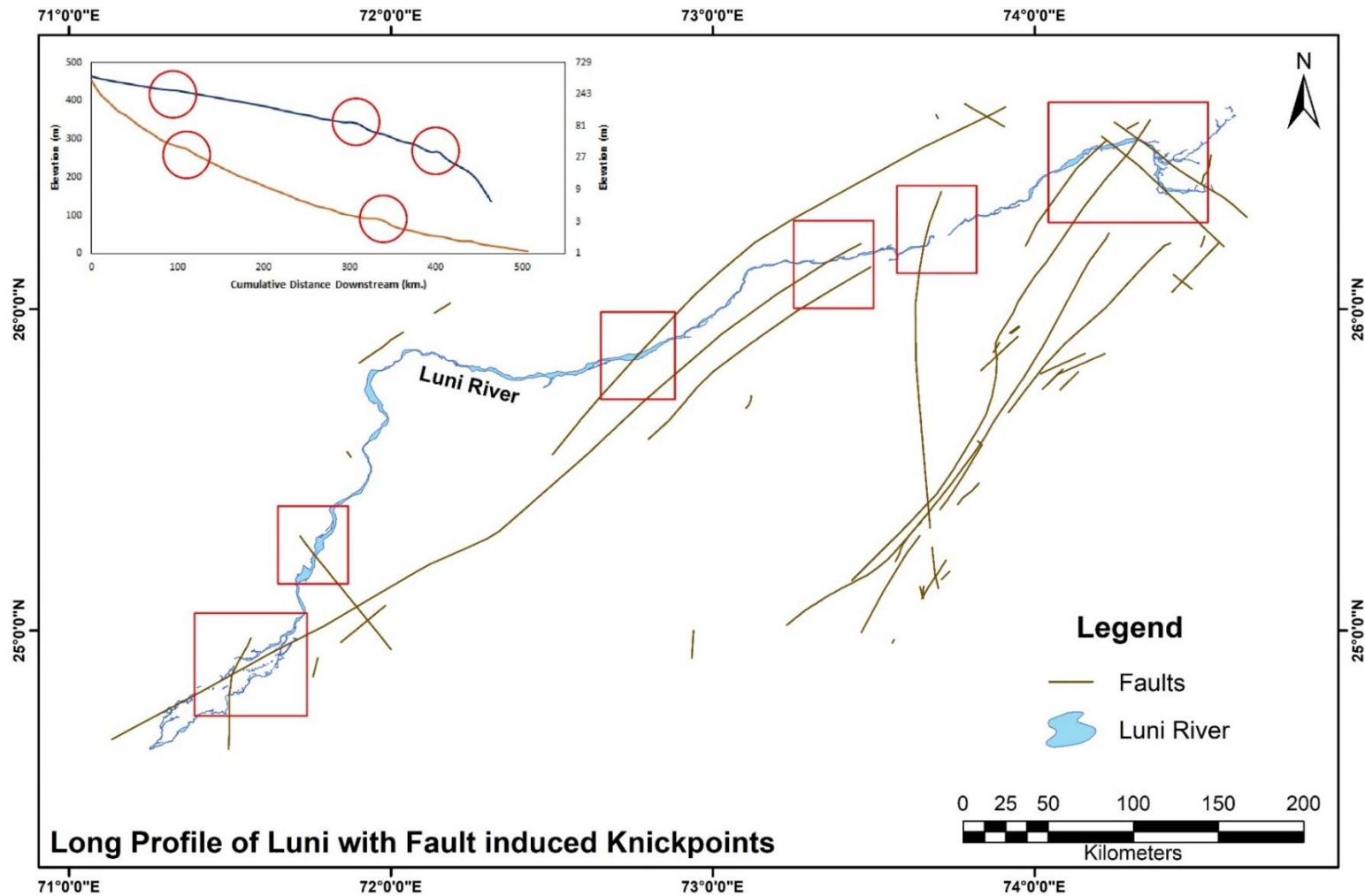
Fig. 4.17: Long profile of Luni river and the fault induced knickpoints along its course. Source: Computed by the researcher based on the SRTM DEM 30 m tiles and overlayed on the lineament map obtained from GSI database.
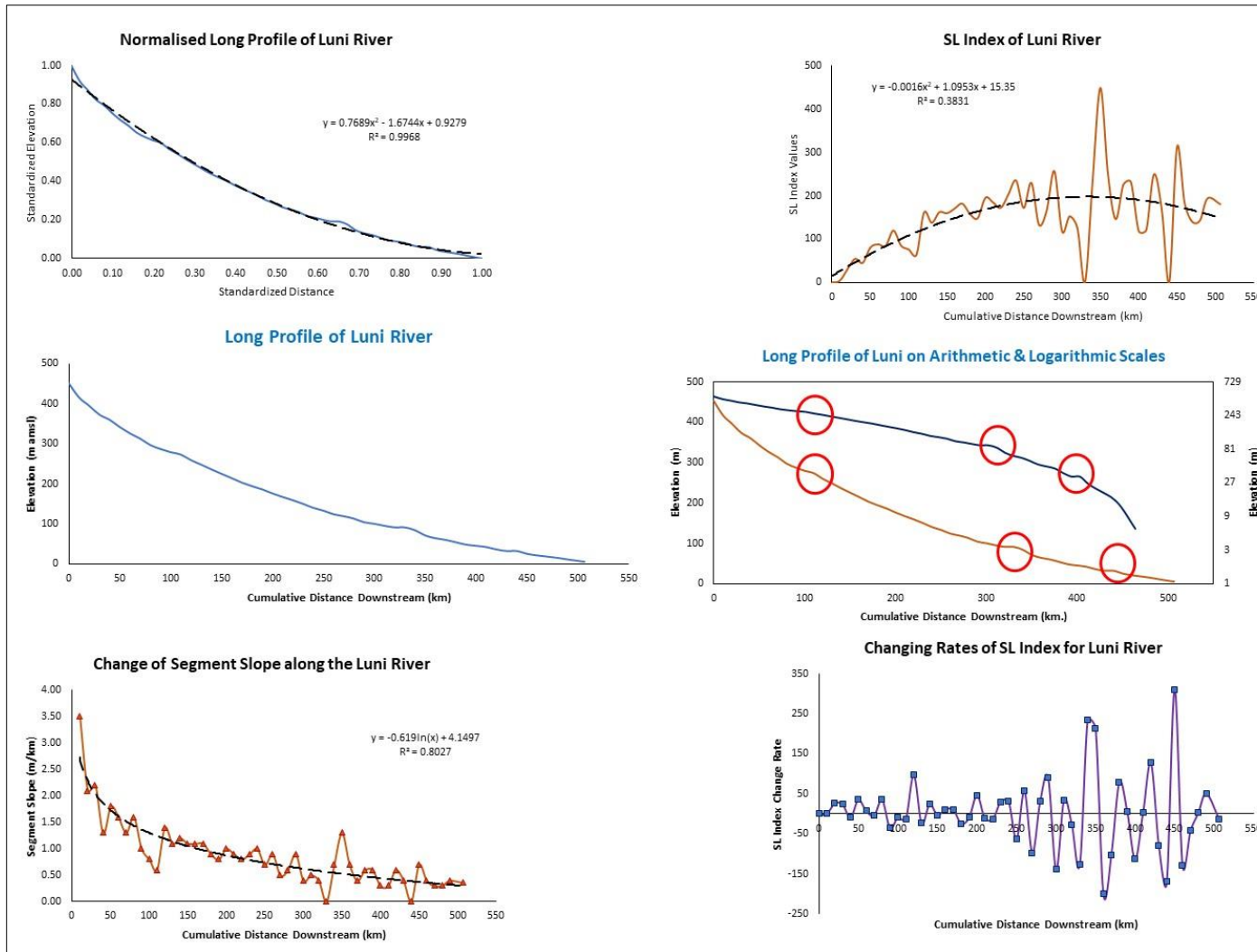
Fig. 4.18: Different aspects of the Long Profile analysis for the Luni river. Source: Computed by the researcher based on the SRTM DEM 30 m tiles.

- **Long Profile and SL Index Overlay**: The long profile and SL index for the seven major tributaries of the Luni river (Fig. 4.19) were calculated (Appendix, Table D) to develop the understanding of micro to macro alterations in the streams due to tectonic influence from the structural lineaments or the diversity in erosion rates. The overlay of the SL index and long profile helps to correlate the points or zone of changes and helps to glance through the primary reasons behind such alterations. The two right bank tributaries of Luni – Mithri and Jojari-have a typical 'concave-upward' long profile shape with a steep yet gradual changing SL index from its source till it meets the Luni. Few minor knicks in the profile and satellite-based image observations say that the differential rates of erosion and the major faults on the western side of the river basins are responsible for such anomalies. The rest five left bank tributaries are found to have a major 'concave-upward' slope in the long profile and a gradual change in the SL index. The Lilri river that originates from the lithological crests of the Aravalli along the eastern side of the Luni river basin shows certain knicks due to the existing fault lines adjoining the Aravalli with a high amount of lithological control. The other major tributaries like Sukri, Kher Nawala originate from the runoff slopes of Aravalli and show a progressive decline in the long profile with few exceptions. A huge amount of sand deposits accumulated on such river channels either due to natural sedimentation, flash flood deposit accumulation, or other anthropogenic alterations. The range of SL index variation is much lower than the main Luni river due to the expanse of Luni flowing a length of >500 km compared to these medium length tributaries. The average rate of change of the SL index for all the tributaries is found to be ~3%, while the mean value of the SL index varies from 69.69 to 108.78 depending on the size, length and expanse of the river channel. A higher SL index imply the influence of tectonics or erosion on the river channel and vice-versa. Hence, all the tributaries of Luni show some limited knickpoints due to a local geomorphic or lithological condition.
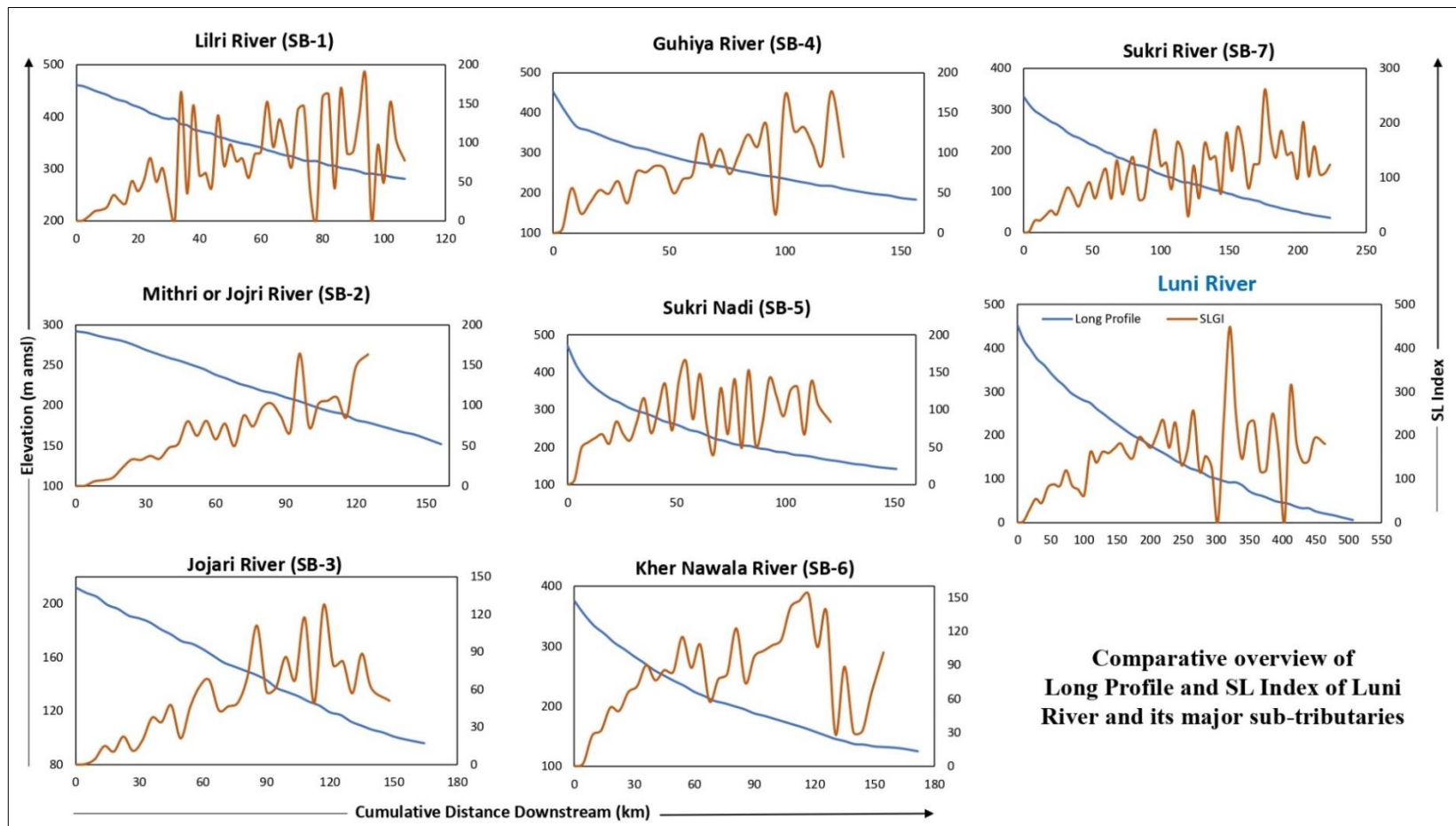
Fig. 4.19: Comparative overview of Long profile and SL index of Luni river and its major tributaries. Source: Computed by the researcher based on the SRTM DEM 30 m tiles.
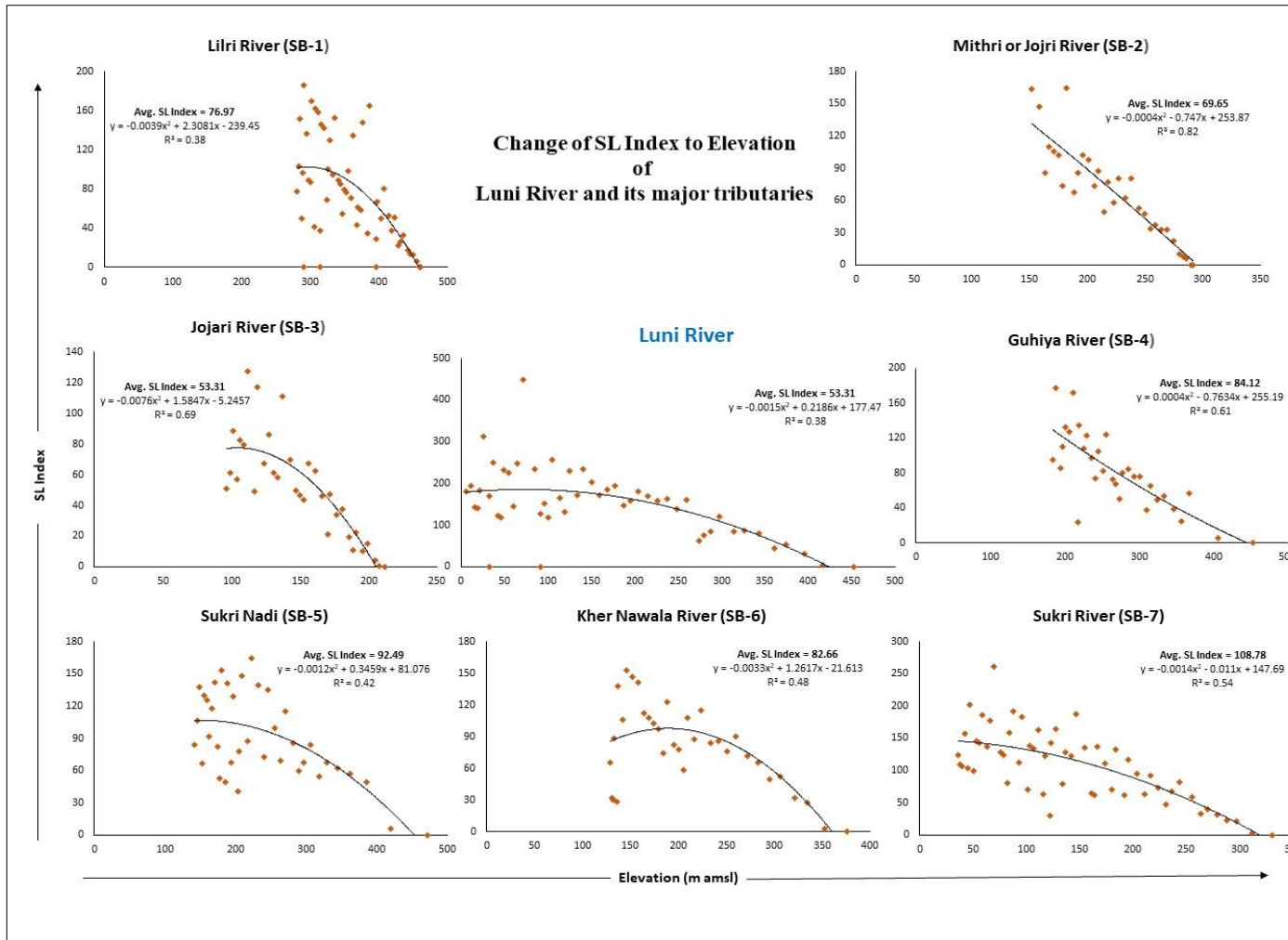
Fig. 4.20: Change of SL index to Elevation of Luni river and its major tributary streams. Source: Computed by the researcher based on the SRTM DEM 30 m tiles.

- **Change of SL Index to Elevation**: The change of SL index to elevation is a better form for evaluating the reasons for variations in the SL index. The key form of the derivation of SL index lies from the variation in elevation along the designated river channel, either for a specific segment or for the whole channel itself. The scatter plot of elevation (m amsl) on the X-axis and the SL index on the Y-axis (Fig. 4.20) represents the distribution of the SL index values over a particular range of elevation. It shows that over which elevation does the river originates and then meets the major higher-order stream. The trend of scattering depends on the significant differences among the correlation values with elevation as an independent factor counting on the elevation values (Roy and Sahu, 2015). The second-degree polynomial trendline shows low to higher positive fitness of the scatter plot with R^2 values ranging in between 0.38 for Luni river to 0.82 for Mithri river. The aberration of the SL values from the trend line explains larger sedimentation in the drainage basins, which is most evident in each of the scatter plots. The sedimentation is progressive in the downstream region of the streams with fewer exceptions especially for the left bank tributaries of Luni bringing down sediments from the relict topography of Aravalli and its footslope region. Some events like flash floods and anthropogenic alteration in the riverscape also tend to change the river behaviour evident from such correlation between SL index and elevation.

4.15 Summary

This chapter outlines the terrain, drainage and areal based morphometric analysis of the Luni river basin and its seven major sub-basins describing the variation of topographic and drainage factors. This helps to characterize and cover the behavioural aspects of the Luni river. The typical observations vary in the dryland river basin of Luni, hence making it exciting and unique to study. The basin boundary delineation of Luni from various sources and its intercomparison based on the shape and linear morphometry has provided a new dimension of analyzing the dryland river basin. It has tried to cover the issues faced in the Luni basin delineation from different DEMs and address the debates over such basin area differences. The CG points and the distribution of mass of a river basin is another new addition to this study. The basin asymmetry exhibits a right aligned Luni river channel with an implication of structural control. The hypsometry and long profile assessment discern the influence of tectonics, variable rates of erosion and the action of geomorphic agents – wind and water on the Luni river basin helping to decipher the evolutionary stage of its geomorphic life cycle.

CHAPTER – 5

ENVIRONMENTAL MECHANISMS AND SENSITIVITY ANALYSIS
OF LUNI RIVER BASIN

5.1 Introduction

The unceasing environmental management mechanisms need a defined and upgraded framework to consider the geomorphological inputs liable for the alterations of landscapes. Past studies conducted by Gregory (1987); Downs and Gregory (1995), and recently by Fryirs (2017) established a range of geomorphic examination to understand the sensitivity of river channels in the context of various internal and external stimuli from the environment and associated anthropogenesis leading to never-ending channel modifications. This kind of understanding of the sensitivity can be accomplished using the reductionist approach with an effective amalgamation of the operative geomorphic agents carving out the current riverscape. The frail landscape of the Luni is sensitive for any sort of high susceptible events like flash floods or unprecedented aggressive encroachments of human activities. Present-day studies show how proactive man-made activities disrupt the interactions of geomorphic agents due to the increasing demand for food, fodder, water and other natural resources threatening the ecology, sediment mobility, hydrology and degrading landscape quality (Kar, 2018; Kar and Kumar, 2020). Hence, discerning the aeolian-fluvial interactions and the eco-sensitive floodout region of the Luni needs to scientifically evaluate and observe the present status of such fluvial landscape. The modern technique to understand landscape sensitivity needs to be used to zone out the degree of response from a sudden and short-lived event like flash floods and the impact of increasing anthropogenic activities using MCDM methods. Such models support bringing out the sensitive zones for flash floods and human activities using some pre-determined thematic layers assigned with criteria weights and positioned in a hierarchy.

5.2 Objective

This chapter deals with the last two objectives of the research. The fourth objective of this study is to evaluate the behaviour and sensitivity of the Luni river using the lens of environmental mechanisms associated with aeolian-fluvial synergy and floodout morphology. At the same time, this research's last or fifth objective focuses on the findings of flash floods and anthropogenic sensitivity within the Luni river basin based on the MCDM-AHP and CSI modelling.

5.3 Methodology

The mapping of sand dunes along the stretch of Luni was selected based on the maximum concentration of the dunes found just after the southwards turn of the Luni channel a few kilometres crossing Balotra, much before the Sukri river joins the Luni. All the available dunes were digitized from the SoI topographical maps and were cross-checked with the present-day Google Earth base map imagery. A conceptual diagram was drawn to cover the topic to explain the aeolian and fluvial mechanisms and their synergy. The fluvial signature in the floodout was mapped in detail using the surface geomorphic features available from the Google Earth imagery. The global surface water occurrence intensity thematic layer explained the variations of riverine flows across 1984-2019 in the floodout region based on Google Earth Engine (GEE) cloud computation. The Landsat 8 OLI bands were used to calculate the spectral indices for the floodout region inorder to bring out the natural status in pre and post-monsoon seasons. The flash floods and anthropogenic sensitivity analysis for the entire Luni river basin were performed to bring out the fifth objective of this study and come up with the correlation between the parameters and the individual sensitivity layers. The sensitivity characterization is done using two types of MCDM processes, AHP and CSI, compared to observe the significant differences obtained from each sensitivity layer. A detailed method for each MCDM process is provided and discussed in detail under the individual sub-heading in the preceding part of this chapter.

Table 5.1: List of data used for analysis in chapter 5.

Sl. No.	Parameters	Data Type	Data Source	Spatial Resolution	Period
1	Topography & Luni River Channel	Line and polygon coverage	SoI Topographical Sheets	1: 50,000	2006
2	Satellite Image based Spectral Indices (floodout)	Raster Grid	Landsat 8 OLI/TIRS C1 L1; Path/Row: 150-43	30 m	May & Oct/Nov 2019
3	Global surface water		Joint Research Centre, European Union	30 m	1984-2020
4	Fluvial Signatures	Polygon coverage	Google Earth Imagery	2 cm = 1 km	2020

Source: Compiled by the researcher.

5.4 Aeolian-Fluvial Interactions within a stretch of Luni river corridor

Dryland regions are characterized by the two dominant geomorphic processes - aeolian and fluvial, which compete to carve new landforms within the arid landscape. The water and wind

are the creator medium responsible for featuring new landforms based on their synergistic erosive mechanism. Such processes have ecological consequences within the specific environmental setting ranging from global to local scales. Aeolian and fluvial processes have been studied independently by tradition, thus making it vital and ambitious to understand their interactions over varied spatial and temporal scales in a dryland framework using an interdisciplinary lens (Belnap et al., 2007). The evolution of the concept of aeolian-fluvial studies in geomorphology dates back from the late 1980s when some studies came up discussing the major types of processes that occur due to river-dune interactions and the resultant landform units, and paleo-signatures formed both in the present and past, respectively (Langford, 1989; Langford and Chan, 1989). Table 5.2 helps comprehend the development of the concepts of aeolian-fluvial interactions and the theoretical framework of each research article. In the past three decades, the ideas have evolved from studying the resultant landforms from river-dune interactions to creating new global inventories and geo-models to study their interactions (Liu and Coulthard, 2015; 2017). The most recent studies involve understanding the landscape ecology, geochemistry (Li et al., 2020); active ingression of either dunes or rivers on each other's pathways (Jia et al., 2021) and a quantitative framework to classify the landscapes generated as a result of coupling impact of aeolian-fluvial synergy (Li et al., 2021). Therefore, the need for an interdisciplinary approach in studying the interactions of dunes and rivers in dryland systems can produce a comprehensive overview of how the present-day processes are occurring and are creating new types of landform units. Such interactive study is done for a small stretch of river Luni which is mapped and examined to understand how the dunes and the stream channel interact.

Table 5.2: Concept contribution and theoretical framework showing the progression of aeolian-fluvial interaction studies.

Reference	Theoretical Framework/Concept Contribution
Li et al., 2021	The quantitative data statistically distinguishes four types of landscapes generated as a result of an aeolian-fluvial environment.
Jia et al., 2021	The desert area has dune-river interactions with either active ingression of dryland rivers with encroaching dunes in dry seasons while lateral cutting of the dunes during rainfall events leading to an unending landform alteration and renewed landscape evolution.
Li et al., 2020	The geomorphic characterization of desert-rivers landscapes with a consolidation of the ecology of the landscape and related geochemistry.
Priddy and Clarke, 2020	The ephemeral flow in dryland rivers produces and preserves sedimentological imprints distinct in nature and traits only observable in sediment cores and not in any outcrops.

Liu and Coulthard, 2017	An interactive computer-based interactive model exhibited the coupled impact of sand dune-river interactions, highlighting how aeolian sediment (dunes) transportation can alter and deflect the dryland river avenue.
Masrahy et al., 2015	A generic framework enlisting varied types of fluvial and aeolian interactions existing among the active depositional systems at the present-day dune-field margins examines their geomorphic complexity.
Liu and Coulthard, 2015	Satellite imagery-based global index of the river - dune interactions with an impact characterization of the aeolian-fluvial geomorphic systems and dominance detection in relevant geomorphic settings worldwide.
Belnap et al., 2011	The need for an interdisciplinary lens to study the linkages between fluvial and aeolian systems focuses on the increasing threat of changing climate and land-use alterations.
Field et al., 2009	An integrative viewpoint presented for the erosional processes notably considering both aeolian and fluvial processes and their synergistic interactions required to extend management practices and deploy appropriate resources for the alterations in climate and land-use patterns.
Maroulis et al., 2007	The pertinent quaternary fluvial and aeolian activity with an active relation to climate change was shown through luminescence dating technique with an exciting outcome of role reversal where the residual dunes are contemporarily exhibiting flood channels.
Bullard et al., 2003	A review showing the links of process-response effectiveness or landscape sensitivity and transitions of dryland environment with spatial-temporal alterations are the vital empowering forces that bring out the geomorphological implications of aeolian-fluvial interactions.
Veiga et al., 2002	A close interaction between the aeolian and fluvial processes developed due to a decline in sea level, leading to dissection of an entire catchment with a side by side setting of non-marine deposits on the shallow and deep marine facies.
Bullard and Livingstone, 2001	The factors controlling the sediment transfer between aeolian and riverine systems, with an additional spotlight availability of moisture, supply of sediments and the frequency of interactive aeolian-fluvial events with a future research prospect.
Langford, 1989	The modern fluvial interactions found in the interdune areas and along the river channel due to streamflow extending and intermixing with the aeolian setup have six possible aeolian-fluvial interaction scenarios.
Langford and Chan, 1989	The past fluvial-aeolian deposits on overbank interdunes and the large erosional flood surfaces were found with four distinct facies with Cutler Formation and Cedar Mesa Sandstone.

Source: Compiled by the researcher.

The interaction mapping (Fig. 5.1) is done along the stretch of the Luni river buffer area, having a width of 4 km. The concentration of dunes is found to be maximum in this specific stretch of the Luni river corridor. The distribution of dunes is mapped from the SoI topographical maps having an average length of ~0.71 km. The shape of the dunes is mainly linear, aligning to the wind direction with few examples of the crescent and parabolic shapes found on the western side of the stretch and along the lower end of the stretch on the eastern bank of Luni. The maximum number of dunes are found to be interconnected with an average height of ~90-100 m. The nature of these dunes is semi-stabilized to most stable ones, with no such shifting signs over the past except for a few exceptional dust storms or peak wind flow events. The maximum concentration of dunes within the study stretch is found on the lower section with a more significant number within a buffer range of ~500 m to 1.5 km. But the recent satellite imageries

show the massive transformation of these dunes as they are razed off to increase more area under cultivation and unprecedented growth of sand mining (Kar and Kumar, 2020) without any enforcement machinery to check and control the destruction of such geoheritage. Over the past decade, the land cover units are being converted into pro-anthropogenic land use, which was also observed in the LULC temporal changes.
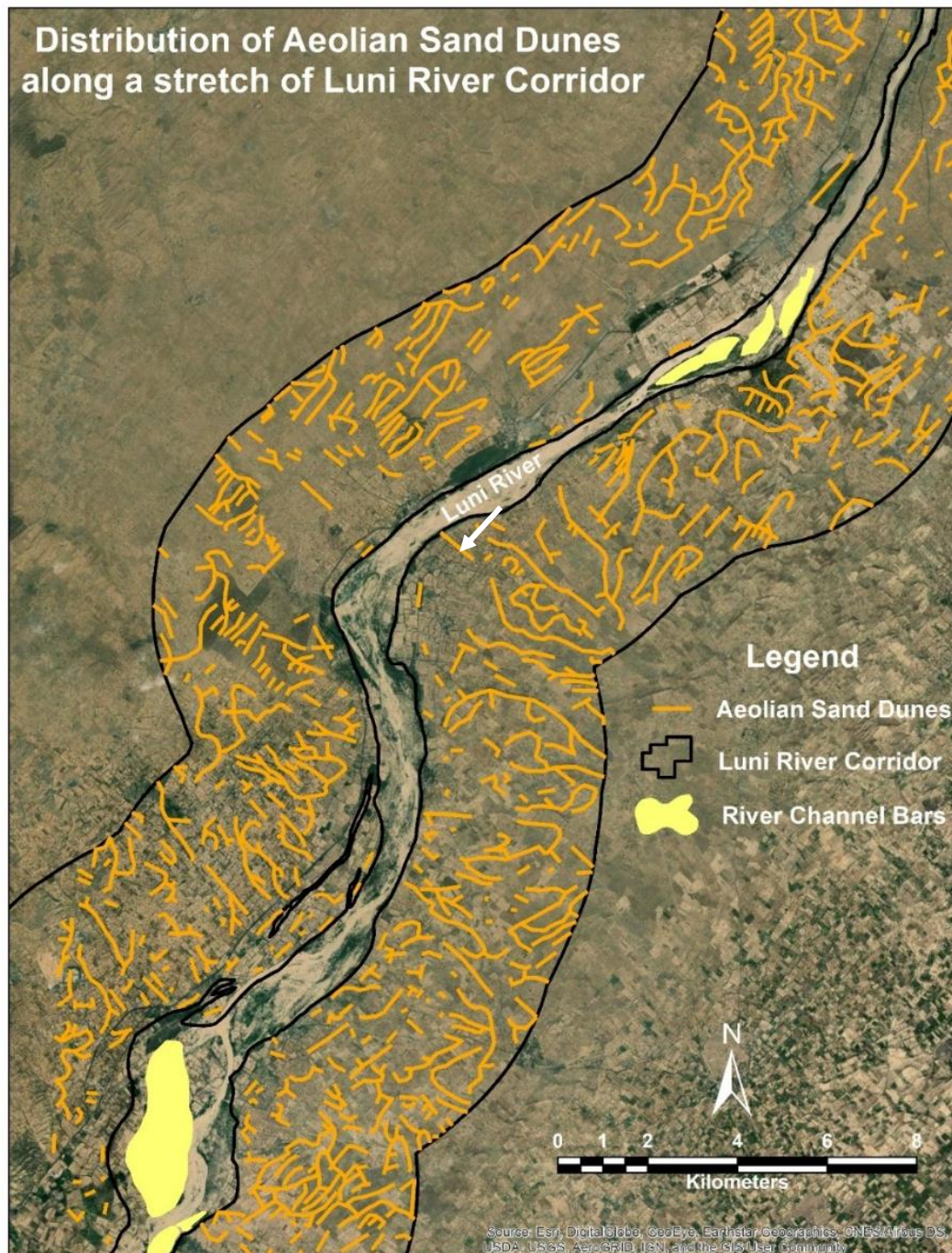
Fig. 5.1: Distribution of aeolian dunes along a stretch of the Luni river corridor. Source: Prepared by the researcher based on SoI topographical maps (2006)
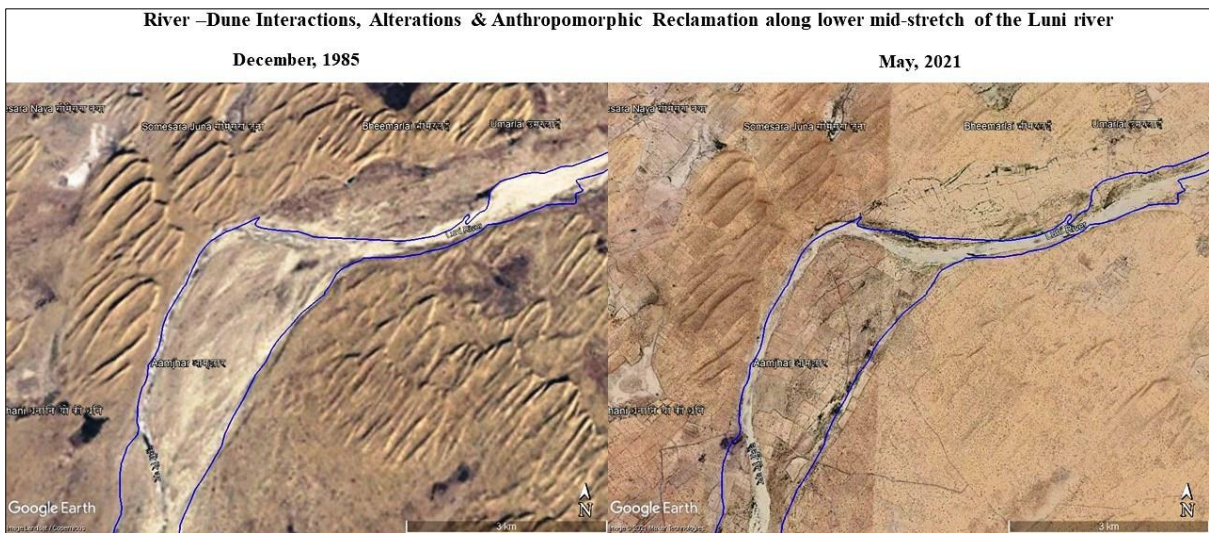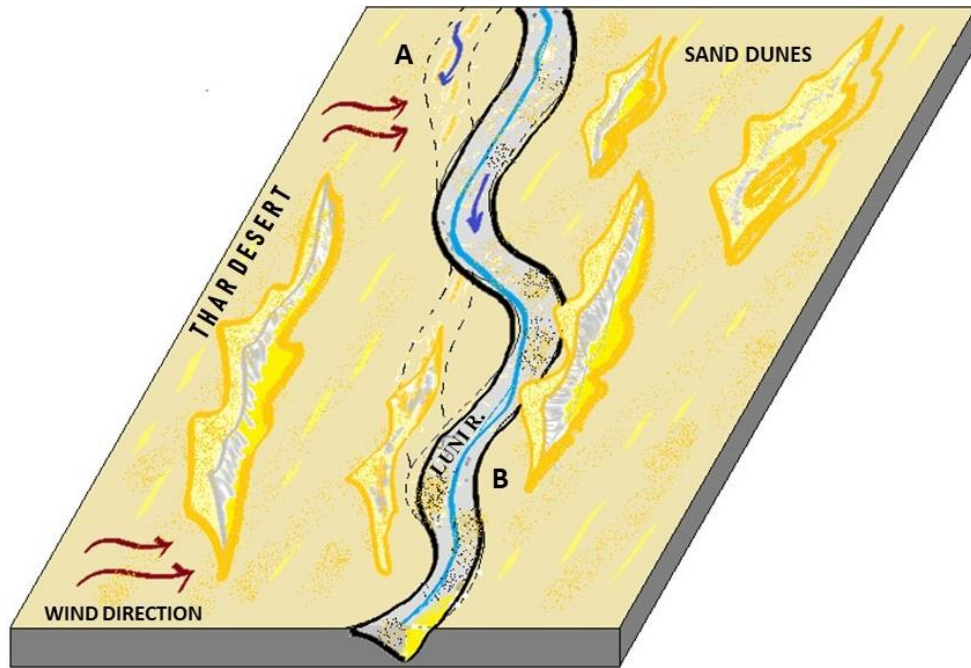
Fig. 5.2.1: Conceptual diagram showing the dune migration and its impact on the Luni river channel. (A) Paleochannel signature of the Luni river (B) High wind flows from the Thar desert result in a semi-stabilized linear dune shifting towards the active Luni river channel, indicating a slow encroachment into the channel. Fig.5.2.2 Temporal river-dune interactions, alterations and anthropomorphic reclamation observed along lower mid-stretch of the Luni river. Source: Prepared by the researcher based on Google Earth imagery.

Dune and river interactions in the Luni river can be best explained through a conceptual diagram, as shown in Fig. 5.2.1 and through the temporal Google Earth imageries as observed in Fig. 5.2.2. A small tract of the Luni river corridor in the Fig. 5.1 is taken to explain the

interactive process operating within the river buffer area. The portion (A) exhibits the paleochannel signature left on the older sandy alluvial tracts of the Luni with a defined migration of the channel towards the right side over time due to erodible sandbanks with significant points of weakness on the shallow river bank. This leads to channel avulsion from a peak flow event due to a high rainfall episode, creating the present-day active channel consisting of the blue thalweg line. Scenario (B) explain how peak wind flows from the Thar desert result in semi-stabilized linear dune shifting towards the active Luni river channel from the left indicating a slow encroachment into the channel. This is also observed in the Fig. 5.2.2 for the year 1985. A stark change is observed in 2021 where the dunes have been reclaimed for agricultural practices, hence altering the Luni corridor in the villages of Aamjhar, Bheemarlai, Somesara Juna and Umarlai in the Sindhari *tehsil* of Barmer district of Rajasthan. The high wind speed intends to carry enough sands from the Thar and while crossing the Luni channel as a topographic drop led to the deposition of sands into the active channel. Thus, sediments brought down by the Luni river are sometimes overpowered by the active aeolian actions leading to an interplay of geomorphic processes. Sometimes high-powered sand/dust storms, locally known as *aandhi*, can lead to blocking and burying the present-day river channels, which might also be a possible reason for channel migration in (A). During a flash flood event steered by high monsoon can also lead to dune destabilization by active lateral channel expansion, undercutting of the dunes, scooping of river bed materials, and higher alluvial sediments deposited in the interdune areas can be the instances from fluvial induced dune and channel erosion in a dryland region like Luni. Liu and Coulthard (2015) have classified aeolian-fluvial interaction into six major types: Fully fluvial dominant, mostly fluvial dominant, balanced, primarily aeolian dominant, fully aeolian dominant and alternating. The riverscape of Luni represented in Fig. 5.1 exhibits a 'balanced' type of interaction as the conditions are mostly stable with no such changes in channel location/length/width due to semi-stabilized to most stable old dunes with fewer instances of alternating types marked by dune encroachment or fluvial erosion as the Luni passes off the dune field.

5.5 Floodout Geomorphology

Floodout can also be referred to as an in-land delta formed out of a dry river which produces a magnificent opportunity to study the riverscape behaviour deriving and validating the principle of uniformitarianism which says "present is key to the past". A floodout is typically not defined as an incarcerating landform, unlike any other typical alluvial river zones. However, here the dryland river scrolls around with various trends of discharge leading to splaying channels,

expanding floodplain widths, and marked with an overall increase in downstream cross-section. Eventually, confined flow and termination of bedload transport, although with rarely occasional large floods, might have records of paleo high flow events that continue across substantial unconfined alluvial surfaces known as "floodout" (Tooth et al., 1999; Tooth, 2000).

A geomorphic sojourn of this unique and fascinating landscape is marked by series of anabranching channels with paleo markers and present-day active and inactive flow avenues. No single-channel drainage mouth exists (Fig. 5.3), similar to any typical river debouching into the sea, creating a delta or tidal/estuarine mouth. A series of channels tend to drain the region, creating a complex fluvial and ecological interaction zone sensitive to any sort of ex-situ changes like land-use alterations or extreme meteorological episodes. The examination of the Wannara creek catchment floodout in western Australia (Gore et al., 2000) can be related to the floodout system of the Luni river explaining the breakdown and debranching drainage channels led to the evolution of floodout sedimentation from the alluvial deposits brought down by the river can create long-lived older sedimentation units with paleo-markers of floods and channel swapping in the past. Layers of thick older to newer sandy alluvium is deposited, creating an unexampled sediment regime (Jaeger et al., 2017) with a new evolving idea to understanding eco-geomorphological thresholds and resilience in dryland river systems (Tooth, 2018).

The absence of vegetation on the river banks reduces the main channel's stability, which leads the river to meander and splay around freely, increasing the width of the floodout area with every new minor splay or avulsed channel that the flowing water of the river has crafted. As with any other drylands, complex interactions are found between slope, sediment transportation, bank sediment material, discharge, vegetation and patterns of tributary drainage results in variable downstream channel change in the floodout (Tooth, 1999; Gore et al., 2000). The fluvial signatures vary according to the response of climatic and anthropogenic factors, where the gradients of adjustments are quantified through the nature of disturbances posed by the preceding factors. High sinuosity and continuous formation of new crenulated channels disrupt the river water flow through converging and diverging streams resulting from peak discharge events that rarely occur within 5 to 10 years, as studied from the hydrological behaviour of Luni. The basic tendency of Luni like dryland rivers are interesting to note, which has this exclusive in-land deltaic formation with a vast expanse of cross-sectional width where the rivers play around the earth's surface with variable sediment distribution and tributary patterns.
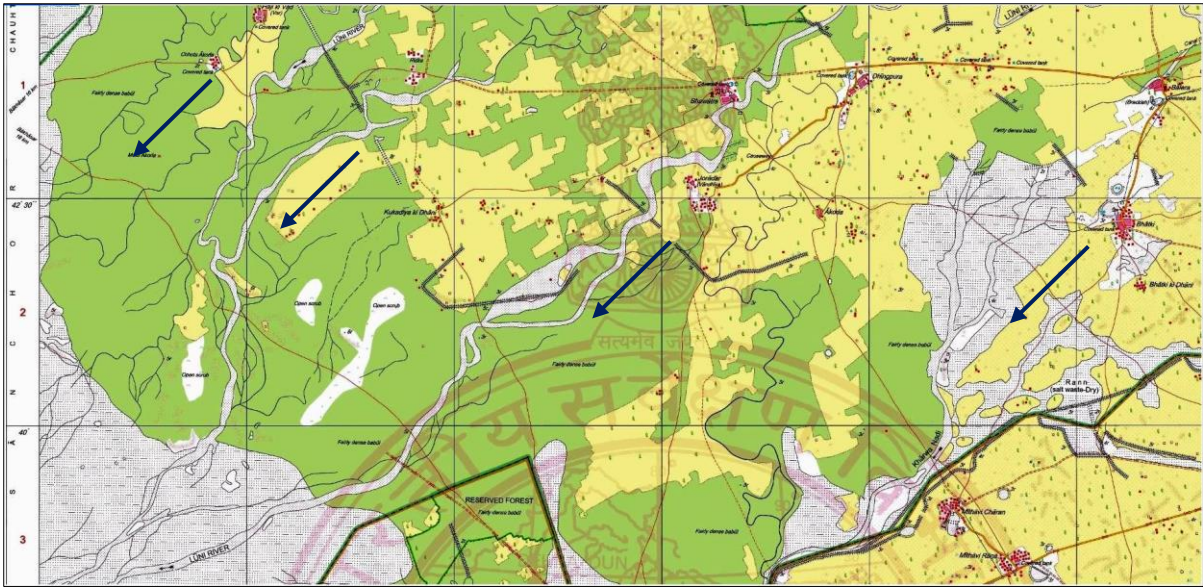
Fig. 5.3: An excerpt from the topographical map number - 40 P/6 showing the Luni Flood out region with diverging anabranches of Luni (marked with blue arrows) and tendency of channel avulsion. Source: Survey of India.

The present study shows that the floodout region extends a few kilometres downstream of Gandhav GDS and continues until the anabranching channels debouch into the Rann of Kutch. The area of floodout is considered to be 1049.44 km^2, and the area of the Rann within the Luni river basin is 464.66 km^2. The geomorphic and fluvial signatures are extensively mapped (Fig. 5.4) to bring out the odyssey of the floodout. Older floodplain dominates the main fluvial area with minimal presence of active and younger floodplains. The channel anabranching incises the stable layers of older alluvium with both lateral splaying and downcutting, especially during the stochastic flow events. The thalweg line shifts annually from one channel to the other but almost remaining constant for the channel on the extreme left adjoining the western boundary. The agricultural practice has led to a high number of geomorphic changes noting down the active land use of the area. Disappearing or the avulse flow lines form ephemeral channels and weakened points during the peak flow events, which are dynamic and can change anytime. Most of the channels are non-perennial and receive flows from monsoon or other rainfall events. Paleochannels exist towards the eastern side of the floodout, which are mapped, and some are geologically explored or dated to bring out their existential age and confirm their way of formation (Ramaswamy et al., 1991 and Kale et al., 2000).
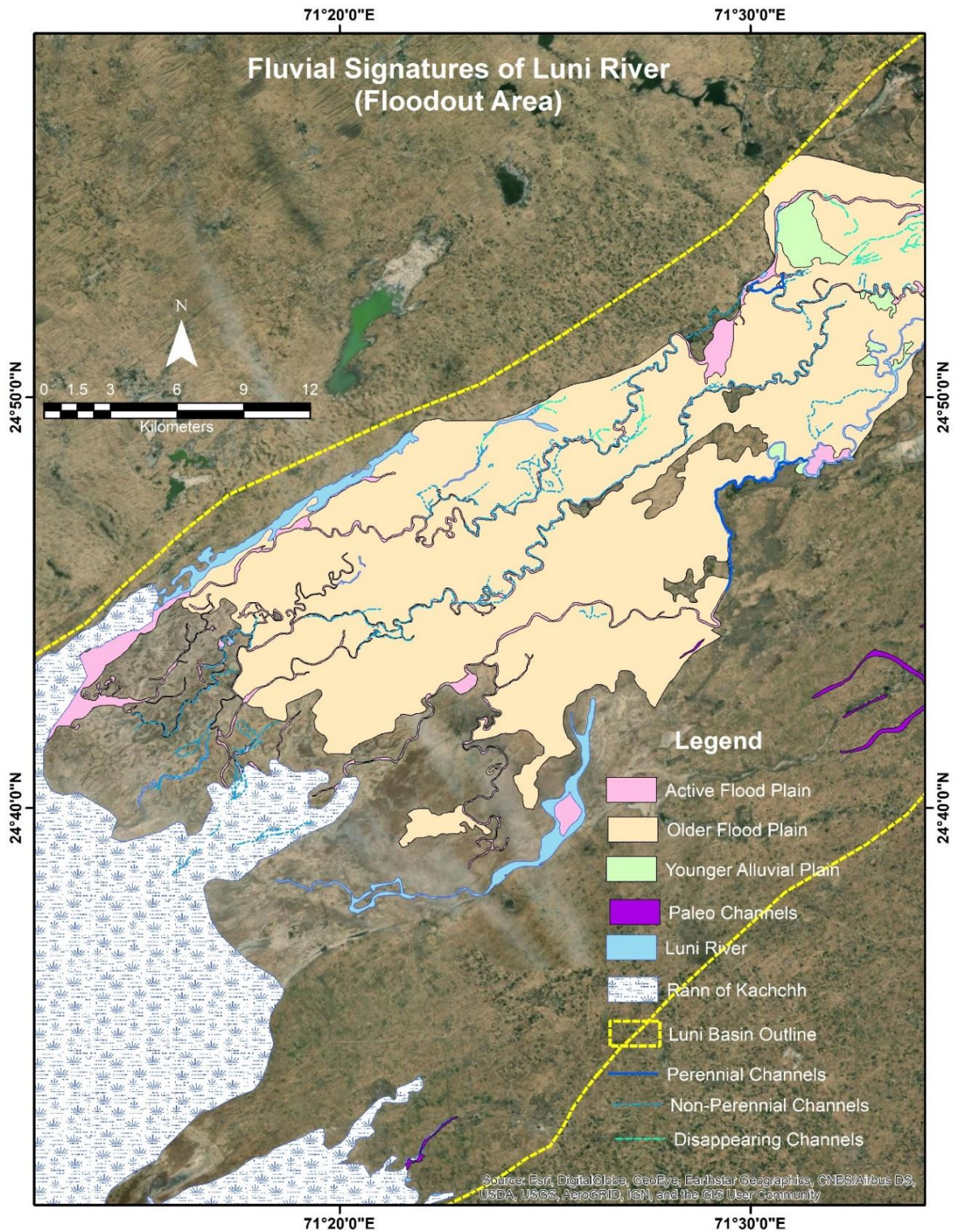
Fig. 5.4: Fluvial Signatures mapped across the Luni river Floodout region. Source: Prepared by the researcher based on Google Earth imagery (2020).

5.6 Global Surface Water Occurrence Intensity of Luni Floodout

The Global Surface Water (GSW) occurrence intensity is mapped out from an advanced geographical dataset, an online storehouse of the GSW datasets based in the famous GEE cloud

computing web explorer. The history of GSW alterations for 37 years, i.e., 1984-2020, could be easily navigated and utilized for the region of interest (ROI). Pekel et al. (2016) introduced this dataset for location-based detection of surface water changes due to anthropogenic and natural stressors. Temporal changes help to discern the alterations that have taken place for a surface water body over time, e.g., the shrinkage of the Aral Sea. Six sets of data are maintained for the GSW: occurrence, occurrence change intensity, seasonality, recurrence, transitions, and maximum water extent. The vitality of surface water changes directly impacts the global hydrological cycle affecting the flux between land and atmosphere through evaporation (Zhan et al., 2019).

Value (TIFF)	Value (GEE)	Symbol	Colour	Label
0	-100	🟥	#FF0000	-100% loss of occurrence
100	0	⬛	#000000	No change
200	100	🟩	#00FF00	100% increase in occurrence
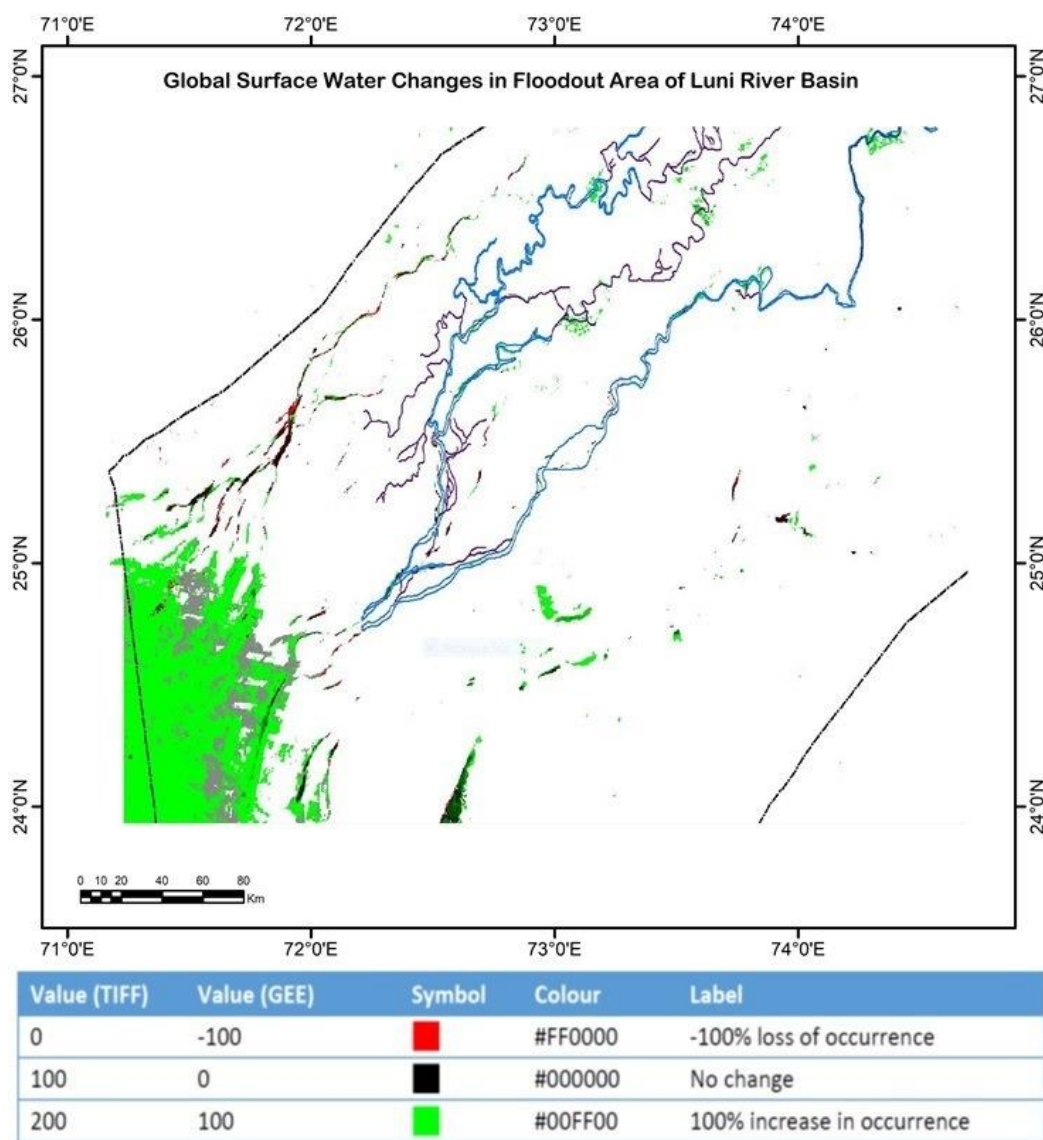
Fig. 5.5: Global Surface Water changes as observed in the Luni floodout area. Source: Prepared by the researcher based on JRC-EU, Global Surface Water Change v.2, GEE (1984-2020).

173

The alterations of GSW in the Luni floodout area (Fig. 5.5) records the ongoing surface water changes reflecting the dynamics of the floodout over the past 37 years. The occurrence change intensity provides information on where surface water occurrence has increased, decreased or remained the same. The increase in water occurrence is shown in green, and the decline are marked in red. The black shaded areas have no significant change in the water occurrence intensity. The colour intensity represents the degree of change (in percentage). For example, dark red areas show a more significant loss of water than light red areas. Some areas appear grey in the maps, which means insufficient data to compute a meaningful change statistic. The overall scenario extracted from the GSW dataset highlights the prime changes in the wetland region of the Rann of Kutch while the channels are stable with some obvious few exceptions. The three prime factors - changing water flows, ephemeral conditions, and sediment regime alterations shape the Rann wetland boundary, which has recorded cent percentage changes over the past years.

5.7 Analysing Luni floodout condition using Remote Sensing spectral indices

Satellite imageries have proved to be the best means of earth observation over past decades. The various spectral bands capture information relevant to understanding a landscape's past and present-day environmental and anthropogenic status with some specialized computer-based image geoprocessing. The current and historical status of vegetation, soil moisture, urban sprawl, croplands, snow, forest fires, thermal conditions and many other natural or man-made factors could be monitored, measured, analyzed and represented using surface reflectance-derived spectral indices normalized differences of the spectral bands with values ranging in between ±1 indicating highest and lowest values.

The Luni floodout could be better comprehended through three types of remote sensing-based spectral indices, namely, NDMI, SAVI and BSI, suitable for judging the dryland status and operative environmental mechanisms during pre (May 2019) post-monsoon (October/November 2019) season. The arid landscapes are specifically susceptible to water and wind erosion due to the sparsely spaced vegetation cover, soil's low organic content, and the increasing anthropogenic disruptions that can easily break the bio-physical crusting having a slow regeneration time (Belnap, 2007). The Luni river floodout region is a sensitive zone compared to any other part of the Luni river basin, for which selecting the best spectral indices was challenging and were based on a series of permutations. Different spectral indices are modified to have an adjusted version highlighting the particular feature that needs enhancement for understanding the environmental setup. For instance, the SAVI scores higher than standard

174

vegetation indices like – NDVI/MNDVI for the floodout region. This is because SAVI considers soil condition and vegetation cover, making it more suitable to describe the vegetal growth and its status in a sparsely vegetated dryland fluvial setup. The barrenness of the floodout region marked with non-perennial channels and minimal streamflow would better expose the barren land through BSI. The inherent moisture conditions acquired in the spectral bands would score over any water indices (NDWI/MNDWI). The moisture index would showcase the consolidated moisture condition available both from the physical water bodies/rivers and the local farmlands natural vegetation. This helps capture and give a fair idea of how moisture is distributed across the floodout in various sources, from natural to man-made features. The following three spectral indices derived from the Landsat satellite imagery are discussed below in association with the Table 5.3 exhibiting the maximum and minimum values –

- **NDMI**: The NDMI helps comprehend the amount of water available from the water bodies and vegetation consolidating both from natural ones and the cultivated croplands. It is traditionally computed as a proportion between the NIR and SWIR values available from the spectral bands of the satellite imagery. Fig. 5.6 shows the pre and post-monsoon conditions of moisture availability in the Luni floodout. May is considered the hottest month in this region, which has a considerable low amount of moisture except for the central section of the floodout infested with the continuous and ephemeral channels. Active farming in this section leads to maximum moisture content during the post-monsoon month and with some noticeable rise of moisture due to monsoon and local rainfall events in the preceding months.

Table 5.3: RS based spectral indices used for analyzing the Luni floodout region.

Sl. No.	RS spectral indices	Abbreviation	Formula	Pre-Monsoon		Post-Monsoon	
				Max.	Min.	Max.	Min.
1	Normalised Difference Moisture Index	NDMI	(NIR - SWIR) / (NIR + SWIR)	0.30	-0.15	0.38	-0.14
2	Soil Adjusted Vegetation Index	SAVI	((NIR - Red) / (NIR + Red + l)) * (1 + L) where, l = 0.5 and L = 1.5	0.74	-0.31	0.65	-0.15
3	Bare Soil Index	BSI	(SWIR+Red) - (NIR+Blue) / (SWIR+Red) + (NIR+Blue)	0.12	-0.23	0.14	-0.24

Source: Compiled by the researcher

- **SAVI**: This index is meant for a low vegetated area with sparse distribution perfectly suitable for showing the soil modified vegetation cover for a dryland landscape unit like the Luni floodout. It is meant to correct the NDVI algorithm by minimizing and modifying the impact of soil brightness, reasonable to bring down the effect of brightness otherwise found in a barren or arid landscape with minimal vegetation cover. In SAVI, the surface reflectance spectral signature is computed as a proportion of R and NIR values having a soil brightness correction factor (L) of 0.5 to bring in most land cover units. In Fig. 5.7, the minimum SAVI values were found to dominate the floodout region in the pre-monsoon month of May except for the areas with few plantations and croplands in the upper and central section of the floodout. The lower end of the floodout remains primarily devoid of vegetation and is dry with zero flows in the channel. At the same time, a considerable change in the scenario is observed during the post-monsoon period as the entire floodout gets an uplifted value of SAVI, indicating a rise of agricultural activities and growth of natural vegetation, having enhanced greenery and health baseline.

- **BSI**: The amount of increase/decrease of soil bareness is vital to understand the condition for an arid river floodout. BSI is the best fit spectral index to extract the bare land from satellite imagery. The analysis of bare land would also help identify the prospective zones of wind erosion playing a decisive role in contributing to dust storms in arid lands. The computation of BSI is based on the ratio of combination having red, blue, near-infrared and short-wave infrared spectral bands used in a standardized pattern. The red and SWIR spectral bands measure the soil mineral composition, while the NIR and blue bands are meant to enrich the presence of vegetation. In Fig. 5.8, the pre-monsoon conditions in May displays exposed soil layers with scanty vegetation in the northern section of the floodout. The aridity of soil layers and the degree of bareness is evident from the low range of maximum and minimum values. The bare conditions have a minimal upliftment in the central section of the floodout after the monsoon in November, as shown with the lighter to darker shades of yellow. The lower values represent the farmlands and cultivated areas, while the dark shades in the Rann of Kutch give an idea about the high exposed soil conditions. A moderate bare soil layer dominates even after the post-monsoon season across the floodout region.

5.8 MCDM-AHP and Composite Index based Sensitivity Analysis

Out of all the different methods that have been applied to map sensitive zones for delineating flash flood or anthropogenic vulnerability, the RS/GIS is believed to be one of the best, cost-

effective, efficient and primary tools for identifying the potential areas of flood occurrence (Rahmati et al., 2016; Das, 2018; Zhang et al., 2021). In the last couple of decades, researchers have found that combining the RS/GIS and MCDM process is one of the best possible ways to address spatial data management (Murmu et al., 2019). AHP is one such MCDM method developed by Thomas Saaty in the 1970s for effectively choosing the best possible alternatives under conflicting criteria with absolute and relative measurements (Saaty, 1986) along with a feedback system framework (Satty and Takizawa, 1984). AHP is a method where problems are divided into different variables, thereby arranging them into hierarchical structures, on the relative importance of pairs of elements and synthesizing the results (Saaty, 1999) with a reliance on expert knowledge (Liu et al., 2021). Thus, the use of RS/GIS has proven to be the most popular tool in use for delineating flood hazard zones with the use of MCDM like AHP (Das et al., 2017; 2018; Das, 2018).

The other type of MCDM used in this research is based on a composite or consolidated scenario, where, instead of putting a certain number of weights for each thematic layer in a hierarchy, each thematic factor can be multiplied, averaged and square-rooted to bring out the core value for assessing a specific zonation. It is sometimes confusing or inaccurate to estimate vulnerability zones with a hierarchical model as it is becoming difficult to choose which parameter scores over the other. An amalgamation of all the thematic parameters can help better discerning the sensitive zones. Thus, composite sensitivity index (CSI) is the blended MCDM having all the measuring or judgement parameters to develop a single zonation map deciphering the disposal of sensitivity. The CSI is mainly applied for judging the coastal vulnerability (Gornitz, 1990; 1991; Sahana et al., 2019; Bera and Maiti, 2021), and hence this study takes upon experimenting the same in determining the two types of sensitive zones (FFSZ and ASZ) as it has decided in the objective. CSI can help express a community's exposure, sensitivity, and adaptive capacity meant for various spatio-temporal scales (Das, 2012). The present study delineates two types of sensitive zones induced by two different natural and man-made factors, respectively. Such a study aims to bring down the future prospective hazards with disaster risk reduction (DRR) and move forward in achieving resiliency in the study area.
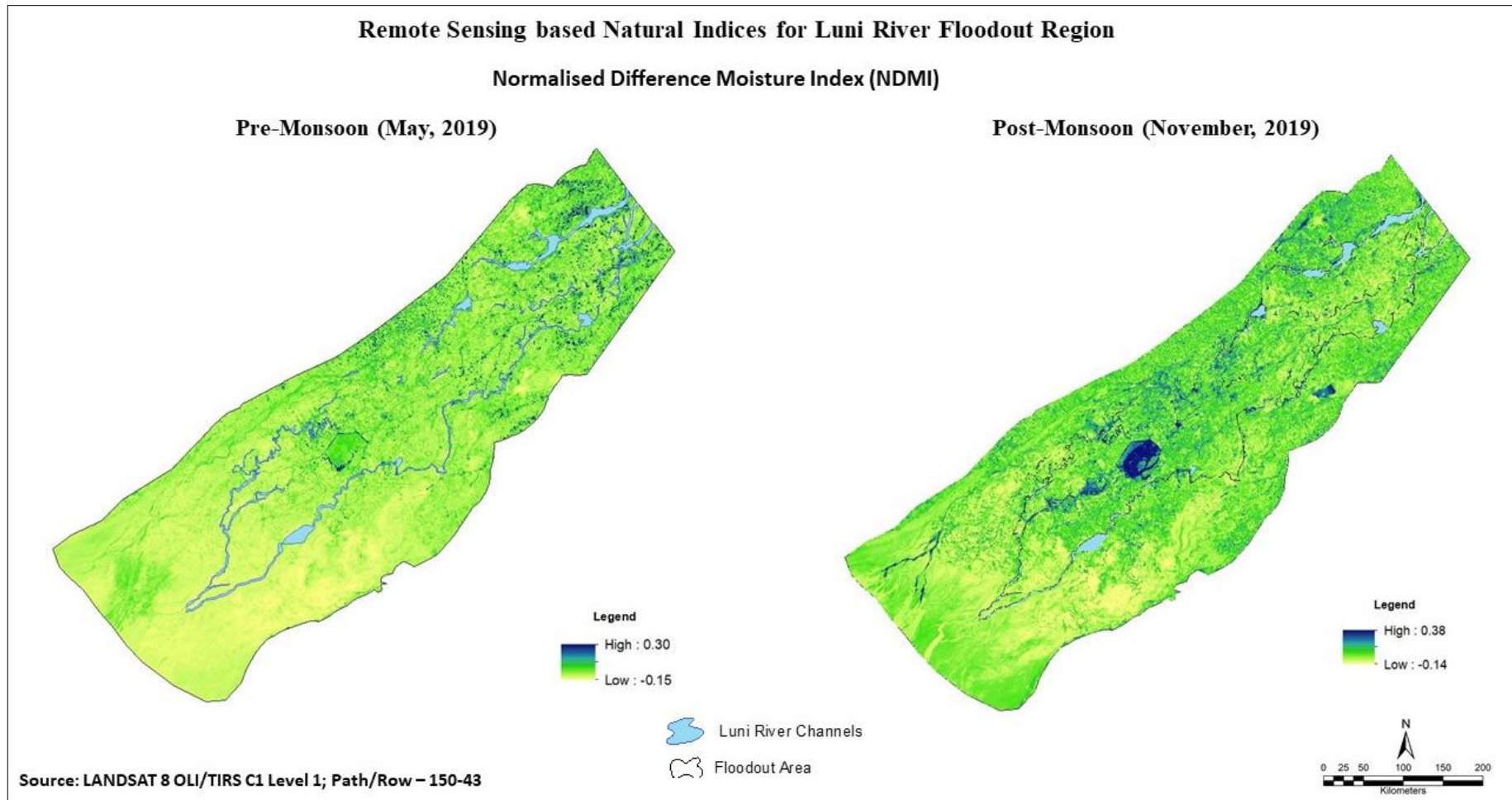
Fig. 5.6: NDMI analysis of the Luni floodout region for Pre (May, 2019) and Post (November, 2019) Monsoon seasons. Source: Prepared by the researcher based on Landsat 8 OLI/TIRS C1 Level 1; Path/Row – 150/43.
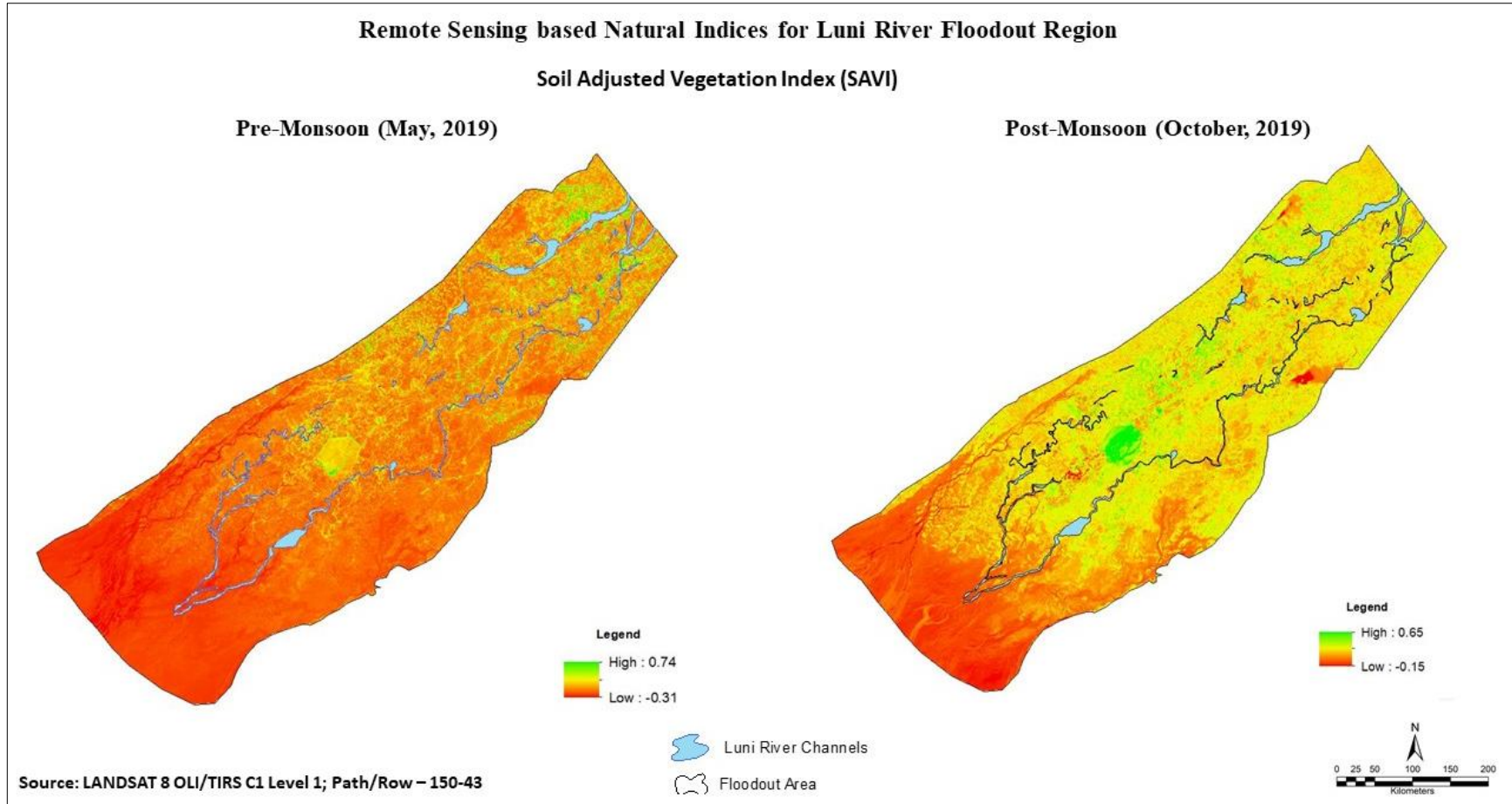
Fig. 5.7: SAVI analysis of the Luni floodout region for Pre (May, 2019) and Post (November, 2019) Monsoon seasons. Source: Prepared by the researcher based on Landsat 8 OLI/TIRS C1 Level 1; Path/Row – 150/43.
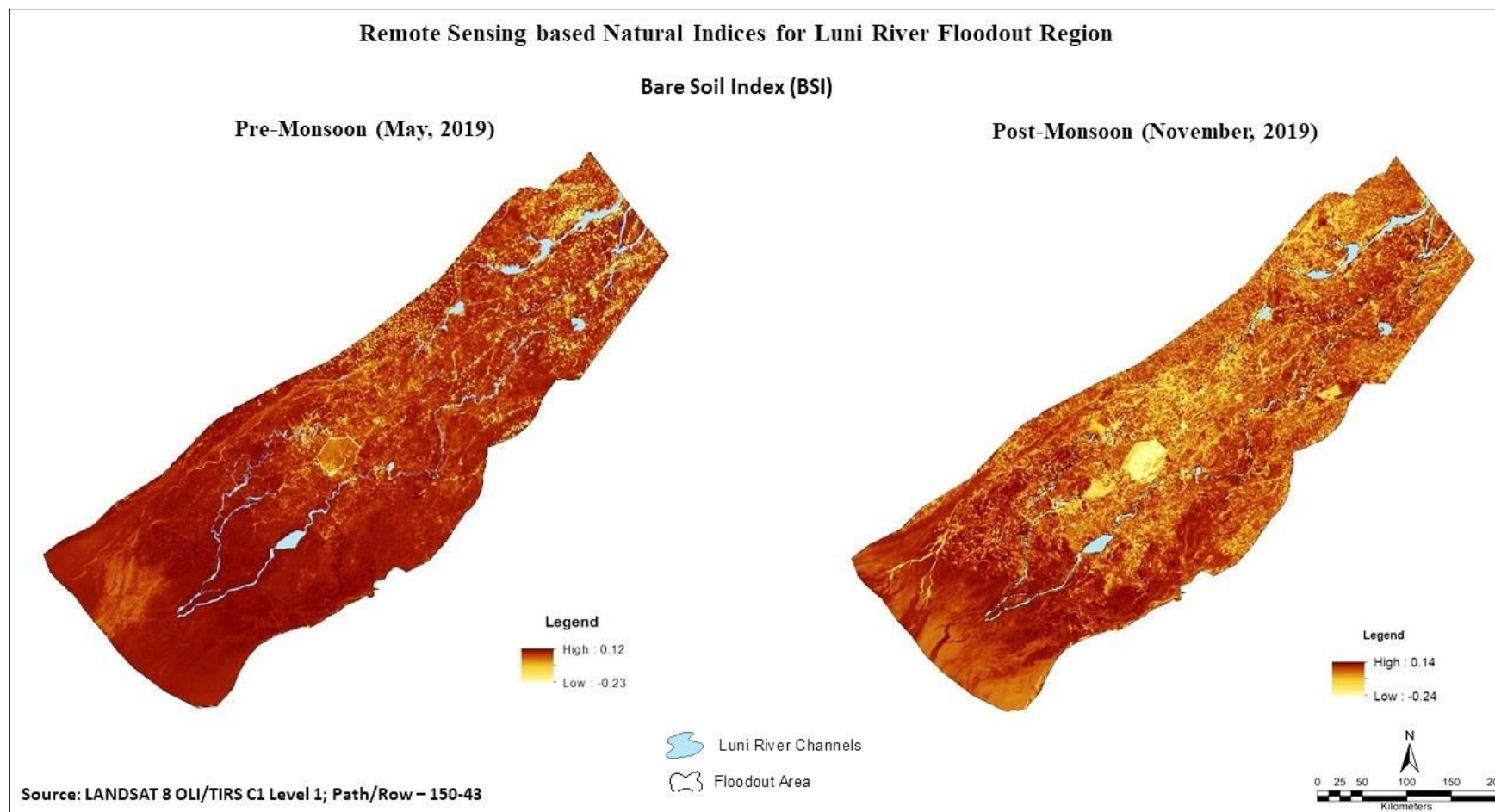
Fig. 5.8: BSI analysis of the Luni floodout region for Pre (May, 2019) and Post (November, 2019) Monsoon seasons. Source: Prepared by the researcher based on Landsat 8 OLI/TIRS C1 Level 1; Path/Row – 150/43.

5.8.1 Preparation of Thematic layers

The thematic parameters considered for the MCDM analysis of flash floods are - Rainfall (Fig. 2.4a), Elevation (Fig. 2.1), Slope (Fig. 4.1a), Relative Relief (Fig. 4.2b), Slope Length (LS) Factor (Fig. 4.1b), Length of Overland Flow (Fig. 4.7b), Topographic Wetness Index (Fig. 4.3d), Stream Power Index (Fig. 4.7c) and Curvature (Fig. 4.1c). Similarly, the thematic layers considered for demarcating ASZs are - Settlement Extent (Fig. 2.14d), Population Density (Fig. 2.14b), Transport Network Density (Fig. 2.13b), Distance from Transport Network (Fig. 2.13c), Cropland (Fig. 2.9c), Pastureland (Fig. 2.9d) and Landuse and Landcover (Fig. 2.12-2019). These parameters were weighed depending upon their relationship with the GWPZ and their respective classes (as gleaned from the relevant literature, expert knowledge and knowhow of the study area), so that a parameter with a higher value indicated it having a more significant impact on the resultant flash flood or anthropogenic susceptible condition. Each thematic layer was brought to a specific spatial resolution either through upscaling or downscaling the dataset to a particular pixel unit which is 30 m. This is of utmost importance to maintain the sanctity and a standard spatial scale of the data fetching the best results for the analysis.

Table 5.4: Saaty's Scale for AHP

1/9	1/7	1/5	1/3	1	3	5	7	9
Extreme	Very strong	Strong	Moderate	Equally	Moderate	Strong	Very strong	Extreme
Less important				Equal				More important

Note: 1/8, 1/6, 1/4, 1/2, 2, 4, 6, 8 can also be used if more classes exist.

Source: Compiled by the researcher.

Table 5.5: Random Index for various N value used for computing consistency

N	1	2	3	4	5	6	7	8	9	10	11	12	13	14	15
RI	0	0	0.58	0.90	1.12	1.24	1.32	1.41	1.45	1.49	1.51	1.54	1.56	1.57	1.59

Source: Adapted from Satty and Vargas (1991)

Table 5.6: The results of consistency aggregated for sensitivity analysis in the Luni basin

Sensitivity	λ max	N	RI	CI	CR	Consistency
Flash Flood	9.54	9	1.45	0.067	0.047	CR<0.1
Anthropogenic	7.41	7	1.32	0.068	0.051	(Yes)

λ max: Maximum eigen value, **N**: Number of factors, **RI**: Random Index, **CI**: Consistency Index, **CR**: Consistency Ratio. Source: Computed by the researcher.

Table 5.7: Reclassified scale for each raster input in AHP analysis.

Sensitivity	1	2	3	4	5
Flash Flood	Most Sensitive		Moderately		Least Sensitive
Anthropogenic			Sensitive		

Source: Computed by the researcher.

5.8.2 Assignment of Weights

The various thematic layers are assigned criteria weights depending on the local understanding of the landscape, and the AHP method was applied as it succinctly summarizes the authors' perceptions and judgments. The verdict matrix (Table 5.8 and 5.10) in AHP considers the final weightage for the chosen factors thought to be most suitable in representing the final sensitive zone (Saaty, 2004). Efforts are still required to eliminate the sensitivity of criteria weight impact on the estimated results for understanding risk (Zhang et al., 2021). So, any sort of minor alterations in defining the criteria weight can put a way forward for an appreciable impact on the outcome of the verdict matrix. (Ohnishi et al., 2011; Zhang et al., 2021).

The weight allocation to the different thematic layers and their respective classes as the assignment of weights for each parameter is essential in integration analysis because the outcome is primarily dependent on relevant weights (Muralitharan and Palanivel, 2015). This is determined mainly by the author's expertise, know-how, and understanding of the different parameters concerning the flash flood and human-induced disturbance potentiality of the study area, as these thematic layers control the flash flood and anthropogenic sensitivity of that area are assigned appropriate weights.

The AHP breaks down the complex multi-criteria decision problem into a hierarchy based on a pairwise comparison of the importance of different criteria and sub-criteria (Saaty, 2005). Additionally, the AHP technique is well suited for assessing the analysis' consistency of the work and induces comparatively less reduces bias in the elicited result (Arulbalaji et al. 2019). The normalization process, through the pairwise comparison matrix, was used to reduce the subjectivity of each parameter, and these were weighed on the Saaty's 1–9-point scale, where 1 denoted equal importance between two different parameters and 9 denoted extreme importance of one parameter in respect to the other (Table 5.4). The weights assigned to each criterion were carefully considered based on published studies and their assumed influence on groundwater availability. The following steps were performed to calculate the weights of the different parameters and to find the consistency-

Step 1: Adding the values in each column of the pairwise matrix (Table 5.8 and 5.10):

$$A_j = \sum_{i,j}^{n} G_{ij} \qquad \text{(Eq. 6)}$$

where A_j = the total values in each column of the pairwise matrix and G_{ij} = the number assigned to each criterion at the ith row and j^{th} column.

Step 2: Dividing each matrix element by its column total to generate a normalized pairwise matrix (Table 5.9 and 5.11):

$$X_{ij} = \frac{G_{ij}}{A_j} \qquad \text{(Eq. 7)}$$

where X_{ij} = the value at i^{th} row and j^{th} column in the normalized pairwise matrix.

Step 3: Dividing the sum of the normalized row of the matrix by the number of criteria used (N) to generate standard weights:

$$W_i = \frac{\sum X_{ij}}{N} \qquad \text{(Eq. 8)}$$

where W_i is the standard weight.

Step 4: Consistency Analysis: After calculating the standard weights, consistency analysis needs to be done. The AHP method tries to assess any ambiguity present through this consistency analysis. The Consistency Index (CI) and the Consistency Ratio (CR), respectively, were computed as below:

$$CI = \frac{\lambda - n}{n - 1} \qquad \text{(Eq. 9)}$$

where CI is the Consistency Index, and n is the number of parameters used in the analysis.

$$CR = \frac{CI}{RI} \qquad \text{(Eq. 10)}$$

where CR is the Consistency Ratio, and RI is the random inconsistency value given by Satty and Vargas (1991) (Table 5.5). The CR value should be ≤ 0.1, as proposed by Saaty (1990), to continue further analysis. If it is greater than 0.1, the inconsistency needs to be ascertained and the calculations revised. The analyses elicited acceptable CR values of less than 0.1 for all the considered parameters (Table 5.6), and thus the computations were furthered using the allotted weights for demarcating the FFSZs and ASZs within the Luni basin.

Table 5.8: Pair-wise comparison AHP Matrix with nine parameters for Flash Flood Sensitivity (FFS).

Parameters	RF	Elev	SL	RR	LSF	LOF	TWI	SPI	CV
RF	1	2	2	3	5	6	7	8	9
Elev	1/2	1	2	3	5	6	7	7	9
SL	1/2	1/2	1	2	2	5	6	6	8
RR	1/3	1/3	1/2	1	3	3	5	5	7
LSF	1/5	1/5	1/2	1/3	1	2	3	5	7
LOF	1/6	1/6	1/5	1/3	1/2	1	3	5	6
TWI	1/7	1/7	1/6	1/5	1/3	1/3	1	3	5
SPI	1/8	1/7	1/6	1/5	1/5	1/5	1/3	1	3
CV	1/9	1/9	1/8	1/7	1/7	1/6	1/5	1/3	1

RF: Rainfall (**A**), **Elev**: Elevation (**B**), **SL**: Slope (**C**), **RR**: Relative Relief (**D**), **LSF**: Slope Length (LS) Factor (**E**), **LOF**: Length of Overland Flow (**F**), **TWI**: Topographic Wetness Index (**G**), **SPI**: Stream Power Index (**H**), **CV**: Curvature (**I**). Source: Computed by the researcher.

Table 5.9: Normalised weight matrix with Criteria Weights (CW) for individual parameters of FFS

Parameters	RF	Elev	SL	RR	LSF	LOF	TWI	SPI	CV	C_W	C_W %
RF	0.32	0.43	0.30	0.29	0.29	0.25	0.22	0.20	0.16	0.28	27.78
Elev	0.16	0.22	0.30	0.29	0.29	0.25	0.22	0.17	0.16	0.24	23.70
SL	0.16	0.11	0.15	0.20	0.12	0.21	0.18	0.15	0.15	0.16	15.98
RR	0.11	0.07	0.08	0.10	0.17	0.13	0.15	0.12	0.13	0.12	11.92
LSF	0.06	0.04	0.08	0.03	0.06	0.08	0.09	0.12	0.13	0.08	7.54
LOF	0.05	0.04	0.03	0.03	0.03	0.04	0.09	0.12	0.11	0.06	5.75
TWI	0.05	0.03	0.03	0.02	0.02	0.01	0.03	0.07	0.09	0.04	3.54
SPI	0.04	0.03	0.03	0.02	0.01	0.01	0.01	0.02	0.05	0.02	2.30
CV	0.04	0.02	0.02	0.01	0.01	0.01	0.01	0.01	0.02	0.01	1.47

Source: Computed by the researcher.

Table 5.10: Pair-wise comparison AHP Matrix with seven parameters for Anthropogenic Sensitivity (AS)

Parameters	SE	PD	TND	DFTN	CL	PL	LULC
SE	1	2	3	3	5	6	7
PD	1/2	1	3	3	5	5	7
TND	1/3	1/3	1	3	3	5	6
DFTN	1/4	1/3	1/3	1	2	3	5
CL	1/5	1/5	1/4	1/3	1	3	5
PL	1/6	1/6	1/5	1/4	1/3	1	3
LULC	1/7	1/7	1/6	1/5	1/5	1/3	1

SE: Settlement Extent (**a**), **PD**: Population Density (**b**), **TND**: Transport Network Density (**c**), **DFTN**: Distance from Transport Network (**d**), **CL**: Cropland (e), **PL**: Pastureland (**f**), **LULC:** Landuse & Landcover (**g**). Source: Computed by the researcher.

Table 5.11: Normalised weight matrix with Criteria Weight for individual parameters of AS

Parameters	SE	PD	TND	DFTN	CL	PL	LULC	C$_W$	C$_W$ %
SE	0.39	0.48	0.38	0.28	0.30	0.26	0.21	0.33	32.65
PD	0.19	0.24	0.38	0.28	0.30	0.21	0.21	0.26	25.87
TND	0.13	0.08	0.13	0.28	0.18	0.21	0.18	0.17	16.93
DFTN	0.10	0.08	0.04	0.09	0.12	0.13	0.15	0.10	10.11
CL	0.08	0.05	0.03	0.03	0.06	0.13	0.15	0.07	7.48
PL	0.06	0.04	0.03	0.02	0.02	0.04	0.09	0.04	4.34
LULC	0.06	0.03	0.02	0.02	0.01	0.01	0.03	0.03	2.64

Source: Computed by the researcher.

5.8.3 AHP based delineation of FFSZ and ASZ

The demarcation of both the flash flood and anthropogenic sensitive zones was done following a dimensionless weighted linear combination method that predicts the degree of sensitivity across the Luni river basin, using the formula given by Malczewski (1999) in ArcGIS 10.3 via its raster calculator tool, wherein:

$$AHP_{FF} = RF \times w + Elev \times w + SL \times w + RR \times w + LSF \times w + LOF \times w +$$
$$TWI \times w + SPI \times w + CV \times w \quad \text{(Eq. 11)}$$

$$AHP_{AS} = SE \times w + PD \times w + TND \times w + DFTN \times w + CL \times w + PL \times w + LULC \times w$$
$$\text{(Eq. 12)}$$

The weight of each layer (w) derived out of the normalized pair matrices as in Table 5.9, and 5.11 were combined on a pixel-wise basis. The final sensitivity raster was re-classified from 1 to 5 into five sensitive categories with 1 being the most sensitive one while 5 being the least sensitive zone (Table 5.7).

5.8.4 CSI based delineation of FFSZ and ASZ

The composite index is based on Gornitz (1990; 1991) methodology, with equal weightage assigned to each thematic layer. A square root algorithm is fitted into the equation to bring out the core value of the mathematic expression from the combination to determine the consolidated sensitive zones. The unitless compiled equal-weighted MCDM is computed using the raster calculator tool in ArcGIS 10.3 as –

$$CSI_{FF} = \frac{\sqrt{A \times B \times C \times D \times E \times F \times G \times H \times I}}{9} \quad \text{(Eq. 13)}$$

$$CSI_{AS} = \frac{\sqrt{a \times b \times c \times d \times e \times f \times g}}{7} \quad \text{(Eq. 14)}$$

5.8.5 Zonation of Flash Flood Sensitive Areas

The changing climate and monsoon pattern is the talk of the decade, especially for the climate scientists leading to the rise of extreme events like flash flood and cloudburst events enhanced the socio-economic losses and aggravating the impact on the landscape, including destroying the livelihood of the local population in a small timeframe (Ali et al., 2019; Panwar and Sen, 2020; Das and Gupta, 2021). Recent studies have shown the increasing incidences of severe meteorological events from – cyclones to floods. In monsoon, peak rainfall episodes lasting for a shorter time (Georgakakos and Hudlow, 1984; Modrick and Georgakakos, 2015) led to rising runoff due to less time for the excessive water to get absorbed into the ground causes flash floods. Such events are those characterized by the rapid rise in water level in the river channel within lean hours of abundant rainfall, proving destructive causing enormous damages to the physical infrastructures with high incurrence of societal and economic losses (Anagnostou et al., 2010; Modrick and Georgakakos, 2015; Pham et al., 2020). No type of warning can be predicted for a flash flood event as per the American Meteorological Society, for which serious risk is associated with it depending on the complex environmental mechanisms interacting with the local riverscape (Georgakakos, 1986; Collier, 2007). The minimal response time of the river basin is a key indicator of flash floods (Pham et al., 2020). Type of basin, drainage systems and associated watershed characteristics along with man-made activities like deforestation, modifications in the river corridor with infrastructures like bridges/canals and land-use changes help determine the flash flood occurrence and its potentiality to cause damages. Increasing rainfall variability, precipitation distribution over the river basin, and timing regulate flash flood and drought incidences.

- **AHP based FFSZ**: The AHP based FFSZs are very distinct and is found to have a definite pattern. Fig. 5.9 displays the most sensitive zones of flash floods are located along the entire eastern section adjoining the Aravalli contributing 5.31% only. This resembles that higher slopes of Aravalli accompanied with short duration and high intensive rainfall with minimal response time can lead to severe flash floods. The adjoining footslope and pediment zone of Aravalli is marked as a quite sensitive zone with 11.55% area. The pediment-pediplain complex with particular variable high slope ground in the central section of the Luni river basin is marked as moderate and poor flash flood sensitive zones with an areal coverage of 18.37% and 26.31%, respectively. Hence this resembles that flash floods are having the most impact on the higher slopes of Aravalli and the immediate foothill region. The entire Luni river comes under the least sensitive area with 38.46%., but the flash flood model

cannot always consider the local factor, especially when done for such a huge area as the intensity of rainfall/cloudburst and higher slope variations or undulation in the riverscape can contribute to a flashy river flow condition. The local monadnock structures in the eastern bank of Luni just near Balotra is a significant source to contribute flashy flows into the Luni after a high rainfall event as locally recorded from the weather stations and river gauge at Gandhav mentioned finds due to mention the report published by Dhir et al. (1982). The typical arid geomorphic condition of Luni leads to a rapid expansion of floods which is being exasperated by the series of earthen dam failures constructed by the local villages for irrigation and domestic uses (Sharma et al., 1982; Sharma and Vangani, 1982). Even though the flood water did not inundate the riverine floodplain for a longer time, and ran out within few days after the flood occurrence.

- **CSI based FFSZ**: The composite index for flash flood sensitivity exhibits a bit different scenario when compared to the AHP based FFSZ. Fig. 5.10 shows a 16.94% area identified as most sensitive to flash floods found to be concentrated along the entire eastern edge of the Luni basin demarcated by the presence of high slope grounds of the Aravalli. No distinguishable pattern was observed for the other sensitive zones as the resultant raster shows a pixel-based value for FFSZs. The undefined weights for the CSI have enhanced the resultant FFSZ raster to have a better pixel-level analysis compared to that of the AHP based FFSZ. The quiet and moderate sensitive zones constitute 28.82% and 24.40%, respectively, with no paternal trend. The poor and least sensitive flash flood areas were found along the western section of the river basin adjoining the trunk stream of Luni with an areal presence of 17.95% and 11.89%, respectively. The variation of the FFSZs derived from AHP and CSI based MCDMs are found to be complimenting and itself validating the results. Despite having specific differences in the areal distribution of flash flood sensitive zones, most to most minor sensitive zones have a close fit. To compare both the MCDMs, it is to the opinion that both the techniques standoff well in their places, but the AHP scores better in portraying the flash flood susceptibility than the composite index. This is because a pattern in the zones of AHP could be found helping to discern the specific sensitive zones systematically rather than a pixel level zonation as derived from the CSI.

Table 5.12.: Comparative areal analysis of AHP and CSI derived FFSZs and ASZs.

| Sensitivity Zonation | Flash Flood Sensitivity (FFSZ) | | | | Anthropogenic Sensitivity (ASZ) | | | |
| | AHP | | CSI | | AHP | | CSI | |
	Area (km²)	Area %	Area (km²)	Area %	Area (km²)	Area %	Area (km²)	Area %
Most Sensitive	2048.27	5.31	6534.10	16.94	629.77	1.63	5339.63	13.79
Quite Sensitive	4456.72	11.55	11119.64	28.82	1301.39	3.36	11784.73	30.44
Moderately Sensitive	7088.99	18.37	9415.58	24.40	7459.74	19.27	14215.92	36.72
Poor Sensitive	10151.99	26.31	6926.26	17.95	15263.08	39.43	6365.12	16.44
Least Sensitive	14837.23	38.46	4587.42	11.89	14058.85	36.32	1007.42	2.60

Source: Computed by the researcher.

Inorder to understand the inter-relationship between the most vital thematic layers and FFSZ, a scatter plot based trend analysis was performed in between AHP and CSI based FFSZ and two key determinant parameters – slope and rainfall (Fig. 5.11). Each raster layer was extracted, and the values were plotted in Excel to develop the individual correlation. The inter-comparison proved to be the most influencing with a very high positive correlation R-squared values varying between 0.85 to 0.93, with a few outliers.

Fig. 5.9: AHP based FFSZs along the Luni river basin. Source: Prepared by the researcher.

Fig. 5.10: CSI based FFSZs along the Luni river basin. Source: Prepared by the researcher.

Fig. 5.11: Correlation between the two most vital thematic parameters determining flash floods – Slope and Rainfall with the AHP and CSI based FFSZs. Source: Computed by the researcher
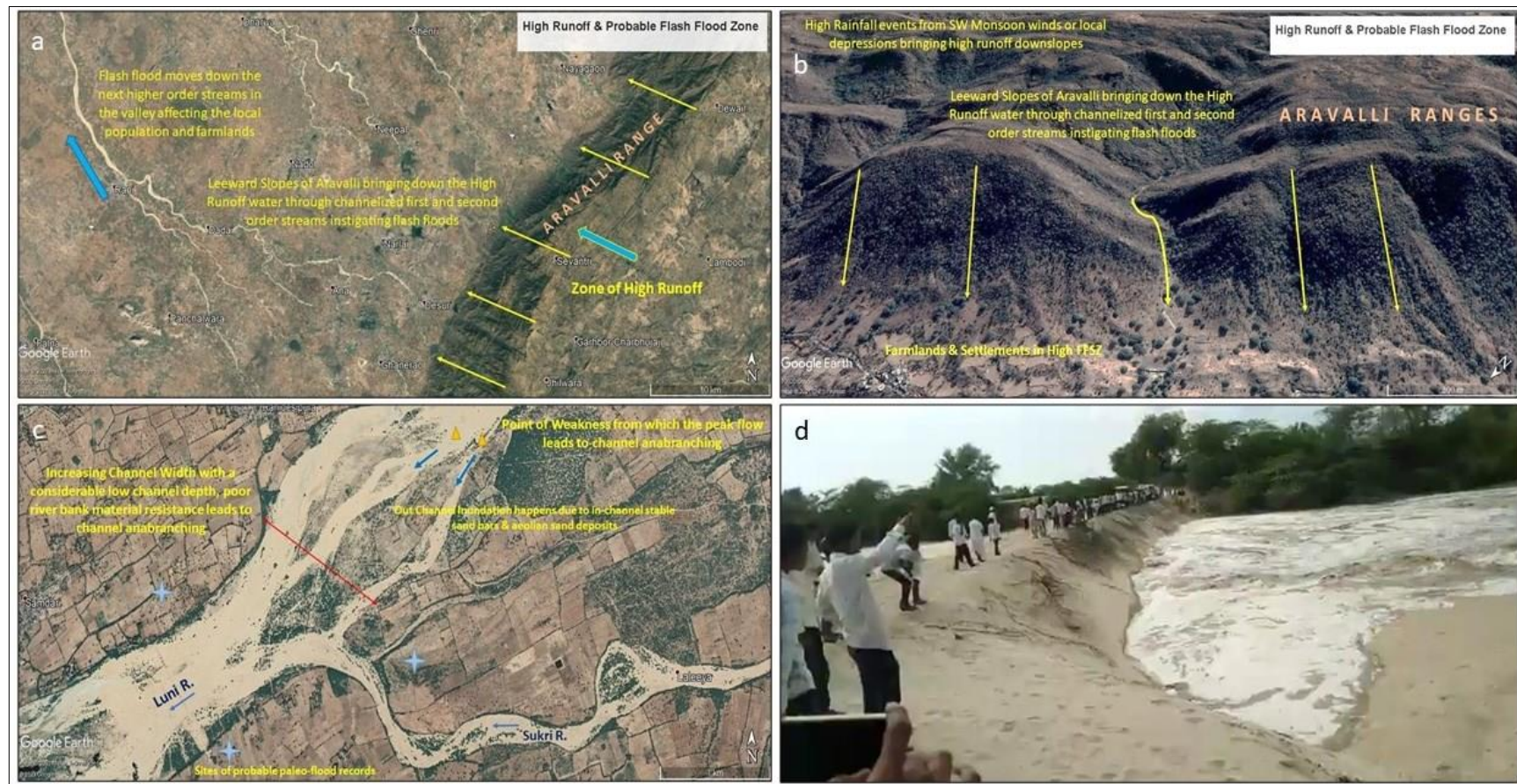
Fig. 5.12: Evidences of flash floods as observed from Google Earth imageries and a video snapshot a. High runoff and possible flash flood occurrence along the central Aravalli region.; b. Eastern view of the central Aravalli ranges explaining the flash flood mechanism in the foot slope; c. Fluvial dynamics and river channel alterations due to flash flood events at the Luni and Sukri river confluence; d. Flash flood waters gushing down the Luni river channel from the uplands near Balotra town and accumulate over a causeway. Source: - a-c: Prepared by the researcher from Google Earth imagery; d. Collected by the researcher from YouTube (Accessed: 20 August 2020).

The evidence of flash floods can be best validated by investigating the eastern section of the Luni river basin having the Aravalli, which has come up as the most FFSZ. However, the variable monsoon and certain local high rainfall episodes can individually create a flash flood situation meant to affect only a shorter stretch of the Luni river as its bed remains dry almost throughout the year. Different situations may arise, causing the flash floods leading to various combinations of possibilities for its occurrence. Google Earth imageries are now a unique modern tool that helps to explain the local topography and geomorphic features with better comprehensive ability. Fig. 5.12a resembles a high runoff and probable flash flood zone along the mid-Aravalli region marked with a westward slope along the eastern section of the Luni basin. Peak and short intensity rainfall events can bring down gushing streamflow leading to flash floods in the foothills inundating the farmlands and local villages (Fig. 5.12b), as happened in the disastrous flash floods of 1979. Fig. 5.12c shows the riverine dynamics and changes in the river channel due to flash floods or even certain sudden high flow events living for a short episode found at the Luni-Sukri confluence above Gandhav GDS. The increasing width of the channel makes it shallow with minimal channel depth. Points of weakness having potency for creation of avulsions and later anabranching was also observed. The most probable sites for paleo-flood dating have also been identified for future studies. Fig. 5.12d is a video snapshot collected from YouTube showing how the dry river suddenly covers up with huge gushing streamflow and accumulates behind a causeway near Balotra.

5.8.6 Zonation of Anthropogenic Sensitive Areas

Anthropogenic interactions are leading to a havoc alteration in the present-day riverscapes all around the globe. Such studies of human pressure on fluvial systems are early (Tarolli and Sofia, 2016) and need to be further done, especially for the Indian geomorphic context. The rise of awareness for saving the geoheritage and conservation of unique geomorphosites (Binni, 2009) is the hour's present concern. The never-ending constructions in the riverine floodplains with the unprecedented rise of population and encroachment into the natural systems have led to the destruction of the local geoheritage or landscape uniqueness, such as razing off the Thar dunes for farming or mining purposes (Kar and Kumar, 2020). The intensity of transport connectivity and its impact on channel morphology due to each intersection have varying impacts on the core fluvial corridor (Roy and Sahu, 2017; 2018; Roy, 2021). The aesthetic beauty of the riverscapes is continuously compromised, for which we need a robust assessment framework to delineate the human-induced sensitivity of the landscape, which in this study is addressed through ASZ of the Luni river basin. The ASZ tries to configure the most to minor

sensitive zones in terms of human activities and their footprints through an amalgamation of various man-based activity thematic layers. Such studies are interdisciplinary and have a lot with geomorphic connectivity, sediment transfer and ecological synergies (Wohl, 2017; Roy and Sahu, 2017; 2018).

- **AHP based ASZ**: Fig. 5.13 exhibits the ASZs for the entire Luni basin. The most interactive human spaces as marked with active farmlands, growing urban settlement extents, population density and transport network (combination of railways and roadways) density are found as most and quite anthropogenically sensitive. However, the Luni river basin accounts for only 1.63% and 3.36% respectively, under such zones. Moderate ASZ is found along the northern, northwestern, southern and in few patches all over the basin represented by a light shade of green having an areal contribution of 19.27%. The rest of the basin is found to have a poor to least human-induced sensitivity marked by 39.43% and 36.32%, respectively. The natural units in the Aravalli and along the dune-river interaction zone in the southwest have fewer human disturabnces and footprints than those in the other parts. The central locations of larger district headquarters towns and cities and their fringe areas are marked as the most sensitive human-impacted areas.

- **CSI based ASZ**: The composite index of ASZ shows much variability compared to the AHP derived one. In Fig. 5.14, most anthropogenic sensitive zones are found to be 13.79%, along with the quite sensitive ones as 30.44%. The moderate sensitive zones have coverage of 36.72%, while the poor and least has an areal coverage of 16.44% and 2.60%, respectively. The two starring differences in the ASZs observed for the most and least sensitive zones are much different compared with the ASZ of AHP. The equal weightage along with a multiplying factor may have elevated the differences observed in the most and least sensitive zones. A pixel-level accounting is observed from the CSI based ASZ. The thematic layers like settlement extent, population density, and transport network density reflect the final ASZ raster, providing a different outlook altogether compared to the AHP based ASZ. The district headquarters, towns and cities like Ajmer (north) and Jodhpur (northwestern edge) have an active ASZ raster profile contribution. The radiating transport networks and impact of croplands have been vital to have lesser degree sensitive zones along the central and northern section of the Luni river basin.

Thus, the first of its kind analysis of human footprint or influence index on the riverscape has proven much beneficial in understanding the vitality of the landscape either degrading because of unending human activities or are found to be least sensitive to any such changes due to less

population density and settlement concentration. Thus, a positive or direct correlation can be established between human presence and landscape alterations. To the opinion derived from the two MCDMs used to investigate the ASZs for the Luni river basin, the composite index finds a better score. It is advantageous in portraying the right scenario in judging the human impact on the riverscape the hierarchical criteria weighted AHP technique.

Inorder to understand the inter-relationship between the most vital thematic layers and ASZ, a scatter plot based trend analysis was performed in between AHP and CSI based ASZ and two key determinant parameters – population density and transport network density (Fig. 5.15). Each raster layer was extracted, and the values were plotted in Excel to develop the individual correlation. The inter-comparison proved to be the most influencing with a very high positive correlation R-squared values varying between 0.87 to 0.98, with a few outliars.
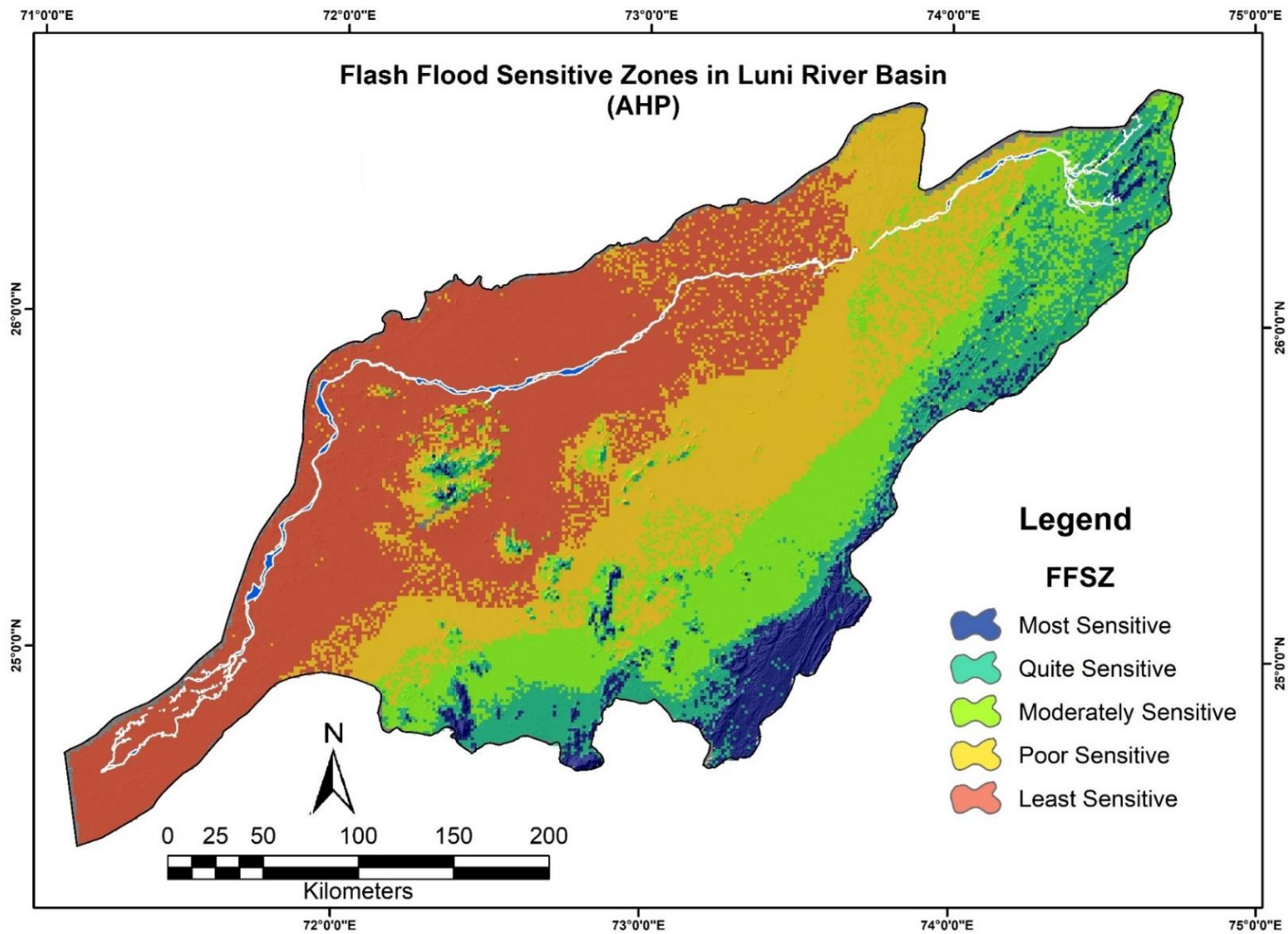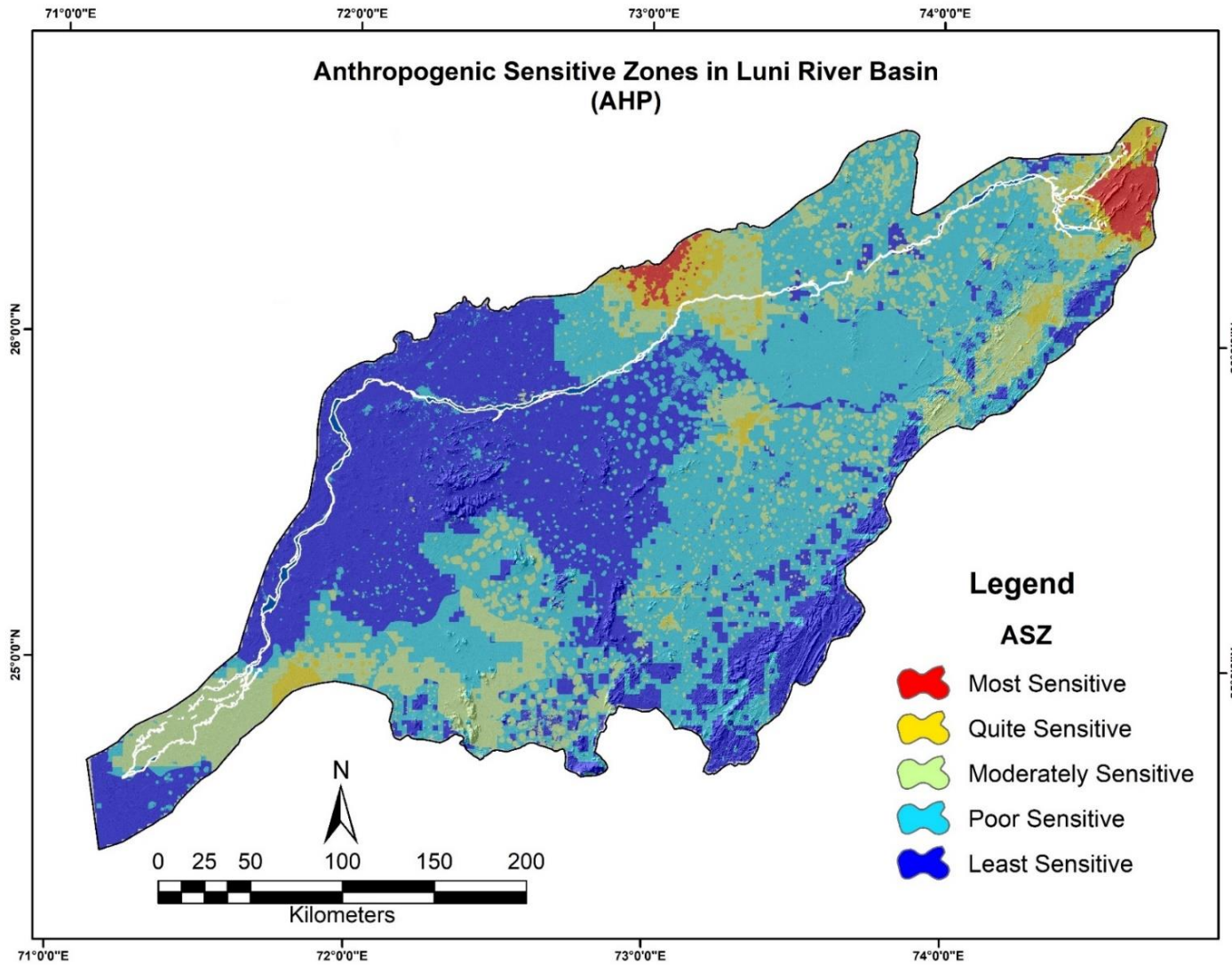
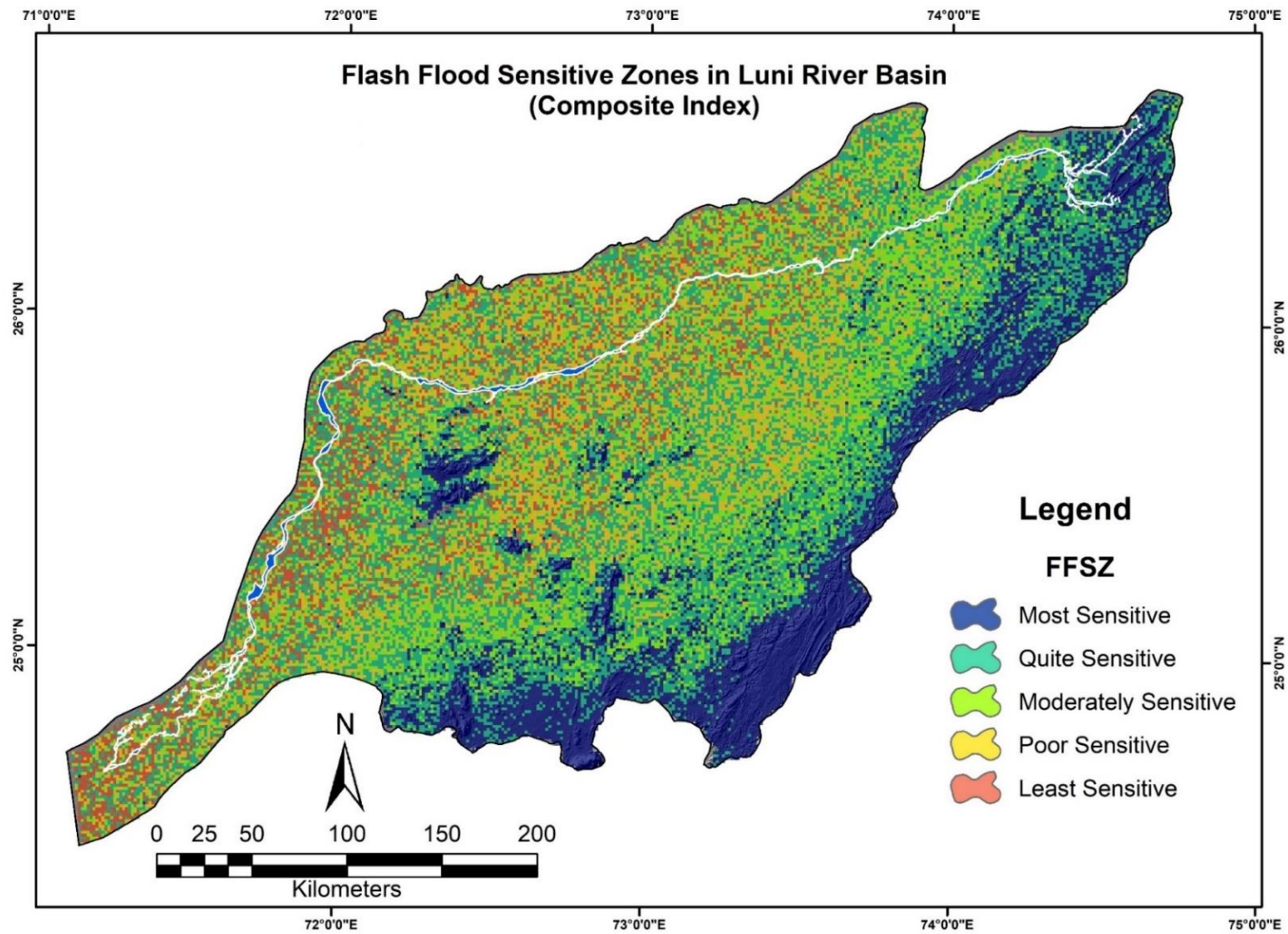Fig. 5.13: AHP based ASZs along the Luni river basin. Source: Prepared by the researcher.

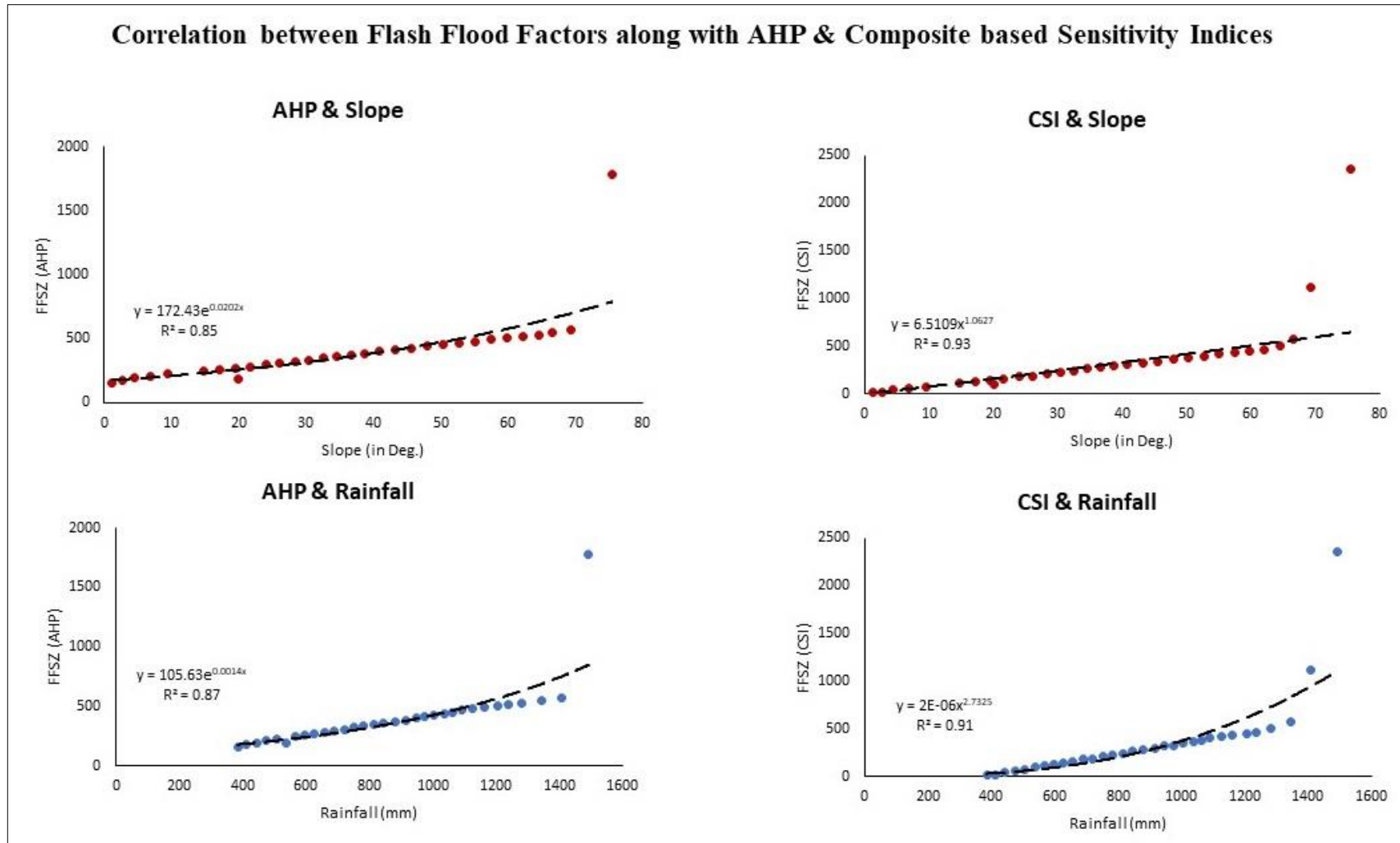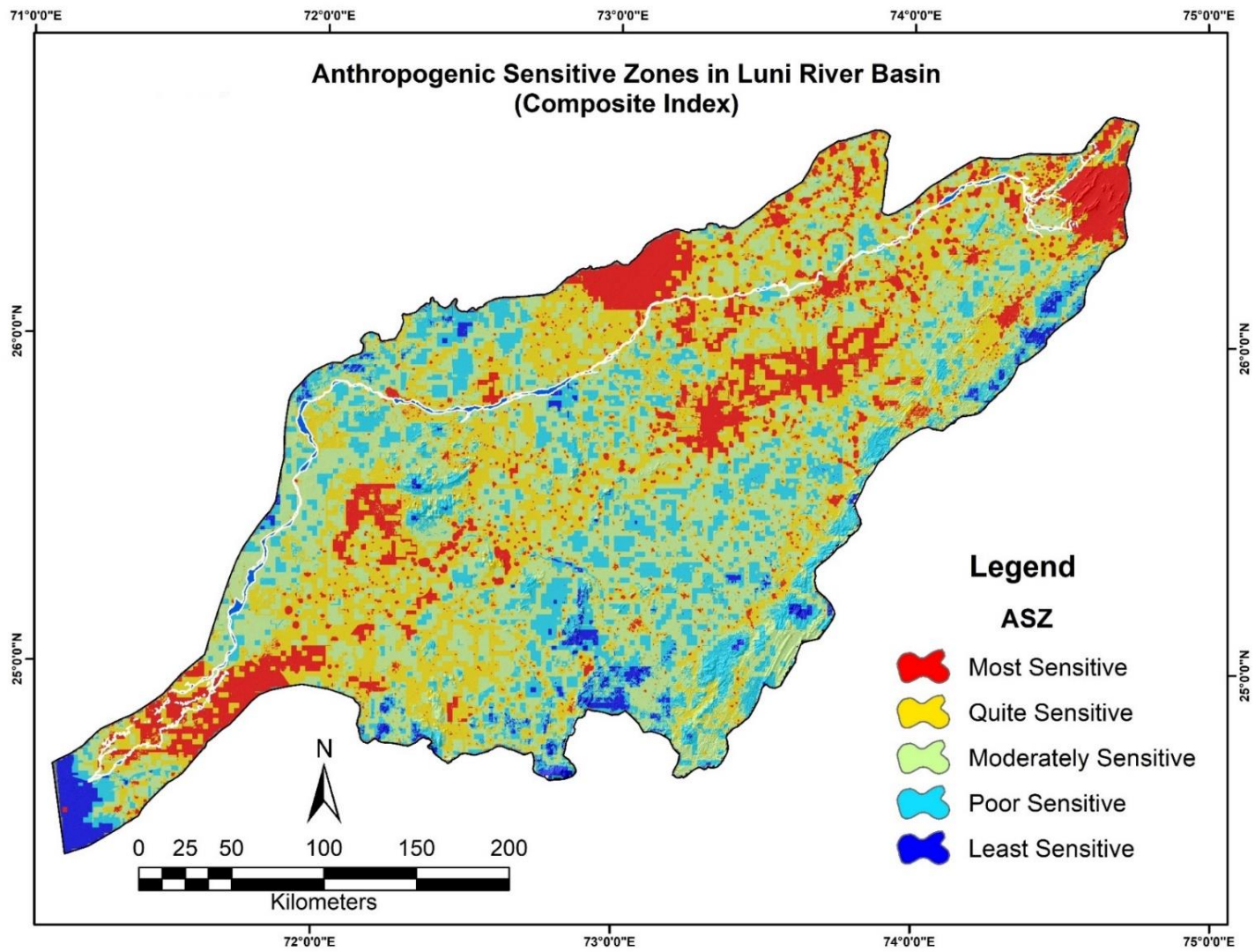Fig. 5.14: CSI based ASZs along the Luni river basin. Source: Prepared by the researcher.
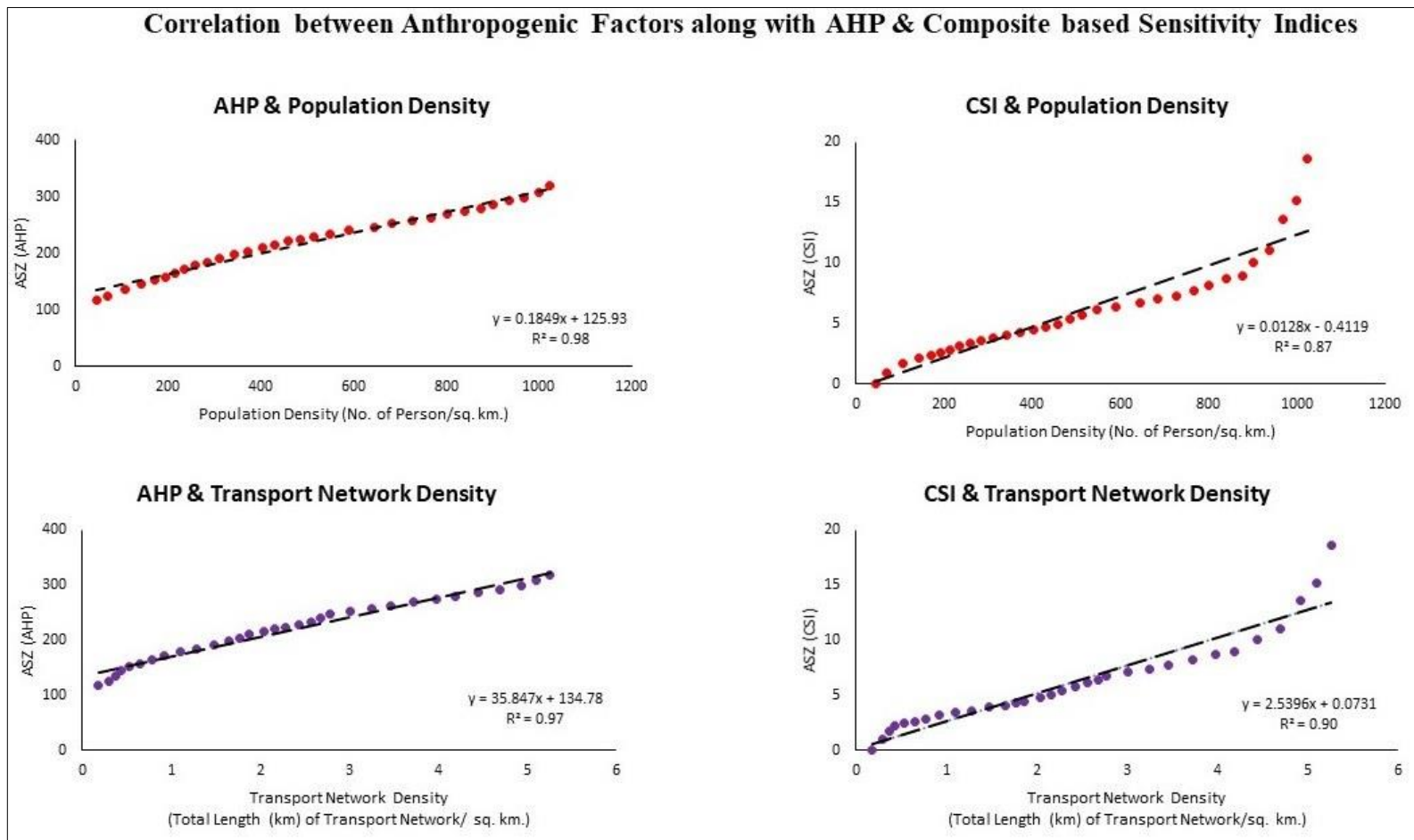
Fig. 5.15: Correlation between the two most vital thematic parameters determining anthropogenic sensitivity – Population density and Transport network density with the AHP and CSI based ASZs. Source: Computed by the researcher.

5.9 Summary

The chapter brings in the vital essence of this research by addressing the last two objectives of the study. The environmental interactions are duly noted, analyzed and presented in this study. The dune-river interactions and their conceptual representation were addressed to bring out the aeolian-fluvial synergy resulting in the domination of different interdune landscape units. A detailed literature review has shown the need and importance for such studies, especially in the Thar desert of the Indian subcontinent. The in-land deltaic system or the floodout is another unique landform feature examined in detail, showcasing the overall geomorphic system and micro-features. For the past 37 years, the water occurrence intensity has exhibited no such significant changes except the various diverging anabranched channels flowing during different timeframes. The natural status of the floodout is also mapped for pre-and post-monsoon seasons using three vital spectral signature-based normalized indices – NDMI, SAVI and BSI. The evident variations were noted and examined to bring out the essential dryland characteristics of the Luni's floodout region. Thus, glimpses of the significant and unique natural phenomenon occurring in the arid landscapes of the Luni river was mapped and investigated with some exciting future scope of research in such regions. Among all the other objectives, the most interesting was understanding the areas sensitive to flash floods and anthropogenic impact on the riverscape using two widely understood MCDM techniques – AHP and CSI. Both the techniques were used based on a specific judgment matrix with a combination of different best-suited thematic parameters for both the FFSZs and ASZs. The FFSZ showed an expected positive relation with rainfall and slope as its crucial determinant factor. The eastern edges along the entire stretch of Aravalli and its foothill zones were marked as most and quite sensitive regions for flash floods. The human-induced landscape disturbances were identified through both the AHP and CSI based techniques to delineate the ASZs throughout the Luni river basin. The towns/cities region and the areas of maximum transport network concentration showed a dominant relationship in the context of the ASZ. Though both techniques yielded a slightly different result, they could at least be compared and mutually validated based on the outcome map.

CHAPTER – 6
CONCLUSION

6.1 Rundown through the Findings

The present study has been extensive to develop the various vital findings, to sum up from all the preceding chapters. A rundown is synoptically presented to discuss how this study is standalone in Indian river science studies. Arid landscapes of the Thar have been historically seen as a dune dominated and aeolian process-related landscape in much ignorance of the dry river channels in this part of physiography. A well-cognized literature foundation was developed to find the significant research gaps and formulate the research questions that have not been addressed to date. Hence, the research objectives were derived from those research questions trying to address feasible ones within the scope of the present degree's timeframe. Fluvial behaviour is a derivative of the characteristic traits solely depending on the environmental setup. The terms often used in defining human psychology was used in a new fashion setting up a specific framework to define the evolution of the Luni riverscape. Environment induced character building and the resultant expression in hydro-geomorphic forms for the Luni river can be defined as the 'psyche' of a river. In short, a framework has been devised to address the core underlayer or the secret behind the present-day river behaviour. The process-intensive complexities have been tried to simplify and break down to equate each step behind the currently viewed riverine behaviour. For instance, noting down the non-perennial, ephemeral conditions along with tectonic induced alterations and larger channel width and shallow depth of the Luni can be better comprehended as these individual traits help to discern the dryland river behaviour.

The second chapter voraciously consists of maps to decipher the ongoing natural and human-induced processes within the Luni river basin. The distribution of administrative units, climatic conditions, bioclimatic variables, soil conditions, land resources, population density and transport networks has been extracted from different sources and introduced for describing the Luni river basin. Each natural and socio-economic unit is mapped to follow up the rest objectives in the succeeding chapters for the MCDMs. The rainfall and temperature were inversely proportional in the context of geographical location as the temperature would increase towards the western section of the river basin while the rainfall decreases towards the west and vice-versa. Wind speed is found to be optimum along the eastern edges, and a rising PET is seen over the extensive cropped areas of the basin. The soil conditions are primarily excellent and fit for cultivation except those affected by salinization/alkalinization. The decadal

LULC has shown a significant rise in farmlands and a decrease in natural vegetation. Active mining activities, levelling of dunes and expanding towns are the major causes for changing land cover units. The maps of population density and transport network exhibit nodal physical infrastructure growth, leading to geomorphic (dis)continuities and active interference with the landscapes.

The third chapter describes the geoscientific facts of the Luni river basin. The geology, geomorphology, lineament distribution, tectonic framework, seismic zones, Bouguer anomaly and hydrogeology of the river basin is explored, and comparative findings were placed with a compact integration of past literature published on the area. The dominant intra-cratonic alluvial filled sediment composition from the residual Aravalli ranges is the main factor describing the geological composition of the Luni river basin. The undifferentiated aeolian and fluvial sediments have led to the development of an older alluvial layer and a well-defined pediment-pediplain complex with the tributaries of Luni originating from the runoff of the Aravalli is entrenched and incising the valley floor. Very few river basins in India are like that of Luni, which has a unique composition of the four dominant seismic zones with varying potency of neo-tectonism. Major lineaments give a detailed insight into the reasons for changes in the river long profile. The potential zones of groundwater movement and recharge with specific yield values are seen to illuminate the hydrogeological condition of the Luni river basin. In the later part of the chapter, hydrological findings subscribe to the character of the Luni as a dry, non-perennial river having an 'extreme late summer regime'. The hydrological conditions of Balotra and Gandhav GDS were intercompared to bring out the significant changes observed in the river flow. Peak events were isolated using the R-B (flashiness) index to develop the flashy flows in the rivers, while the average annual gauge height and discharge were plotted along with its derivates like the stream power and rating curve. The unimodal hydrograph and the water level plots for both the GDS interpret the only river flow source as from the monsoon. A specialized index to compute the amount of zero flow was observed monthly, with the exception found only during the rainy season of the southwest monsoon. The probable reasons for zero flow are less rainfall in the stream and may be due to lack of consistent data readings, quick water percolation through the pervious sandy river bed or surface water extraction for irrigating the farmlands or domestic use before the hydrological data could be collected at a specific GDS. Downstream discharge has certain anomalies limited to few years, only suggesting Luni to be a 'losing' stream. Thus, the geoscientific study of the Luni basin has highlighted the significant balances and essential ingredients to explore the

riverine system's geophysical properties, exemplifying the specific reasons for ephemeral behaviour.

The terrain characterization provides a proven foundation regarding the importance of comprehending river behaviour. Slope, topographic and drainage characterization has been solved in the fourth chapter towards fulfilling the second part of the third objective of the research. The entire river basin of Luni has been a variable terrain process-response system depending on elevation and drainage classification. Higher slopes and initial stream orders were observed along the Aravalli ranges, while the terrain remains flat primarily with particular undulations in the pediment-pediplain zone. The modern geomorphometric features were solved along with the traditional ones to enhance the terrain configuration. The basin characterization was done as Luni's catchment is different from those delineated using a single pour point in a GIS environment. The Luni watershed was derived from previous highly cited literature and the various spatial resolution DEMs to develop an inter-comparison to understand the Luni basin's variations in shape and size. The debate of omitting the western section of the watershed adjacent to the Luni main channel was addressed by showing how small runoff ephemeral channel's inability to join with the Luni because of lack of streamflow and power to reach and meet up with Luni. Seven major sub-basins of Luni were delineated, and areal morphometric parameters were examined to bring out their impact on the central river basin. The CG analysis is a unique one for understanding how the gravitational force varies across the various source derived river basins and their striking expanse and presence in the arid landscape of Thar. The tectonic induced and topographic titling of the Luni river basin was computed using the AF index. The hypsometric analysis of the Luni and its major seven sub-basins showed that most of them are in the senile/old stage of evolutionary history as most of the sediment-source zones (Aravalli) is in the residual monadnock stage. Long profile and its derivates like SL index, segment slope and their changing rates have shown the structural lineament induced knickpoints and anomalies on the river profile suggesting rejuvenation or sudden slope alterations due to local anthropogenic activities.

The final chapter deals with the last two objectives of this research showing up the environmental interactions and status-quo of only the compelling stretches of the Luni river having unique geomorphology and delineating the flash flood and anthropogenic sensitive zones for the entire Luni basin. The aeolian-fluvial interactions and the conceptual framework of river-dune interaction have been mapped and investigated for a specific lower stretch of Luni. The interplay of semi-stabilized dune movement, sand storm-induced sediment filling of

the dry river channel of Luni and peak flow in Luni leading to minor or moderate changes in the dune field has been explored. An in-land deltaic system called the floodout is geomorphologically defined and understands its natural condition in pre-and post-monsoon seasons. The water occurrence intensity layer from 1984-2020 has been phenomenal in deriving the small to significant changes in the ecohydrological sensitivities of the region. The flash flood and anthropogenic sensitive zones were delineated using two widely used MCDMs – AHP and composite index. The outcomes for flash floods were higher in the high grounds of Aravalli and its adjacent regions. While the human footprints found maximum through the population, transport network densities and settlement extent layers registered the peak sensitive zones known as most anthropogenically sensitive and are susceptible to geomorphic (dis)continuities in the riverscape of the Luni basin.

6.2 Key Challenges

Bohra (2007) notes down the most deplorable water-stressed situation in the Thar desert region of India, especially that of the districts of western Rajasthan known for acute water shortage, scanty rainfall and droughts. The only water source is underground aquifers, which dry up with scorching and thirsty deserts, making lives challenging. Luni river is dry throughout the year, except some water gushing down the stream during the monsoon season is the primary source of surface freshwater. This source is becoming unfit for human use as harmful effluents from the textile industries and other local manufacturing units are directly dumped into the dry river leading to its conversion to a mere wastewater canal, especially near Jodhpur and Balotra. This wastewater is affecting the eco-sensitive fluvial system of the Luni river and hampering the lives of the local population with the spread of several water-borne diseases and causing severe illness to the poor villages. Since the river remains dry and the underlying river bed material has a composition of pervious sand and gypsum layers, it enhances the contaminants to meet with the groundwater and leads to its quality degradation. Scarce water availability and effluent contamination are paying a heavy price for farming and domestic consumption, leaving it unfit for any use. Recently, an order issued by the Rajasthan Pollution Control Board (RPCB) to lock down more than 800 textile units adjoining the Luni river in Balotra has been reported by the [media](). These units have been asked to remain suspended unless the 18 MLD reverse osmosis (RO) sewerage water treatment plant (SWTP) starts its operations to decrease pollution levels in the local environment of Balotra.

The other issues that were observed while conducting this research included the quality, irregularity and erroneous maintenance of the hydrological dataset by the concerned data

maintenance authorities. Most of the gauge and discharge datasets were computed from certain observed ones and found as a misfit. The accurate picture of hydrological analysis is difficult to be represented and come up with some compelling and conclusive findings discussing the Luni river's hydrological phenomenon. Unfortunately, the GD, sediment and river water quality datasets for the dryland rivers of western India are ill-maintained, and some actual hydro-meteorological events have been missed in this regard. Zero flows recorded in the GDS of Luni are not always meant to have no river water flow but are casually filled by the local data observer without any proper measurements. Data gap makes the hydrological comprehension problematic for predicting streamflow or discerning any concussive configuration of the fluvial system. The dearth of an integrated depository maintaining annual or monthly basis state or district level natural hazard inventory is much needed to procure and validate the findings of disaster risk sensitivity is a much need of the hour. Such data can help comprehend vital statistics and develop an integrated disaster profile of the state or district.

6.3 Way Forward

The future research possibilities are exciting with the reconstruction of paleo-floods, paleo-channels and paleo-climatic events using the luminescence dating technique on the fluvial sediments or aeolian dunes along the river corridor of Luni. The most discussed geoscientific fact-finding projects regarding the presence of the Saraswati river can also be verified promptly after applying such a technique to quantify the evolution of the Luni's riverscape. The isostatic balance formed by the unending natural sediment cycle from erosion of the Aravalli highlands to the prime deposition of eroded sediments by the active geomorphic agencies needs to be investigated in the Thar areas of India. Drylands have always been known for dunes and active aeolian processes, but sometimes peak riverine events like flash floods alter the riverscape to a much larger extent which needs to be thoroughly studied in future. This research is promising and new in the Indian context as such exhaustive mapping of the dryland river of Luni and its significant sub-basins have been much less addressed. The dune-river synergy and their active impacts creating new landscape units are not much observed in the Luni basin area. Aeolian and fluvial interactions are the hour's need to understand better the geomorphic domination and the core carving reasons of the drylands under the interdisciplinary lens. The concept of landscape 'memory' bearing the imprints of the records of tectonics, surface processes, and climatic variability can be comprehended to understand the progression better. Weaker socio-economic profiles, changing land covers, increasing risks of natural hazards are the way forward topics that can be analyzed in dryland regions as they are sensitive to climate change.

The development and execution of better enforceable policies could be devised by restricting the rising human footprints and conserving the water balance in the region. Islam and Ghosh (2021) have demonstrated the need for a community-based approach in evaluating the flood risks along with the drivers of alterations and in-depth impact analysis on the social, economic and physical infrastructural components. Hence, river perception surveys can also be a better subsequent study involving the local communities thriving on the Luni river for their sustenance and livelihood.

Recent studies conducted by Pani and Carling (2020) show a current framework with the facilitating amalgamation of geoscientific and hydrological data to solicit a better river management system in the Luni river. A practical and viable method for understanding ground and surface water interactions in desert regions is of utmost importance. It was found that the data assimilation approach stitching the geophysical, hydrological data along with socio-economic surveyed profiles of the region endorsed by the active application of RS and GIS tools results in identifying the deplorable zones sensitive to either flash floods or active human influence. Better management plans can be designed to check erosion, floods and growing alterations of land use, mitigate the potency of future hazards through a detailed disaster risk reduction analysis and enhance social resiliency to promote an eventual sustainable livability.

BIBLIOGRAPHY

1. Abboud, I.A. and Nofal, R.A., 2017. Morphometric analysis of wadi Khumal basin, western coast of Saudi Arabia, using remote sensing and GIS techniques. Journal of African Earth Sciences, 126, pp.58-74. DOI: https://doi.org/10.1016/j.jafrearsci.2016.11.024.

2. Agnihotri, I., Punia, M.P. and Sharma, J.R., 2021. Spatiotemporal Analysis of Maximum and Minimum Temperature within a Basin: A Case Study of West-Flowing River Basin of Kutch, Saurashtra and Marwar, India. Journal of the Indian Society of Remote Sensing, pp.1-8. DOI: https://doi.org/10.1007/s12524-021-01340-7.

3. Ahmed, M.A. and Ahmad W.A., 2013. Barren Land Index Assessment Land Use-Land Cover Changes in Himreen Lake and surrounding area East of Iraq. Journ. of Env. and Earth Sc., vol. 3, no. 4, pp. 15-26.

4. Ali, H., Modi, P. and Mishra, V., 2019. Increased flood risk in Indian sub-continent under the warming climate. Weather and Climate Extremes, 25, p.100212. DOI: https://doi.org/10.1016/j.wace.2019.100212

5. Al-Masrahy, M.A. and Mountney, N.P., 2015. A classification scheme for fluvial–aeolian system interaction in desert-margin settings. Aeolian Research, 17, pp.67-88. DOI: https://doi.org/10.1016/j.aeolia.2015.01.010

6. Ambili, V. and Narayana, A.C., 2014. Tectonic effects on the longitudinal profiles of the Chaliyar River and its tributaries, southwest India. Geomorphology, 217, pp.37-47. DOI: https://doi.org/10.1016/j.geomorph.2014.04.013.

7. Anagnostou, M.N., Kalogiros, J., Anagnostou, E.N., Tarolli, M., Papadopoulos, A. and Borga, M., 2010. Performance evaluation of high-resolution rainfall estimation by X-band dual-polarization radar for flash flood applications in mountainous basins. Journal of hydrology, 394(1-2), pp.4-16. DOI: https://doi.org/10.1016/j.jhydrol.2010.06.026

8. Anand, A. K., and Pradhan, S. P., 2019. Assessment of active tectonics from geomorphic indices and morphometric parameters in part of Ganga basin. Journal of Mountain Science, 16(8), 1943-1961. DOI: https://doi.org/10.1007/s11629-018-5172-2

9. Antón, L., De Vicente, G., Muñoz-Martín, A. and Stokes, M., 2014. Using river long profiles and geomorphic indices to evaluate the geomorphological signature of continental scale drainage capture, Duero basin (NW Iberia). Geomorphology, 206, pp.250-261. DOI: https://doi.org/10.1016/j.geomorph.2013.09.028.

10. Arulbalaji, P., Padmalal, D. and Sreelash, K., 2019. GIS and AHP techniques based delineation of groundwater potential zones: a case study from southern Western Ghats, India. Scientific reports, 9(1), pp.1-17. DOI: https://doi.org/10.1038/s41598-019-38567-x

11. Ayaz, S. and Dhali, M.K., 2020. Longitudinal profiles and geomorphic indices analysis on tectonic evidence of fluvial form, process and landform deformation of Eastern Himalayan Rivers, India.

Geology, Ecology, and Landscapes, 4(1), pp.11-22. DOI: https://doi.org/10.1080/24749508.2019.1568130.

12. Bajpai, V.N., 2004. Hydrogeological evolution of the Luni river basin, Rajasthan, western India: A review. Journal of Earth System Science, 113(3), pp. 427-451. DOI: https://doi.org/10.1007/BF02716735

13. Bajpai, V.N., Roy, T.S. and Tandon, S.K., 2001. Subsurface sediment accumulation patterns and their relationships with tectonic lineaments in the semi-arid Luni river basin, Rajasthan, Western India. Journal of Arid environments, 48(4), pp.603-621. DOI: https://doi.org/10.1006/jare.2000.0766

14. Baker, D.B., Richards, R.P., Loftus, T.T. and Kramer, J.W., 2004. A new flashiness index: Characteristics and applications to midwestern rivers and streams 1. JAWRA Journal of the American Water Resources Association, 40(2), pp.503-522. DOI: https://doi.org/10.1111/j.1752-1688.2004.tb01046.x.

15. Barling, R. D., Moore, I. D., Grayson, R. B., 1994. A quasi-dynamic wetness index for characterizing the spatial distribution of zones of surface saturation and soil water content. Water Resources Research, 30, 1029–1044. DOI: https://doi.org/10.1029/93WR03346

16. Belnap, J., Munson, S.M. and Field, J.P., 2011. Aeolian and fluvial processes in dryland regions: the need for integrated studies. Ecohydrology, 4(5), pp.615-622. DOI: https://doi.org/10.1002/eco.258

17. Bendjoudi, H. and Hubert, P., 2002. The Gravelius compactness coefficient: critical analysis of a shape index for drainage basins.

18. Bera, R. and Maiti, R., 2021. An assessment of coastal vulnerability using geospatial techniques. Environmental Earth Sciences, 80(8), pp.1-18. DOI: https://doi.org/10.1007/s12665-021-09616-4

19. Beven, K.J. and Kirkby, M.J., 1979. A physically based, variable contributing area model of basin hydrology/Un modèle à base physique de zone d'appel variable de l'hydrologie du bassin versant. Hydrological Sciences Journal, 24(1), pp.43-69.

20. Bini, M., 2009. Geomorphosites and the conservation of landforms in evolution. Mem. Descr. Carta Geol. d'It, 87, pp.7-14.

21. Biron, P.M., Buffin-Bélanger, T., Larocque, M., Choné, G., Cloutier, C.A., Ouellet, M.A., Demers, S., Olsen, T., Desjarlais, C. and Eyquem, J., 2014. Freedom space for rivers: a sustainable management approach to enhance river resilience. Environmental management, 54(5), pp.1056-1073. DOI: https://doi.org/10.1007/s00267-014-0366-z.

22. Biswas, S.K., 2016, November. Tectonic framework, structure and tectonic evolution of Kutch Basin, western India. In Conference GSI (pp. 129-150).

23. Black, P.E., 1972. Hydrograph responses to geomorphic model watershed characteristics and precipitation variables. Journal of hydrology, 17(4), pp.309-329. DOI: https://doi.org/10.1016/0022-1694(72)90090-X

24. Blanton, P. and Marcus W.A., 2009. Railroads, roads and lateral disconnection in the river landscapes of the continental United State. Geomorphology. 112(3-4):212–227. DOI: https://doi.org/10.1016/j.geomorph.2009.06.008

25. Blanton, P. and Marcus, W.A., 2014. Roads, Railroads, and floodplain fragmentation due to transportation infrastructure along rivers. Ann Assoc Am Geogr. 104(3):413–431.

26. Bohra, N.K., 2007. Ecological studies on Luni river basin. Nature, Environment and Pollution Technology, 6(1), pp.29-35.

27. Boulton, S.J., 2020. Geomorphic response to differential uplift: river long profiles and knickpoints from Guadalcanal and Makira (Solomon Islands). Frontiers in Earth Science, 8, p.10.DOI:https://doi.org/10.3389/feart.2020.00010.

28. Brunsden, D. and Thornes, J.B., 1979. Landscape sensitivity and change. Transactions of the Institute of British Geographers, pp.463-484.

29. Brunsden, D., 2001. A critical assessment of the sensitivity concept in geomorphology. Catena, 42(2-4), pp.99-123. DOI: https://doi.org/10.1016/S0341-8162(00)00134-X.

30. Buchhorn, M., Smets, B., Bertels, L., De Roo, B., Lesiv, M., Tsendbazar, N. - E., Herold, M. and Fritz, S., 2020. Copernicus Global Land Service: Land Cover 100 m: collection 3: epoch 2019: Globe. DOI: 10.5281/zenodo.3939050. (https://lcviewer.vito.be/download). Accessed on - 15 September, 2020.

31. Bull, L.J. and Kirkby, M.J. eds., 2002. Dryland rivers: hydrology and geomorphology of semi-arid channels. John Wiley & Sons.

32. Bullard, J.E. and Livingstone, I., 2002. Interactions between aeolian and fluvial systems in dryland environments. Area, 34(1), pp.8-16. DOI: https://doi.org/10.1111/1475-4762.00052

33. Bullard, J.E. and McTainsh, G.H., 2003. Aeolian-fluvial interactions in dryland environments: examples, concepts and Australia case study. Progress in Physical Geography, 27(4), pp.471-501.DOI:https://doi.org/10.1191/0309133303pp386ra

34. Bullard, J.E. and McTainsh, G.H., 2003. Aeolian-fluvial interactions in dryland environments: examples, concepts and Australia case study. Progress in Physical Geography, 27(4), pp.471-501.DOI:https://doi.org/10.1191/0309133303pp386ra.

35. Bullard, J.E. and Nash, D.J., 2000. Valley-marginal sand dunes in the south-west Kalahari: their nature, classification and possible origins. Journal of Arid Environments, 45(4), pp.369-383. DOI: https://doi.org/10.1006/jare.2000.0646

36. Burrough, P.A., 1986. Principles of geographical information systems for land resources assessment. Clarendon.

37. Castelltort, S., Goren, L., Willett, S.D., Champagnac, J.D., Herman, F. and Braun, J., 2012. River drainage patterns in the New Zealand Alps primarily controlled by plate tectonic strain. Nature Geoscience, 5(10), pp.744-748. DOI: https://doi.org/10.1038/ngeo1582

38. Center for International Earth Science Information Network - CIESIN - Columbia University. 2018. Gridded Population of the World, Version 4 (GPWv4): Population Density, Revision 11. Palisades, NY: NASA Socioeconomic Data and Applications Center (SEDAC). DOI: https://doi.org/10.7927/H49C6VHW. Accessed on - 30 September, 2020.

39. CGWB, Watershed Atlas of India, 2012. River Basin Map of Luni.

40. Chandrashekar, H., Lokesh, K.V., Sameena, M., Roopa, J. and Ranganna, G., 2015. Proc. Int. Conf. on Water Resources, Coastal and Ocean Engineering (Mangalore) vol. 4 ed. G.S. Dwarakish (Elsevier Procedia), pp. 1345 – 1353.

41. Chatterjee, A. and Ray, J.S., 2018. Geochemistry of Harappan potteries from Kalibangan and sediments in the Ghaggar River: Clues for a dying river. Geoscience Frontiers, 9(4), pp.1203-1211.

42. Chatterjee, A., Ray, J.S., Shukla, A.D. and Pande, K., 2019. On the existence of a perennial river in the Harappan heartland. Scientific reports, 9(1), pp.1-7. DOI: https://doi.org/10.1038/s41598-019-53489-4

43. Chen, C.Y. and Yu, F.C., 2011. Morphometric analysis of debris flows and their source areas using GIS. Geomorphology, 129(3-4), pp.387-397. DOI: https://doi.org/10.1016/j.geomorph.2011.03.002

44. Chorley, R.J., Malm, D.E. and Pogorzelski, H.A., 1957. A new standard for estimating drainage basin shape. American journal of science, 255(2), pp.138-141.

45. Chow, V.T., Maidment, D.R. and Mays, L.W., 1988. Applied hydrology. Mc-Graw Hill, New York.

46. Chu-Rong, X.I.N.G., You-Gui, F.E.N.G., Gui-Jun, Y.A.N.G., Ping, W.A.N.G. and Wen-Jiang, H.U.A.N.G., 2009. Method of estimating vegetation coverage based on remote sensing. Remote Sensing Technology and Application, 24(6), pp.849-854.

47. Collier, C.G., 2007. Flash flood forecasting: What are the limits of predictability? Quarterly Journal of the Royal Meteorological Society: A journal of the atmospheric sciences, applied meteorology and physical oceanography, 133(622), pp.3-23. DOI: https://doi.org/10.1002/qj.29

48. Cox, R.T., 1994. Analysis of drainage-basin symmetry as a rapid technique to identify areas of possible Quaternary tilt-block tectonics: An example from the Mississippi Embayment. Geological society of America bulletin, 106(5), pp.571-581. DOI: https://doi.org/10.1130/0016-7606(1994)106<0571:AODBSA>2.3.CO;2

49. CWC River Basin Report, 2014. West Flowing Rivers of Kutch and Saurashtra including Luni. v.2.0. New Delhi.

50. Das S., Gupta A., and Ghosh S., 2017. Exploring groundwater potential zones using MIF techniques in semi-arid region: a case study of Hingoli district, Maharashtra. Spat Inf Res 25(6), pp. 749–756. DOI: https://doi.org/10.1007/s41324-017-0144-0

51. Das, S. and Gupta, A., 2021. Multi-criteria decision based geospatial mapping of flood susceptibility and temporal hydro-geomorphic changes in the Subarnarekha basin, India. Geoscience Frontiers, 12(5), p.101206. DOI: https://doi.org/10.1016/j.gsf.2021.101206

52. Das, S., 2012. The role of natural ecosystems and socio-economic factors in the vulnerability of coastal villages to cyclone and storm surge. Natural Hazards, 64(1), pp.531-546. DOI: https://doi.org/10.1007/s11069-012-0255-9

53. Das, S., 2018. Geographic information system and AHP-based flood hazard zonation of Vaitarna basin, Maharashtra, India. Arabian Journal of Geosciences, 11(19), pp.1-13. DOI: https://doi.org/10.1007/s12517-018-3933-4

54. Das, S., 2021a. Hydro-geomorphic characteristics of the Indian (Peninsular) catchments: Based on morphometric correlation with hydro-sedimentary data. Advances in Space Research, 67(8), pp.2382-2397.DOI:https://doi.org/10.1016/j.asr.2021.01.043.

55. Das, S., and Pardeshi, S.D., 2018. Morphometric analysis of Vaitarna and Ulhas River basins, Maharashtra, India: using geospatial techniques. Applied Water Science, 8(6), pp.1-11. DOI: https://doi.org/10.1007/s13201-018-0801-z

56. Das, S., Kandekar, A.M., Sangode, S.J., 2021b. Lithologic controls on the geomorphic evolution of the central Western Ghats: An example from the Aghnashini Catchment, Karnataka, India. Journal of the Geological Society of India (*In Press*)

57. Das, S., Pardeshi, S.D., Kulkarni, and P.P., Doke, A., 2018. Extraction of lineaments from different azimuth angles using geospatial techniques: a case study of Pravara basin, Maharashtra, India. Arab J. Geosci 11, p. 160. DOI: https://doi.org/10.1007/s12517-018-3522-6

58. Das, S., Roy, S. and Sengupta, S., 2020. Drainage Basin Morphometry and its Relation to Erosion Susceptibility in the Barakar River Basin, Jharkhand and West Bengal. Journ. of Ind. Geomorph., vol. 8, pp. 73-89.

59. De Reu, J., Bourgeois, J., Bats, M., Zwertvaegher, A., Gelorini, V., De Smedt, P., ... Van Meirvenne, M., 2013. Application of the topographic position index to heterogeneous landscapes. Geomorphology, 186, 39-49. https://doi.org/10.1016/j.geomorph.2012.12.015.

60. Dhir, R.P., Kar, A., Wadhawan, S.K., Rajaguru, S.N., Misra, V.N., Singhvi, A.K. and Sharma, S.B., 1992. Lineaments, In: Singhvi, Thar Desert in Rajasthan: land, man and environment, A.K. and Kar, A. (eds), pp 29–32. Bangalore: Geological Society of India.

61. Dhir, R.P., Kolarkar, A.S., Sharma, K.D., Vangani, N.S., Saxena, S.K., Sen, A.K., Ramakrishna, Y.S., Murthy, K.N.K., Singh, N. and Tak, B.L., 1982. July 1979 Flash Flood in The Luni: A Case Study.

62. Downs, P.W. and Gregory, K.J., 1993. The sensitivity of river channels in the landscape system. In Landscape sensitivity (pp. 15-30).

63. Downs, P.W. and Gregory, K.J., 1995. Approaches to river channel sensitivity. The Professional Geographer, 47(2), pp.168-175. DOI: https://doi.org/10.1111/j.0033-0124.1995.00168.x

64. Downs, P.W. and Gregory, K.J., 1995. Approaches to river channel sensitivity. The Professional Geographer, 47(2), pp.168-175. DOI: https://doi.org/10.1111/j.0033-0124.1995.00168.x

65. Draut, A.E., 2012. Effects of river regulation on aeolian landscapes, Colorado River, southwestern USA. Journal of Geophysical Research: Earth Surface, 117(F2). DOI: https://doi.org/10.1029/2011JF002329

66. Elfeki, A., Masoud, M. and Niyazi, B., 2017. Integrated rainfall–runoff and flood inundation modeling for flash flood risk assessment under data scarcity in arid regions: Wadi Fatimah basin case study, Saudi Arabia. Natural Hazards, 85(1), pp.87-109. DOI: https://doi.org/10.1007/s11069-016-2559-7

67. Escadafal, R. and Bacha, S., 1996. Strategy for the dynamic study of desertification.

68. European Space Agency (ESA) and Université catholique de Louvain (UCLouvain), 2009. Globcover 2009. http://due.esrin.esa.int/page_globcover.php. Accessed on – 15 September, 2020.

69. Evans, I.S., 1980. An integrated system of terrain analysis and slope mapping. Zeitschrift für Geomorphologie. Supplementband Stuttgart, (36), pp.274-295.

70. Faniran, A., 1968. The index of drainage intensity: a provisional new drainage factor. Aust J Sci, 31(9), pp.326-330.

71. FAO (Food and Agricultural Organization), 1983. Soils resources, management and conservation service, Guidelines: land evaluation for rainfed agriculture. FAO.

72. Field, J.P., Breshears, D.D. and Whicker, J.J., 2009. Toward a more holistic perspective of soil erosion: why aeolian research needs to explicitly consider fluvial processes and interactions. Aeolian Research, 1(1-2), pp.9-17. DOI: https://doi.org/10.1016/j.aeolia.2009.04.002

73. Fongers, D., Manning, K. and Rathbun, J., 2007. Application of the Richards-Baker Flashiness Index to gaged Michigan rivers and streams. DEQ Michigan's Nonpoint Source Program.

74. Friedrich, K. 1996. Digitale Reliefgliederungsverfahren zur Ableitung bodenkundlich relevanter Flaecheneinheiten. Frankfurter Geowissenschaftliche Arbeiten D 21, Frankfurt/M., online.

75. Friedrich, K. 1998. Multivariate distance methods for geomorphographic relief classification. in Heinecke, H., Eckelmann, W., Thomasson, A., Jones, J., Montanarella, L., Buckley, B. (eds.): Land Information Systems - Developments for planning the sustainable use of land resources. European Soil Bureau - Research Report 4, EUR 17729 EN, Office for official publications of the European Communities, Ispra, pp. 259-266.

76. Fryirs, K., Spink, A. and Brierley, G., 2009. Post-European settlement response gradients of river sensitivity and recovery across the upper Hunter catchment, Australia. Earth Surface Processes and Landforms, 34(7), pp.897-918. DOI: https://doi.org/10.1002/esp.1771.

77. Fryirs, K.A. and Brierley, G.J., 2012. Geomorphic analysis of river systems: an approach to reading the landscape. John Wiley & Sons, ch. 11, pp. 205-234.

78. Fryirs, K.A., 2017. River sensitivity: A lost foundation concept in fluvial geomorphology. Earth Surface Processes and Landforms, 42(1), pp.55-70. DOI: https://doi.org/10.1002/esp.3940.

79. Fuller, I.C., Gilvear, D.J., Thoms, M.C. and Death, R.G., 2019. Framing resilience for river geomorphology: Reinventing the wheel?. River Research and Applications, 35(2), pp.91-106. DOI: https://doi.org/10.1002/rra.3384.

80. Gad, A.A., 2015. Land capability classification of some western desert Oases, Egypt, using remote sensing and GIS. The Egyptian Journal of Remote Sensing and Space Science, 18(1), pp. S9-S18. DOI: https://doi.org/10.1016/j.ejrs.2015.06.002

81. Gallant, J.C., Dowling, T.I. 2003. A multiresolution index of valley bottom flatness for mapping depositional areas. Water Resources Research, 39(12), 1347.

82. García, J.H., Ollero, A., Ibisate, A., Fuller, I.C., Death, R.G. and Piégay, H., 2021. Promoting fluvial geomorphology to "live with rivers" in the Anthropocene Era. Geomorphology, 380, p.107649.DOI:https://doi.org/10.1016/j.geomorph.2021.107649.

83. Georgakakos, K.P. and Hudlow, M.D., 1984. Quantitative precipitation forecast techniques for use in hydrologic forecasting. Bulletin of the American Meteorological Society, 65(11), pp.1186-1200. DOI: https://doi.org/10.1175/1520-0477(1984)065<1186:QPFTFU>2.0.CO;2

84. Georgakakos, K.P., 1986. On the design of national, real-time warning systems with capability for site-specific, flash-flood forecasts. Bulletin of the American Meteorological Society, 67(10), pp.1233-1239. DOI: https://doi.org/10.1175/1520-0477(1986)067<1233:OTDONR>2.0.CO;2

85. Ghosh, A. and Maiti, R., 2021. Development of new composite index on channel sensitivity using AHP, FR and ensemble model and its application on the Mayurakshi river of Eastern India. International Journal of River Basin Management, pp.1-18. DOI: https://doi.org/10.1080/15715124.2021.1879092.

86. González-Hidalgo, J.C., Peña-Monné, J.L. and de Luis, M., 2007. A review of daily soil erosion in Western Mediterranean areas. Catena, 71(2), pp.193-199. DOI: https://doi.org/10.1016/j.catena.2007.03.005

87. Gore, D., Brierley, G., Pickard, J. and Jansen, J., 2000. Anatomy of a floodout in semi-arid eastern Australia. Zeitschrift fur Geomorphologie, 122, pp. 113-139.

88. Gornitz, V., 1990. Vulnerability of the East Coast, USA to future sea level rise. Journal of Coastal research, pp.201-237.

89. Gornitz, V., 1991. Global coastal hazards from future sea level rise. Palaeogeography, Palaeoclimatology, Palaeoecology, 89(4), pp.379-398. DOI: https://doi.org/10.1016/0031-0182(91)90173-O

90. Goudie, A.G., 2004. Encyclopedia of geomorphology (Vol. 2). Routledge, London, p. 1156.

91. Goudie, A.S. and Middleton, N.J., 2006. Desert dust in the global system. Springer Science & Business Media.

92. Goudie, A.S., 1987. Change and instability in the desert environment. In Horizons in Physical Geography (pp. 250-267). Palgrave, London.

93. Goudie, A.S., 2013. Arid and Semi-Arid Geomorphology. Cambridge University Press., ch. 5, pp. 205-245.

94. Graf, W.L., 1988. Fluvial processes in dryland rivers (Vol. 346). New York: Springer-Verlag.

95. Grant, G.E., 1997. A geomorphic basis for interpreting the hydrologic behaviour of large river basins (pp. 105-116). CRC Lewis Publishers.

96. Gravelius, H., 1914. Flusskunde. Goschen Verlagshan dlung Berlin. Morphometry of drainage basins. Elsevier, Amsterdam.

97. Gregory, K.J. and Walling, D.E., 1968. The variation of drainage density within a catchment. Hydrological Sciences Journal, 13(2), pp.61-68. DOI: https://doi.org/10.1080/02626666809493583

98. Gregory, K.J., 1987. Environmental effects of river channel changes. Regulated Rivers: Research & Management, 1(4), pp.358-363.

99. Gregory, K.J., 2019. Human influence on the morphological adjustment of river channels: The evolution of pertinent concepts in river science. River Research and Applications, 35(8), pp.1097-1106. DOI: https://doi.org/10.1002/rra.3455.

100. Grohmann, C.H., 2017. Comparison of roving-window and search-window techniques for characterising landscape morphometry. Computers and Geosciences 35, pp. 2164–2169. DOI: https://doi.org/10.1016/j.cageo.2008.12.014.

101. Ground Water Department (GWD), Govt. of Rajasthan, 2013. Hydrogeological Atlas of Rajasthan, Luni River Basin. European Union State Partnership Programme, Rolta India Ltd.

102. Guisan, A., Weiss, S.B. and Weiss, A.D., 1999. GLM versus CCA spatial modeling of plant species distribution. Plant ecology, 143(1), pp.107-122. DOI: https://doi.org/10.1023/A:1009841519580

103. Haas, J. and Ban, Y., 2017. Sentinel-1A SAR and sentinel-2A MSI data fusion for urban ecosystem service mapping. Remote Sensing Applications: Society and Environment, 8, pp.41-53. DOI: https://doi.org/10.1016/j.rsase.2017.07.006

104. Haines, A.T., Finlayson, B.L. and McMahon, T.A., 1988. A global classification of river regimes. Applied Geography, 8(4), pp.255-272. DOI: https://doi.org/10.1016/0143-6228(88)90035-5

105. Harinath, V. and Raghu, V., 2013. Morphometric analysis using Arc GIS techniques a case study of Dharurvagu, south eastern part of Kurnool district, Andhra Pradesh, India. International Journal of Science and Research (IJSR), India Online ISSN, pp.2319-7064.

106. Hong, H., Panahi, M., Shirzadi, A., Ma, T., Liu, J., Zhu, A.X., Chen, W., Kougias, I. and Kazakis, N., 2018. Flood susceptibility assessment in Hengfeng area coupling adaptive neuro-fuzzy inference system with genetic algorithm and differential evolution. Science of the total Environment, 621, pp.1124-1141. DOI: https://doi.org/10.1016/j.scitotenv.2017.10.114.

107. Horton, R.E., 1932. Drainage-basin characteristics. Eos, transactions American geophysical union, 13(1), pp.350-361.

108. Horton, R.E., 1945. Erosional development of streams and their drainage basins; hydrophysical approach to quantitative morphology. Geological society of America bulletin, 56(3), pp.275-370.

109. Hu, X., Zhang, L., Ye, L., Lin, Y. and Qiu, R., 2017. Locating spatial variation in the association between road network and forest biomass carbon accumulation. Ecological Indicators, 73, pp.214-223. DOI: https://doi.org/10.1016/j.ecolind.2016.09.042

110. Huggett, R.J., 1988. Dissipative systems: implications for geomorphology. Earth Surface Processes and Landforms, 13(1), pp.45-49. DOI: https://doi.org/10.1002/esp.3290130107

111. Islam, A., Ghosh, S., 2021. Community-Based Riverine Flood Risk Assessment and Evaluating Its Drivers: Evidence from Rarh Plains of India. Appl. Spatial Analysis. DOI: https://doi.org/10.1007/s12061-021-09384-5

112. Iwahashi, J. and Pike, R.J., 2007. Automated classifications of topography from DEMs by an unsupervised nested-means algorithm and a three-part geometric signature. Geomorphology, 86(3-4), pp.409-440. DOI: https://doi.org/10.1016/j.geomorph.2006.09.012

113. J.C., Nanson, G.C., Price, D.M. and Pietsch, T., 2007. Aeolian–fluvial interaction and climate change: source-bordering dune development over the past~ 100 ka on Cooper Creek, central Australia. Quaternary Science Reviews, 26(3-4), pp.386-404. DOI: https://doi.org/10.1016/j.quascirev.2006.08.010

114. Jaeger, K.L., Sutfin, N.A., Tooth, S., Michaelides, K. and Singer, M., 2017. Geomorphology and sediment regimes of intermittent rivers and ephemeral streams. In Intermittent rivers and ephemeral streams. Academic Press, pp. 21-49. DOI: https://doi.org/10.1016/B978-0-12-803835-2.00002-4

115. Jain, M., Tandon, S.K., Singhvi, A.K., Mishra, S. and Bhatt, S.C., 2005. Quaternary alluvial stratigraphical development in a desert setting: a case study from the Luni River basin, Thar Desert of western India. Fluvial Sedimentology VII, International Association of Sedimentologists. Special Publication, 35, pp. 349-371.

116. Jain, V., Sonam, A.S., Singh, A., Sinha, R. and Tandon, S., 2020. Evolution of modern river systems: an assessment of 'landscape memory' in Indian river systems. Episodes Journal of International Geoscience, 43(1), pp.535-551. DOI: https://doi.org/10.18814/epiiugs/2020/020035

117. Jia, X., Wang, H. and Li, Y., 2021. Desert channel erosion, accretion characteristics and their implications for aeolian–fluvial interactions: a case study in a desert watershed in the Ordos Plateau, China. Environmental Earth Sciences, 80(10), pp.1-14. DOI: https://doi.org/10.1007/s12665-021-09656-w

118. Johnson, B.A. and Iizuka, K., 2016. Integrating OpenStreetMap crowdsourced data and Landsat time-series imagery for rapid land use/land cover (LULC) mapping: Case study of the Laguna de

Bay area of the Philippines. Applied Geography, 67, pp.140-149. DOI: https://doi.org/10.1016/j.apgeog.2015.12.006

119.   Kale, V.S., Singhvi, A.K., Mishra, P.K. and Banerjee, D., 2000. Sedimentary records and luminescence chronology of Late Holocene palaeofloods in the Luni River, Thar Desert, northwest India. Catena, 40(4), pp.337-358.

120.   Kale, V.S., Sengupta, S., Achyuthan, H. and Jaiswal, M.K., 2014. Tectonic controls upon Kaveri River drainage, cratonic Peninsular India: Inferences from longitudinal profiles, morphotectonic indices, hanging valleys and fluvial records. Geomorphology, 227, pp.153-165. DOI: https://doi.org/10.1016/j.geomorph.2013.07.027.

121.   Kar, A. and Kumar, A., 2020. Evolution of arid landscape in India and likely impact of future climate change. Episodes J. Int. Geosci., 43(1), pp.511-523. DOI: https://doi.org/10.18814/epiiugs/2020/020033

122.   Kar, A., 2018, Desertification: Causes and effects. In: D. Bartlett and R.P. Singh (eds.), Exploring Natural Hazards: A Case Study Approach. CRC Press, Taylor & Francis Group, Boca Raton, USA, pp. 159-205.

123.   Keller, E.A. and Pinter, N., 1996. Active tectonics (Vol. 338). Upper Saddle River, NJ: Prentice Hall.

124.   Keller, E.A. and Pinter, N., 2002. Active tectonics. Earthquakes, Uplift, and Landscape. Prentice Hall, New Jersey.

125.   Khan, A., Govil, H., Kumar, G. and Dave, R., 2020. Synergistic use of Sentinel-1 and Sentinel-2 for improved LULC mapping with special reference to bad land class: a case study for Yamuna River floodplain, India. Spatial Information Research, pp.1-13. DOI: https://doi.org/10.1007/s41324-020-00325-x

126.   Khan, S. and Fryirs, K., 2020. An approach for assessing geomorphic river sensitivity across a catchment based on analysis of historical capacity for adjustment. Geomorphology, 359, p.107135. DOIhttps://doi.org/10.1016/j.geomorph.2020.107135.

127.   Khan, T. and Khan, M.S., 2016. Geochemistry of the sandstones of Punagarh basin: Implications for two source terranes and Arabian-Nubian connection of Aravalli craton? Journal of the Geological Society of India, 88(3), pp.366-386.

128.   Khonde, N., Singh, S.K., Maurya, D.M., Rai, V.K., Chamyal, L.S. and Giosan, L., 2017. Tracing the vedic saraswati river in the great rann of kachchh. Scientific reports, 7(1), pp.1-6.

129.   Kirby, E., and Whipple, K.X., 2012. Expression of active tectonics in erosional landscapes. J. Struct. Geol., v.44, pp.54–75. DOI: https://doi.org/10.1016/j.jsg.2012.07.009.

130.   Knighton, A.D. and Nanson, G.C., 1997. Distinctiveness, diversity and uniqueness in arid zone river systems. Arid Zone Geomorphology: Process, Form and Change in Drylands, Thomas DSG (ed). 2nd Edition, John Wiley & Sons, pp.185-203.

131.   Knighton, D., 1998. Fluvial forms and processes: a new perspective. Routledge.

132.   Kühni, A. and Pfiffner, O.A., 2001. The relief of the Swiss Alps and adjacent areas and its relation to lithology and structure: topographic analysis from a 250-m DEM. Geomorphology, 41(4), pp.285-307. DOI: https://doi.org/10.1016/S0169-555X(01)00060-5

133.   Lal, R., 1990. Soil erosion in the tropics: principles and management. McGraw Hill.

134.   Langbein, W.B., 1947. Topographic characteristics of drainage basins.

135.   Langbein, W.B., 1949. Annual floods and the partial-duration flood series. Eos, Transactions American Geophysical Union, 30(6), pp.879-881.

136.   Langford, R.P. and Chan, M.A., 1989. Fluvial-aeolian interactions: Part II, ancient systems. Sedimentology, 36(6), pp.1037-1051. DOI:https://doi.org/10.1111/j.13653091.1989.tb01541.x

137.   Langford, R.P., 1989. Fluvial-aeolian interactions: Part I, modern systems. Sedimentology, 36(6), pp.1023-1035.DOI:https://doi.org/10.1111/j.1365-3091.1989.tb01540.x

138.   Larkin, Z.T., Ralph, T.J., Tooth, S., Fryirs, K.A. and Carthey, A.J.R., 2020. Identifying threshold responses of Australian dryland rivers to future hydroclimatic change. Scientific reports, 10(1), pp.1-15. DOI: https://doi.org/10.1038/s41598-020-63622-3.

139.   Larkin, Z.T., Ralph, T.J., Tooth, S., Fryirs, K.A. and Carthey, A.J.R., 2020. Identifying threshold responses of Australian dryland rivers to future hydroclimatic change. Scientific reports, 10(1), pp.1-15.DOI: https://doi.org/10.1038/s41598-020-63622-3

140.   Lee, C.S. and Tsai, L.L., 2009. A quantitative analysis for geomorphic indices of longitudinal river profile: a case study of the Choushui River, Central Taiwan. Environmental Earth Sciences, 59(7), pp.1549-1558. DOI: https://doi.org/10.1007/s12665-009-0140-3.

141.   Leopold, L.B., 1968. Hydrology for urban land planning: A guidebook on the hydrologic effects of urban land use (Vol. 554). US Department of the Interior, Geological Survey.

142.   Li, D., He, D., Santosh, M., Ma, D. and Tang, J., 2015. Tectonic framework of the northern Junggar Basin part I: The eastern Luliang Uplift and its link with the East Junggar terrane. Gondwana Research, 27(3), pp.1089-1109.

143.   Li, X., Yan, P. and Liu, B., 2020. Geomorphological classification of aeolian-fluvial interactions in the desert region of north China. Journal of Arid Environments, 172, p.104021. DOI: https://doi.org/10.1016/j.jaridenv.2019.104021

144.   Li, X., Yan, P., Cao, L. and Liu, B., 2021. Distinct Aeolian-fluvial Interbedded Landscapes in Three Watersheds of the Northern China. Chinese Geographical Science, pp.1-12. DOI: https://doi.org/10.1007/s11769-021-1211-y

145.   Lisenby, P.E., Fryirs, K.A. and Thompson, C.J., 2020. River sensitivity and sediment connectivity as tools for assessing future geomorphic channel behavior. International Journal of River Basin Management, 18(3), pp.279-293. DOI: https://doi.org/10.1080/15715124.2019.1672705.

146. Liu, B. and Coulthard, T.J., 2015. Mapping the interactions between rivers and sand dunes: implications for fluvial and aeolian geomorphology. Geomorphology, 231, pp.246-257. DOI: https://doi.org/10.1016/j.geomorph.2014.12.011

147. Liu, B. and Coulthard, T.J., 2017. Modelling the interaction of aeolian and fluvial processes with a combined cellular model of sand dunes and river systems. Computers & Geosciences, 106, pp.1-9. DOI: https://doi.org/10.1016/j.cageo.2017.05.003

148. Liu, P., Zhu, B. and Wang, P., 2021. A weighting model based on best–worst method and its application for environmental performance evaluation. Appl. Soft Comput., 103: 107168. DOI: https://doi.org/10.1016/j.asoc.2021.107168

149. Malczewski, J., 1999. GIS and multicriteria decision analysis. John Wiley & Sons.

150. Marçal, M., Brierley, G. and Lima, R., 2017. Using geomorphic understanding of catchment-scale process relationships to support the management of river futures: Macaé Basin, Brazil. Applied Geography, 84, pp.23-41. DOI: https://doi.org/10.1016/j.apgeog.2017.04.008.

151. Maroulis, J.C., Nanson, G.C., Price, D.M. and Pietsch, T., 2007. Aeolian–fluvial interaction and climate change: source-bordering dune development over the past~ 100 ka on Cooper Creek, central Australia. Quaternary Science Reviews, 26(3-4), pp.386-404. DOI: https://doi.org/10.1016/j.quascirev.2006.08.010

152. Maune, D. F., 2001. Digital Elevation Model Technologies and Applications: The DEM User's Manual (Bethesda, MD: American Society for Photogrammetry and Remote Sensing).

153. McKenney, M.S. and Rosenberg, N.J., 1993. Sensitivity of some potential evapotranspiration estimation methods to climate change. Agricultural and Forest Meteorology, 64(1-2), pp.81-110. DOI: https://doi.org/10.1016/0168-1923(93)90095-Y.

154. Melton, M.A., 1957. An analysis of the relations among elements of climate, surface properties, and geomorphology. Columbia Univ New York.

155. Menier, D., Mathew, M., Pubellier, M., Sapin, F., Delcaillau, B., Siddiqui, N., Ramkumar, M. and Santosh, M., 2017. Landscape response to progressive tectonic and climatic forcing in NW Borneo: Implications for geological and geomorphic controls on flood hazard. Scientific reports, 7(1), pp.1-18. DOI: https://doi.org/10.1038/s41598-017-00620-y

156. Miller, V.C., 1953. A Quantitative Geomorphic Study of Drainage Basin Characteristics in the Clinch Mountain Area Virginia and Tennessee. Columbia University New York.

157. Mishra, M., Dugesar, V., Prudhviraju, K.N., Patel, S.B. and Mohan, K., 2019. Precision mapping of boundaries of flood plain river basins using high-resolution satellite imagery: A case study of the Varuna river basin in Uttar Pradesh, India. Journal of Earth System Science, 128(4). DOI: https://doi.org/10.1007/s12040-019-1146-1.

158. Mo, K., Chen, Q., Chen, C., Zhang, J., Wang, L. and Bao, Z., 2019. Spatiotemporal variation of correlation between vegetation cover and precipitation in an arid mountain-oasis river basin in northwest China. Journal of Hydrology, 574, pp.138-147. DOI:

https://doi.org/10.1016/j.jhydrol.2019.04.044

159. Modrick, T.M. and Georgakakos, K.P., 2015. The character and causes of flash flood occurrence changes in mountainous small basins of Southern California under projected climatic change. Journal of Hydrology: Regional Studies, 3, pp.312-336. DOI: https://doi.org/10.1016/j.ejrh.2015.02.003

160. Montgomery, D., and Brandon, M., 2002. Topographic controls on erosion rates in tectonically active mountain ranges. Earth Planet. Sci. Lett., v.201, pp.481–489. DOI: https://doi.org/10.1016/S0012-821X(02)00725-2.

161. Moore, I. D., Grayson, R. B., & Ladson, A. R. (1991). Digital terrain modelling: a review of hydrological, geomorphological, and biological applications. Hydrological processes, 5(1), 3-30.

162. Moore, I.D. and Burch, G.J., 1986. Physical basis of the length-slope factor in the universal soil loss equation. Soil Science Society of America Journal, 50(5), pp.1294-1298.

163. Moore, I.D., Grayson, R.B. and Ladson, A.R., 1991. Digital terrain modelling: a review of hydrological, geomorphological, and biological applications. Hydrological processes, 5(1), pp.3-30.

164. Mouratidis, A. and Kehagia, F., 2014. On the Track of Road Evolution. Journal of Infrastructure Development, 6(1), pp.1-15.

165. Muralitharan, J. and Palanivel, K., 2015. Groundwater targeting using remote sensing, geographical information system and analytical hierarchy process method in hard rock aquifer system, Karur district, Tamil Nadu, India. Earth Science Informatics, 8(4), pp.827-842. DOI: https://doi.org/10.1007/s12145-015-0213-7

166. Murmu, P., Kumar, M., Lal, D., Sonker, I. and Singh, S.K., 2019. Delineation of groundwater potential zones using geospatial techniques and analytical hierarchy process in Dumka district, Jharkhand, India. Groundwater for Sustainable Development, 9, p.100239. DOI: https://doi.org/10.1016/j.gsd.2019.100239

167. Murphy, B.W., Murphy, C., Wilson, B.R., Emery, K.A., Lawrie, J., Bowman, G., Lawrie, R. and Erskine, W., 2004, July. A revised land and soil capability classification for New South Wales. In The 13th International Soil Conservation Organization Conference, Brisbane.

168. Nardi, F., Biscarini, C., Di Francesco, S., Manciola, P. and Ubertini, L., 2013. Comparing a large-scale DEM-based floodplain delineation algorithm with standard flood maps: The Tiber River Basin case study. Irrigation and Drainage, 62(S2), pp.11-19. DOI: https://doi.org/10.1002/ird.1818.

169. Nexer, M., Authemayou, C., Schildgen, T., Hantoro, W.S., Delcaillau, S.B., Pedoja, K., Husson, L., and Regard, V. (2015) Evaluation of morphometric proxies for uplift on sequence of coral reef terraces: A case study from Samba Island (Indonesia). Geomorphology, v.241, pp.145-159. DOI:https://doi.org/10.1016/j.geomorph.2015.03.036.

170. Nir, D., 1957. The ratio of relative and absolute altitudes of Mt. Carmel: a contribution to the problem of relief analysis and relief classification. Geographical Review, 47(4), pp.564-569.

171. Nozaki, K., 2006. The generalized Bouguer anomaly. Earth, planets and space, 58(3), pp.287-303.

172. Ohnishi, S.I., Saito, T., Yamanoi, T. and Imai, H., 2011, September. A weights representation for absolute measurement AHP using fuzzy sets theory. In 2011 5th International Symposium on Computational Intelligence and Intelligent Informatics (ISCIII), pp. 67-70. IEEE. DOI: https://doi.org/10.1109/ISCIII.2011.6069744

173. O'Loughlin, E. M., 1986. Prediction of surface saturation zones in natural catchments by topographic analysis. Water Resources Research, 22(5), 794-804.

174. Pal, G.N., 1991. Quaternary landscape and morphostratigraphy in the lower reaches of the Luni basin. In: Proceedings of Quaternary landscape of Indian Subcontinent, Desai N, Ganpathi S and Patel R K (eds), pp 79–90. Vadodra, Geology Department, M.S. University, Baroda.

175. Pani, P. and Carling, P., 2020. A Water Balance Analysis to Support Sustainable River Basin Management in Desert River Luni, India: Report of Research Exchange June 2019. The India-UK Water Centre; UK Centre for Ecology and Hydrology, Wallingford and IITM Pune. https://iukwc.org/sites/default/files/images/Pani%20RE%20Report.pdf.

176. Panwar, V. and Sen, S., 2020. Examining the economic impact of floods in selected Indian states. Climate and Development, 12(3), pp.281-296. DOI: https://doi.org/10.1080/17565529.2019.1614897

177. Parker, B.M., Sheldon, F., Phinn, S. and Ward, D., 2018. Changes in foliage projective cover and its implications for mapping groundwater dependent vegetation across a precipitation gradient. Ecohydrology, 11(4), p.e1937. DOI: https://doi.org/10.1002/eco.1937

178. Parson, A.J., Bracken, L., Poeppl, R.E., Wainwright, J., Keesstra, S.D., 2015. Introduction to special issue on connectivity in water and sediment dynamics. Earth Surf Process Landforms. 40(9):1275–127. DOI: https://doi.org/10.1002/esp.3714

179. Parsons, A.J. and Abrahams, A.D., 2009. Geomorphology of desert environments. In Geomorphology of desert environments. Springer, Dordrecht.

180. Patel, P.P. and Sarkar, A., 2010. Terrain characterization using SRTM data. Journal of the Indian Society of Remote Sensing, 38(1), pp.11-24. DOI: https://doi.org/10.1007/s12524-010-0008-8

181. Patel, P.P., 2013. GIS Techniques for Landscape Analysis - Case Study of the Chel River Basin, West Bengal. Proceedings of State Level Seminar on Geographical Methods in the Appraisal of Landscape, Dept. of Geography, Dum Dum Motijheel Mahavidyalaya, Kolkata, 20th March, 2012, pp 1-14.

182. Patel, P.P., and Sarkar, A., 2009. Application of SRTM Data in Evaluating the Morphometric Attributes: A Case Study of The Dulung River Basin" in Practicing Geographer, Vol. 13 (2), pp. 249-265.

183. Pekel, J.F., Cottam, A., Gorelick, N. and Belward, A.S., 2016. High-resolution mapping of global surface water and its long-term changes. Nature, 540(7633), pp.418-422. DOI: https://doi.org/10.1038/nature20584

184. Pham, B.T., Avand, M., Janizadeh, S., Phong, T.V., Al-Ansari, N., Ho, L.S., Das, S., Le, H.V., Amini, A., Bozchaloei, S.K. and Jafari, F., 2020. GIS based hybrid computational approaches for flash flood susceptibility assessment. Water, 12(3), p.683. DOI: https://doi.org/10.3390/w12030683

185. Pike, R.J. and Wilson, S.E., 1971. Elevation-relief ratio, hypsometric integral, and geomorphic area-altitude analysis. Geological Society of America Bulletin, 82(4), pp.1079-1084.

186. Pratama, G. and Kusratmoko, E., 2018, April. Flashiness Index of Several Rivers in the Citarum Basin, West Java. In IOP Conference Series: Earth and Environmental Science (Vol. 145, No. 1, p. 012107). IOP Publishing.

187. Priddy, C.L. and Clarke, S.M., 2020. The sedimentology of an ephemeral fluvial–aeolian succession. Sedimentology, 67(5), pp.2392-2425. DOI: https://doi.org/10.1111/sed.12706

188. Rahmati, O., Haghizadeh, A. and Stefanidis, S., 2016. Assessing the accuracy of GIS-based analytical hierarchy process for watershed prioritization; Gorganrood River Basin, Iran. Water resources management, 30(3), pp.1131-1150. DOI: https://doi.org/10.1007/s11269-015-1215-4

189. Ramasamy, S.M., Bakliwal, P.C. and Verma, R.P., 1991. Remote sensing and river migration in Western India. Remote Sensing, 12(12), pp.2597-2609. DOI: https://doi.org/10.1080/01431169108955288.

190. Reid, H.E. and Brierley, G.J., 2015. Assessing geomorphic sensitivity in relation to river capacity for adjustment. Geomorphology, 251, pp.108-121. DOI:https://doi.org/10.1016/j.geomorph.2015.09.009.

191. Reid, I. and Frostick, L.E., 1997. Channel form, flows and sediments in deserts. In Arid Zone Geomorphology, ed. D.S.G. Thomas. Chichester: Wiley, pp. 205–29.

192. Renard, K.G., Foster, G.R., Weesies, G.A., McCool, D.K. and Yoder, D.C., 1997. Predicting soil erosion by water: a guide to conservation planning with the Revised Universal Soil Loss Equation (RUSLE) (Vol. 703). Washington, DC: United States Department of Agriculture.

193. Rhoads, B.L., 1988. Mutual adjustments between process and form in a desert mountain fluvial system. Annals of the Association of American Geographers, 78(2), pp.271-287.

194. Riley, S.J., DeGloria, S.D. and Elliot, R., 1999. Index that quantifies topographic heterogeneity. intermountain Journal of sciences, 5(1-4), pp.23-27.

195. Roy, A.B. and Chatterjee, A., 2015. Tectonic framework and evolutionary history of the Bengal Basin in the Indian subcontinent. Current Science, pp.271-279.

196. Roy, A.B. and Jakhar, S.R., 2001. Late Quaternary drainage disorganisation and migration and extinction of the Vedic Saraswati; Current Science, 81 1188–1195.

197. Roy, D.B., Tandon, S.K. and Singh, V., 2021. Drainage evolution in a Holocene landscape that hosted a 'lost river' system in the Punjab-Haryana plains, NW India. Quaternary International, 585, pp.99-110. DOI: https://doi.org/10.1016/j.quaint.2021.01.029

198. Roy, S. and Sahu, A.S., 2015. Quaternary tectonic control on channel morphology over sedimentary low land: a case study in the Ajay-Damodar interfluve of Eastern India. Geoscience Frontiers, 6(6), pp.927-946. DOI: https://doi.org/10.1016/j.gsf.2015.04.001.

199. Roy, S. and Sahu, A.S., 2017. Potential interaction between transport and stream networks over the lowland rivers in Eastern India. Journal of environmental management, 197, pp.316-330. https://doi.org/10.1016/j.jenvman.2017.04.012

200. Roy, S. and Sahu, A.S., 2018. Road-stream crossing an in-stream intervention to alter channel morphology of headwater streams: case study. International Journal of River Basin Management, 16(1), pp.1-19. DOI: https://doi.org/10.1080/15715124.2017.1365721

201. Roy, S., 2021. Impact of linear transport infrastructure on fluvial connectivity across the catchments of West Bengal, India. Geocarto International, pp.1-26. DOI: https://doi.org/10.1080/10106049.2021.1903576

202. Saaty, T. L., 1986. Absolute and relative measurement with the AHP. The most livable cities in the United States. Socio-Economic Planning Sciences, 20(6), pp. 327-331. DOI: https://doi.org/10.1016/0038-0121(86)90043-1

203. Saaty, T. L., 1999. Fundamentals of the analytic network process. Proceedings of the ISAHP 1999, pp. 1–14.

204. Saaty, T. L., and Takizawa, M., 1986. Dependence and independence: From linear hierarchies to nonlinear networks. European journal of operational research, 26(2), pp. 229-237. DOI: https://doi.org/10.1016/0377-2217(86)90184-0

205. Saaty, T.L., 1990. An exposition of the AHP in reply to the paper "remarks on the analytic hierarchy process". Management science, 36(3), pp.259-268.

206. Saaty, T.L., 2004. Decision making—the analytic hierarchy and network processes (AHP/ANP). Journal of systems science and systems engineering, 13(1), pp.1-35. DOI: https://doi.org/10.1007/s11518-006-0151-5

207. Saaty, T.L., 2005. Making and validating complex decisions with the AHP/ANP. Journal of Systems Science and Systems Engineering, 14(1), pp.1-36.

208. Saaty, T.L., and Vargas, L.G., 1991. Prediction, Projection and Forecasting: Applications of the Analytic Hierarchy Process in Economics, Finance. Politics, Games and Sports, //Kluwer Academic.

209. Sahana, M., Hong, H., Ahmed, R., Patel, P.P., Bhakat, P. and Sajjad, H., 2019. Assessing coastal island vulnerability in the Sundarban Biosphere Reserve, India, using geospatial technology. Environmental Earth Sciences, 78(10), pp.1-22. DOI: https://doi.org/10.1007/s12665-019-8293-1

210. Saini, H.S., Alok, A. and Pant, N.C., 2020. The lost Saraswati River of Northwestern Indian plains: Status and way forward. Episodes, 43(1), pp.524-534.DOI:https://doi.org/10.18814/epiiugs/2020/020034

211. Sandercock, P.J., Hooke, J.M. and Mant, J.M., 2007. Vegetation in dryland river channels and its interaction with fluvial processes. Progress in Physical Geography, 31(2), pp.107-129. DOI: https://doi.org/10.1177/0309133307076106.

212. Saxena, B.K. and Rao, K.V.S., 2016. Estimation of wind power density at a wind farm site located in Western Rajasthan region of India. Procedia Technology, 24, pp.492-498. DOI: https://doi.org/10.1016/j.protcy.2016.05.084.

213. Schumm, S.A., 1956. Evolution of drainage systems and slopes in badlands at Perth Amboy, New Jersey. Geological society of America bulletin, 67(5), pp.597-646.

214. Seeber, L. and Gornitz, V., 1983. River profiles along the Himalayan arc as indicators of active tectonics. Tectonophysics, 92(4), pp.335-367.

215. Sharma, K.D. and Vangani, N.S., 1982. Flash flood of July 1979 in the Luni basin—a rare event in the Indian desert. Hydrological Sciences Journal, 27(3), pp.385-397. DOI: https://doi.org/10.1080/02626668209491117

216. Sharma, K.D., Vangani, N.S. and Choudhari, J.S., 1984. Sediment transport characteristics of the desert streams in India. Journal of Hydrology., 67, pp. 261–272. DOI: https://doi.org/10.1016/0022-1694(84)90245-2

217. Sharma, K.D., Vangani, N.S., Chatterji, P.C. and Singh, G., 1982. A severe flood in Luni Basin, western Rajasthan during July 1979–A case study. Mausum, 33, pp. 377-384.

218. Singh, A., 1989. Review article digital change detection techniques using remotely-sensed data. International journal of remote sensing, 10(6), pp.989-1003. DOI: https://doi.org/10.1080/01431168908903939

219. Singh, M., Sinha, R. and Tandon, S.K., 2021. Geomorphic connectivity and its application for understanding landscape complexities: a focus on the hydro-geomorphic systems of India. Earth Surface Processes and Landforms, 46(1), pp.110-130. DOI: https://doi.org/10.1002/esp.4945

220. Smith, G. H., 1935. The relative relief of Ohio. Geographical review, 25(2), 272-284.

221. Smith, K.G., 1950. Standards for grading texture of erosional topography. American journal of Science, 248(9), pp.655-668.

222. Sonam and Jain, V., 2018. Geomorphic effectiveness of a long profile shape and the role of inherent geological controls in the Himalayan hinterland area of the Ganga River basin, India. Geomorphology, *304*, pp.15-29. DOI: https://doi.org/10.1016/j.geomorph.2017.12.022.

223. Steinhausen, M.J., Wagner, P.D., Narasimhan, B. and Waske, B., 2018. Combining Sentinel-1 and Sentinel-2 data for improved land use and land cover mapping of monsoon regions. International journal of applied earth observation and geoinformation, 73, pp.595-604. DOI: https://doi.org/10.1016/j.jag.2018.08.011

224. Stevens, F.R., Gaughan, A.E., Linard, C. and Tatem, A.J., 2015. Disaggregating census data for population mapping using random forests with remotely-sensed and ancillary data. PloS one, 10(2), p.e.0107042. DOI: https://doi.org/10.1371/journal.pone.0107042

225. Stoddart, D.R., 1965. The shape of atolls. Marine Geology, 3(5), pp.369-383. DOI: https://doi.org/10.1016/0025-3227(65)90025-3.

226. Strahler, A., 1953. Hypsometric analysis of erosional topography. Bull. Geol. Soc. Am, 63, pp.923-938.

227. Strahler, A.N., 1956. Quantitative slope analysis. Geological Society of America Bulletin, 67(5), pp.571-596.

228. Sukristiyanti, S., Maria, R. and Lestiana, H., 2018, February. Watershed-based morphometric analysis: a review. In IOP conference series: earth and environmental science (Vol. 118, No. 1, p. 012028). IOP Publishing. DOI: https://doi.org/10.1088/1755-1315/118/1/012028.

229. Taloor, A.K., Joshi, L.M., Kotlia, B.S., Alam, A., Kothyari, G.C., Kandregula, R.S., Singh, A.K. and Dumka, R.K., 2021. Tectonic imprints of landscape evolution in the Bhilangana and Mandakini basin, Garhwal Himalaya, India: a geospatial approach. Quaternary International, 575, pp.21-36. DOI: https://doi.org/10.1016/j.quaint.2020.07.021

230. Taloor, A.K., Ray, P.K.C., Jasrotia, A.S., Kotlia, B.S., Alam, A., Kumar, S.G., Kumar, R., Kumar, V. and Roy, S., 2017. Active tectonic deformation along reactivated faults in Binta basin in Kumaun Himalaya of north India: inferences from tectono-geomorphic evaluation. Zeitschriftfür Geomorphologie, 61(2), pp.159-180. DOI: https://doi.org/10.1127/zfg/2017/0417

231. Tarolli, P. and Sofia, G., 2016. Human topographic signatures and derived geomorphic processes across landscapes. Geomorphology, 255, pp.140-161. DOI: https://doi.org/10.1016/j.geomorph.2015.12.007

232. Thomas, D. S. G., and R. J. Allison, eds. 1993. Landscape Sensitivity. Chichester: John Wiley & Sons.

233. Thomas, D.S. ed., 2011. Arid zone geomorphology: process, form and change in drylands. John Wiley & Sons.

234. Thomas, D.S.G. and Allison, R.J., 1993. The sensitivity of landscapes. Landscape Sensitivity. John Wiley, Chichester, pp.1-12.

235. Thomas, M.F., 2001. Landscape sensitivity in time and space—an introduction. Catena, 42(2-4), pp.83-98.DOI: https://doi.org/10.1016/S0341-8162(00)00133-8.

236. Thornbury, W.D., 1954. Principles of geomorphology (Vol. 78, No. 2, p. 157). LWW.

237. Thornes, J.B., 1980. Erosional processes of running water and their spatial and temporal controls: a theoretical viewpoint. Soil erosion, pp.129-182.

238. Tooth, S. and Nanson, G.C., 2011. Distinctiveness and diversity of arid zone rivers. In Arid Zone Geomorphology: Process, Form and Change in Drylands (pp. 269-300). Wiley. ISBN (Print): 978-0-470-97569-5

239. Tooth, S., 2000. Downstream changes in dryland river channels: The Northern Plains of arid central Australia. Geomorphology, 34(1-2), pp.33-54. DOI: https://doi.org/10.1016/S0169-555X(99)00130-0

240. Tooth, S., 2018. The geomorphology of wetlands in drylands: Resilience, nonresilience, or…?. Geomorphology, 305, pp. 33-48. DOI: https://doi.org/10.1016/j.geomorph.2017.10.017

241. Tooth, S., Miller, A.J. and Gupta, A., 1999. Floodouts in central Australia. Varieties of fluvial form, pp.219-247.

242. UNEP (United Nations Environment Programme), 1997. World atlas of desertification 2ED. UNEP, London.

243. Veiga, G.D., Spalletti, L.A. and Flint, S., 2002. Aeolian/fluvial interactions and high-resolution sequence stratigraphy of a non-marine lowstand wedge: the Avilé Member of the Agrio Formation (Lower Cretaceous), central Neuquén Basin, Argentina. Sedimentology, 49(5), pp.1001-1019. DOI:https://doi.org/10.1046/j.13653091.2002.00487.x

244. Vijith, H., Prasannakumar, V., Sharath Mohan, M.A., Ninu Krishnan, M.V. and Pratheesh, P., 2017. River and basin morphometric indexes to detect tectonic activity: a case study of selected river basins in the South Indian Granulite Terrain (SIGT). Physical Geography, 38(4), pp.360-378. DOI:https://doi.org/10.1080/02723646.2017.1283478

245. Vittala, S.S., Govindaiah, S. and Gowda, H.H., 2004. Morphometric analysis of sub-watersheds in the Pavagada area of Tumkur district, South India using remote sensing and GIS techniques. Journal of the Indian Society of Remote Sensing, 32(4), pp.351-362. DOI: https://doi.org/10.1007/BF03030860.

246. Vittala, S.S., Govindaiah, S. and Gowda, H.H., 2008. Prioritization of sub-watersheds for sustainable development and management of natural resources: An integrated approach using remote sensing, GIS and socio-economic data. Current Science, pp.345-354.

247. Wang, C., Liu, S., Deng, L., Liu, Q. and Yang, J., 2014. Road lateral disconnection and crossing impacts in river landscape of Lancang River Valley in Yunnan Province, China. Chinese geographical science, 24(1), pp.28-38. DOI: https://doi.org/10.1007/s11769-014-0653-x

248. Wells, M., 2001. An Assessment of Soil Capability for On-Site Effluent Disposal East Carnarvon, Western Australia. Resource Management Technical Report No.79.

249. Werritty, A. and Leys, K.F., 2001. The sensitivity of Scottish rivers and upland valley floors to recent environmental change. Catena, 42(2-4), pp.251-273. DOI: https://doi.org/10.1016/S0341-8162(00)00140-5.

250. Wheater, H.S., Sorooshian, S. and Sharma, K., 2008. Modelling hydrological processes in arid and semi-arid areas: an introduction to the workshop. Hydrological Modelling in Arid and Semi-Arid Areas, Cambridge University Press, Cambridge, U.K.

251. Wohl, E., 2016. Spatial heterogeneity as a component of river geomorphic complexity. Progress in Physical Geography, 40(4), pp.598-615. DOI: https://doi.org/10.1177/0309133316658615.

252. Wohl, E., 2017. Connectivity in rivers. Progress in Physical Geography, 41(3), pp.345-362. DOI: https://doi.org/10.1177/0309133317714972

253. Wohl, E., 2018. Geomorphic context in rivers. Progress in Physical Geography: Earth and Environment, 42(6), pp.841-857. DOI: https://doi.org/10.1177/0309133318776488.

254. World Bank, 2017. Major River Basins of the World. Data Catalog.

255. Yizhaq, H., Ashkenazy, Y. and Tsoar, H., 2009. Sand dune dynamics and climate change: A modeling approach. Journal of Geophysical Research: Earth Surface, 114(F1). DOI: https://doi.org/10.1029/2008JF001138.

256. Yokoyama, R., Shirasawa, M. and Pike, R.J., 2002. Visualizing topography by openness: a new application of image processing to digital elevation models. Photogrammetric engineering and remote sensing, 68(3), pp.257-266.

257. Zhan, S., Song, C., Wang, J., Sheng, Y. and Quan, J., 2019. A global assessment of terrestrial evapotranspiration increase due to surface water area change. Earth's future, 7(3), pp. 266-282. DOI: https://doi.org/10.1029/2018EF001066

258. Zhang, G., Jia, Q., Wang, W., Wang, P., Zhao, Q., Sun, X., Xie, X., Zhao, Z. and Tang, W., 2018. On tectonic framework and evolution of the South China Sea. Chinese Journal of Geophysics, 61(10), pp.4194-4215.DOI: https://doi.org/10.6038/cjg2018L0698

259. Zhang, H., Shao, Z., Hua, B., Huang, X., Zhao, J., Wu, W. and Fan, Y., 2021. Evaluating the weight sensitivity in AHP-based flood risk estimation models. arXiv preprint arXiv:2107.13368.

260. Zhang, Y.-G., Nearing, M.A., Liu, B.Y., Van Pelt, R.S., Stone, J.J., Wei, H. and Scott, R.L., 2011. Comparative rates of wind versus water erosion from a small semiarid watershed in southern Arizona, USA. Aeolian Research, 3, pp. 197–204. DOI: https://doi.org/10.1016/j.aeolia.2011.03.006

261. Zimmer, M.A., Kaiser, K.E., Blaszczak, J.R., Zipper, S.C., Hammond, J.C., Fritz, K.M., Costigan, K.H., Hosen, J., Godsey, S.E., Allen, G.H. and Kampf, S., 2020. Zero or not? Causes and consequences of zero-flow stream gage readings. Wiley Interdisciplinary Reviews: Water, 7(3), p.e1436. DOI: https://doi.org/10.1002/wat2.1436

APPENDIX

Table A: Hypsometric analysis of Luni river basin and its major seven sub-basins.

Luni River Basin		Lilri R SB 1		Mithri or Jojri R SB 2		Jojari R SB 3		Guhiya N SB 4		Sukri N SB 5		Kher Nawala N SB 6		Sukri R SB 7	
X	Y	X	Y	X	Y	X	Y	X	Y	X	Y	X	Y	X	Y
1.00	0.00	1.00	0.00	1.00	0.00	1.00	0.00	1.00	0.00	1.00	0.00	1.00	0.00	1.00	0.00
0.91	0.04	0.97	0.04	0.99	0.05	0.98	0.02	0.93	0.04	1.00	0.01	0.83	0.03	0.95	0.02
0.74	0.09	0.88	0.08	0.95	0.10	0.91	0.08	0.75	0.09	0.79	0.06	0.46	0.08	0.73	0.07
0.50	0.13	0.81	0.13	0.86	0.15	0.81	0.13	0.59	0.13	0.46	0.10	0.27	0.13	0.45	0.12
0.29	0.18	0.74	0.17	0.74	0.20	0.70	0.18	0.39	0.18	0.27	0.15	0.18	0.18	0.22	0.16
0.17	0.23	0.66	0.22	0.61	0.26	0.56	0.24	0.28	0.22	0.15	0.20	0.08	0.23	0.10	0.21
0.11	0.27	0.54	0.26	0.50	0.31	0.45	0.29	0.23	0.27	0.09	0.24	0.05	0.28	0.06	0.26
0.05	0.32	0.44	0.30	0.39	0.36	0.35	0.35	0.20	0.31	0.08	0.29	0.04	0.33	0.03	0.30
0.04	0.36	0.33	0.35	0.28	0.42	0.27	0.40	0.17	0.36	0.07	0.34	0.03	0.38	0.02	0.35
0.03	0.41	0.21	0.39	0.21	0.47	0.21	0.46	0.15	0.41	0.06	0.39	0.03	0.44	0.01	0.40
0.02	0.45	0.11	0.43	0.13	0.52	0.18	0.51	0.12	0.45	0.06	0.43	0.02	0.49	0.01	0.44
0.02	0.50	0.06	0.48	0.04	0.58	0.13	0.57	0.08	0.50	0.05	0.48	0.02	0.54	0.01	0.49
0.01	0.54	0.03	0.52	0.00	0.63	0.08	0.62	0.05	0.54	0.04	0.53	0.01	0.59	0.00	0.54
0.00	0.59	0.01	0.56	0.00	0.68	0.03	0.67	0.02	0.59	0.04	0.58	0.01	0.64	0.00	0.58
0.00	0.64	0.01	0.61	0.00	0.73	0.01	0.73	0.01	0.63	0.03	0.62	0.01	0.69	0.00	0.63
0.00	0.68	0.00	0.65	0.00	0.79	0.00	0.78	0.01	0.68	0.02	0.67	0.00	0.74	0.00	0.67
0.00	0.73	0.00	0.69	0.00	0.84	0.00	0.84	0.00	0.73	0.01	0.72	0.00	0.79	0.00	0.72
0.00	0.77	0.00	0.74	0.00	0.89	0.00	0.89	0.00	0.77	0.01	0.76	0.00	0.85	0.00	0.77
0.00	0.82	0.00	0.78	0.00	1.00	0.00	1.00	0.00	0.82	0.01	0.81	0.00	0.90	0.00	0.81
0.00	0.86	0.00	0.83					0.00	0.86	0.00	0.86	0.00	1.00	0.00	0.86
0.00	0.91	0.00	0.87					0.00	0.91	0.00	0.91			0.00	0.91
0.00	1.00	0.00	0.91					0.00	1.00	0.00	1.00			0.00	1.00
		0.00	1.00												

SB: Sub-Basin, R: River, N: Nadi. Source: Computed by the researcher.

Table B: Long Profile and associated SL Index parameters for Luni river basin

D (m)	E (m)	SD (km)	CD (km)	StdD	StdE	Fall (h1-h2)	ln D	ln D2 - ln D1	SLGI (h1-h2)/(ln D2 - lnD1)	Avg. SLGI	SLGI Change	SLGI Change Rate %	Avg. SLGI Change Rate %	SS
0	452	0	0	0.00	1.00	x	-6.91	x	0.00	153.78	0	x		x
10000	417	10	10	0.02	0.92	35	2.30	9.21	3.80		0	x		3.50
20000	396	10	20	0.04	0.87	21	3.00	0.69	30.30		26.50	14.89	2.02	2.10
30000	374	10	30	0.06	0.83	22	3.40	0.41	54.26		23.96	13.47		2.20
40000	361	10	40	0.08	0.80	13	3.69	0.29	45.19		-9.07	-5.10		1.30
50000	343	10	50	0.10	0.76	18	3.91	0.22	80.67		35.48	19.94		1.80
60000	327	10	60	0.12	0.72	16	4.09	0.18	87.76		7.09	3.99		1.60
70000	314	10	70	0.14	0.69	13	4.25	0.15	84.33		-3.42	-1.92		1.30
80000	298	10	80	0.16	0.65	16	4.38	0.13	119.82		35.49	19.95		1.60
90000	288	10	90	0.18	0.63	10	4.50	0.12	84.90		-34.92	-19.63		1.00
100000	280	10	100	0.20	0.61	8	4.61	0.11	75.93		-8.97	-5.04		0.80
110000	274	10	110	0.22	0.60	6	4.70	0.10	62.95		-12.98	-7.29		0.60
120000	260	10	120	0.24	0.57	14	4.79	0.09	160.90		97.95	55.05		1.40
130000	249	10	130	0.26	0.54	11	4.87	0.08	137.43		-23.47	-13.19		1.10
140000	237	10	140	0.28	0.52	12	4.94	0.07	161.93		24.50	13.77		1.20
150000	226	10	150	0.30	0.49	11	5.01	0.07	159.44		-2.49	-1.40		1.10
160000	215	10	160	0.32	0.47	11	5.08	0.06	170.44		11.00	6.18		1.10
170000	204	10	170	0.34	0.44	11	5.14	0.06	181.44		11.00	6.18		1.10
180000	195	10	180	0.36	0.42	9	5.19	0.06	157.46		-23.99	-13.48		0.90
190000	187	10	190	0.38	0.41	8	5.25	0.05	147.96		-9.49	-5.34		0.80
200000	177	10	200	0.39	0.38	10	5.30	0.05	194.96		46.99	26.41		1.00
210000	168	10	210	0.41	0.36	9	5.35	0.05	184.46		-10.49	-5.90		0.90
220000	160	10	220	0.43	0.35	8	5.39	0.05	171.97		-12.49	-7.02		0.80
230000	151	10	230	0.45	0.33	9	5.44	0.04	202.47		30.50	17.14		0.90

240000	141	10	240	0.47	0.30	10	5.48	0.04	234.96	32.50	18.26	1.00
250000	134	10	250	0.49	0.29	7	5.52	0.04	171.48	-63.49	-35.68	0.70
260000	125	10	260	0.51	0.27	9	5.56	0.04	229.47	57.99	32.59	0.90
270000	120	10	270	0.53	0.26	5	5.60	0.04	132.48	-96.99	-54.51	0.50
280000	114	10	280	0.55	0.24	6	5.63	0.04	164.98	32.50	18.26	0.60
290000	105	10	290	0.57	0.22	9	5.67	0.04	256.47	91.49	51.42	0.90
300000	101	10	300	0.59	0.21	4	5.70	0.03	117.99	-138.48	-77.83	0.40
310000	96	10	310	0.61	0.20	5	5.74	0.03	152.49	34.50	19.39	0.50
320000	92	10	320	0.63	0.19	4	5.77	0.03	125.99	-26.50	-14.89	0.40
330000	92	10	330	0.65	0.19	0	5.80	0.03	0.00	-125.99	-70.81	0.00
340000	85	10	340	0.67	0.18	7	5.83	0.03	234.48	234.48	131.78	0.70
350000	72	10	350	0.69	0.15	13	5.86	0.03	448.47	213.99	120.26	1.30
360000	65	10	360	0.71	0.13	7	5.89	0.03	248.48	-199.99	-112.40	0.70
370000	61	10	370	0.73	0.12	4	5.91	0.03	145.99	-102.49	-57.60	0.40
380000	55	10	380	0.75	0.11	6	5.94	0.03	224.99	79.00	44.40	0.60
390000	49	10	390	0.77	0.10	6	5.97	0.03	230.99	6.00	3.37	0.60
400000	46	10	400	0.79	0.09	3	5.99	0.03	118.49	-112.49	-63.22	0.30
410000	43	10	410	0.81	0.08	3	6.02	0.02	121.49	3.00	1.69	0.30
420000	37	10	420	0.83	0.07	6	6.04	0.02	248.99	127.49	71.65	0.60
430000	33	10	430	0.85	0.06	4	6.06	0.02	169.99	-79.00	-44.40	0.40
440000	33	10	440	0.87	0.06	0	6.09	0.02	0.00	-169.99	-95.54	0.00
450000	26	10	450	0.89	0.04	7	6.11	0.02	311.49	311.49	175.06	0.70
460000	22	10	460	0.91	0.04	4	6.13	0.02	181.99	-129.49	-72.78	0.40
470000	19	10	470	0.93	0.03	3	6.15	0.02	139.49	-42.50	-23.88	0.30
480000	16	10	480	0.95	0.02	3	6.17	0.02	142.49	3.00	1.69	0.30
490000	12	10	490	0.97	0.01	4	6.19	0.02	193.99	51.50	28.94	0.40
500000	12	16.59	507	1.00	0.00	6	6.23	0.03	180.21	-13.78	-7.74	0.36
506589	6	**506.59**								**176.41**		

D: Distance, E: Elevation, SD: Segment Distance, CD: Cumulative Distance, StdD: Standard Distance, StdE: Standard Elevation, h1 & h2: Elevation of 1st and 2nd observations respectively, ln: natural logarithmic, SLGI: Stream Length Gradient Index SS: Segment Slope. Source: Computed by the researcher.

Table C: Long Profiles of Luni river and its seven major tributaries.

Luni River Basin		Lilri R SB 1		Mithri or Jojri R SB 2		Jojari SB 3		Guhiya N SB 4		Sukri N SB 5		Kher Nawala N SB 6		Sukri R SB 7	
Dist (km)	Elev (m)	Dist (km)	Elev (m)	Dist (km)	Elev (m)	Dist (km)	Elev (m)	Dist (km)	Elev (m)	Dist (km)	Elev (m)	Dist (km)	Elev (m)	Dist (km)	Elev (m)
0	452	0	461	0	292	0	212	0	453	0	471	0	376	0	331
10	417	2	459	5	290	5	208	5	406	4	419	5	353	4	312
20	396	4	455	10	286	10	205	10	367	8	385	10	334	8	297
30	374	6	450	15	283	15	199	15	357	12	362	15	321	12	288
40	361	8	446	20	280	20	196	20	346	16	344	20	306	16	279
50	343	10	442	25	275	25	191	25	334	20	329	25	295	20	270
60	327	12	436	30	269	30	189	30	325	24	319	30	283	24	264
70	314	14	432	35	264	35	186	35	315	28	306	35	272	28	255
80	298	16	429	40	259	40	181	40	310	32	297	40	260	32	244
90	288	18	423	45	255	45	177	45	301	36	290	45	251	36	236
100	280	20	419	50	250	50	172	50	293	40	281	50	242	40	231
110	274	22	414	55	245	55	170	55	285	44	270	55	234	44	224
120	260	24	407	60	238	60	166	60	278	48	264	60	224	48	216
130	249	26	403	65	233	65	161	65	274	52	256	65	217	52	211
140	237	28	398	70	227	70	156	70	269	56	246	70	209	56	204
150	226	30	396	75	223	75	153	75	264	60	241	75	205	60	196
160	215	32	396	80	218	80	150	80	256	64	232	80	200	64	192
170	204	34	386	85	215	85	147	85	251	68	222	85	195	68	184
180	195	36	384	90	210	90	143	90	245	72	217	90	188	72	180
190	187	38	376	95	206	95	137	95	241	76	209	95	184	76	174
200	177	40	373	100	201	100	134	100	236	80	205	100	179	80	167
210	168	42	370	105	196	105	131	105	230	84	203	105	174	84	164
220	160	44	368	110	192	110	127	110	225	88	197	110	169	88	161
230	151	46	362	115	189	115	124	115	219	92	194	115	164	92	155
240	141	48	359	120	182	120	119	120	218	96	188	120	158	96	147
250	134	50	355	125	179	125	117	125	211	100	186	125	152	100	142
260	125	52	352	130	175	130	112	130	206	104	180	130	146	104	137

270	120	54	349	135	171	135	109	135	201	108	178	135	142	108	134
280	114	56	347	140	167	140	106	140	197	112	175	140	137	112	128
290	105	58	344	145	164	145	104	145	194	116	170	145	136	116	123
300	101	60	341	150	159	150	101	150	188	120	166	150	133	120	122
310	96	62	336	156.56	152	155	99	156.44	184	124	163	155	132	124	118
320	92	64	333			164.39	96			128	159	160	131	128	116
330	92	66	329							132	155	165	129	132	111
340	85	68	326							136	153	171.66	125	136	107
350	72	70	324							140	149			140	103
360	65	72	320							144	146			144	101
370	61	74	316							151.04	142			148	96
380	55	76	315											152	93
390	49	78	315											156	88
400	46	80	311											160	84
410	43	82	307											164	82
420	37	84	306											168	79
430	33	86	302											172	76
440	33	88	300											176	70
450	26	90	298											180	66
460	22	92	295											184	63
470	19	94	291											188	59
480	16	96	291											192	56
490	12	98	289											196	53
506.59	6	100	288											200	51
		102	285											204	47
		104	283											208	45
		106.73	281											212	42
														216	40
														220	38
														223.58	36

Source: Computed by the researcher.

Table D: SL index of the major Luni river tributaries.

Lilri R SB1		Mithri or Jojri R SB2		Jojari SB3		Guhiya N SB4		Sukri N SB5		Kher Nawala N SB6		Sukri R SB7	
Dist (km)	SLGI	Dist (km)	SLGI	Dist (km)	SLGI	Dist (km)	SLGI	Dist (km)	SLGI	Dist (km)	SLGI	Dist (km)	SLGI
0	0	0	0	0	0	0	0	0	0	0	0	0	0
2	0.26	5	0.23	5	0.47	5	5.52	4	6.27	5	2.70	4	2.29
4	5.77	10	5.77	10	4.33	10	56.27	8	49.05	10	27.41	8	21.64
6	12.33	15	7.40	15	14.80	15	24.66	12	56.72	15	32.06	12	22.20
8	13.90	20	10.43	20	10.43	20	38.24	16	62.57	20	52.14	16	31.28
10	17.93	25	22.41	25	22.41	25	53.78	20	67.22	25	49.30	20	40.33
12	32.91	30	32.91	30	10.97	30	49.36	24	54.85	30	65.82	24	32.91
14	25.95	35	32.44	35	19.46	35	64.87	28	84.33	35	71.36	28	58.38
16	22.47	40	37.44	40	37.44	40	37.44	32	67.40	40	89.87	32	82.38
18	50.94	45	33.96	45	33.96	45	76.41	36	59.43	45	76.41	36	67.92
20	37.96	50	47.46	50	47.46	50	75.93	40	85.42	50	85.42	40	47.46
22	52.46	55	52.46	55	20.98	55	83.94	44	115.41	55	83.94	44	73.44
24	80.45	60	80.45	60	45.97	60	80.45	48	68.96	60	114.93	48	91.94
26	49.97	65	62.47	65	62.47	65	49.97	52	99.95	65	87.45	52	62.47
28	67.47	70	80.96	70	67.47	70	67.47	56	134.94	70	107.95	56	94.46
30	28.99	75	57.98	75	43.48	75	72.47	60	72.47	75	57.98	60	115.95
32	0.00	80	77.47	80	46.48	80	123.96	64	139.45	80	77.47	64	61.98
34	164.95	85	49.48	85	49.48	85	82.47	68	164.95	85	82.47	68	131.96
36	34.99	90	87.48	90	69.98	90	104.97	72	87.48	90	122.47	72	69.98
38	147.96	95	73.98	95	110.97	95	73.98	76	147.96	95	73.98	76	110.97
40	58.49	100	97.48	100	58.49	100	97.48	80	77.98	100	97.48	80	136.47
42	61.49	105	102.48	105	61.49	105	122.98	84	40.99	105	102.48	84	61.49
44	42.99	110	85.98	110	85.98	110	107.48	88	128.98	110	107.48	88	64.49
46	134.98	115	67.49	115	67.49	115	134.98	92	67.49	115	112.48	92	134.98
48	70.49	120	164.48	120	117.48	120	23.50	96	140.98	120	140.98	96	187.97
50	97.99	125	73.49	125	48.99	125	171.48	100	48.99	125	146.98	100	122.48
52	76.49	130	101.99	130	127.48	130	127.48	104	152.98	130	152.98	104	127.48

54	79.49	135	105.99	135	79.49	135	132.48	108	52.99	135	105.99	108	79.49
56	54.99	140	109.99	140	82.49	140	109.99	112	82.49	140	137.48	112	164.98
58	85.49	145	85.49	145	56.99	145	85.49	116	142.49	145	28.50	116	142.49
60	88.49	150	147.49	150	88.49	150	176.98	120	117.99	150	88.49	120	29.50
62	152.49	156.56	163.53	155	60.99	156.44	95.19	124	91.49	155	30.50	124	121.99
64	94.49			164.39	51.01			128	125.99	160	31.50	128	62.99
66	129.99							132	129.99	165	64.99	132	162.49
68	100.49							136	67.00	171.66	101.06	136	133.99
70	69.00							140	137.99			140	137.99
72	141.99							144	106.49			144	71.00
74	145.99							151.04	83.83			148	182.49
76	37.50											152	112.49
78	0.00											156	192.49
80	157.99											160	157.99
82	161.99											164	81.00
84	41.50											168	124.49
86	169.99											172	127.49
88	87.00											176	260.99
90	89.00											180	177.99
92	136.49											184	136.49
94	185.99											188	185.99
96	0.00											192	142.49
98	97.00											196	145.49
100	49.50											200	99.00
102	151.50											204	201.99
104	103.00											208	103.00
106.73	77.25											212	157.50
												216	107.00
												220	109.00
												223.58	123.91

Source: Computed by the researcher.

List of Research Papers presented in Conferences

Sl. No.	Dates	Sub-Theme	Research Paper Presented	Co-Author	Organization Body	Venue
1	21 to 23 January 2021	Geomorphology of Extreme Events	Mapping Flash Flood Risk Zones and Analysing its Sensitivity for Luni River Basin, India		32nd Annual Conference of Indian Institute of Geomorphologist (IGI)	Dept. of Geography, West Bengal State University
2	6 to 8 March 2020	Water Resource Management	An Assessment of River Behaviour and Sensitivity in Arid Environment, Luni Basin, India	Dr. Padmini Pani	XIV IGU-India International Conference	Dept. of Geography, The University of Burdwan, W.B.

XIV INTERNATIONAL GEOGRAPHICAL UNION (IGU)-INDIA

International Conference

on

Agriculture, Food, Water, Biodiversity and Health in Changing Climate

March 6-8, 2020

Golden Jubilee Year

Department of Geography, The University of Burdwan, Burdwan-713104, West Bengal, India

Certificate of Participation

This is to certify that Prof. / Dr. / Mr. / Ms. *Jayesh Mukherjee*

of *Jawaharlal Nehru University*

has participated as Paper Presenter in XIV INTERNATIONAL GEOGRAPHICAL UNION (IGU)-INDIA International

Conference on 6-8 March 2020, organized by the Department of Geography, The University of Burdwan, Burdwan-713104,

West Bengal, India, in collaboration with Association of Bengal Geographers.

Title of Paper Presented *An Assessment of River - - - - - - - - Luni Basin, India*

Prof. Yukio Himiyama
President, IGU

Prof. R. B. Singh
Secretary General, IGU

Prof. N. C. Jana
Convener

Prof. N. C. Saha
Vice Chancellor

32nd Annual Conference of the Indian Institute of Geomorphologists (IGI)

Focal Theme: Geomorphology for Human Adaptation to Changing Environment

Organized by

Department of Geography, West Bengal State University

This is to certify that ~~Prof.~~ / ~~Dr.~~ / Sri/ ~~Smt.~~ .... JAYESH MUKHERJEE ....

of .... **Jawaharlal Nehru University, New Delhi** .... presented a paper

entitled *Mapping Flash Flood Risk Zones and Analyzing its Sensitivity for Luni River Basin,*

India .... in the 32nd Annual

Conference of The Indian Institute of Geomorphologists (IGI) on 21st to 23rd January 2021.

Prof. Subhamita Chaudhuri
Convener

Dr. Sayantan Das
Organising Secretary

239